Single cell electroporation on chip

Ana Valero

The research described in this thesis was carried out at the BIOS Lab-on-a-Chip Group of the MESA+ Institute for Nanotechnology of the University of Twente, Enschede, The Netherlands. The project was financially supported by the Dutch Technology Foundation (STW – project number TMM.6016) and Agrotechnology and Food Innovations (Wageningen, The Netherlands).

Promotiecommissie:

Voorzitter	Prof. dr. ir. J. van Amerongen	
Secretaris	Prof. dr. ir. J. van Amerongen	Universiteit Twente
Promotor	Prof. dr. ir. A. van den Berg	Universiteit Twente
Co-promotor	Prof. dr. S.M.H. Andersson	Universiteit Twente
Leden	Prof. dr. ir. N.F. de Rooij	University of Neuchâtel
	Prof. dr. W. Kruijer	Universiteit Twente
	Prof. dr. C.G. Figdor	Universiteit Twente
	Dr. R. Luttge	Universiteit Twente

Valero Valero, Ana
Single cell electroporation on chip
PhD thesis University of Twente, Enschede, The Netherlands
ISBN 90-365-2416-4
Publisher: Wöhrmann Print Service, Zutphen, The Netherlands
Cover design: Jeroen Huijben and Ana Valero

SINGLE CELL ELECTROPORATION ON CHIP

PROEFSCHRIFT

ter verkrijging van
de graad van doctor aan de Universiteit Twente,
op gezag van de rector magnificus,
prof. dr. W.H.M. Zijm,
volgens het besluit van het College voor Promoties
in het openbaar te verdedigen
op donderdag 12 oktober 2006 om 13.15 uur

door

Ana Valero Valero

geboren op 16 augustus 1978
te Zaragoza, Spanje

Dit proefschrift is goedgekeurd door:

Promotor:	Prof. dr. ir. A. van den Berg
Co-promotor:	Prof. dr. S.M.H. Andersson

A mis padres y mis hermanos

Contents

1

Aim and outline of thesis

In this chapter a brief introduction to the aims of this project, single cell electroporation on a chip, is given. The advantages of microfluidic lab-on-a-chip devices for biological analysis are discussed. Finally an overview is presented of the subjects treated in the following chapters of this thesis.

1.1 Single cell electroporation on a chip

In the last decade, electric field pulse techniques have gained increasing importance in cellular and molecular biology, in gene transfection technology, and in medicine. In particular the method of electroporation, as well as that of electrofusion, have become powerful tools for cell modification and for the physical chemical study of electrically induced structural rearrangements in membranes [1, 2]. Electroporation is the phenomenon that induces breakdown of the cell membrane lipid bilayer, which results in the formation of transient or permanent pores in the membrane; molecules can enter and leave the cell during this permeabilized state [1, 3]. The electroporation process is obtained by exposing the cell temporarily to an external electric field: application of strong, rapid electric pulses to the cell membrane results in increased permeability and conductance of the membrane [4-6].

Although there are a number of model approaches toward theories for electropermeabilization, it is fair to say that the detailed mechanisms of field-induced restructuring of membranes in electroporation process are unknown [2].

A drawback of conventional electroporation studies that are carried out in bulk liquid is the large number of parameters to take into account. Each electric field application uses specific electrical parameters (e.g. pulse waveform, field intensity, number and duration of the pulses, interpulse interval) and specific conditions of the cell suspension (like temperature, pH, ionic strength, growth phase, osmolarity) that all need to be optimized [2, 4, 7]. The most important drawback of conventional bulk electroporation is, however, that it works with batches of thousands of cells, leading to low cell survival and low transfection efficiency.

Additionally, while electroporation appears to be a universal phenomenon, the outcome of an electroporation protocol is cell type specific and varies among cells in a given population; each cell is affected separately and differently and shows its own characteristic response to the applied external electric field [3]. Such individuality in response depends on the dimension of the cell, its shape, its relative position to the direction of the electric field, and the structure of particular parts of the membrane [7].

Several of these shortcomings can be overcome by performing the procedure on individual cells: single cell electroporation. Single cell electroporation makes it possible to investigate cell-to-cell variations in a population, and it also helps to unravel the fundamental kinetic and thermodynamic properties of electric-field-induced pore formation and properties of transpore mass transport, and diffusion [8]. Thus, single cell electroporation is an interesting and promising approach and opens up a new window of opportunities in manipulating the genetic, metabolic, and synthetic contents of single targeted cells in tissue slices, cell cultures, in microfluidic channels or at specific loci on chip-based devices.

Microfabrication techniques have been used for many applications in biology and medicine. The applications can be divided into four domains: tools for molecular biology and biochemistry, tools for cell biology, medical devices, and biosensors [9, 10]. Microstructured devices provide significantly enhanced functionality with respect to conventional devices (flow-cytometry, patch clamp, cell sorting). Moreover, microfabrication can enable devices with novel capabilities. These enhancing and enabling qualities are conferred when microfabrication is used appropriately to address the right types of problems [11].

The investigation of living cells, isolated organelles, viruses and macromolecules in chip-based devices is, however, a rather new field of research. Recent advances in Lab-on-a-Chip (LOC) techniques have increased the potential of high-throughput biochemical assays on individual mammalian cells. Of particular interest is the ability to parallelize up-front assay protocols and still be able to examine and treat every individual cell in the assay separately retrieving single-cell event information [12-14].

This thesis describes the development and functionality of microfluidic cell trap chips to perform single cell electroporation. Part of the project was a cooperation between the University of Twente (UT) and the University of Wageningen (WUR). The work at UT was performed in the BIOS Lab-on-a-Chip group (BIOS – part of the faculty of Electrical Engineering, Mathematics and Information Technology) of the MESA$^+$ Institute for Nanotechnology, and at WUR in the institute for Agrotechnology and Food Innovations. The project was financed by STW ("Stichting Technische Wetenschappen" – Dutch Technology

Foundation) under projectnumber TMM.6016 and Agrotechnology and Food Innovations (Wageningen, The Netherlands).

1.2 Thesis outline

Below an overview of the matters of each chapter of this thesis is shown.

In chapter 2 the fundamentals of the electrical permeabilization of cell membranes, electroporation, are discussed. Moreover, the ability of microtechnology to perform single cell electroporation is treated and the current status on micro-electroporation devices for analysis, transfection or pasteurization of biological cells is presented.

In chapter 3 different cell trapping mechanisms that can be implemented in microfluidic devices are described. The design and fabrication of microfluidic devices containing mechanical trapping sites, micromachined filters, is presented, and the flow behaviour as well as functionality of these cell traps is characterized.

In chapter 4 an application of this microfluidic cell trap device is shown: the analysis of apoptosis in HL60 cells. The silicon-glass chip enabled the immobilization of HL60 cells and real time monitoring of the apoptotic process. Fluorescent dyes were used to discriminate between viable, apoptotic and necrotic cells.

Chapter 5 presents the results of single cell electroporation of HL60 and C2C12 cells performed in different cell trapping devices. A detailed electrical characterization for single cell electroporation is discussed and successful gene transfection and protein expression in single cells is presented.

In chapter 6 the results of modeling the cell trapping device are described. The potential distribution in the cell trap chip is modeled using a Finite Element Model, as well as the voltage drop over the cell. An electrical circuit model is developed to simulate/verify whether it is possible to detect the increase in current when cell electroporation takes place. Experiments were done to investigate

whether the current 'jump' occurs at the same moment as optical detection of electroporation (i.e. staining).

Chapter 7 describes the results of a study in which a microfluidic trapping device and a flow-through device were used to electroporate yeast cells. The electroporation process was visualized using the membrane-impermeable fluorescent DNA stain PI and turned out to be a progressive process.

Chapter 8 describes the transfection by electroporation of a green fluorescent-erk1 fusion protein and subsequent erk1 protein tracking in mouse myoblastic cells (C2C12) and in human mesenchymal stem cells (hMSCs) using microfluidic single cell trapping devices.

Finally, in chapter 9 the conclusions of the work described in the previous chapters of the thesis are summarized. Furthermore, several issues are suggested that can be useful for improvement of single cell electroporation on a chip.

1.3 References

[1] D. C. Chang, B. M. Chassy and J. A. Saunders, -*Guide to electroporation and electrofusion;* San Diego: Academic Press. (1992).

[2] E. Neumann, A. E. Sowers and C. A. Jordan, -*Electroporation and Electrofusion in Cell Biology;* Plenum Press, New York (1989).

[3] Y. Huang and B. Rubinsky - *Micro-electroporation: improving the efficiency and understanding of electrical permeabilization of cells;* Biomedical microdevices, **2 (2)**, (1999), pp 145-150.

[4] S. Y. Ho and G. S. Mittal - *Electroporation of cell membranes: A review;* Critical reviews in biotechnology, **16 (4)**, (1996), pp 349-362.

[5] F. Ryttsen, C. Farre, C. Brennan, S. G. Weber, K. Nolkrantz, K. Jardemark, D. T. Chiu and O. Orwar - *Characterization of single-cell electroporation by using patch-clamp and fluorescence microscopy;* Biophysical Journal, **79 (4)**, (2000), pp 1993-2001.

[6] J. C. Weaver and Y. A. Chizmadzhev - *Theory of electroporation: A review;* Bioelectrochemistry and bioenergetics, **41** (1996), pp 135-160.

[7] E. Ferret, C. Evrard, A. Foucal and P. Gervais - *Volume changes of isolated human K562 leukemia cells induced by electric field pulses;* Biotechnology and Bioengineering, **67 (5)**, (2000), pp 520-528.

[8] J. Olofsson, K. Nolkrantz, F. Ryttsen, B. A. Lambie, S. G. Weber and O. Orwar - *Single-cell electroporation;* Current Opinion in Biotechnology, **14 (1)**, (2003), pp 29-34.

[9] H. Andersson and A. van den Berg, -*Lab on a chips for Cellomics;*Kluwer academic publishers (2004).

[10] P. C. H. Li, -*Microfluidic Lab-on-a-Chip for Chemical and Biological Analysis and Discovery* CRC Press (2006).

[11] J. Voldman, M. Gray and M. Schmidt - *Microfabrication in biology and medicine;* Annual Review of Biomedical Engineering, **1** (1999), pp 401-425.

[12] N. J. Dovichi and D. Pinkel - *Analytical biotechnology - Tools to characterize cells and their contents - Editorial overview;* Current Opinion in Biotechnology, **14 (1)**, (2003), pp 3-4.

[13] S. A. Sundberg - *High-throughput and ultra-high-throughput screening: solution- and cell-based approaches;* Current Opinion in Biotechnology, **11 (1)**, (2000), pp 47-53.

[14] A. Tixier-Mita, J. Jun, S. Ostrovidov, M. Chiral, B. Frenea, B. Le Pioufle and H. Fujita, -*Proceedings of MicroTotal Analysis System;* microTAS, (2004), pp 180-183.

2

Electroporation of cells: fundamentals and status*

In this chapter the electrical permeabilization of cell membranes, often referred to as electroporation, is presented. The history, principles and potential application of electroporation in biology and food sciences are described. The ability of microtechnology to perform single cell electroporation is discussed and a review is given on micro-electroporation devices for analysis, transfection or pasteurization of biological cells.

* Parts of this chapter are published in: M.B. Fox, D.C. Esveld, A. Valero, R. Luttge, H.C. Mastwijk, P.V. Bartels, A. van den Berg and R.M. Boom – *Electroporation of cells in microfluidic devices: a review*; Analytical and Bioanalytical Chemistry, 385 (3) (2006), pp 474-485.

2.1 Introduction

Living biological cells contain many membranes, first at the outer boundary (the plasma membrane), and then further in, at the boundary of the nucleus, mitochondria, endoplasmic reticulum and many other subcellular structures. The function of these cell membranes is to isolate regions of different materials, but also to selectively control the transport of ions and molecules from one region to the other. Cells are protected by a selective cytoplasmic membrane which prevents the unregulated transport of any large molecules. Therefore, introducing exogenous molecules into a cell is not an easy task. The difficulties are due to the molecule charge, their molecular weight, hydrophilicity or other physio-chemical properties. In areas such as biotechnology, medicine, cancer and cell research it is important to transport across the cell membrane chemical species that are not compatible with the normal cell membrane function. Accordingly, several methods have been developed to introduce or remove species/molecules through the cell membrane including: mechanical (e.g. microinjection), chemical (e.g. ATP-based active transport), biological (e.g. viral vectors), electrical (e.g. electroporation). The latter, electrical permeabilization or electroporation, is discussed in this chapter.

First, the history and biophysical fundamentals of electroporation is reviewed briefly (section 2.2). This is followed by a description of the principles of conventional bulk electroporation (section 2.3). In section 2.4 single cell electroporation is discussed on and why it should be performed in microfluidic devices. Finally, in section 2.5 an overview of various micro-electroporation devices that are currently available is given.

2.2 Electroporation: history and biophysical fundamentals

Electroporation is a phenomenon that makes the living cell membrane permeable to chemical species that normally cannot cross the membrane by exposing the cell to strong, rapid electric pulses (Figure 2-1) [1]. It is a simple, flexible, and relatively nontoxic physical method which relies on the transient

permeation of the cell membrane induced by the application of a strong electric pulse (typically 1-4 kV cm^{-1} for 1 μs to a few ms) [2]. Although the mechanism is not fully understood, electroporation has become a widely used technique in biotechnology to incorporate various molecules (e.g. DNA and RNA fragments, proteins, antibodies, drugs, fluorescent probes, etc.) into many different types of cells (e.g. bacteria, yeasts, plant and mammalian cells) [3, 4].

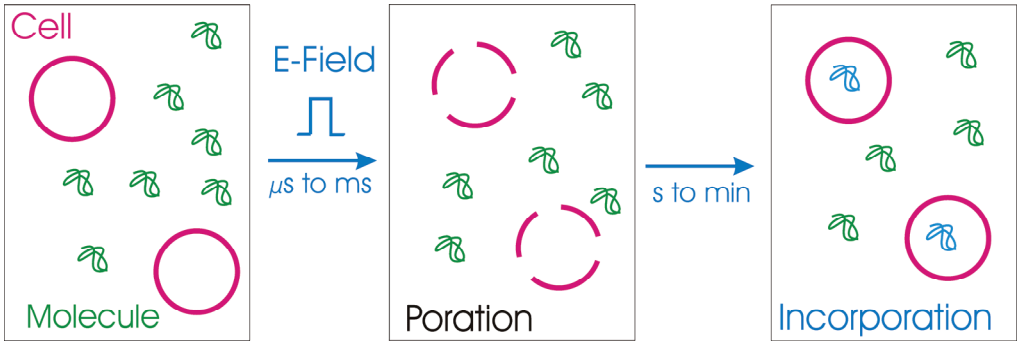

Figure 2-1: Schematic drawing of electroporation.

Application of large electric fields to cells over long times compared to the charging time of the membranes (approximately one microsecond for the plasma membrane of mammalian cells) [5] results in charge redistribution, and the build-up of a transmembrane voltage in addition to the resting voltage. Once the transmembrane voltage exceeds a few hundred millivolts, structural rearrangements begin, which lead to membrane instabilities. The unstable membrane then alters its shape, forming aqueous pathways that possibly are nano-scale pores [3], and the membrane rapidly acquires some type of new electrical conduction pathways. Mass transfer can now occur through these pores under electrical control or by diffusion.

There are a number of early reports on the effects of electric fields on the living cell membrane. In 1958, the nodes of Ranvier of nerves were reported to be involved in some type of 'breakdown' [6]. A decade later, in the late 1960s, Sale and Hamilton reported the damaging effects of strong electric fields on microorganisms and erythrocytes, suggesting non thermal membrane interactions [7-9]. Dielectric breakdown of the cell membrane due to an induced electric field and release of intracellular components was first observed in the early 1970s [10-12]. During the late 1970s the ability of the membrane to reseal after exposure to an electric field

was discovered [13-15]. It was also found that by varying pulse parameters, this induced electric field could either have no effect on the cell membrane permeability, cause reversible permeabilization of the cell membrane or cause irreversible cell membrane breakdown [16, 17]. Further evidence for chemical transport through membranes was observed in experiments with red blood cells [18-23]. Erythrocytes were also used to demonstrate DNA delivery into a cell associated with dielectric breakdown of the cell membrane [24]. However, the first to demonstrate cell transfection *in vitro* through DNA electro-transfer were Neumann *et al.* and Wong and Neumann in 1982 [25, 26]. Since the early nineties electroporation is a routine technique in biotechnology and genetic engineering [3].

While electroporation is commonly used in biotechnology, the mechanism which leads to the permeabilization of the living cell membrane in an electrical field is not fully understood. Several approaches are reported in literature to describe the membrane permeabilization, such as energy balance theories and electromechanical and stochastic pore population theory. Below, a brief overview of these theories is given. However, nowadays none of them are fully accepted.

Crowley used the electromechanical instability theory to describe membrane breakdown [10]. Crowley's theory assumes that the electrostatic compressing force decreases the membrane thickness. Due to the fact that the bilayer volume is incompressible, the membrane area must increase, and this leads to an increased wedge shaped conformation of lipids. Consequently, the membrane breakdown can be explained as a result of the destabilized bilayer due to the shift of phase equilibrium toward non-lamellar phases [10, 27]. Though supported by some experimental evidence, Crowley's theory cannot distinguish the reversible membrane breakdown from irreversible membrane rupture. Theories that also support membrane breakdown due to mechanical stress are given by Bryant and Wolfe and Wilhelm *et al.*: Bryant and Wolfe proposed that cell lysis was due to isotropic mechanical surface tension produced in deforming the cell rather than due to electric field produced in the membrane [28]. Wilhelm *et al.* combined models of pore formation with those of mechanical stress to describe membrane breakdown [29].

Other theories incorporate the concepts of pre-existing pores, defects or fluctuations in the cell membrane integrity to explain the process of electroporation. Neumann and Boldt proposed electroporation as a phase transition from hydrophobic pathways to hydrophilic ones in the lipid layers [30], whereas Cheromordik suggested that there are initially small hydrophobic pores or defects, which become enlarged and hydrophilic under an electric field [31]. The denaturation model speculates that the membrane could be permeated at the protein channels, where it undergoes denaturation by Joule heating or by electrical modification [32].

Weaver and Powell describe electropores as dynamic and transient structures in the lipid bilayer membrane [33]. In their model either the electric field rapidly creates small pores in the membrane or tiny pores already exist in the membrane. Due to the large electrical potential (caused by the electrical pulse) these pores expand. Weaver and Barnett developed pore population models to predict the number of electropores and the pore population rate in a membrane [34]. Electropores will remain stable, provided that energy is expended for edge formation and is gained by increasing the pore areas. According to Weaver's model, these stable pores provide the pathway for foreign substances to enter the cell. The pores have, however, never been unquestionable verified or observed in the membrane of mammalian cells. Regardless, this is the most common theory and hence the term electroporation is commonly employed [35].

Experimental studies were also performed in an attempt to understand the mechanism of membrane permeabilization and how it correlates to electrical fields. Chang and Reese visualized electroporation of red blood cells using rapid-freezing electron microscopy [36]. Although Chang and Reese describe their observations as being electroporation events, it is now thought that the pores in their work were secondary effects and not related to the permeabilization event itself: these pores appeared after the delivery of the electric pulse as a result from the influx of water and subsequent rapid swelling of the cell.

Other ways to study the dynamics of electroporation are based on detecting changes in membrane resistance with patch or voltage clamps [31, 37] or by measuring the transmembrane potential. During electroporation, the transmembrane potential can be determined by staining the cell membrane with a voltage-

sensitive fluorescent dye and recording the experiment using digital video microscopy [17, 38].

In conclusion, despite the wide use of electroporation in biotechnology the fundamental understanding is limited. Researchers all over the world have reported solid evidence that electroporation is a physical phenomenon. Although the results are scattered and the kinetic models are diverse, researchers agree that electroporation is a complex dynamic process in which the pore structure and process time sequence are subject to variations depending on the physical and electrical conditions employed. Moreover, there are only a few experimental techniques to investigate the fundamentals of the electroporation process. Developing a fundamental understanding on the biophysics of cell membrane permeabilization in an electrical field is of central importance for the efficient use of electroporation in biotechnology. Microdevices as a platform to perform electroporation provide an essential tool to obtain this fundamental knowledge about electroporation.

2.3 Bulk Electroporation

Conventional *in vitro* electroporation of cells is conceptually simple. It involves placing a suspension of cells between two electrodes connected to a high voltage electrical field generator (Figure 2-2). Whole populations of cells are electroporated in homogenous fields of a few kilovolts per centimeter. The electric fields are created between large electrodes, separated several millimeters up to some centimeters, by applying hundreds to thousands of volts to them. The electrical behavior of a cell is dominated by the cell membrane, which behaves essentially as a local capacitor with low but complex conductance, and by the electrolytic conduction of the intra- and extra-cellular domains. Therefore the potential drop over the cell (V) occurs almost entirely across the cytoplasmic membrane of thickness d, leading to very large electric fields within the phospholipid bilayer ($E_m \sim V/d$) [2].

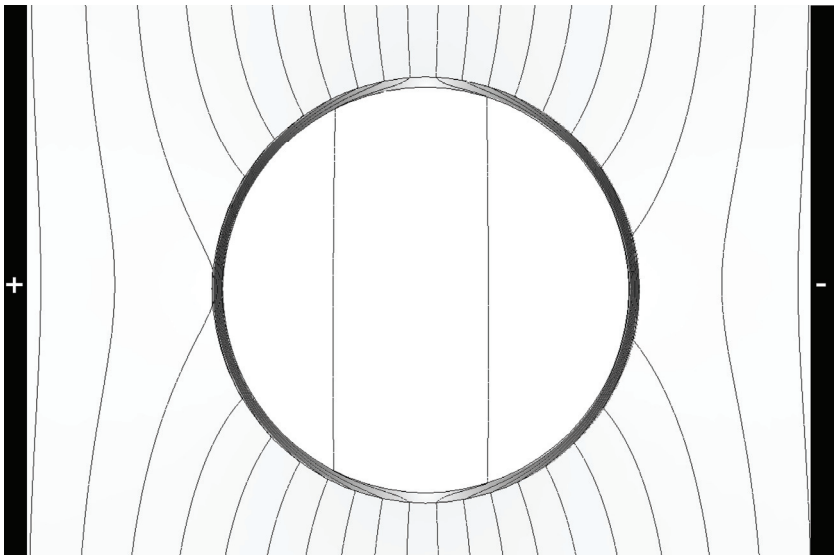

Figure 2-2: Schematic representation of a cell in an electric field. Black depicts high electric field strengths, white depicts low electric field strengths. The lines are equipotential lines.

According to experimental observations and the transient aqueous pore mechanism hypothesis [3-5, 39-42], the main features of electroporation involve a) application of short electrical pulses (10^{-6} to 10^{-1} s), b) charging of lipid bilayer membranes developing an induced transmembrane electrical potential of typically 200 mV–1 V, and a resultant electrical field across the membrane of the order of 10^{8} V/m (for a typical cell membrane thickness of 5 nm), c) rapid, localized structural rearrangements within the membrane, d) transitions to water-filled membrane structures which perforate the membrane: "aqueous pathways", "pores" or "hydrophilic pores", and e) tremendous increase in ionic and molecular transport through the membrane. Whether the membrane system fully recovers or not depends on many factors, which will be discussed in section 2.3.5.

2.3.1 Induced transmembrane potential

The induced transmembrane potential is not evenly distributed over the cell surface. The potential difference is highest at the membrane sites closest to the electrodes and lowest at the membrane sites furthest away from the electrodes [43-45]. Several mathematical equations have been developed to associate the induced

transmembrane potential to various properties of the biomembrane, external medium and electrical conditions [17, 44, 46-48].

When a cell in suspension is exposed to an electric field, the Maxwell equation describing the current in the region near the cell is given by

$$\Delta \cdot J + \frac{\partial \rho}{\partial t} = 0 \qquad \text{eq. (1)}$$

where J is the current density, ρ the resistivity, and t the time. If charges are not generated in a cell during the electric field treatment, this relation simplifies to

$$\Delta \cdot J = 0 \qquad \text{eq. (2)}$$

and since the electric field is the gradient of the electric potential, the Maxwell equation (eq.1) becomes

$$\Delta^2 \psi = 0 \qquad \text{eq. (3)}$$

where ψ denotes the electric potential.

For DC electric fields, the solution to the Maxwell relation for a field-induced transmembrane potential, $\Delta\psi$, can be expressed as

$$\Delta\psi(E, M, t) = -f \cdot g \cdot E \cdot r \cdot \cos\theta(M) \cdot \left(1 - \exp - \left(\frac{t}{\tau}\right)\right) \qquad \text{eq. (4)}$$

where ψ is the electric potential [V], M is the point of interest on the membrane, f is the cell factor, g is the relative electric permeability of the membrane, E the applied electric field strength [V/m], r the cell radius [m], θ the angle between the direction of E and M, t is the time after the field is turned on [s], and τ is the characteristic time constant/relaxation time of the membrane [s].
If an AC electric field is used the equation for the field-induced potential, $\Delta\psi$ is as follows

$$\Delta\psi(E, M, t) = \frac{-f^* \cdot g \cdot E \cdot r \cdot \cos\theta(M) \cdot \left(1 - \exp - \left(\frac{t}{\tau}\right)\right)}{\left[1 + (2 \cdot \pi \cdot f \cdot \tau)^2\right]^{0.5}} \qquad \text{eq. (5)}$$

where f^* is the frequency of the applied AC field [Hz] and g (relative electric permeability) is given in equation 6.

$$g = \frac{2 \cdot \sigma_e \cdot \sigma_i}{(2\sigma_e + \sigma_m)(2\sigma_m + \sigma_i) + \left(\frac{r}{d_m}\right)\sigma_m(2\sigma_e + \sigma_i)} \qquad \text{eq. (6)}$$

where σ_e, σ_i and σ_m are the electrical conductivities of the external suspending medium, the cytoplasm, and the cell membrane respectively [S/m], and d_m is the membrane thickness [m].

$$\tau = r \cdot C_m \cdot \left(\frac{1}{\sigma_i} + \frac{1}{2\sigma_e}\right) \qquad \text{eq. (7)}$$

where C_m is the membrane capacitance per unit area [F/m^2].

For the case that the pulse duration is much larger than the membrane charging time (~1μs) [5] ($T >> \tau$), and the cell membrane is considered as pure dielectric ($g = 1$), equation 4 can be reduced to simple, time-independent forms:

a) For spherical cells where f=1.5,

$$\Delta\psi = 1.5 \cdot E \cdot R \cdot \cos\theta \qquad \text{eq. (8)}$$

b) For elongated cells where f = 0.5,

$$\Delta\psi_{\max} \approx 0.5 \cdot E \cdot L \qquad \text{eq. (9)}$$

where L is the characteristic long dimension of the cell [m] and the cell is parallel to E.

Taking into account the intrinsic resting potential, $\Delta\psi_{mo}$, which is present in every living cell and is maintained by the cell membrane pumps, equation 8 becomes:

$$\Delta\psi = 1.5 \cdot E \cdot R \cdot \cos\theta - \Delta\psi_{mo} \qquad \text{eq. (10)}$$

According to equation 10, the electrical potential which develops across the cell membrane is not symmetric relative to the two electrodes because of the intrinsic resting potential difference ($\Delta\psi_{mo}$ = -70 mV) and is also a function of angle. Due to this, it is argued that the first pore is always initiated in the anodic pole of the cell where the resting potential enhances the induced transmembrane potential. Once the pore forms, redistribution of potential takes place and the next pores form on the cathodic pole of the cell. The equation also shows that the transmembrane potential is proportional to the cell size, which suggests that among a population of cells with different sizes, the same electrical field may cause

different transmembrane potentials. This explains why conventional bulk electroporation that works with batches of cells leads to low cell survival and low transfection efficiency.

If the transmembrane potential exceeds the breakdown voltage, the membrane undergoes irreversible electroporation that finally leads to membrane rupture and cell inactivation. For most biomembranes, a transmembrane potential of 1V is sufficient to induce irreversible membrane breakdown and thus kill the cells [49]. Experimental studies suggest that the threshold for electroporation is 300-350 mV [50-52]. An induced transmembrane potential in mammalian cells around the threshold for electroporation results in reversible electroporation; i.e., the pores will be resealed within time [3]. For bacteria it is assumed that the same picture applies.

In summary, in conventional bulk electroporation protocols a suspension of cells is placed between two electrodes. Electrical pulses are generated between the electrodes in order to induce cell membrane permeabilization. Conventional electroporation is a trial-and–error procedure. Numerous empirical studies have been conducted in order to get more insight in the electroporation process in which electrical parameters such as amplitude, frequency, pulse number, pulse type and electrode geometry are varied and the consequence of those on cell viability or its ability to incorporate molecules. Procedures for selecting the electrical parameters are described by Chang *et al.* [3] who provide other research as reference points.

2.3.2 Structural membrane reorganisation

In electroporation, the permeable state of the cell membrane is induced during the onset of the pulse. However, the structural reorganisation of the membrane takes places on a much longer time scale, as observed by conductance measurement, light scattering and digitized video-imaging [38, 53-57]. Gabriel *et al.* concluded by direct video-imaging that the electric field strength determines the geometry of the part of the cell membrane that is porated while the pulse length controls the density of defects in this poration area [54].

2.3.3 Molecular transport

Diffusion and electrophoresis have been shown to be the major mechanisms of molecular and ionic transport through electroporated membranes [58]. Experimental measurements confirmed that diffusion plays a major role in the transport of small molecules [59], while electrophoresis accounts for the transport of macromolecules such as DNA [60, 61].

Several factors need to be considered in the transport of molecules through the pores created by electroporation, e.g., the size and shape of a molecule as well as its electric charge. Simple size exclusion by the membrane is straightforward, as the membrane will sieve molecules with inappropriately large size [62]. Weaver [40, 63] described that an enhanced uptake of small ions and molecules over a prolonged time may occur if a long macromolecule (e.g. unbranched dextrans, other polymers, DNA) temporarily resides with a fraction of its length inside a pore. He named it the "foot-in-the-door" hypothesis and assumes that the long molecule interacts repulsively with the pore walls, tending therefore to hold the pore open (inhibit resealing) until the long molecule leaves the pore. This is relevant to diffusive and electrophoretic post-pulse transport.

Electrostatic exclusion can also be significant for the transmembrane transport. Small hydrophilic pores represent a large resistance because of an energy repulsion associated with the lower dielectric constant of the membrane interior regions and interaction with the charged headgroups of the phospholipids [1, 40]. Moreover, pores tend to expand to quickly discharge the membrane capacitance (an essential aspect of reversible electroporation). Creation of pores larger than 1 nm also benefits molecular transport. Neutral and charged molecules need to fit into a pore, or to expand the pore, to be transported through the electroporated membrane.

A contribution by electroosmosis has been suggested [60], but the pore length (5 nm) along which coupling to flow can occur is small and electroosmosis has not been emphasized subsequently. Moreover, endocytosis might occur as a secondary transport processes after cells have been stimulated [64-66].

Another possible contribution that has received little attention is the presence of the resting potential during the relatively long time of post-pulse

membrane recovery. Even though this resting potential is small, it may generate a significant electrophoretic contribution to the transport of ions and charged molecules [34]. A broad, quantitative description of molecular transport has not yet been achieved.

2.3.4 Membrane recovery: pore resealing

Pore formation is known to be a fast process (reported to occur on time scales of 10 ns [67]). Pore resealing, however, is a much slower process and normally occurs on a time scale of seconds [68]. Besides, mechanisms for membrane recovery remain still unclear [63]. In the post electric pulse stage, the induced transmembrane potential is replaced by the resting potential, which is two or more orders of magnitude smaller. This potential cannot be immediately discharged through the pores due to their high impedance. But membrane recovery depends not only on this, other factors such as temperature (and the resultant thermal fluctuations) and membrane composition also play a role [63]. Furthermore, membrane recovery does not ensure long-term cell viability; also other factors like active processes play a significant role [5, 63].

2.3.5 Factors that affect electroporation

One of the most important drawbacks of electroporation studies is the large number of parameters to take into account. Each electric field application uses specific electrical parameters (amplitude, length, shape, number and duration of the pulses, interpulse interval) and specific conditions of the cell suspension (temperature, pH, ionic strength, growth phase, osmolarity), which need to be optimized [4, 17, 69].

The composition of the electroporation buffer is one of the most critical factors affecting electroporation. Media supplemented with small amounts of divalent cations like Ca^{2+} and Mg^{2+} in millimolar concentrations were found to promote cell viability. Furthermore the pH of the electroporation buffer is also of high importance, since the composition and pH of this buffer has to mimic the composition of the cytoplasm of the cell. A pH of 7.2 is an appropriate value since

it is approximately the intracellular pH. Moreover, the use of ice cold buffers (0-4 °C) avoids the rapid resealing of electrically porated cells [4, 70].

In summary, fine-tuning of electroporation involves various parameters that can significantly influence cell viability. For this optimization, studies to determine cell viability before and after electroporation events are crucial.

2.3.6 Electroporation applications

The electroporation technique is used in many *in vitro* and *in vivo* applications, mainly at the cellular level but also at the whole tissue level. Reversible electroporation is used as a technique to introduce foreign molecules in cells while the pores are opened. Electroporation has been used for the introduction of components in the cell, like proteins [71], DNA [70], Rb^+ ions [72-74] or drugs [74]. Current applications include gene transfer in mammalian and plant cells, genetic transformation in bacteria and yeast, *in vitro* and *in vivo* drug delivery, production of hybridoma and human monoclonal antibodies [3]. It is foreseen that electroporation will become an important technology in the treatment of gene diseases at the single cell-level, notably with stem cells; e.g. in treatment of autoimmune diseases. Moreover, electroporation can also be applied in cancer treatment through the introduction of drugs into malignant cells.

In contrast to reversible electroporation, where the cell viability is maintained, irreversible electroporation is used as a low thermal pasteurization technique, called pulsed electric fields (PEF). To inactivate microorganisms, short (typically 2 μs), high electric field (typically more than 10 kV cm^{-1}) pulses are applied to a food product [75, 76]. On a large scale of 1000 L hr^{-1} and more, PEF is particularly suitable as an alternative to heat pasteurization of pumpable foods [77], like fruit juices [78, 79] or dairy products [80], and to increase the release of intracellular contents from plant cells, for example for the extraction of sugar from sugar beet cells [81, 82].

2.4 Single Cell Electroporation

2.4.1 Why single cell electroporation

While bulk electroporation appears to be a universal phenomenon, the outcome of an electroporation protocol is cell type specific and varies among cells in a given population: as discussed in section 2.3 each cell is affected separately and shows its own characteristic response to the external electric field [83]. Such individuality in response depends on the dimension of the cell, its shape, its relative position to the direction of the electric field, and the structure of particular parts of the membrane [69]. Moreover, there is no effective and real time feedback on the permeability status of the cell membrane during and shortly after electroporation.

These and other deficiencies of bulk electroporation could be resolved by performing electroporation in individual cells. Therefore, single cell electroporation (SCE) is an interesting and promising approach that opens up a new window of opportunities in manipulating the genetic, metabolic, and synthetic contents of single targeted cells in tissue slices, cell cultures, in microfluidic channels or at specific loci on a chip-based device.

Several methods to target single cells by electroporation have been reported: solid microelectrodes [84], electrolyte-filled capillaries [85], micropipettes (patch-clamp electrodes) [86, 87] and a diversity of chip structures which will be reviewed in more detail in section 2.5. These new techniques make it possible to electroporate a cell without affecting adjacent cells, and thus provide ways to manipulate the biochemical content of single cells and even to sub-cellular structures (such as organelles), *in vivo* and *in vitro*.

In summary, single cell electroporation makes it possible to investigate cell-to-cell variations in a population, and it also helps to unravel the fundamental kinetics and thermodynamic properties of electric-field-induced pore formation and the properties of transpore mass transport [88].

2.4.2 Why SCE in microfluidic devices

For successful single cell electroporation, the cell must either be isolated or the electric field must be focused well to target a particular cell. Microfabricated

devices are ideally suitable to fulfill both functions of isolating single cells as well as focusing of the electric field. In addition, the use of microfluidic devices for cell electroporation applications offers clear advantages compared to common electroporation setups. First of all, by applying microelectronic pattern techniques, the distances between the electrodes in the microchips can be made very small, which means that relatively low potential differences are sufficient to give high electric field strengths in the regions between the electrodes. The electrical design of the pulser is therefore much simpler, which permits us to choose from a wider range of pulsers. This allows pulse forms other than the common block or exponential decay pulse shapes to be used [89]. Cell handling and manipulation are also easier, as the channels and electrode structures are comparable to the sizes of the cells. As the hydrodynamic regime used in microfluidics is much different to that used in large scale equipment, it is possible to make use of specific hydrodynamic effects associated with this regime. The coupling between cell electroporation and separation or detection of the released components is also more direct, as it can be integrated onto the same device. This makes it even possible to trap single cells and to determine intracellular content or other properties, which is hardly feasible using laboratory-scale equipment. In addition, only small amounts of cells and difficult-to-produce reagents, such as specific plasmids, are needed. On top of this, in situ optical inspection and real time monitoring of the electroporation process (using fluorescent probes for example) also becomes possible, as the microdevices can be made transparent. However, the experimental results published so far have been mainly qualitative because the field of microtechnology is relatively new. Finally, the area-to-volume ratio in microdevices is relatively large, which results in faster heat dissipation per unit surface area. This makes it possible to distinguish between heat and electric field effects, in contrast to the usual PEF experiments, where temperature increases of 10 °C and more are observed [90, 91], although this advantage is less important in transfection and analysis microdevices.

In the next section, a review is given on microfluidic devices for cell electroporation. This work is published in Anal. Bioanal. Chem., 385 (3) (2006), pp.474-485.

2.5 Electroporation of cells in microfluidic devices: a review

One of the first single cell electroporation devices was made by Lundqvist [84, 85, 88, 92], who studied the electroporation of individual cells using two carbon fiber microelectrodes. These microelectrodes, which had diameters of 5 μm, were moved within 2-5 μm of the cellular membrane with a micromanipulator. Single cells could be selected from a solution and successfully electroporated with 1 volt-millisecond square wave pulses. This setup gives a high degree of freedom when selecting cells, even in a complex multicellular system, and even for organelles, as was demonstrated by staining only the exonuclear cytoplasmic region with fluorescein. Gene transfection with GFP (green fluorescent protein) plasmids has also been accomplished [84]. Although this design demonstrated the possibilities of single cell electroporation, it is a labour-intensive technique, comparable to already existing patch-clamp techniques. Moreover, the cell is not brought into a confined geometry, which makes it unsuitable for automation.

Therefore, a more common approach is to use a microfluidic system which can handle small amounts of cells, combined with an electrical treatment based on integrated, fixed electrodes. These electroporation microdevices can be roughly divided into three categories depending on their application.

I. Devices for analyzing cellular properties or intracellular content

II. Devices for transfecting cells

III. Devices for inactivating/pasteurizing cells

We now consider each of these in turn.

2.5.1 Devices for analyzing cellular properties or intracellular content

Electroporation microdevices are mainly used in the field of analysis, as the advantages are numerous, including the very small sample size needed, the high separation efficiencies obtained, and the ability to combine the technique with sensitive measurement methods. Applications of electroporation microdevices to analysis vary from those devices which measure true electroporation properties, like

the pore formation process, to those where electroporation is only an aid for further analysis of the cell content, notably by capillary electrophoresis (CE). Another application involves measuring the cell concentration in a bulk fluid.

CE is a technique that has evolved significantly due to the use of microtechnology [93]. The capillary structures are relatively simple to make in several materials, the devices are suitable for coupling to sensitive detection methods, and they are cheap to produce [93-96]. In conventional CE of cell content, a batch of cells is lysed after which a small sample is analysed [97]. However, since the average properties of a larger group of cells are measured, valuable information is lost.

Therefore, one of the most promising challenges in CE (and microtechnology in general) is to be able to analyze the contents of a single cell [98]. Whereas cell lysis can be accomplished by methods like chemical lysis [99], electroporation has the advantage that no chemicals need to be added to the system, which could disturb the measurements. Gao *et al.* [100] used electroporation in a microfluidic device to release the cellular content. Their design consists of a simple crossed channel, in which erythrocyte cells are loaded using a pressure gradient (Fig 2-3 a). When a cell arrives at the crossing, an EOF is used to direct the cell into the separation channel, after which the flow is stopped for 15 s to allow the cell to attach to the wall. The cell is then electroporated using a one-second 1400 V pulse. In this way, the single cell glutathione content was measured in a reproducible way without the need to use disturbing lysing agents. McClain *et al.* [101] also reported on a CE chip for single cell analysis, in which continuous 450 V m^{-1} square wave pulses with a DC offset of 675 V m^{-1} were used. The DC offset provides the necessary potential for separation, while the added pulses are used for electroporation. A non-pulsed, but high DC current would result in too much Ohmic heating. Using this device, cells which were previously loaded with several fluorescent stains were electroporated, which was followed by the separation and measurement of the stains.

Although these are effective demonstrations of single cell electroporation coupled to separation and analysis, more advanced designs have been proposed for the electroporation of biological cells. In a series of articles [83, 102-104], Huang and Rubinsky presented a microfluidic device in which a single cell is captured and

electroporated for analysis purposes. This chip (Figure 2-3 b) [83, 103] consists of two chambers in n+ polysilicon, separated by a 1 μm thick silicon nitride membrane with a hole. The hole diameter (2 to 10 μm) in the membrane is smaller than the cell diameter. Pulses are applied via the conducing n+ polysilicon layer. Since the thin polysilicon layer is translucent, it is possible to observe the chip while treating biological cells. Cells are pumped through the top chamber, followed by immobilization of one cell in the hole by lowering the pressure in the bottom chamber. The electrode distance is 900 μm, but the electric field is focused in the pore of the silicon nitride membrane. Therefore, only pulses of 0 to 120 V are needed for cell electroporation. The electroporation and resealing process can be followed in time by impedance measurements as the cell plugs the hole (thereby strongly changing the impedance). With this chip, Huang *et al.* were able to show the natural difference in electroporation behaviour between human prostate adenocarcinoma and rat hepatocyte cells. The n+ polysilicon electrode was replaced in later publications [103] by an Ag/AgCl electrode, since the polysilicon electrodes hindered the precise characterization of the electrical properties of the cell membrane. This was caused by the complicated electrochemical behaviour at the electrode-electrolyte interface, particularly for DC and low frequency pulses. By staining human prostate adenocarcinoma cells with YOYO-1 (a membrane-impermeable fluorescent DNA stain) it was possible to combine an impedance measurement with an optical measurement [104]. This combination showed that the impedance measurement is a suitable way of measuring cell electroporation behaviour in the microdevice. With the same design, it was also demonstrated that it was possible to study the response of cells to specific chemical substances, in this case Triton X-100, which is a cell lysis reagent.

Valero *et al.* [105] used a different geometry to trap cells and subsequently electroporate them in order to study the electroporation behaviour. Their design consists of a chip with two crossing channels, where one side of the crossing is partially blocked; leaving special designed trapping sites with small flow channels behind the trapping sites (Figure 2-3 c). The trapping sites have a size which is approximately the size of a cell (10-12 μm), whereas the subsequent flow channel is 3 μm wide, preventing the cells to flow any further than the trapping site. Gold wires inserted in the entrance reservoirs are used as electrodes. Using

electroosmotic flow, human promyelocytic leukemic (HL60) cells were directed towards the trapping sites, where they were trapped and subsequently electroporated as the electric field was focused at the trapping sites. This device was applied to the study of apoptosis (controlled cell death), where the cells were observed visually while they were stained in the trapping site with fluorescent FLICA and propidium iodide.

As well as the aforementioned trapping devices, several flow-through devices have also been reported. Lee and Tai [106] reported on a microdevice used for the lysis of cells for analysis, consisting of a straight, 30 μm high microchannel with an electrode structure at the bottom perpendicular to the fluid flow (Figure 2-3 d). The electrode structure consists of interdigitated gold electrodes with a saw-tooth structure to enhance the electric field gradient. The tips of the saw-tooth structure are separated by 5μm. Cells are introduced by pressure-driven flow and dielectrophoretically directed towards the tips of the electrode, where 20 V, 100 μs pulses were used to electroporate the cells. Various cell types, such as yeast cells, plant protoplasts and *E. coli* could be electroporated. Although the design could be further optimized, the authors showed the ability of the device to electroporate small numbers of cells on the microscale, while concentrating the cells near the electrodes in order to increase electroporation efficiency.

Suehiro *et al.* [107] used a variation of the device designed by Lee and Tai to measure the cell concentration. The device used by Suehiro has a straight 12 μm wide electrodes at a glass wafer (Figure 2-3 e), with a 5 μm clearance in between the electrodes, instead of the saw-tooth structure used by Lee and Tai. Yeast cells from the pressure-driven fluid flow are directed dielectrophoretically towards the surface between the interdigitated electrodes using a 5 V, 100 kHz AC voltage, thereby changing the impedance between the electrodes. Since the impedance change is correlated to the time allowed for the cells to migrate towards the electrode structure and the cell concentration, it is possible to use the device to measure cell concentrations. However, the impedance changes are relatively small, which limits the sensitivity to 10^4 CFU/ml for yeast cells. In order to increase the sensitivity, Suehiro *et al.* [108] increased the dielectrophoretic voltage stepwise to 20 V, in order to electroporate the trapped cells. The electroporated cells have an improved conductivity because of the fractured membrane, which causes the lowest sensitivity

limit to jump to 10^2 CFU/ml. This method has also been applied to bacterial *E. coli* cells [109]. As the sensitivity decreased, the form of the pulses used for electroporation had to be improved to make them continuous block pulses of a limited time, in order to avoid contamination by products generated by electrode degradation.

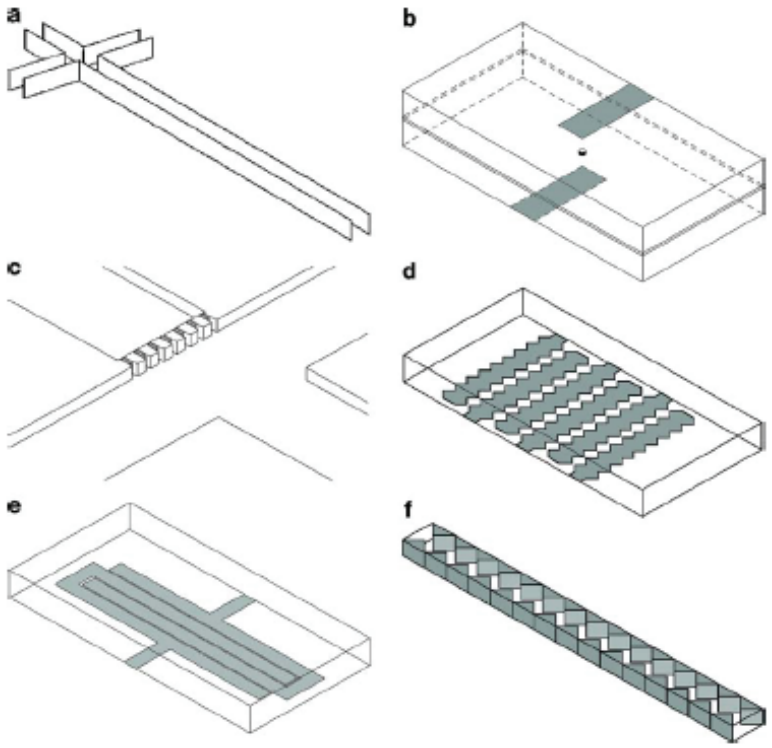

Figure 2-3: Schematic representation of different analytical microfluidic electroporation devices. Not to scale. **a** Gao *et al.*[100]; **b** Huang and Rubinsky [83, 102-104] ; **c** Valero *et al.* [105]; **d** Lee and Tai [106]; **e** Suehiro *et al.* [107]; **f** Lu *et al.*[110]

Lu *et al.* [110] also used the advantageous saw-tooth structure for their more advanced microelectrode structure in order to enhance the electric field strength. A straight, 50 μm high microchannel was constructed on Pyrex glass, where the side-walls consist of gold saw-tooth shaped electrodes with a tip distance of 30 μm (Figure 2-3f), supported by the polymer SU-8. Using pressure-driven flow, cells are directed through the channel and electroporated at the place where the electrodes are closest to each other (where the electric field strength is the highest). To avoid electrolysis in the channel, a continuous alternating voltage of 6-8.5 V at 5-10 kHz is applied to electroporate the cells. It was possible with this device to electroporate

human carcinoma (HT-29) cells, as assessed using fluorescent acridine orange and propidium iodide staining. Although this design was aimed to induced cell lysis and therefore the release of intracellular content for further analysis, it could be used for transfection purposes as well, since transfection could take place in the channel and then the transfected cells could be sample for further culturing.

2.5.2 Transfection designs

Transfection of cells with foreign DNA is often accomplished by reversible electroporation [4] . However, the treatment protocols are often suboptimal [3] and based upon the application of long duration pulses (ms) with a relatively low electric field strengths, which results in excess amounts of inactivated cells. Furthermore, cells exposed to electric fields can be sensitive to substances in the medium such as Al^{3+} ions, which can become solubilized from the electrodes [111]. It is possible to control the circumstances better in microfluidic devices, and hence increase the efficiency of transfection. Besides this advantage, only small amounts of transfection material are needed, and it is possible to make structures where the transfection of more cells in a parallel fashion is possible. Several microfluidic designs have been published, some aiming at single cell transfection, others at the transfection of larger amounts of cells.

Lin *et al.* [112] constructed a device made of PMMA that consisted of a 0.2 mm high, 5 mm wide channel with integrated gold electrodes at the top and the bottom of the channel at the electroporation spot (Figure 2-4a). Since the electrode distance was relatively small, only 10 ms pulses of 10 V were required for electroporation. The efficiency of this simple design was proven by transfecting human hepatocellular carcinoma cells (Huh-7) with β-galactosidase and green fluorescent protein genes.

While Lin *et al.* used a small electrode distance to focus the electric field, it is possible to do this by introducing a constriction between the two electrodes. Khine *et al.* [113] used this concept in their design (Figure 2-4b), which was originally developed as a multiple patch-clamp array [114]. Although the constriction itself increases the electric field strength, this effect is enhanced in this design by applying

a gentle underpressure and sucking a cell partially into the constriction, thereby blocking the constriction completely. The cell cannot pass the constriction because the cell diameter (12-17 μm) is approximately four times larger than the constriction (3.1 μm). Low potentials of less than 1 V could be applied using an Ag/AgCl electrode. The release of calcein and the uptake of trypan blue from HELA cells after electroporation were followed visually, although transfection with DNA has not yet been accomplished in this device type.

Huang and Rubinsky, who designed an electroporation analysis device with a microhole in a silicon nitride membrane, also adapted this analysis-oriented design [115] to make it applicable to cell transfection. They did this by creating a flow-through channel on top of a silicon nitride membrane of approximately 1.5 times the size of the cells (Figure 2-4c). The hole in the membrane is situated in the middle of the channel. Once a cell is brought into the microchannel, it is captured in the microhole by a backside pressure, electroporated, uploaded with the desired foreign molecules and then released, exiting the channel on the other side. The microhole in the silicon nitride membrane provides the necessary enhancement of the electric field. Using this design, it was possible to stain cells with fluorescent YOYO-1 using 100 ms, 10 V pulses and transfect them with an enhanced green fluorescence protein-gene.

While all these transfection oriented designs were aimed at cells in solution, Lin *et al.* [112, 116, 117] created a microfluidic design aimed at the transfection of animal cells growing on a solid surface (Figure 2-4d). The chip consists of a glass wafer with a gold interdigitated electrode structure, which is sealed with a PDMS mold to form a cavity. Cells grow on the glass surface. The interdigitated electrode structure can be used to electroporate the surface-bound cells. In this way, it was possible to transfect Huh-7 cells, human embryonic kidney cells and HUVEC primary cells with GFP DNA. By adding an extra anode electrode above the interdigitated structure, negative DNA plasmids were directed to the cathodes by an electrophoretic potential [117] prior to electroporation, creating a local high concentration of plasmids near the cells at the cathodes. Improved cell transfection was demonstrated by the relatively high concentration of transfected cells near the cathodes as compared to experiments where no electrophoretic forces were used.

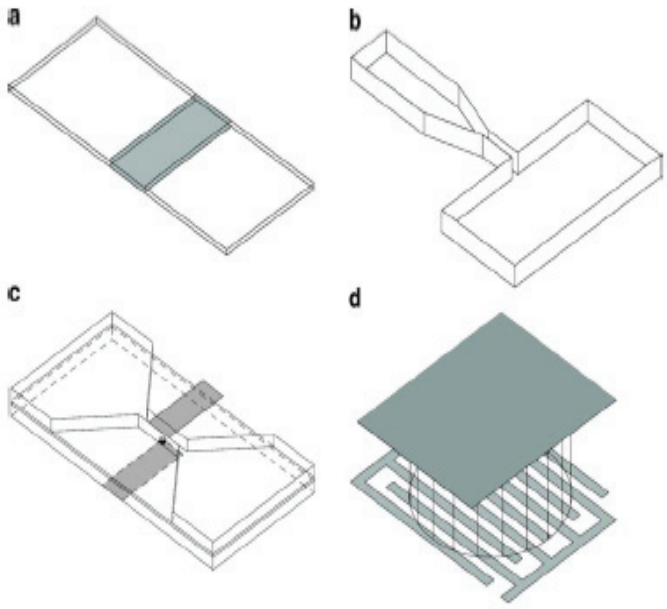

Figure 2-4: Schematic representation of various different transfection microfluidic electroporation devices. Not to scale. **a** Lin *et al.* [112]; **b** Khine *et al.* [113]; **c** Huang and Rubinsky [115]; **d** Lin *et al.*[112, 116, 117]

2.5.3 Pasteurization design

In the food processing industry, electroporation is used for the pasteurization of liquid foods in what is known as pulsed electric field (PEF) processing [75]. Pasteurization is used to render all spoilage bacteria present in the liquid foods inactive. Therefore, irreversible electroporation of all the cells need to take place. Because of this, and due to the fact that bacterial cells are in general significantly smaller than eukaryotic cells (1-5 μm), higher electric fields are needed in PEF than in electroporation for transfection and/or analysis purposes. Although microtechnology seems a less obvious choice for PEF applications because voluminous flows are processed, the use of microdevices avoids the risks involved with using high voltages and causes any heat generated to be rapidly dissipated. Because of this, microdevices should aid the exploration of other possibilities in the field of PEF.

The first PEF microreactor was presented by Fox *et al.* [118], which consisted of a 50 μm deep channel with a 10 μm deep, 30 μm long constriction to

focus the electric field between the two electrodes (Figure 2-5). It was possible to make a comparison with a pre-existing laboratory setup [91], with a typical constriction size of 1×2 mm, using artificial vesicles loaded with carboxyfluorescein as a model system. This comparison showed that, despite the difference in length scales, the two devices were comparable when 2 μs square wave pulses of 0 to 800 V were used. Vesicle electroporation in both devices was studied using the transmembrane potential and the total amount of energy added as criteria for comparison. The total amount of energy added did not turn out to be a good parameter for comparing the laboratory setup to the microtechnological setup, as this criterion is mainly determined by the device. However, the transmembrane potential was a good parameter to use when comparing vesicle breakdown, as it describes effects happening in the vesicle itself, which eliminates structural effects.

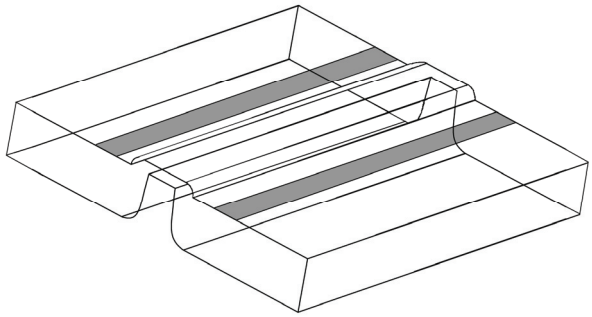

Figure 2-5: Schematic representation of the PEF microreactor [118]. Not to scale.

2.5.4 Technical comparison between the microfluidic devices

2.5.4.1 Electrode properties

The properties of the microdevices discussed above have been summarized in table 2-I. High electric field strengths are required for electroporation. Two different strategies are used to achieve this in the discussed microdevices: the electrodes can be positioned in close proximity, or the electric current can be focused into a small flow constriction. The first approach has been applied by several authors [106, 108, 110, 112]. However, depending on the pulse scheme and pulse duration, this will inevitably lead to electrode degradation due to electrolysis.

Table 2-I: Technical specifications of the different electroporation microdevices

Publication	Materials	Focusing by Constriction or electrode?	Typical size	Electrode material	Electrode distance	Mechanism of movement[1]	Flow-through/ static
[83]	n+polysilicon siliconnitiride	Constriction	2-10 μm	n+polysilicon Ag/AgCl	900 μm	PDF	Static
[105]	Silicon	Constriction	8-12 μm	Au wires, not integrated	Very large	EOF	Static
[100]	Soda-lime glass	No focusing	-	ND, not integrated	Very large	PDF & EOF	Flow-through
[101]	White crown glass	No focusing	-	ND	Very large	EOF	Flow-through
[106]	Silicon	Electrode	~16 μm	Au	5 μm	PDF & DEP	Flow-through
[108]	Glass	Electrode	5 μm	Cr	5 μm	DEP	Flow-through
[110]	Pyrex glass & SU-8	Electrode	130 μm	Au	30 μm	PDF	Flow-through
[112]	PMMA	Electrode	0.2 mm	Au	0.2 mm	PDF	Flow-through
[113]	PDMS	Constriction	4×3.1 μm	Ag/AgCl, not integrated	Very large	PDF	Static
[116]	Glass, PDMS	Electrode	100 μm	Au	100 μm	-	Static
[115]	Silicon. Silicon Nitride	Constriction	6 μm	Pt	N.D.	PDF	Flow-through
[118]	Glass	Constriction	30 μm	Pt	70 μm	PDF	Flow-through

PDF: pressure driven flow, *EOF*: electroosmotic flow, *DEP*: dielectrophoresis, *N.D.* Not determined

Electrolysis occurs when the potential difference is larger than the redox potential of the liquid and the pulse duration is longer than the time taken to charge the electrical double layer. Since the pulses applied in electroporation are usually higher than the redox potential, electrolysis will often take place. The close proximity of the electrodes will result in the contamination of the load with electrode material. Moreover, the local electric field will degrade as the electrodes are corroded. Nevertheless, this approach is suitable for analysis-oriented designs, where single cells must be electroporated in a controlled way with a limited number

of pulses. However, in designs where pulses must be applied continuously, such as those intended for transfection or pasteurization, this approach has some serious drawbacks. The stronger electric field strengths present at the electrode surface might result in the formation of gas due to the electrolysis of water. Gas bubbles should be avoided in the microdevices as the breakdown potential of gas is much lower than that of water, and so arcing can occur, which seriously damages the electrode. If the average electrical current is low, the rate of electrolysis is also low and the gas dissolves and is transported away. In many cases this is not sufficient.

The rate of electrolysis can be reduced by applying shorter pulses and thus reducing the current or by applying bipolar pulses instead of unipolar pulses, which makes the time averaged current zero. If bipolar pulses are applied, electrolytic reactions still occur, but are then partially reversed during the successive pulse. Electrolysis can also be reduced by increasing the resistance between the electrodes, as the total current will also be reduced.

The other approach, taken in several devices [83, 105, 113, 118], is more promising for designs where long intervals of pulses or continuous pulses are required. These designs make use of a constriction of the channel, which results in a high electrical resistance. The main potential drop in these devices is not in the vicinity of the electrode, which therefore prevents electrode degradation. Another option for decreasing the resistance would be to use low conductivity fluids. However, the composition of the fluid is restricted by biological constraints in many cases.

Although the design and properties of the electrodes are more important in high than in low current applications, it is crucial to have a good electrode structure. Various materials have been used so far, including different metals, polysilicon and Ag/AgCl electrodes. For impedance measurements where high accuracy is needed, Ag/AgCl electrodes offer the best choice, since there is no polarization at the electrode surface. Polysilicon, which has elusive electrode surface properties, is a less obvious choice as electrode material. Metal electrodes seem to be the best choice as electrodes for other applications, as the electrodes are easy to incorporate into the production process and the behaviour at the surface is well known, although complex. The electrodes used in the microdevices reported here are unprotected electrodes, except in one case [106], which makes them more

susceptible to degradation by electrolysis. As discussed above, electrolysis can result in corrosion of metal electrodes [119] and degradation is even observed in the case of noble metal electrodes, as large fragments can break from the electrode at high electric field strengths, as reported by Lee [106] and Fox [118]. Lee [106] proposed a solution to this where a very thin Teflon layer was applied onto the electrodes. The electrode was therefore separated from the fluid. This technique has also been used in large scale PEF equipment [120-123]. It would be logical to think that such an approach should be copied in future microtechnological structures, for example by applying dedicated coatings [124] . However, care is required here, as the isolating layer will alter the form of the pulse form. It will act as a high pass filter, blocking low frequencies and the DC component and therefore complicating the analysis and interpretation of the results.

2.5.4.2 Cell handling

A clear distinction can be made between static devices and flow-through devices as summarized in table 2-II. Static designs are most commonly used for single cell measurements, as they facilitate sample introduction, treatment and analysis. To analyze single cell content, it is essential to restrict the released cell content to a small volume in order to prevent dilution beyond the detection limit. Secondly, the separation of cellular debris and cell content is required for many analysis methods. The biological cell is retained at a defined place, for example via suction at a small channel opening, and the extracted cell content can then be separated into a very narrowly defined volume. To study single cell properties like impedance, the cell should be directed towards one place and be immobilized there.

Flow-through devices are generally used for analysis devices where many cells are electroporated, as well as transfection devices, as it is important to collect a sample of the transfected cells for replication. This is even more important for a PEF device, as larger quantities of cells need to be treated in a production environment. To treat large quantities, a commercial PEF microreactor might be scaled-up by mass parallelization instead of scaling-up by size.

Table 2-II: Electroporation and cell properties of the different electroporation microdevices

Publication	Purpose	Potential difference used	Electric field strength ($kVcm^{-1}$)	Pulse time	Tested cells	Cell size	Measurement method
[83]	Analysis	0-60 V	N.D.	2 μs-100 ms	Human prostate adenocarcinoma cells, rat hepatocytes	20 μm	YOYO-1
[105]	Analysis	100 V	N.D.	Continuous DC	Human promyelocytic leukemic cells (HL60)	10 μm	PI/FLICA
[100]	Analysis	1400 V	N.D.	1 s	Erythrocytes	10 μm	CE
[101]	Analysis	1125 V	0.6	Continuous DC & block pulses	Jurkat	N.D.	OG, CF, Calcein AM
[106]	Analysis	20 V	~ 2	100 μs	*S. cerevisiae, E.coli,* plant protoplasts	2-35 μm	Cell counting
[108]	Analysis	20 V	N.D.	± 20 s AC	*S. cerevisiae*	5 μm	Impedance
[110]	Analysis	6-8.5 V	~ 1-2	5-10 kHz AC	HT-60 cells	10 μm	AO/PI
[112]	Transfection	10 V	0.5	5 ms	*Huh-7* (human hepatocellular carcinoma cells	N.D.	GFP/β-galactosidase plasmids
[113]	Transfection	1 V	N.D.	6.5 ms	HELA cells	10 μm	Calcein AM, tryphan blue
[116]	Transfection	100 V	0.1-0.4	N.D.	Several endothelial cells	±10 μm	GFP
[115]	Transfection	10 V	~ 2.5	100 ms	Human prostate adenocarcinoma cells (ND-1)	N.D.	YOYO-1 Enhanced GFP plasmids
[118]	Inactivation	800 V	100	2 μs	Artificial vesicles	200 nm	CF

PI: Propidium iodide, *CE*: capillary electrophoresis, *AO*: acridine orange, *GFP*: green fluorescent protein, *CF*: carboxyfluorescein, *OG*: Oregon green, *N.D.* Not determined

2.5.4.3 Detection

While some researchers have just begun to look into the development of microdevices that perform both single cell electroporation and subsequent analysis of the cell content [100, 101], most of the electroporation microdevice research performed so far has focused on analyzing and understanding the electroporation process itself. Membrane integrity analysis is often performed optically, by measuring the uptake or release of fluorescent markers such as YOYO-1, PI, acridine orange, FLICA, calcein AM or CF. Measuring impedance is another technique that is often used to follow electroporation; this has the advantages of a fast, online response and a noninvasive nature. Transfection analysis has been performed with GFP genes and β-galactosidase genes. Once again, the GFP genes were used because they make optical detection easier.

2.5.4.4 Cell types

Almost all of the devices reported have been tested with animal cells, or at least with cells that are relatively large in size, such as yeast and plant cells. Because the transmembrane potential over a cellular membrane is linearly related to the size of the cell, relatively low electric field strengths are sufficient for the electroporation of large cells, which makes testing easier. Secondly, the large cell size makes it easy to visually inspect the effects of the electric fields on the cells. This approach has been applied in most microdevices, and fluorescent markers have been used to study the cellular response microscopically in situ. An additional advantage of using large cells is that they are in the same size regime as the microtechnological devices. Hence, it is possible to trap them at certain locations in the microdevice, which is preferred for single cell measurements. To perform single cell measurements on smaller cells, for example bacterial cells, smaller structures with sizes on the order of 1 μm or even smaller are required. It is much more challenging to make microfluidic structures with these sizes, and so the development of devices aimed at bacterial electroporation has been retarded. Secondly, observing with a microscope becomes less feasible as the dimensions of a cell become comparable to wavelengths associated with light. Hence, more research is needed to improve single cell bacterial electroporation measurements.

2.5.5 Future trends

2.5.5.1 Materials

Microchips are expensive to product because of the costs of the substrate material and the many steps involved in the production process, such as photolithographic, etching and cleaning [125]. This is not an issue for research prototypes as well as for devices which can be cleaned and then reused. However, such costs are a major issue for disposable devices intended for routine analysis. The need to reduce the cost has driven the general trend towards the production of polymeric microfluidic devices [126]. Polymers are cheap compared to glass or silicon substrate and applicable for mass production technologies such as injection molding, hot embossing or the phase separation micromolding process. Since many different types of polymers are available, which differ in their mechanical, optical and temperature properties as well as in resistance chemical attack, polymer based devices can be tailored to any application. A similar trend can be expected for microfluidic electroporation devices, as some devices are already polymer based [112, 113] or partially polymer based [110]. One point to consider is the fabrication of the electrodes, which sometimes requires different techniques than glass based microdevices. The deposition can often only be done with a shadow mask, which limits the dimensional accuracy [125].

2.5.5.2 Integration of detection

As well as non-silicon chips, we also expect the progressive integration of electroporation with subsequent measurements in future electroporation microdevices. Most existing analysis designs are able to monitor phenomena like fluorescence uptake of impedance changes at the area of electroporation. Gao [100] and McClain [101] showed that it was possible to combine electroporation with intracellular content analysis based on CE. However, the electroporation process itself in these devices is relatively rough, and more sophisticated devices with full control over the electroporation process as well as cell debris separation and subsequent intracellular cell content analysis have not been reported yet. Therefore, it is expected that integrated devices where combinations of electroporation,

separation and analysis occur will emerge, such as devices with integrated chromatography, electrophoresis or isoelectric focusing steps for separation and mass spectroscopy, electrochemical and fluorescent methods for analysis. Secondly, the present designs usually require multiple manual steps in order to insert the cells, electroporation them and measure the effects. Until now, no devices have been reported where all these steps have been integrated in an automated way, preferably with multiple samples in parallel, which could greatly enhance the application of microtechnological analysis.

2.5.5.3 Intelligent handling

If the analysis and operation are integrated onto a microfluidic device, it becomes possible to manipulate the cell or fluid flow based on a previously measured signal. The electroporation process can be triggered by the detection of a single or sufficient number of cells between the electrodes. This can be combined with concentration methods that are used to reduce the volume, such as specially designed flow structures [127], electric field methods like dielectrophoresis [128] or electrophoresis, which has been demonstrated by transfecting surface bound cells in a local high concentration of plasmids [117]. It is also possible to select suitable cells prior to electroporation or to use a fluorescent or electrical response to separate the cells after electroporation.

2.5.5.4 Beyond simple pulses

The use of microtechnology allows the voltage required to reach sufficiently high electric field strength to be lowered. This makes it easier to use more advanced pulse forms then those currently provided by commercial high voltage pulsers. Until now, mainly exponential decay and square wave pulses have been used with pulse lengths the micro- and milliseconds. However, recent publications [129] show that more advanced pulse forms can produce very different effects. The group of Schoenbach [89, 130-133]demonstrated that high frequency pulses with pulse durations in the order of 10 to 100 ns can cause intracellular damage but they allow the extracellular membrane to remain intact. This opens up new possibilities in the field of apoptosis induction [134], gene delivery to the nucleus or altered cell

functions, depending on the electrical pulse duration. Microtechnology offers the ability to study these effects.

2.6 Conclusions

Biological transport barriers are based on lipid bilayer membranes. One of the major consequences of electroporation phenomena is the increased membrane permeability which allows molecular transport to occur. Electric field pulses that raise the transmembrane potential to 0.2 to 1 V are hypothesized to create primary aqueous pathways (hydrophilic pores) with minimum size of ~1 nm. A dynamic interaction involving both external membrane charging and internal membrane discharging governs a rapidly evolving pore population, which alternately controls electrical behavior and molecular transport. Secondary phenomena can arise from chemical imbalances and from cell stimulation. Overall, while electroporation is commonly used for loading cells with small to large molecules the mechanism which leads to the permeabilization of the living cell membrane in an electrical field is not fully understood. Developing a fundamental understanding on the biophysics of cell membrane permeabilization in an electrical field is of central importance for the efficient use of electroporation. Microdevices as a platform to perform electroporation could (partially) fulfill these necessities.

In recent years, several publications on microfluidic devices have focused on the process of electroporation. The microfluidic electroporation devices are designed for cell analysis, transfection or pasteurization. This range of applications has resulted in a variety in designs: microchips in which cells move through a treatment zone, microchips in which cells are trapped at a specific location, and devices in which the cells are surface-bound. Relatively low voltages are required in such systems due to the close electrode spacing employed, which is even enhanced further in some cases by applying a constriction between the electrodes. This approach reduces electrolytic damage to the electrodes. Detection is usually performed by fluorescent visualization or via noninvasive impedance measurements. Most of the devices reported so far have focused on just the electroporation process itself, but integration with separation and detection processes is expected to add further value to the concept of an integrated electroporation microfluidic chip in the near future. The field of single cell content

analysis where the cell content is released by electroporation is particularly promising, as it is difficult to accomplish in larger structures. Polymeric chips are expected for single-use electroporation devices. Furthermore, microfluidic devices can facilitate research into intracellular electroporation by applying advanced pulse schemes.

2.7 References

[1] J. C. Weaver and Y. A. Chizmadzhev - *Theory of electroporation: a review;* Bioelectrochemistry and Bioenergetics., **41** (1996), pp 135-160.

[2] H. Isambert - *Understanding the electroporation of cells and artificial bilayer membranes;* Physical Review Letters, **80 (15)**, (1998), pp 3404-3407.

[3] D. C. Chang, B. M. Chassy, J. A. Saunders and -*Guide to electroporation and electrofusion ;* San Diego: Academic Press. (1992).

[4] E. Neumann, A. E. Sowers and C. A. Jordan, -*Electroporation and Electrofusion in Cell Biology;* New York: Plenum Press (1989).

[5] J. C. Weaver - *Electroporation of cells and tissues;* IEEE Transactions on Plasma Science, **28 (1)**, (2000), pp 24-33.

[6] R. Stämpfli - *Reversible Electrical Breakdown of the Excitable Membrane of a Ranvier Node;* An. Acad. Brasil. Ciens., **30** (1958), pp 57-63.

[7] W. A. Hamilton and A. J. H. Sale - *Effects of high electric fields on microorganisms II Mechanism of action of the lethal effect. ;* Biochimica et biophysica acta, **148** (1967), pp 789-800.

[8] A. J. H. Sale and A. Hamilton - *Effects of High Electric Fields on Microorganisms: I. Killing of Bacteria and Yeasts;* Biochimica et Biophysica Acta, **148** (1967), pp 781-788.

[9] A. J. H. Sale and W. A. Hamilton - *Effects of high electric fields on micro-organisms III Lysis of erythrocytes and protoplasts;* Biochimica et biophysica acta, **163** (1968), pp 37-43.

[10] J. M. Crowley - *Electrical breakdown of biomolecular lipid membranes as an electromechanical instability;* Biophysical Journal, **13** (1973), pp 711-724.

[11] E. Neumann and K. Rosenheck - *Permeability changes induced by electric impulses in vesicular membranes;* Journal of Membrane Biology, **10** (1972), pp 279-290.

[12] U. Zimmermann, J. Vienken and G. Pilwat - *Dielectric breakdown of cell membranes;* Biophysical Journal, **14 (11)**, (1974), pp 881-899.

[13] K. J. Kinosita and T. Y. Tsong - *Hemolysis of human erythrocytes by a transient electric field;* Proc. Natl. Acad. Sci. USA, **74 (5)**, (1977), pp 1923-1927.

[14] P. F. Baker and D. E. Knight - *Calcium-dependent exocytosis in bovine adrenal medullary cells with leaky plasma membranes;* Nature, **276** (1978), pp 620-622.

[15] B. Gauger and F. W. Bentrup - *A Study of Dielectric Membrane Breakdown in the Fucus Egg;* Journal of Membrane Biology, **48 (3)**, (1979), pp 249-264.

[16] R. Benz, F. Beckers and U. Zimmermann - *Reversible electrical breakdown of lipid bilayer membranes: a charge-pulse relaxation study;* Journal of Membrane Biology, **48 (2)**, (1979), pp 181-204.

[17] S. Y. Ho and G. S. Mittal - *Electroporation of cell membranes: A review;* Critical Reviews in Biotechnology, **16 (4)**, (1996), pp 349-362.

[18] U. Zimmermann, F. Riemann and G. Pilwat - *Enzyme Loading of Electrically Homogeneous Human Red Blood Cell Ghosts Prepared by Dielectric Breakdown;* Biochimica et Biophysica Acta, **436** (1976), pp 460-474.

[19] K. J. Kinosita and T. Y. Tsong - *Formation and Resealing of Pores of Controlled Sizes in Human Erythrocyte Membrane;* Nature, **268** (1977), pp 438-441.

[20] K. J. Kinosita and T. Y. Tsong - *Survival of Sucrose-loaded Erythrocytes in Circulation;* Nature, **272** (1978), pp 258-260.

[21] J. Teissie and T. Y. Tsong - *Electric Field Induced Transient Pores in Phospholipid Bilayer Vesicles;* Biochemistry, **20** (1981), pp 1548-1554.

[22] U. Zimmermann, P. Scheurich, G. Pilwat and R. Benz - *Cells with Manipulated Functions: New Perspectives for Cell Biology, Medicine and Technology;* Angew. Chem. Int. Ed. Eng., **20** (1981), pp 325-344.

[23] V. L. Sukhorukov, H. Mussauer and U. Zimmermann - *The effect of electrical deformation forces on the electropermeabilization of erythrocyte membranes in low- and high-conductivity media;* Journal of Membrane Biology, **163 (3)**, (1998), pp 235-245.

[24] D. Auer, G. Brandner and W. Bodemer - *Dielectric Breakdown of the Red Blood Cell Membrane and Uptake of SV 40 DNA and Mammalian Cell RNA;* Naturwiss, **63** (1976), pp 391.

[25] E. Neumann, M. Schaefer-Ridder, Y. Wang and P. H. Hofschneider - *Gene transfer into mouse lyoma cells by electroporation in high electric fields;* Journal of EMBO, **1** (1982), pp 841-845.

[26] T. K. Wong and E. Neumann - *Electric field mediated gene transfer;* Biochemical and Biophysical Research Communications, **107** (1982), pp 584-587.

[27] B. Rubinsky, "Micro-electroporation in celllomics" -*Lab on a chips for Cellomics;*Andersson H. and van den Berg A., Eds.,Kluwer academic publishers (2004).

[28] G. Bryant and J. Wolfe - *Electromechanical stresses produced in the plasma membranes of suspended cells by applied electric fields;* Journal of Membrane Biology, **96** (1987), pp 129-139.

[29] C. Wilhelm, M. Winterhalter, U. Zimmermann and R. Benz - *Kinetics of Pore-Size during Irreversible Electrical Breakdown of Lipid Bilayer-Membranes;* Biophysical Journal, **64 (1)**, (1993), pp 121-128.

[30] E. Neumann and E. Boldt, "Membrane electroporation:The dye method to determine the cell membrane conductivity. " -*In: Horizons in Membrane Biotechnology;*eds. C. Nicolau, D. Chapman, Wiley-Liss (1990).

[31] L. V. Chernomordik, "Electropores in lipids bilayers and cell membranes" - *in Guide to Electroporation and Electrofusion;*D.C. Chang, Editor.Academic Press, Inc.San Diego, CA. (1992).

[32] T. Y. Tsong, "Time sequence of molecular events in electroporation" -*in Guide to Electroporation and Electrofusion;*D.C. Chang, Editor.Academic Press, Inc.San Diego, CA. (1992).

[33] J. C. Weaver and K. T. Powell, "Theory of electroporation" -*in Electroporation and Electrofusion in Cell Biology;*E. Neumann, Editor. Plenum Press: New York, NY (1989).

[34] J. C. Weaver and A. Barnett, "Progress toward a theoretical model for electroporation mechanism: membrane electrical behavior and molecular transport" -*in Guide to Electroporation and Electrofusion;*D.C. Chang, Editor. 1992, Academic Press, Inc.San Diego, CA. (1992).

[35] L. M. Mir - *Therapeutic perspectives of in vivo cell electropermeabilization;* Bioelectrochemistry, **53 (1)**, (2001), pp 1-10.

[36] D. C. Chang and T. S. Reese - *Changes in Membrane-Structure Induced by Electroporation as Revealed by Rapid-Freezing Electron-Microscopy;* Biophysical Journal, **58 (1)**, (1990), pp 1-12.

[37] R. W. Glaser, S. L. Leikin, L. V. Chernomordik, V. F. Pastushenko and A. I. Sokirko - *Reversible Electrical Breakdown of Lipid Bilayers - Formation and Evolution of Pores;* Biochimica Et Biophysica Acta, **940 (2)**, (1988), pp 275-287.

[38] M. Hibino, M. Shigemori, H. Itoh, K. Nagayama and K. Kinosita - *Membrane Conductance of an Electroporated Cell Analyzed by Submicrosecond Imaging of Transmembrane Potential;* Biophysical Journal, **59 (1)**, (1991), pp 209-220.

[39] T. Y. Tsong - *Electroporation of Cell-Membranes;* Biophysical Journal, **60 (2)**, (1991), pp 297-306.

[40] J. C. Weaver - *Electroporation - A General Phenomenon for Manipulating Cells and Tissues;* Journal of Cellular Biochemistry, **51 (4)**, (1993), pp 426-435.

[41] J. C. Weaver and Y. A. Chizmadzhev, "Electroporation" -*Handbook of Biological Effects of Electromagnetic Fields;*In C. Polk and E. Postow, editors, CRC Press, Boca Raton, 2nd edition (1996).

[42] U. Zimmermann, -*The Effects of High Intensity Electric Field Pulses on Eukaryotic Cell Membranes: Fundamentals and Applications;*CRC Press, Boca Raton (1996).

[43] T. Clementz, A. Christiansson and A. Wieslander, "Effect of electrical potential on membrane organization and fuction" -*In: Advances in Membrane Fluidity Volume 3: Physiological Regualtion of Membrane Fluidity;* Aloia R.C., Curtain C.C. and Gordon L.M., Eds., Alan R.Liss, Inc., New York. (1988).

[44] D. Gross - *Electromobile surface charge alters membrane potential changes induced by applied electric fields;* Biophysical Journal, **54** (1988), pp 879-884.

[45] T. C. Tomov and I. C. Tsoneva - *Changes in the surface charge of cells induced by electrical pulses.;* Bioelectrochemistry and Bioenergetics, **22** (1989), pp 127-133.

[46] E. Neumann, "The relaxation hysterisis of membrane electroporation" -*Electroporation and electrofusion in Cell Biology;*Neumann E., Sowers A. E. and Jordan C.A., Eds., Plenum Press, New York (1989).

[47] E. Neumann - *Membrane Electroporation and Direct Gene-Transfer;* Bioelectrochemistry and Bioenergetics, **28 (1-2)**, (1992), pp 247-267.

[48] J. Teissie and M. P. Rols - *An Experimental Evaluation of the Critical Potential Difference Inducing Cell-Membrane Electropermeabilization;* Biophysical Journal, **65 (1)**, (1993), pp 409-413.

[49] J. C. Weaver, "Electroporation theory: Concepts and mechanisms" -*Methods in Molecular Biology;*Humana Press, Inc., Totowa, NJ (1995).

[50] M. Bier, S. M. Hammer, D. J. Canaday and R. C. Lee - *Kinetics of sealing for transient electropores in isolated mammalian skeletal muscle cells;* Bioelectromagnetics, **20 (3)**, (1999), pp 194-201.

[51] B. Gabriel and J. Teissie - *Direct observation in the millisecond time range of fluorescent molecule asymmetrical interaction with the electropermeabilized cell membrane;* Biophysical Journal, **73 (5)**, (1997), pp 2630-2637.

[52] R. C. Lee, D. J. Zhang and J. Hannig - *Biophysical injury mechanisms in electrical shock trauma;* Annual Review of Biomedical Engineering, **2** (2000), pp 477-509.

[53] N. Asgharian and Z. A. Schelly - *Electric field-induced transient birefringence and light scattering of synthetic liposomes;* Biochimica Et Biophysica Acta-Biomembranes, **1418 (2)**, (1999), pp 295-306.

[54] B. Gabriel and J. Teissie - *Time courses of mammalian cell electropermeabilization observed by millisecond imaging of membrane property changes during the pulse;* Biophysical Journal, **76 (4)**, (1999), pp 2158-2165.

[55] M. Hibino, H. Itoh and K. Kinosita - *Time Courses of Cell Electroporation as Revealed by Submicrosecond Imaging of Transmembrane Potential;* Biophysical Journal, **64 (6)**, (1993), pp 1789-1800.

[56] S. Kakorin and E. Neumann - *Kinetics of the electroporative deformation of lipid vesicles and biological cells in an electric field;* Berichte Der Bunsen-Gesellschaft-Physical Chemistry Chemical Physics, **102 (4)**, (1998), pp 670-675.

[57] K. J. Kinosita and T. Y. Tsong - *Voltage-induced conductance in human erythrocyte membranes;* Biochimica et Biophysica Acta, **55** (1979), pp 479– 497.

[58] H. T. Tien and A. Ottova - *The bilayer lipid membrane (BLM) under electrical fields;* IEEE Transactions on Dielectrics and Electrical Insulation, **10 (5)**, (2003), pp 717-727.

[59] E. Tekle, R. D. Astumian and P. B. Chock - *Selective and Asymmetric Molecular-Transport across Electroporated Cell-Membranes;* Proceedings of the National Academy of Sciences of the United States of America, **91 (24)**, (1994), pp 11512-11516.

[60] D. S. Dimitrov and A. E. Sowers - *Membrane Electroporation - Fast Molecular-Exchange by Electroosmosis;* Biochimica Et Biophysica Acta, **1022 (3)**, (1990), pp 381-392.

[61] V. A. Klenchin, S. I. Sukharev, S. M. Serov, L. V. Chernomordik and Y. A. Chizmadzhev - *Electrically Induced DNA Uptake by Cells Is a Fast Process Involving DNA Electrophoresis;* Biophysical Journal, **60 (4)**, (1991), pp 804-811.

[62] C. Chen, S. W. Smye, M. P. Robinson and J. A. Evans - *Membrane electroporation theories: a review;* Medical and Biological Engineering & Computing, **44** (2006), pp 5-14.

[63] J. C. Weaver - *Electroporation of biological membranes from multicellular to nano scales;* IEEE Transactions on Dielectrics and Electrical Insulation, **10 (5)**, (2003), pp 754-768.

[64] L. V. Chernomordik, A. V. Sokolov and V. G. Budker - *Electrostimulated Uptake of DNA by Liposomes;* Biochimica Et Biophysica Acta, **1024 (1)**, (1990), pp 179-183.

[65] M. P. Rols, P. Femenia and J. Teissie - *Long-Lived Macropinocytosis Takes Place in Electropermeabilized Mammalian-Cells;* Biochemical and Biophysical Research Communications, **208 (1)**, (1995), pp 26-35.

[66] S. Satkauskas, M. F. Bureau, A. Mahfoudi and L. M. Mir - *Slow accumulation of plasmid in muscle cells: Supporting evidence for a mechanism of DNA uptake by receptor-mediated endocytosis;* Molecular Therapy, **4 (4)**, (2001), pp 317-323.

[67] M. Tarek - *Membrane electroporation: A molecular dynamics simulation;* Biophysical Journal, **88 (6)**, (2005), pp 4045-4053.

[68] J. Teissie, M. Golzio and M. P. Rols - *Mechanisms of cell membrane electropermeabilization: A minireview of our present (lack of ?) knowledge;* Biochimica Et Biophysica Acta-General Subjects, **1724 (3)**, (2005), pp 270-280.

[69] E. Ferret, C. Evrard, A. Foucal and P. Gervais - *Volume changes of isolated human K562 leukemia cells induced by electric field pulses;* Biotechnology and Bioengineering, **67 (5)**, (2000), pp 520-528.

[70] G. L. Prasanna and T. Panda - *Electroporation: Basic principles, practical considerations and applications in molecular biology;* Bioprocess Engineering, **16 (5)**, (1997), pp 261-264.

[71] S. Y. Ho, G. S. Mittal and J. D. Cross - *Effects of high field electric pulses on the activity of selected enzymes;* Journal of Food Engineering, **31 (1)**, (1997), pp 69-84.

[72] E. H. Serpersu and T. Y. Tsong - *Activation of electrogenic Rb+ transport of (Na,K)-ATPase by an electric field;* Journal of Biological Chemistry, **259 (11)**, (1984), pp 7155-7162.

[73] E. H. Serpersu, T. Y. Tsong and K. Kinosita - *Reversible and irreversible modification of erythrocyte membrane permeability by electric field;* Biochimica et biophysica acta, **812 (3)**, (1985), pp 779-785.

[74] T. Y. Tsong and K. Kinosita - *Use of voltage pulses for the pore opening and drug loading and the subsequent resealing of red blood cells.;* Bibliotheca haematologica (Basel), **51** (1985), pp 108-114.

[75] D. Knorr, A. Angersbach, M. N. Eshtiaghi, V. Heinz and D. U. Lee - *Processing concepts based on high intensity electric field pulses;* Trends in Food Science & Technology, **12 (3-4)**, (2001), pp 129-135.

[76] P. C. Wouters, N. Dutreux, J. P. P. M. Smelt and H. L. M. Lelieveld - *Effects of pulsed electric fields on inactivation kinetics of Listeria innocua;* Applied and Environmental Microbiology, **65 (12)**, (1999), pp 5364-5371.

[77] G. V. Barbosa-Canovas, U. R. Pothakamury, M. M. Gongora-Nieto and B. G. Swanson, -*Preservation of foods with pulsed electric fields. Food science and technology;*San Diego: Academic Press. 1. (1999).

[78] H. C. Mastwijk and P. V. Bartels - *Pulsed electric field (PEF) processing in the fruit juice and dairy industries;* The international review of food science and technology,, (2004), pp 106-108.

[79] S. Min, Z. T. Jin, S. K. Min, H. Yeom and Q. H. Zhang - *Commercial-scale pulsed electric field processing of orange juice;* Journal of Food Science, **68 (4)**, (2003), pp 1265-1271.

[80] H. W. Yeom, G. A. Evrendilek, Z. T. Jin and Q. H. Zhang - *Processing of yogurt-based products with pulsed electric fields: Microbial, sensory and physical evaluations;* Journal of Food Processing and Preservation, **28 (3)**, (2004), pp 161-178.

[81] K. E. Belghiti and E. Vorobiev - *Mass transfer of sugar from beets enhanced by pulsed electric field;* Food and Bioproducts Processing, **82 (C3)**, (2004), pp 226-230.

[82] M. N. Eshtiaghi and D. Knorr - *High electric field pulse pretreatment: potential for sugar beet processing;* Journal of Food Engineering, **52 (3)**, (2002), pp 265-272.

[83] Y. Huang and B. Rubinsky - *Micro-electroporation: improving the efficiency and understanding of electrical permeabilization of cells.;* Biomedical microdevices, **2 (2)**, (1999), pp 145-150.

[84] J. A. Lundqvist, F. Sahlin, M. A. Aberg, A. Stromberg, P. S. Eriksson and O. Orwar, *-Altering the biochemical state of individual cultured cells and organelles with ultramicroelectrodes.;* Proceedings of the national academy of sciences USA, **95**, (1998), pp 10356-10360.

[85] K. Nolkrantz, C. Farre, A. Brederlau, R. I. D. Karlsson, C. Brennan, P. S. Eriksson, S. G. Weber, M. Sandberg and O. Orwar - *Electroporation of single cells and tissues with an electrolyte-filled capillary;* Analytical Chemistry, **73 (18)**, (2001), pp 4469-4477.

[86] K. Haas, W. C. Sin, A. Javaherian, Z. Li and H. T. Cline - *Single-cell electroporation for gene transfer in vivo;* Neuron, **29 (3)**, (2001), pp 583-591.

[87] J. L. Rae and R. A. Levis - *Single-cell electroporation;* Pflugers Archiv-European Journal of Physiology, **443 (4)**, (2002), pp 664-670.

[88] J. Olofsson, K. Nolkrantz, F. Ryttsen, B. A. Lambie, S. G. Weber and O. Orwar - *Single-cell electroporation;* Current Opinion in Biotechnology, **14 (1)**, (2003), pp 29-34.

[89] K. H. Schoenbach, S. J. Beebe and E. S. Buescher - *Intracellular effect of ultrashort electrical pulses;* Bioelectromagnetics, **22 (6)**, (2001), pp 440-448.

[90] H. L. M. Lelieveld - *A food industry's view;* in Novel food processing technologies, (2005), pp 145-156.

[91] I. E. Pol, H. C. Mastwijk, P. V. Bartels and E. J. Smid - *Pulsed-electric field treatment enhances the bactericidal action of nisin against Bacillus cereus;* Applied and Environmental Microbiology, **66 (1)**, (2000), pp 428-430.

[92] F. Ryttsen, C. Farre, C. Brennan, S. G. Weber, K. Nolkrantz, K. Jardemark, D. T. Chiu and O. Orwar - *Characterization of single-cell electroporation by using patch-clamp and fluorescence microscopy;* Biophysical Journal, **79 (4)**, (2000), pp 1993-2001.

[93] J. L. Zabzdyr and S. J. Lillard - *New approaches to single-cell analysis by capillary electrophoresis;* Trac-Trends in Analytical Chemistry, **20 (9)**, (2001), pp 467-476.

[94] J. A. Jankowski, S. Tracht and J. V. Sweedler - *Assaying Single Cells with Capillary Electrophoresis;* Trac-Trends in Analytical Chemistry, **14 (4)**, (1995), pp 170-176.

[95] E. X. Vrouwe, R. Luttge and A. van den Berg - *Direct measurement of lithium in whole blood using microchip capillary electrophoresis with integrated conductivity detection;* Electrophoresis, **25 (10-11)**, (2004), pp 1660-1667.

[96] E. S. Yeung - *Study of single cells by using capillary electrophoresis and native fluorescence detection;* Journal of Chromatography A, **830 (2)**, (1999), pp 243-262.

[97] E. Verpoorte - *Microfluidic chips for clinical and forensic analysis;* Electrophoresis, **23 (5)**, (2002), pp 677-712.

[98] N. R. Munce, J. Z. Li, P. R. Herman and L. Lilge - *Microfabricated system for parallel single-cell capillary electrophoresis;* Analytical Chemistry, **76 (17)**, (2004), pp 4983-4989.

[99] A. R. Wheeler, K. Morishima, D. W. Arnold, A. B. Rossi and R. N. Zare, Proceedings of micro-TAS, (2000), pp 623-626.

[100] J. Gao, X. F. Yin and Z. L. Fang - *Integration of single cell injection, cell lysis, separation and detection of intracellular constituents on a microfluidic chip;* Lab on a Chip, **4 (1)**, (2004), pp 47-52.

[101] M. A. McClain, C. T. Culbertson, S. C. Jacobson, N. L. Allbritton, C. E. Sims and J. M. Ramsey - *Microfluidic devices for the high-throughput chemical analysis of cells;* Analytical Chemistry, **75 (21)**, (2003), pp 5646-5655.

[102] R. Davalos, Y. Huang and B. Rubinsky - *Electroporation: Bio-electrochemical mass transfer at the nano scale;* Microscale Thermophysical Engineering, **4 (3)**, (2000), pp 147-159.

[103] Y. Huang and B. Rubinsky - *Microfabricated electroporation chip for single cell membrane permeabilization;* Sensors and Actuators A-Physical, **89 (3)**, (2001), pp 242-249.

[104] Y. Huang, N. S. Sekhon, J. Borninski, N. Chen and B. Rubinsky - *Instantaneous, quantitative single-cell viability assessment by electrical evaluation of cell membrane integrity with microfabricated devices;* Sensors and Actuators A-Physical, **105 (1)**, (2003), pp 31-39.

[105] A. Valero, F. Merino, F. Wolbers, R. Luttge, I. Vermes, H. Andersson and A. van den Berg - *Apoptotic cell death dynamics of HL60 cells studied using a microfluidic cell trap device;* Lab on a Chip, **5 (1)**, (2005), pp 49-55.

[106] S. W. Lee and Y. C. Tai - *A micro cell lysis device;* Sensors and Actuators A-Physical, **73 (1-2)**, (1999), pp 74-79.

[107] J. Suehiro, R. Yatsunami, R. Hamada and M. Hara - *Quantitative estimation of biological cell concentration suspended in aqueous medium by using dielectrophoretic impedance measurement method;* Journal of Physics D-Applied Physics, **32 (21)**, (1999), pp 2814-2820.

[108] J. Suehiro, M. Shutou, T. Hatano and M. Hara - *High sensitive detection of biological cells using dielectrophoretic impedance measurement method combined with electropermeabilization;* Sensors and Actuators B-Chemical, **96 (1-2)**, (2003), pp 144-151.

[109] J. Suehiro, T. Hatano, M. Shutou and M. Hara - *Improvement of electric pulse shape for electropermeabilization-assisted dielectrophoretic impedance measurement for high sensitive bacteria detection;* Sensors and Actuators B-Chemical, **109 (2)**, (2005), pp 209-215.

[110] H. Lu, M. A. Schmidt and K. F. Jensen - *A microfluidic electroporation device for cell lysis;* Lab on a Chip, **5 (1)**, (2005), pp 23-29.

[111] J. W. Loomis-Husselbee, P. J. Cullen, R. F. Irvine and A. P. Dawson - *Electroporation can cause artifacts due to solubilization of cations from the electrode plates;* Biochemical Journal, **277** (1991), pp 883-885.

[112] Y. C. Lin, C. M. Jen, M. Y. Huang, C. Y. Wu and X. Z. Lin - *Electroporation microchips for continuous gene transfection;* Sensors and Actuators B-Chemical, **79 (2-3)**, (2001), pp 137-143.

[113] M. Khine, A. Lau, C. Ionescu-Zanetti, J. Seo and L. P. Lee - *A single cell electroporation chip;* Lab on a Chip, **5 (1)**, (2005), pp 38-43.

[114] J. Seo, C. Ionescu-Zanetti, J. Diamond, R. Lal and L. P. Lee - *Integrated multiple patch-clamp array chip via lateral cell trapping junctions;* Applied Physics Letters, **84 (11)**, (2004), pp 1973-1975.

[115] Y. Huang and B. Rubinsky - *Flow-through micro-electroporation chip for high efficiency single-cell genetic manipulation;* Sensors and Actuators A-Physical, **104 (3)**, (2003), pp 205-212.

[116] Y. C. Lin, M. Li, C. S. Fan and L. W. Wu - *A microchip for electroporation of primary endothelial cells;* Sensors and Actuators A-Physical, **108 (1-3)**, (2003), pp 12-19.

[117] Y. C. Lin, M. Li and C. C. Wu - *Simulation and experimental demonstration of the electric field assisted electroporation microchip for in vitro gene delivery enhancement;* Lab on a Chip, **4 (2)**, (2004), pp 104-108.

[118] M. Fox, E. Esveld, R. Luttge and R. Boom - *A new pulsed electric field microreactor: comparison between the laboratory and microtechnology scale;* Lab on a Chip, **5 (9)**, (2005), pp 943-948.

[119] B. Roodenburg, J. Morren, H. E. Berg and S.W.H. de Haan - *Metal release in a stainless steel Pulsed Electric Field (PEF) system: Part I. Effect of different pulse shapes; theory and experimental method;* Innovative Food Science & Emerging Technologies, **6 (3)**, (2005), pp 327-336.

[120] J. Dunn and J. S. Pearlman, -*High pulsed voltage systems for extending the shelf life of pumpable food products.;*United States (1987).

[121] N. M. Efremov, B. Y. Adamiak, V. I. Blochin, S. J. Dadashev, K. I. Dmitriev, V. N. Semjonov, V. F. Levashov and V. F. Jusbashev - *Experimental investigation of the action of pulsed electrical discharges in liquids on biological objects;* IEEE Transactions on Plasma Science, **28 (1)**, (2000), pp 224-229.

[122] P. Lubicki and S. Jayaram - *High voltage pulse application for the destruction of the Gram-negative bacterium Yersinia enterocolitica;* Bioelectrochemistry and Bioenergetics, **43 (1)**, (1997), pp 135-141.

[123] B. Mazurek, P. Lubicki and Z. Staroniewicz - *Effect of short HV pulses on bacteria and fungi;* IEEE transactions on dielectrics and electrical insulation, **2** (1995), pp 418-425.

[124] D. R. Baer, P. E. Burrows and A. A. El-Azab - *Enhancing coating functionality using nanoscience and nanotechnology;* Progress in Organic Coatings, **47 (3-4)**, (2003), pp 342-356.

[125] H. Becker and C. Gärtner - *Polymer microfabrication methods for microfluidic analytical applications;* Electrophoresis, **21 (1)**, (2000), pp 12-26.

[126] D. R. Reyes, D. Iossifidis, P. A. Auroux and A. Manz - *Micro total analysis systems. 1. Introduction, theory, and technology;* Analytical Chemistry, **74 (12)**, (2002), pp 2623-2636.

[127] G. L. Lettieri, A. Dodge, G. Boer, N. F. de Rooij and E. Verpoorte - *A novel microfluidic concept for bioanalysis using freely moving beads trapped in recirculating flows;* Lab on a Chip, **3 (1)**, (2003), pp 34-39.

[128] J. Voldman, R. A. Braff, M. Toner, M. L. Gray and M. A. Schmidt - *Holding forces of single-particle dielectrophoretic traps;* Biophysical Journal, **80 (1)**, (2001), pp 531-541.

[129] K. J. Mueller, V. L. Sukhorukov and U. Zimmermann - *Reversible Electropermeabilization of Mammalian Cells by High-Intensity, Ultra-Short Pulses of Submicrosecond Duration;* Journal of Membrane Biology, **184 (2)**, (2001), pp 161-170.

[130] N. Y. Chen, K. H. Schoenbach, J. F. Kolb, R. J. Swanson, A. L. Garner, J. Yang, R. P. Joshi and S. J. Beebe - *Leukemic cell intracellular responses to nanosecond electric fields;* Biochemical and Biophysical Research Communications, **317 (2)**, (2004), pp 421-427.

[131] A. G. Pakhomov, A. Phinney, J. Ashmore, K. Walker, J. F. Kolb, S. Kono, K. H. Schoenbach and M. R. Murphy - *Characterization of the cytotoxic effect of high-intensity, 10-ns duration electrical pulses;* IEEE Transactions on Plasma Science, **32 (4)**, (2004), pp 1579-1586.

[132] K. H. Schoenbach, F. E. Peterkin, R. W. Alden and S. J. Beebe - *The effect of pulsed electric fields on biological cells: Experiments and applications;* IEEE Transactions on Plasma Science, **25 (2)**, (1997), pp 284-292.

[133] M. Stacey, J. Stickley, P. Fox, V. Statler, K. Schoenbach, S. J. Beebe and S. Buescher - *Differential effects in cells exposed to ultra-short, high intensity electric fields: cell survival, DNA damage, and cell cycle analysis;* Mutation Research-Genetic Toxicology and Environmental Mutagenesis, **542 (1-2)**, (2003), pp 65-75.

[134] S. J. Beebe, P. M. Fox, L. J. Rec, L. K. Willis and K. H. Schoenbach - *Nanosecond, high-intensity pulsed electric fields induce apoptosis in human cells;* Faseb Journal, **17 (11)**, (2003), pp 1493-1495.

3

Design, realization and characterization of microfluidic devices for cell trapping

In this chapter an overview of different cell trapping mechanisms that can be implemented in microfluidic devices is presented. Subsequently, the design and fabrication of microfluidic devices containing mechanical trapping sites – micromachined filters – is discussed. The flow behaviour as well as the functionality of the cell traps is characterized by using particles and cells.

3.1 Introduction

In order to manipulate single cells several techniques are established, like optical tweezers and vacuum pipettes [1-4]. Single cell handling in microfluidic lab-on-a-chip devices was introduced by several authors previously [5-12]. Particles and cells can be transported within a microfluidic device by means of hydrodynamic flow (pressure driven) [13-16] or electrokinetic forces (e.g. electroosmotic and/or electrophoretic) [17-21]. In this chapter cell trapping and cell transport mechanisms on microfluidic devices are considered. First, a brief overview of different cell trap mechanisms in microfluidic devices is presented (section 3.2). This is followed by a description of the design and fabrication of two different mechanical cell trap devices (section 3.3). Finally, in section 3.4 a study of flow behaviour of particles and cells within the microfluidic cell trap is given.

3.2 Cell trapping in microfluidic devices

This section presents a brief overview about different mechanisms for trapping living cells in microsystems/microfluidic devices [5] and some examples. By cell trapping, cells are maintained at a specific location allowing well-controlled manipulations like injection, electroporation or analysis of the trapped cells. Below an overview of a variety of methods to trap cells in chips such as mechanical, electrical, optical, antibody based and ultrasonic wave trapping is discussed.

3.2.1 Mechanical cell trapping

Mechanical cell trapping on microdevices is based on integrated microstructures with specific geometries which are capable of trapping cells that are transported in a fluid. Microfabricated mechanical filters have been described for trapping different cell types from blood [12, 22, 23]. These filters were made of arrays of rectangular, parallel channels on chip of a width and height that would not allow particles larger than the channels to enter the channel network along the axis parallel to the chip surface. The flow-through microfluidic device realized by Andersson *et al.* [24] traps beads in a confined volume surrounded by vertical silicon bars.

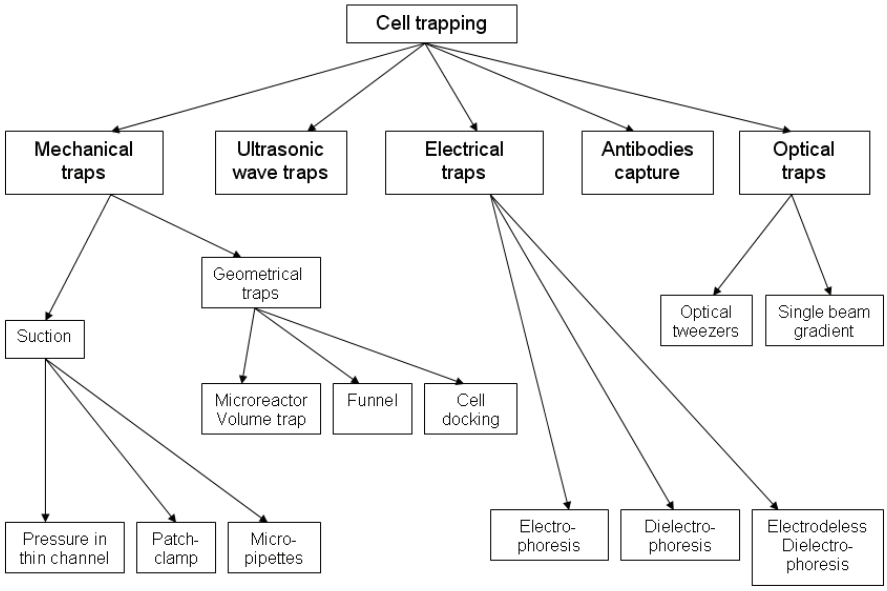

Figure 3-1: Overview of the different cell trapping methods.

This structure concentrates several beads in a defined area as represented in the Figure 3-2a. By adapting the internal geometries of the channel to those proposed by Yun *et al.* [25] and/or M. Denoual *et al.* [26] single cell trapping is possible. The trapping sites behave as funnels and capture single cell in suspension in the buffer in fixed position against fluid flow.

Yang *et al.* [15] present another solution to trap cells in a microfluidic chip: an integrated dam structure inside the channel performs docking and alignment of cells. The trapping sites are along this dam structure which allows the fluid flowing through but retains the cells against it as shown in Figure 3-2b.

Trapping single cells in a flow-through manner is also presented by Huang et al. [27]. Two microfluidic channels are interconnected through a single micron size hole made in a silicon nitride membrane. The cell-containing solution flows through the top channel and is sucked by the bottom channel. This suction creates a pressure gradient that traps cells like shown in Figure 3-3a. In another example, as realized by Tixier-Mita *et al.* [28] and shown in Figure 3-3b, several cells are trapped simultaneously.

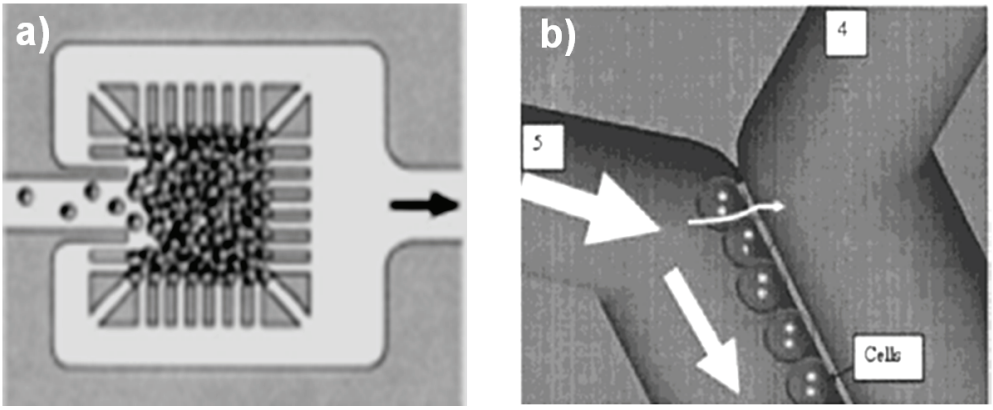

Figure 3-2: (a) Top view of confined volume for beads trapping [24] (b) top view of the dam structure for cells docking [15].

The principle above is known from the so-called patch-clamp technique. The patch-clamp is based on a pressure gradient to trap cells on microholes. Patch-clamping is mostly employed to measure a current through a cell membrane. Various geometries and techniques can be employed for the miniaturization of this trapping concept as shown for example by Hediger *et al.* [29].

A totally different approach to trap cells may be obtained by using micropipettes. These devices have been successfully used by Rusu *et al.* [30] to aspire beads and drawn them out of an optical trap.

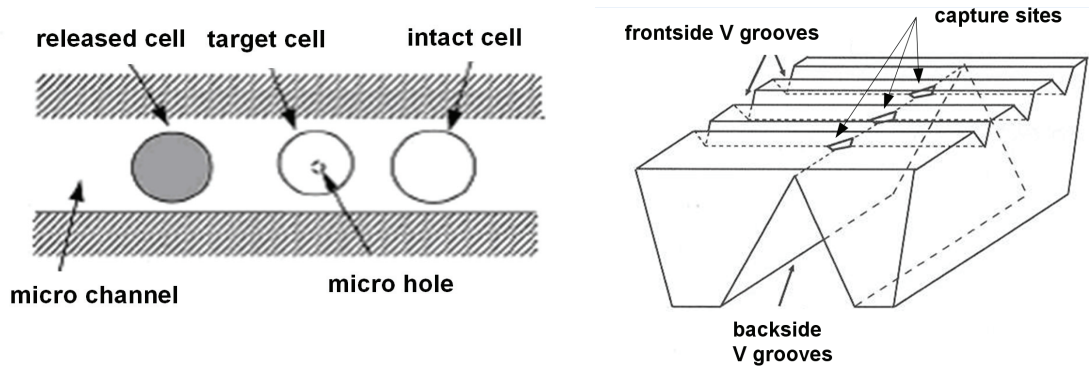

(a) (b)

Figure 3-3: (a) Single cell trapping by suction through microhole in 30 µm wide channel [27] (b) 3D view of a structure allowing trapping several cells in different emplacement and in the same time by suction through microholes [28].

3.2.2 Electrical cell trapping

The electric-field approach to trap cells is well suited for miniaturization because of the ease of microscale generation and structuring of an electric field on microchips. In addition the no-direct contact with biological particles represents an advantage. Different electrokinetic phenomena take place when applying DC or AC electric field in the buffer containing the biological particles. By applying DC current or voltage, electrophoresis occurs, which is based on the Coulomb forces exerted on the charged biological particles. The combination of electrophoresis and the induced drag forces (moving charged particles) of the flow leads to a constant particle velocity represented by the electrophoretic mobility. This phenomenon can thus be used to retain or trap cells.

A non-uniform AC electric field leads to another phenomenon called dielectrophoresis (DEP). During DEP, biological particles polarize and experience an attractive or repelling force from the high electric field area. The nature of the force depends on the electrical properties of the biological particles. A microsystem based on dielectrophoresis for cell sorting, trapping and manipulation is presented by Müller *et al.* [31] and shown in Figure 3-4a. Chou *et al.* [32] use geometrical constrictions in the flow channel to squeeze an electric field applied to a conductive solution as shown in Figure 3-4b. The internal constrictions result in confinement of an electric field gradient which leads to dielectrophoresis in presence of polarized particles.

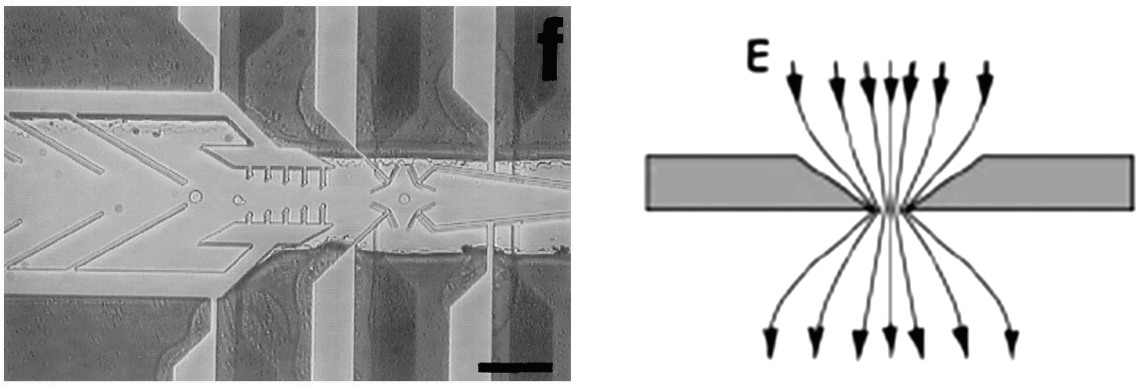

(a) (b)

Figure 3-4: (a) Top view of dielectrophoretic device to trap and sort cells [31] (b) geometrical constriction generating electric field gradient [32] .

3.2.3 Optical cell trapping

Another technique to trap cells is by using optical tweezers: Biological particles can be trapped by highly focused laser light. Particles trapped in the laser beam are moved by scattering forces toward the focus, i.e. the point of highest intensity. Ozkan *et al.* [9] present a microsystem employing optical tweezers to handle cells.

3.2.4 Antibody-based cell trapping

Trapping of living cells is also possible by using antibodies. The antibodies trap the cells by linking themselves to specific proteins on the cell membrane. For example, Le Pioufle *et al.* [33] integrated a layer of antibodies in their microsystem to trap specific cells. The selectivity of the cells is determined by the nature of the antibodies. Specific cells are concentrated in specific areas and thus cell sorting and trapping is performed at once.

3.2.5 Ultrasonic wave trapping

Trapping of cells can also be done with ultrasonic waves. A standing-wave field creates an acoustic radiation force on cells; this force depends on the size of the cell and its acoustic parameters. Particles with higher acoustic impedance than the surrounding medium are trapped in the antinodes of the standing-wave field. Wiklund *et al.* [34] present this ultrasonic trapping technique as a tool for biological particle separation.

3.2.6 Comparison of cell trap mechanisms

When to be implemented in microfluidic devices for cell trapping and manipulation, each of electrical, optical and ultrasonic trapping techniques require additional external equipment to generate and control the electric signals, high focused laser beam or ultrasonic wave, respectively. Moreover, the antibody-based mechanism requires the integration of the biological layer, the use of specific cells and proteins and is not a reversible process. Therefore, these four techniques are

not easily implemented in chips. Integrated microstructures acting as mechanical trapping sites are however, easy to implement and do not require external equipment. Due to the simplicity of this method and consequently the device itself, mechanical cell trapping is highly preferred in microdevices.

In section 3.3 the design and fabrication of chips containing mechanical trapping sites is discussed.

3.3 Mechanical cell trap microdevices: design and fabrication

3.3.1 Filter trapping device

A chip is developed to trap cells using a filter as trapping sites. The device is based on a cross-flow configuration of equally distributed flow channel length between the cross and the reservoirs. The schematic design, including channel dimensions, is shown in Figure 3-5a and a SEM-picture of the trapping sites is depicted in Figure 3-5b. The cell trapping microstructures act as a filter element: i.e. fluid (medium/buffer) can flow through the traps and narrow slits, whereas the cells are captured in the cavities. This filter immobilizes cells in a predefined location where manipulations of the cells can be performed. For immobilization of cells the cross-sectional dimensions of the traps must be smaller than the cells' average diameter. Several different geometries of the mechanical trap were designed to experimentally determine their trapping efficiency. The trapping microstructures differ from each other in the shape, size, number of trapping sites as well as the number of exits (narrow openings between traps). The dimensions of the main channels are: length 12 mm, width 200 μm and depth 15 μm, while the trapping channels are: 30 μm in length, 3 μm wide and 15 μm deep. These devices are fabricated with the process that is described in section 3.3.4. The four access holes to the channels (denoted R1 to R4 in Figure 3-5a) can be used as inlet, outlet or blocked access that allows the configuration of the flow direction and further modifications of it.

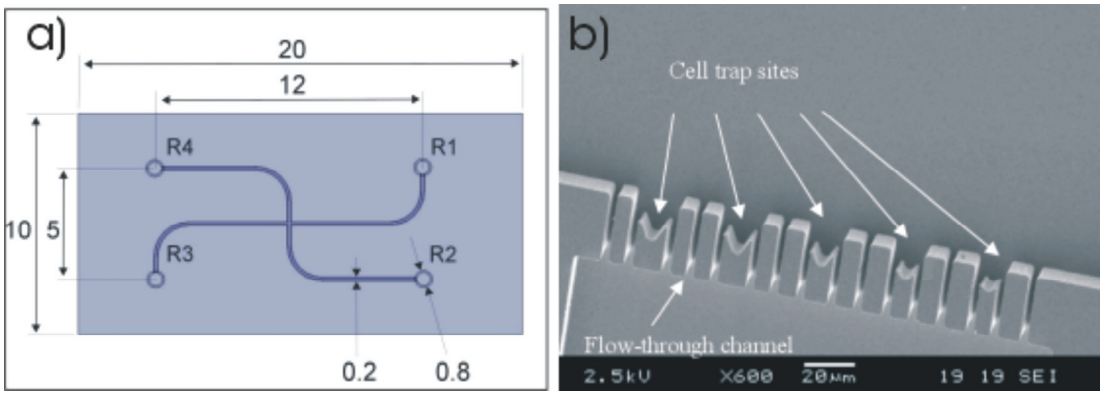

Figure 3-5: (a) Schematic drawing of microfluidic cell trap device (dimensions in mm) and (b) SEM picture of the trapping sites.

3.3.2 Suction trapping device

The suction trapping device consists of two channels that are connected by microholes. These microholes act as trapping sites for the living cells. The two microfluidic channels of 50 µm and 20 µm width, top and bottom respectively, and the nine trapping sites of 4 µm widths are etched to a depth of 15 µm. The fabrication process is identical to the process of the filter trapping devices and it is given in section 3.3.4. There are two designs of trapping structures, a straight trap (type 1), and a trap with two side channels (type 2) as shown in Figure 3-6.

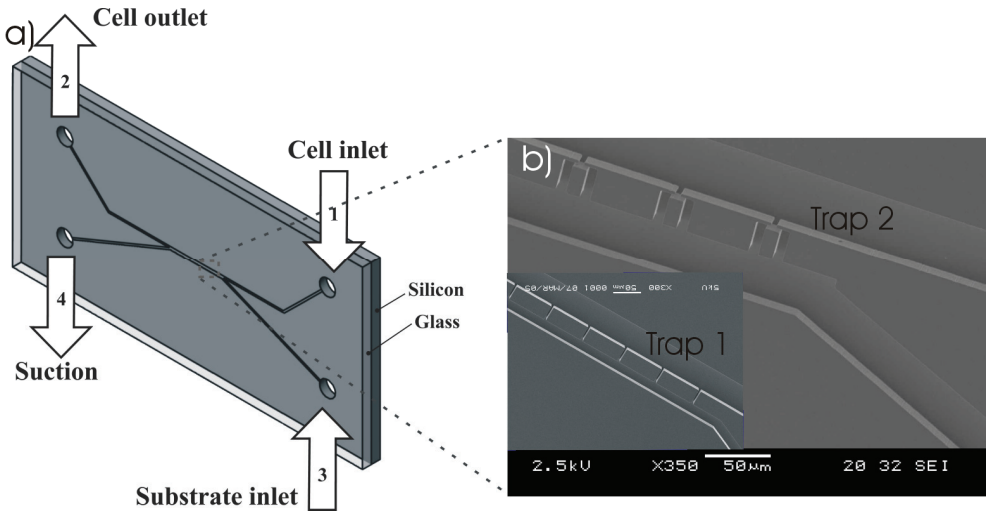

Figure 3-6: (a) Schematic drawing of microfluidic cell trap device and (b) SEM pictures of the two designs for the trapping structures.

The cell sample flows along the upper channel, while the lower channel creates a pressure gradient by suction on the bottom access holes. The result is that the cells which are transported by the liquid in the upper channel are trapped in the cavities.

3.3.3 Selection of material and microtechnology

This section reports on the reasons why (specific) choices for materials and fabrication are made. The microfluidic chips contain channels which are patterned in a first substrate. Then, this patterned substrate is covered by a second non-patterned substrate to close the channels. The two substrates have to be strongly joined together to avoid any leakage. The transparency of the substrates is needed to visualize the channels and the trapping process.

The chips can be made from two glass substrates bonded together by fusion bonding which corresponds with the requirements above. The patterning of common used types of glass like Borofloat or Pyrex would be then an optimal choice. Feature sizes in the same range as the cells are required in order to get the cells trapped. For this purpose, narrow openings which consist in vertical sidewalls are needed, but due to the amorphous crystalline structure of these types of glass wet etching techniques (e.g. HF etching) can not be used. However, glass and in particular fused silica can be etched directionally by a dry etching technique. Recent investigations performed in the *MESA*+ Cleanroom report an aspect ratio of directional dry etching of 13:1, but RIE of fused silica is still in its infancy. In case of glass-silicon, the trapping structures are etched in the silicon. Compared to the directional etching of fused silica, a significantly higher aspect ratio can be achieved in Silicon and (D)RIE of silicon is a well-developed etching technique (in contrast to fused silica etching). Therefore, silicon is preferred as base material for the chips. It has, however, two main disadvantages, i.e. its non-transparency and its electrical conductivity. These drawbacks can be bypassed by using a glass cover plate and deposition of silicon oxide on the silicon substrate. In case of silicon-glass (Pyrex), anodic bonding can be used to seal the chips.

3.3.4 Fabrication of the devices

Both devices are a stack of 2 wafers, silicon and glass (Pyrex). A scheme of the fabrication process is shown in Figure 3-7. In the silicon substrate the microfluidic channels and trapping sites are etched by reactive ion etching (RIE) using the Bosch process (a-d). Access holes are powderblasted from the back side of the silicon wafer (e). After this step the silicon wafer is thermally oxidized at 1100 °C (g). Finally, a Pyrex wafer is anodically bonded to the silicon wafer (h), which allows the visualization of the channels as well as the trapping process.

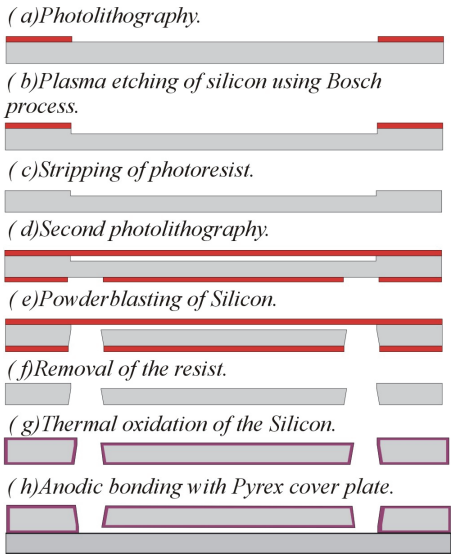

Figure 3-7: Schematic of the fabrication process.

3.4 Characterization of the cell trap microdevices

This section presents the results of microfluidic operations using cell models and cells in a microchip for immobilization and manipulation at the single cell level. Two methods of electrokinetic cell transport are introduced that direct individual cells towards micromechanical trapping sites. The first method utilizes flow-controlled movement of a defined cell suspension volume by the so-called pinched sample injection used on capillary electrophoresis microchips. The second method is based on a combination of electrokinetic focusing similar to the sheath flow technique used in flow-cytometry and electrokinetic gating by employing the cells' electrophoretic mobility. These batch-type cell handling and capturing protocols are

experimentally demonstrated and characterized for suspensions of 10 μm polystyrene beads modeling white blood cells, 4 μm fluorescent beads representing red blood cells and human promyelocytic leukemic HL60 cells. The experimental results show that for both flow transport mechanisms the cell trapping methods function well within these microfluidic devices, single cells can be transported and trapped in a highly controllable way. Therefore, these microfluidic cell trap devices open up new possibilities for single cell analysis. However, from the experiments we can also conclude that for beads (cell suspension models) sometimes contradictive particulate behaviour can occur and supplementary tests with living cells are necessary to fully verify the chip performance as new cell assay. To allow real-time monitoring of several cells simultaneously and individually, it is the idea to perform a continuous sequence to move cells towards a microfluidic trap, investigate them under manipulation and release the treated cell batch towards a waste reservoir, while a new batch of cells is charged onto the trapping features. Thus, the application of integrated microfluidic operations by flow programming represents now a well-designed way of handling single cells at high-throughput [35].

3.4.1 Materials and methods

3.4.1.1 Single cell trapping and cell transport mechanisms

Two different methods to introduce the cells to the traps can be distinguished. The first method was derived from the pinched injection principle of capillary electrophoresis microchips to form a defined sample plug of defined length [36]. The second method is based on the sheath flow techniques already established in conventional and microfluidic flow cytometry [37-39]. In method one, cells are transported via the center channel using electrokinetic pinching towards the trapping sites (Figure 3-8a). In a second step non-captured cells are transported to the waste reservoir by washing with fresh buffer from the side channel (Figure 3-8b). In method two, the cells are loaded by a continuous stream from the side channel which is driven by an electrokinetic gating flow from the centre channel (Figure 3-8c) towards the trapping sites. Introducing a sheath flow across the trap in the centre channel will allow controlling the distance between the traps and the cells that follow the electrical field lines on defined trajectories (Figure

3-8d). Thus, the microchip facilitates transport and immobilization of individual cells in a repetitive (batch-wise) manner and offers thus new possibilities for high-throughput single-cell assays.

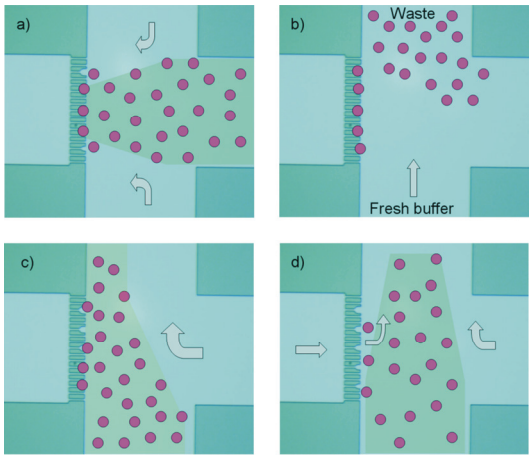

Figure 3-8: Schematic overview of cross channel structure for trapping of single cells; two methods to capture and release cells: based on pinching (a, b) and based on sheath flow (c, d).

The two driving mechanisms for cell transport implemented in the devices are electroosmotic flow [17-21] carrying the cells by the bulk fluid and individual cell movement based on the cell's electrophoretic mobility [40, 41]. Generally speaking EOF-type microfluidic devices are preferred for biomedical/chemical separation and analysis applications since their characteristic flat velocity profiles reduce sample plug dispersion, and consequently can improve the device performance. In our device four fluid ports need to be controlled, which is rather complex for pressure-driven flow where four pressure controllers will be needed. Also the presence of very low flow rates in the device makes electric- field mediated cell transport preferable over pressure-driven flow.

3.4.1.2 Microchips: layouts and fabrication

The design and fabrication process of the cell trap device has been described previously in sections 3.3.1 and 3.3.3. Several different geometries of the mechanical trap were designed to experimentally determine their trapping efficiency, of which the best designs were used in this work.

Commercially available capillary electrophoresis microchips (Micronit Microfluidics B.V., The Netherlands) were used to carry out control experiments concerning flow switching of cell suspension model by means of the sheath flow method. A picture of the used device, made of Borofloat glass, is shown in Figure 3-9 [42]. The channel structure is realized by etching with hydrofluoric acid, while the access holes (R1-R5) are made by powder blasting. The channels are 100 μm wide (top of channel) and 30 μm deep. The length of each channel section is defined as the distance from the access holes to the cross point of the channels (X): R1-X, R2-X, R4-X, R5-X are each 0.6 cm and R3-X is 8.5 cm.

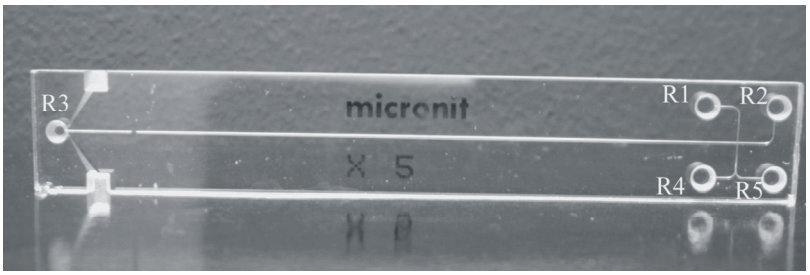

Figure 3-9: Picture of microfluidic device used for executing control experiments concerning the sheath flow method.

3.4.2 Reagents and suspension samples

3.4.2.1 Bead suspensions

Since microfluidic handling of mammalian cell suspensions is not trivial and special care has to be taken if experiments with biological material are pursued, beads were used as a model for a cell suspension. The size distribution of the beads and the conductivity of the solution are adapted to the properties of cells in growth medium. The first cell suspension model mimics a red blood cell suspension: a 5 mM sodium phosphate buffer solution (Merck, Darmstadt, Germany) at pH 8 is loaded with fluorescent beads of an average size distribution of 4 μm (Bangs Laboratories, Inc., USA). For modeling white blood cells in suspension (i.e., suspended HL60 cells) non-fluorescent polystyrene (PS) beads with an average size distribution of 10 μm (Bangs Laboratories, Inc., USA) were loaded in the same buffer.

3.4.2.2 Cell suspensions (HL60 cells)

For experiments with living cells, HL60 cells (white blood cells) were used. These human promyelocytic leukemic HL60 cells were obtained from the German Collection of Microorganisms (Braunschweig, Germany). HL60 cells were cultured in RPMI-1640 medium (BioWhittaker, Verviers, Belgium) supplemented with 10% heat-inactivated and filter-sterilized Fetal Calf Serum, 100 IU/mL penicillin, 100 mg/mL streptomycin, 2 mM L-Glutamine and 250 mg/mL fungizone. Supplements and antibiotics were all obtained from Life Technologies (Grand Island, NY, USA). Cell cultures were maintained in a 5%-CO_2 humidified atmosphere at 37 ºC. The medium was refreshed every 3–4 days.

3.4.3 Microchip preparation and coating

The experiments were performed either on bare or coated microchips. When an electric field is applied to an uncoated glass microfluidic channel, electroosmotic flow is the mechanism that drives the cell suspension (or cell suspension model solution). Prior to experiments, the chips for EOF-control were conditioned by rinsing with 100 mM NaOH. In this way all the silanol groups of the wall become activated and we attain the same surface charge for each experiment. Afterwards, NaOH is first replaced by flowing DI water and then by phosphate buffer solution.

When the interior of the channel structure is coated, electroosmotic flow can be suppressed, and in this case the electrophoretic mobility of the cells (or cell models) is the mechanism that drives the cells when an electric field is applied. In order to suppress EOF, chips were coated with polyacrylamide, according to the procedure of Hjertén for fused-silica capillaries [43]. In brief, the chip was filled with a solution of 40 μL of 3-(trimethoxysilyl)propyl methacrylate (Aldrich, Milwaukee, WI, USA) in 10 mL water adjusted to pH 3.5 with acetic acid (Merck) and allowed to react overnight. The channels were subsequently washed with water and filled with a mixture of 3% w/v acrylamide (Aldrich), 0.1% v/v N,N,N',N'-tetramethylethylenediamine (Sigma) and 0.1% w/v potassium persulfate (Aldrich) in water. During the polymerization reaction, the chip was covered with a microscope slide to keep out oxygen from the air. After 30 minutes the solution

was removed and the channels were washed with water, after which the chip was ready for use.

3.4.4 Instrumentation

In order to perform optical inspection of the microfluidic devices during the experiments, chips were mounted on a XYZ translation stage of an inverted microscope (Leica DM/IRM, Wetzlar, Germany). The microscope system is equipped with 3 objectives (20x, 40x and 50x magnification). A computer-controlled CCD camera (Colorview 8) is mounted on the microscope for image recording. Video imaging was used to visualize the flow control of the cells and/or beads in the channels of the chips. A computer-controlled high-voltage power supply (CU 411, IBIS technologies B.V., Hengelo, The Netherlands) with 4 independently controllable voltage outputs was used to apply electric fields to the microfluidic devices. Gold wires were immersed in the reservoirs of a chip holder making the electrical connection from the fluid in the chip to the high voltage power supply unit.

3.4.5 Results and discussion

3.4.5.1 Flow control based on EOF in a capillary electrophoresis microchip

In order to familiarize with the different concepts of electrohydrodynamic flow switching of cells/beads from one channel to another, capillary electrophoresis microchips were used (see section 3.4.1.2, Figure 3-9). In these devices the cell suspension model for red blood cells (4 μm beads) was loaded to reservoir R1 and the EOF was applied as driving force for the beads. Steering of these beads along the flow trajectories of the fluid was successfully achieved. Figure 3-10 shows flow patterns at the cross point (X) and at the Y-splitter between reservoirs R4 and R5 of the microchip. Figure 3-10a depicts electrokinetically focused fluorescent beads at the cross-channel junction. The flows from R2 and R3 in the centre channel focus the beads, thus that they can not spread into the centre channel. The centre channel flows also act as gating flows in the subsequent switching steps at the Y-

junction between reservoir R4 and R5. By manipulating the voltages applied to the reservoirs (R1 – R5, see Figure 3-9), it is possible to program the flow direction of the beads towards either one or both of the reservoirs R4 and R5. Since this device was manufactured specifically for electrophoretic separation, the configuration employing flows from R2 and R3 as sheath flows for the bead-loaded solution (that enters the cross from reservoir R1) suffers from an asymmetrical layout. Due to this difference in channel length, the voltages applied to R3 and R2 (VR3 and VR2, respectively) to obtain an evenly distributed split of the bead-flow are not identical. By changing the voltage applied to one of the reservoirs (VR3 or VR2), other split-ratios can be obtained. Observations confirmed that when a voltage of 500 V is applied to reservoirs R3 and R2, while R1 to set to 300 V and R4 & R5 remain grounded (0 V), an asymmetric splitting between the flows was found. This result is depicted in Figure 3-10c. Reducing the potential at reservoir R2 to 200 V compensates for the flow restriction and allows an almost equal stream of beads to both reservoirs R4 and R5 (Figure 3-10b). When the voltage to reservoir R3 is increased (and/or the voltage to reservoir R2 decreased further), the bead flow can be directed towards reservoir R5 (not shown).

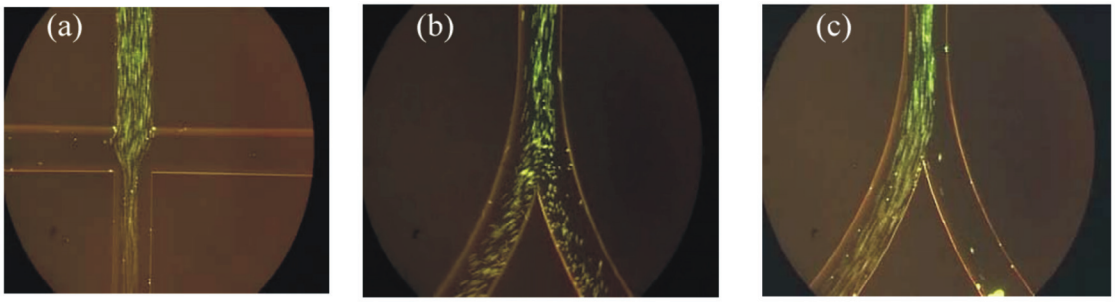

Figure 3-10: Video prints of fluorescent beads in microfluidic flow-through device showing the flow control based on EOF and sheath flow. Flow profiles are described in detail in text.

The conclusion of this series of experiments is that gating by sheath flow using EOF is an attractive option to control the flow direction of cell suspension models in microfluidic devices. Therefore, the principle seems a promising method to control the flow (and capture) of living cells in microfluidic devices with trapping sites for single cell analysis and we translated the protocol to the cell trap microchip described in the following section.

3.4.5.2 EOF-control of bead and HL60 cell suspensions in a cell trap microchip

To characterize pinched flow control for cell immobilization uncoated cell trap microchips were used (see section 3.4.1 2) and the cell suspension model for white blood cells (~10 μm beads) was loaded by EOF as the driving force for the beads. The voltage scheme used for driving the beads towards the trapping sites was: 100 V at the sample compartment (R1), 0 V at the reservoir behind the trap (R3) and 50 V at the other two reservoirs (R2 and R4). Therefore, with this voltage scheme, the beads move towards the traps. When some of the beads are trapped, as shown in Figure 3-11a, the trapping sites are blocked, causing a higher flow restriction across the traps. Moreover, when the first beads are captured, a plug of beads is formed in the center channel. At this moment, it is observed that the introduced beads align into a vortex-type flow pattern within the center channel, moving in the direction of the EOF, while no new beads enter the channel from the reservoir. Clearly, the flow profile is a combination of electroosmotic and hydrodynamic flow (caused by a pressure built up due to blocking of the trapping sites): in the middle of the channel pressure driven flow (PDF) dominates, whereas close to the channel walls EOF is the main driving force of the bead-flow. Thus, a stable bi-directional flow is established [44]. This effect can be seen in Figure 3-11b.

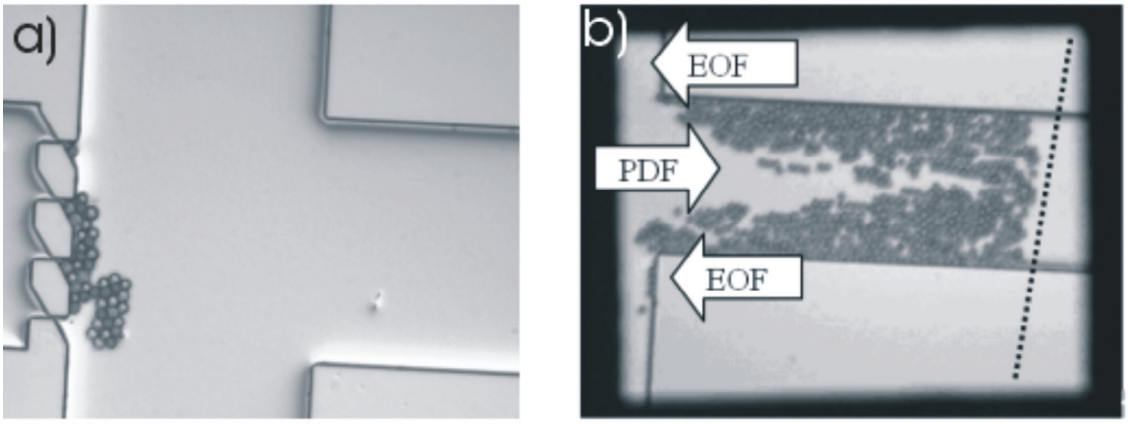

Figure 3-11: a) Images of the polystyrene beads trapped at the trapping sites, resulting in a high flow restriction. b) Image of vortex-type flow of beads (with pseudo-stationary boundary at the dotted line).

This pseudo-static flow phenomenon is, however, not observed for identical experiments with HL60 cells. In the case of working with HL60 cells on the same chip configuration cells still could be addressed towards the traps (no vortex-type flow phenomenon) even when the first cells reached the capture sites. The results of real-time observations of a specific biochemical process inside of the HL60 cells have been reported elsewhere [45]. From these observations we can conclude that the used cell suspension model of the PS beads in phosphate buffer is an inappropriate model for the suspended HL60 cells, since the living cells (being trapped in the same way as the beads) behave mechanically and electrically differently. A living cell could become an active part of the microfluidic network (e.g. by electropermeabilization), which we cannot fully explain. Instead, we present more insight on the described phenomenon of pseudo-static bead circulation as given in section 3.4.5.4, which can be very well described by microfluidic flow simulation.

3.4.5.3 Electrophoretic control of bead and HL60 cell suspensions in a cell trap microchip

To further investigate the electrophoretic motion and capturing behaviour of cells, experiments were performed in a coated cell trap microchip first with the cell model suspension of 10 μm polystyrene beads and subsequently with HL60 cells (see Figures 3-5 and 3-12 for layouts and notations). Here, the attention is pointed to "electrokinetic sheathing" at suppressed EOF.

Prior to applying the voltages, 100 μl of the bead solution was introduced in the inlet reservoir (R2) of the device (side channel with respect to the cross channel section) and phosphate buffer was introduced in each of the other reservoirs (R1, R3, and R4). After filling the reservoirs, the following voltage scheme was applied: 0 V at the sample compartment (R2) and the reservoir behind the trap (R3), 200 V on reservoir R1 and 100 V on the waste reservoir (R4). In figure 3-12a the transport of the beads is shown when this potential configuration is applied: the beads follow the electric field lines towards reservoir R1. Subsequently, the voltage at reservoir R1 is set to 0 V and consequently the motion of the beads changes towards R4, (Figure 3-12b). The voltage setting applied at reservoir R3 leads to repel the beads from the traps, which is in agreement with the concept of sheath flow, but now

exploiting electrical field lines. However, when the voltage at R3 is set to 300V, the beads move towards the trap (Figure 3-12c) and can be captured for as long as this voltage scheme is applied. By setting the voltages at reservoirs R1 and R3 back to their initial values (200 V and 0 V, respectively) the beads are released from the traps, as shown in Figure 3-12d. Subsequently, this transport and trapping concept was used for experiments with HL60 cells. For the above mentioned voltage settings, the behaviour and trapping of HL60 cells was identical to the results obtained with cell suspension models. Figure 3-13 follows an individual cell on its trajectory during the sheathing step (see section 3.4.1.1, Figure 3-8d) of the cell transport protocol in due course of time. Figure 3-13a incorporates four distance lines (L1-L4) from the edge of the trapping feature to the schematically indicated electric field lines, which guides the eye for the interpretation of electrophoretic cell movement depicted in the subsequent in Figures 3-13(b-e).

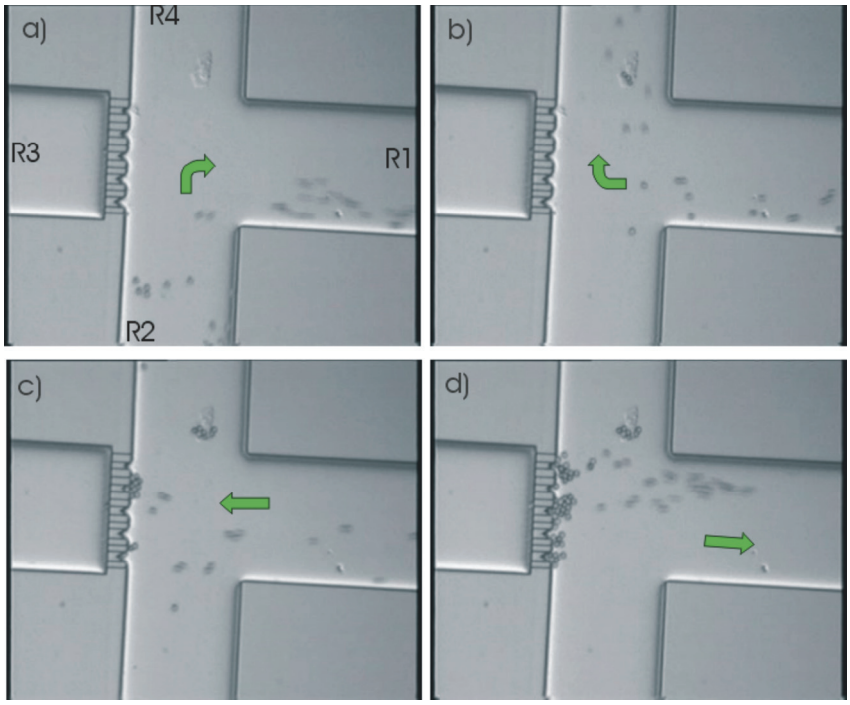

Figure 3-12: Figure 6: Images of electrophoretic movement of polystyrene beads in the coated cell trapping device. The arrows indicate the direction of the bead flow for various voltage settings (see text for details).

To summarize, during electrophoretically driven transport, the cells and beads show very similar behaviour and the original idea of using beads as a model

compounds for cells is confirmed to be useful. Clearly, these experiments show that the transport and trapping of beads and cells can be controlled by means of the cells' electrophoretic mobility.

Figure 3-13: Schematic indication of a cell trajectory (arrow) guiding the eye by the four distance lines L1-L4, which are given by the focused field line pattern (green area) (a); these distances refer to the trajectory position of the individual cell followed within the subsequent video frames (b-e).

3.4.5.4 Flow modeling of 10 µm bead suspension

The flow transport behaviour of living cells and beads are identical when electrophoretic mobility is the main force to drive the cells through the chip (section 3.4.5.3). This is however, not the case when EOF is used in the cell-trap microchip (section 3.4.5.2). Therefore, the 10 µm polystyrene beads seem a less appropriate model for HL60 cells when both the electroosmotic and electrophoretic driving forces are present. Since we observed the phenomenon of recirculation of beads (Figure 3-11b), a flow simulation study was performed to understand this particulate behaviour of the 10 µm polystyrene beads in suspension. The beads tended to group together forming a sort of plug. This plug of beads, of approximately 500 µm length, strongly influences the conductivity of the channel, creating a higher resistance and accordingly raises the voltage drop at this location. Thus, due to the bead-plug formation, the potential distribution over the channel rearranges and this leads to recirculation of beads. This recirculation-phenomenon can be explained by using a CFDRC-ACE+ (CFD Research Company) model. With such a model, flow trajectories can be plotted, but it requires input of the potential distribution across the channel area. For the estimation of this potential distribution the simulation program 20-sim (Controllab Products B.V., Enschede) was used to define an electrical network model by assigning different conductivities to the various channel sections. Figure 3-14 shows the equivalent electrical circuit. When the trapping sites are blocked, both the electrical and hydraulic trap

resistance will be very high (ca. 1000 times higher). Across the bead-plug it was assumed to have an increased specific resistance of about a factor of 2. Consequently, the potential distribution shifted followed by the adaptation of the electric field strength in the network. Accordingly the EOF in the channel section containing the bead-plug increases while it decreases in the rest of the channels.

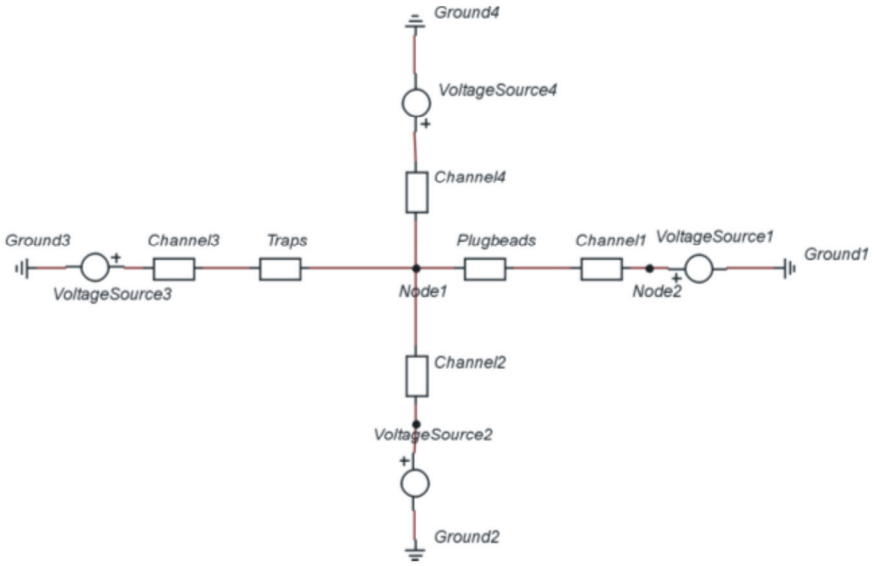

Figure 3-14: Equivalent electrical circuit of the cell trap device and the plug of beads.

The EOF will almost only take place in the bead-plug whereas the flow in the other zones will virtually stop and generate hydraulic impedance to the system. Back flow is simulated by the built-up reservoir level difference. In a CFDRC ACE+ model this was approximated by assuming impedances infinitely high (blocked flow). The resulting flow trajectories of the beads are shown in Figure 3-15. The colors of the particle trace plot indicate the effective velocity of the beads in m/s. In the vertical plane the velocity profile is shown as a combination of EOF (near the channel walls) and pressure-driven flow in the core of the channel in opposite direction.

Since the polystyrene beads are big (10 μm) compared to the channel depth (15 μm), they experience a net force by the EOF and pressure-driven flow such that trajectories will slightly differ from the simulated paths. In case of experiments, the electric field will be disturbed by the beads and charging effect of the beads can play a role. Nevertheless the calculated values were close to the observed velocities of the bead trajectories during the experiment described in section 3.4.5.2. It is

believed that due to the complex nature of HL60 cells simple flow models, as presented above, will not suffice to describe their particulate behaviour during electrohydrodynamic flow. However, for electrophoretic transport a good comparison between beads and cells can be made.

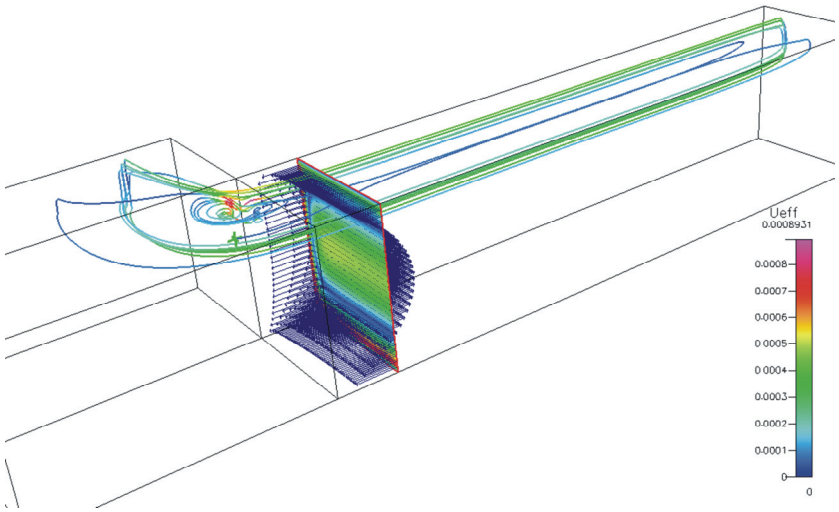

Figure 3-15: Simulated vortex flow in CFDRC. This model plots in color the bead trajectories. In the vertical plane the velocity profile is shown as a combination of EOF (near the channel walls) and PDF (in the core of the channel)

3.4.6 Concluding remarks

In this work, results are presented on the flow behaviour of cell models and cells in microfluidic devices that are designed to be used for trapping and manipulation of single cells. Two methods to address cells towards the trapping sites are investigated: pinched injection by applying electroosmotic flow and sheathing based on the electrophoretic behaviour of the beads and cells respectively. The first series of experiments showed that the concept of electrohydrodynamic focusing and gating using EOF is a good and reliable method to control beads (section 3.4.5.1). If this concept is used for transporting the cell suspension model using 10 μm polystyrene beads in the cell trap microchip (section 3.4.5.2), recirculation of these beads was observed, whereas this effect did not occur for HL60 cells. Therefore, it seems that a cell suspension model based on polystyrene beads is not an appropriate model for HL60 cells transported by EOF in the cell trap microchip. However, from the series of experiments only exploiting

electrophoretic forces (section 3.4.5.3) it was observed that the transport and trapping of HL60 cells and the cell suspension model is successful and very much identical.

The results show that for both transport mechanisms the cell trapping methods function well: single cells can be transported, trapped and manipulated in a controllable and precise way. Thus, the studied microfluidic cell trap protocols open up new possibilities for single cell analysis and new approaches for applications in drug discovery, combinatorial chemistry, and bioanalysis. Since we observed that cell and bead suspensions can show contradictive particulate behaviour we conclude that specific care must be taken if cell models are employed to verify microfluidic manipulation for cell assays.

3.5 References

[1] E. Ferrari, V. Emiliani, D. Cojoc, V. Garbin, M. Zahid, C. Durieux, M. Coppey-Moisan and E. Di Fabrizio - *Biological samples micro-manipulation by means of optical tweezers;* Microelectronic Engineering, **78-79** (2005), pp 575-581.

[2] K. König - *Laser tweezers and multiphoton microscopes in life sciences;* Histochemistry and Cell Biology, **114** (2000), pp 79-92.

[3] N. Munce, J. Li, P. Herman and L. Lilge -*Single Cell Analysis on a Microchip Platform using Optical Tweezers and Optical Scissors;* Proc. Microfluidics, BioMEMS and Medical Microsystems, **4982**, (2003), pp 28-36.

[4] M. Ozkan, T. Pisanic, J. Scheel, C. Barlow, S. Esener and S. N. Bhatia - *Electro-optical platform for the manipulation of live cells;* Langmuir, **19 (5)**, (2003), pp 1532-1538.

[5] H. Andersson and A. van den Berg - *Microfluidic devices for cellomics: a review;* Sensors and Actuators B, **92 (3)**, (2003), pp 315-325.

[6] J. Enger, M. Goksor, K. Ramser, P. Hagberg and D. Hanstorp - *Optical tweezers applied to a microfluidic system;* Lab on a Chip, **4 (3)**, (2004), pp 196-200.

[7] V. I. Furdui, J. K. Kariuki and D. J. Harrison - *Microfabricated electrolysis pump system for isolating rare cells in blood;* Journal of Micromechanics and Microengineering, **13 (4)**, (2003), pp S164-S170.

[8] P. C. H. Li, L. de Camprieu, J. Cai and M. Sangar - *Transport, retention and fluorescent measurement of single biological cells studied in microfluidic chips;* Lab on a Chip, **4 (3)**, (2004), pp 174-180.

[9] M. Ozkan, M. Wang, C. Ozkan, R. Flynn, A. Birkbeck and S. Esener - *Optical manipulation of objects and biological cells in microfluidic devices;* Biomedical Microdevices, **5 (1)**, (2003), pp 61-67.

[10] J. Seo, C. Ionescu-Zanetti, J. Diamond, R. Lal and L. P. Lee - *Integrated multiple patch-clamp array chip via lateral cell trapping junctions;* Applied Physics Letters, **84 (11)**, (2004), pp 1973-1975.

[11] A. R. Wheeler, W. R. Throndset, R. J. Whelan, A. M. Leach, R. N. Zare, Y. H. Liao, K. Farrell, I. D. Manger and A. Daridon - *Microfluidic device for single-cell analysis;* Analytical Chemistry, **75 (14)**, (2003), pp 3581-3586.

[12] P. Wilding, L. J. Kricka, J. Cheng, G. Hvichia, M. A. Shoffner and P. Fortina - *Integrated cell isolation and polymerase chain reaction analysis using silicon microfilter chambers;* Analytical Biochemistry, **257 (2)**, (1998), pp 95-100.

[13] S. Eyal and S. R. Quake - *Velocity-independent microfluidic flow cytometry;* Electrophoresis, **23 (16)**, (2002), pp 2653-2657.

[14] E. A. Schilling, A. E. Kamholz and P. Yager - *Cell lysis and protein extraction in a microfluidic device with detection by a fluorogenic enzyme assay;* Analytical Chemistry, **74 (8)**, (2002), pp 1798-1804.

[15] M. S. Yang, C. W. Li and J. Yang - *Cell docking and on-chip monitoring of cellular reactions with a controlled concentration gradient on a microfluidic device;* Analytical Chemistry, **74 (16)**, (2002), pp 3991-4001.

[16] L. Zhu, Q. Zhang, H. H. Feng, S. Ang, F. S. Chauc and W. T. Liu - *Filter-based microfluidic device as a platform for immunofluorescent assay of microbial cells;* Lab on a Chip, **4 (4)**, (2004), pp 337-341.

[17] J. Gao, X. F. Yin and Z. L. Fang - *Integration of single cell injection, cell lysis, separation and detection of intracellular constituents on a microfluidic chip;* Lab on a Chip, **4 (1)**, (2004), pp 47-52.

[18] L. Kremser, D. Blaas and E. Kenndler - *Capillary electrophoresis of biological particles: Viruses, bacteria, and eukaryotic cells;* Electrophoresis, **25 (14)**, (2004), pp 2282-2291.

[19] J. Kruger, K. Singh, A. O'Neill, C. Jackson, A. Morrison and P. O'Brien - *Development of a microfluidic device for fluorescence activated cell sorting;* Journal of Micromechanics and Microengineering, **12 (4)**, (2002), pp 486-494.

[20] P. C. H. Li and D. J. Harrison - *Transport, manipulation, and reaction of biological cells on-chip using electrokinetic effects;* Analytical Chemistry, **69 (8)**, (1997), pp 1564-1568.

[21] E. X. Vrouwe, R. Luttge and A. van den Berg - *Direct measurement of lithium in whole blood using microchip capillary electrophoresis with integrated conductivity detection;* Electrophoresis, **25 (10-11)**, (2004), pp 1660-1667.

[22] O. Bakajin, R. H. Carlson, C. Chou, S. Chan, C. Gabel, J. Knight, T. Cox and R. Austin, *-Sizing, Fractionation and Mixing of Biological Objects via Microfabricated Devices;* MicroTAS, (1998), pp 103-198.

[23] R. H. Carlson, C. V. Gabel, S. S. Chan, R. H. Austin, J. P. Brody and J. W. Winkelman - *Self-sorting of white blood cells in a lattice;* Physical Review Letters, **79 (11)**, (1997), pp 2149-2152.

[24] H. Andersson, W. van der Wijngaart, P. Enoksson and G. Stemme - *Micromachined flow-through filter-chamber for chemical reactions on beads;* Sensors and Actuators B, **67 (1-2)**, (2000), pp 203-208.

[25] K. Yun, S. Lee, G. M. Lee and E. Yoon, *-Desing and fabrication of micro/nano-fluidic chip performing single-cell positioning and nanoliter drug injection for single-cell analysis;* Proceedings of MicroTAS, **2**, (2002), pp 652-654.

[26] M. Denoual, K. Aoki, A. Mita-Tixier and H. Fujita, *-A microfluidic device for long-term study of individual cells* Proceedings of MicroTAS, **1**, (2003), pp 531-534.

[27] Y. Huang and B. Rubinsky - *Flow-through micro-electroporation chip for high efficiency single-cell genetic manipulation;* Sensors and Actuators A, **104 (3)**, (2003), pp 205-212.

[28] A. Tixier-Mita, Y. Mita, K. Cozic, M. Frénéa, B. Le Pioufle and H. Fujita, *-To place cells as an array using aspiration technique* Proceedings of MicroTAS, **2**, (2002), pp 888-890.

[29] S. Hediger, A. Sayah and M. A. M. Gijs - *Fabrication of a novel microsystem for the electrical characterisation of cell arrays;* Sensors and Actuators B, **56 (1-2)**, (1999), pp 175-180.

[30] C. Rusu, R. van't Oever, M. J. de Boer, H. V. Jansen, J. W. Berenschot, M. L. Bennink, J. S. Kanger, B. G. de Grooth, M. Elwenspoek, J. Greve, J. Brugger and A. van den Berg - *Direct integration of micromachined pipettes in a flow channel for single DNA molecule study by optical tweezers;* Journal of Microelectromechanical Systems, **10 (2)**, (2001), pp 238-246.

[31] T. Muller, G. Gradl, S. Howitz, S. Shirley, T. Schnelle and G. Fuhr - *A 3-D microelectrode system for handling and caging single cells and particles;* Biosensors & Bioelectronics, **14 (3)**, (1999), pp 247-256.

[32] C. F. Chou, J. O. Tegenfeldt, O. Bakajin, S. S. Chan, E. C. Cox, N. Darnton, T. Duke and R. H. Austin - *Electrodeless dielectrophoresis of single- and double-stranded DNA;* Biophysical Journal, **83 (4)**, (2002), pp 2170-2179.

[33] B. Le Pioufle, P. Surbled, H. Nagai, Y. Murakami, K. S. Chun, E. Tamiya and H. Fujita - *Living cells captured on a bio-microsystem devoted to DNA injection;* Materials Science & Engineering C-Biomimetic and Supramolecular Systems, **12 (1-2)**, (2000), pp 77-81.

[34] M. Wiklund, S. Nilsson and H. M. Hertz - *Ultrasonic trapping in capillaries for trace-amount biomedical analysis;* Journal of Applied Physics, **90 (1)**, (2001), pp 421-426.

[35] M. A. McClain, C. T. Culbertson, S. C. Jacobson, N. L. Allbritton, C. E. Sims and J. M. Ramsey - *Microfluidic devices for the high-throughput chemical analysis of cells;* Analytical Chemistry, **75 (21)**, (2003), pp 5646-5655.

[36] L. L. Shultz-Lockyear, C. L. Colyer, Z. H. Fan, K. I. Roy and D. J. Harrison - *Effects of injector geometry and sample matrix on injection and sample loading in integrated capillary electrophoresis devices;* Electrophoresis, **20 (3)**, (1999), pp 529-538.

[37] A. Y. Fu, H. P. Chou, C. Spence, F. H. Arnold and S. R. Quake - *An integrated microfabricated cell sorter;* Analytical Chemistry, **74 (11)**, (2002), pp 2451-2457.

[38] G. B. Lee, C. I. Hung, B. J. Ke, G. R. Huang and B. H. Hwei - *Micromachined pre-focused 1 x N flow switches for continuous sample injection;* Journal of Micromechanics and Microengineering, **11 (5)**, (2001), pp 567-573.

[39] A. Wolff, I. R. Perch-Nielsen, U. D. Larsen, P. Friis, G. Goranovic, C. R. Poulsen, J. P. Kutter and P. Telleman - *Integrating advanced functionality in a microfabricated high-throughput fluorescent-activated cell sorter;* Lab on a Chip, **3 (1)**, (2003), pp 22-27.

[40] F. Omasu, Y. Nakano and T. Ichiki - *Measurement of the electrophoretic mobility of sheep erythrocytes using microcapillary chips;* Electrophoresis, **26 (6)**, (2005), pp 1163-1167.

[41] A. Pfetsch and T. Welsch - *Determination of the electrophoretic mobility of bacteria and their separation by capillary zone electrophoresis;* Fresenius Journal of Analytical Chemistry, **359 (2)**, (1997), pp 198-201.

[42] Q. S. Pu, R. Luttge, H. J. G. E. Gardeniers and A. van den Berg - *Comparison of capillary zone electrophoresis performance of powder-blasted and hydrogen fluoride-etched microchannels in glass;* Electrophoresis, **24 (1-2)**, (2003), pp 162-171.

[43] S. Hjertén - *High-performance Electrophoresis; elimination of electroendosmosis and solute adsorption;* Journal of Chromatography, **347** (1985), pp 191-198.

[44] G. L. Lettieri, A. Dodge, G. Boer, N. F. de Rooij and E. Verpoorte - *A novel microfluidic concept for bioanalysis using freely moving beads trapped in recirculating flows;* Lab on a Chip, **3 (1)**, (2003), pp 34-39.

[45] A. Valero, F. Merino, F. Wolbers, R. Luttge, I. Vermes, H. Andersson and A. van den Berg - *Apoptotic cell death dynamics of HL60 cells studied using a microfluidic cell trap device;* Lab on a Chip, **5 (1)**, (2005), pp 49-55.

4

Apoptotic cell death dynamics of HL60 cells studied using a microfluidic cell trap device*

In this chapter the design, fabrication and experimental results of a microfluidic cell trap device for analysis of apoptosis in HL60 cells are described. The silicon-glass chip enables the immobilization of these cells and real time monitoring of the apoptotic process. Induction of apoptosis, either electric field mediated or chemically induced, was addressed. Fluorescent dyes were used to discriminate between viable, apoptotic and necrotic cells.

* Parts of this chapter are published in: A. Valero, F. Merino, F. Wolbers, R. Luttge, I. Vermes, H. Andersson and A. van den Berg – *Apoptotic cell death dynamics of HL60 cells studied using a microfluidic cell trap device*; Lab on a Chip, 5 (1) (2005), pp 49-55.

4.1 Introduction

There are many ways to die, but nature only knows two, programmed cell death (apoptosis) and accidental cell death (necrosis). The term apoptosis defines a genetically encoded cell death program, which is morphologically, biochemically and molecularly distinct from necrosis [1, 2]. Apoptosis is a kinetic event [3]. The entire duration of apoptosis, from onset to total disintegration of the cell is relatively short and of variable length in comparison to duration of cell cycle time. The various inducers of apoptosis start the process by activation of intracellular cysteine-aspartic acid proteases (caspases) [4, 5]. The process of their activation is considered to be the key event of apoptosis.

Apoptosis is studied both as a target for drug discovery and as a cellular process. Suppression or enhancement of apoptosis is known to cause or contribute to many diseases such as cancer, neurodegenerative diseases and AIDS [1]. Apoptosis occurs normally during the period of embryogenesis and goes on during post-embryonic life, thus controlling cell numbers and organ size in a dynamic balance between cell proliferation and cell death. Apoptosis is a very complex biological process to study. For example, the duration of apoptosis is short, involves single cells with morphological changes only after the "point of no return", ending in phagocytosis without reaction in the neighbour cells [1].

At present there are about 300 different apoptosis–related kits and techniques that are developed for apoptosis detection and quantification [6]. However, all of these techniques have a number of limitations, the most important of which is that cells must be stained, fixed or destroyed for analysis, meaning that intact cells cannot be analyzed today[1, 2]. There are no methods available for studying apoptosis at the single cell level. In addition, cell preparation for analysis is time consuming (at least 15-30 min) and therefore real time monitoring of the cell death cascade is not possible or it can only be reconstructed from flow cytometry measurements of cells samples stained at different stages of the apoptotic process. Further, conventional bioanalytical techniques need highly sophisticated equipments and technicians to perform these measurements which are very labour-consuming and expensive. Hence, there is a real need for simple chip technology to

study apoptosis in real time at the single cell level with high-throughput that will provide valuable additional and complementary information to existing conventional methods to analyze the process of apoptosis [7-10].

Recent advances in microfluidic Lab-on-a-Chip techniques have increased the potential of high-throughput biochemical assays on individual mammalian cells. Of particular interest is the ability to parallelize up-front assay protocols and still be able to examine and treat every individual cell in the assay separately retrieving single-cell event information [11-13].

Studying apoptosis on chip is a completely new approach which has almost not been explored at all. Until today, only three reports on apoptosis analysis on chips were presented [14-16]. In all three reports either cell labeling, cell lysis or very advanced optical system are required. Hence, none of the drawbacks for the conventional techniques were circumvented.

In this contribution real time monitoring of individual cells is addressed presenting the geometrical design, chip fabrication and first results of apoptosis studies in a new microfluidic assay format. The cross-flow devices introduced in this study offer to broaden the tools to characterize single cells in a format that allows integration of high-throughput techniques with unique assay functionality, for example, to identify the apoptotic cascade in the case of HL60 cells.

Integration techniques such as known from microelectronics allow placing electrodes close to a single cell either to stimulate the cell or reading the cell impedance, which can give a measure for the cell status [17, 18]. High-throughput is achieved if electrodes and cells are arranged in an array (parallel) fashion. The device as introduced here presents an intermediate step towards this class of operations by first positioning cells in pre-defined locations of the chip leading to a one dimensional array of cells under investigation. In this stage of development optical detection is performed to compare the results to classical methods [3]. Numbering-up of devices and two dimensional arrayed cell investigations can increase the throughput of observed events. Translating the optical information in cell impedance spectra can help to further optimize automated operation on a large number of cells without the need for complex optical and robotic equipment.

The aim of this work is to eventually be able to measure apoptotic cell death dynamics on a chip in real-time on single cell level. A new microfluidic chip has been developed in which the apoptotic process can be optically followed. Electric field mediated and chemically induced cell death has been attempted. Exposure of cells to a fluorochrome-labelled inhibitor of caspases (FLICA) labels cells after caspase activation and arrest further progress of the apoptotic cascade [3, 19]. Loss of membrane integrity (late apoptosis and necrosis) was observed by exposing cells to propidium iodide (PI).

4.2 Background of apoptosis

All living organisms from unicellular bacteria to multicellular animals are products of cell division. Most scientists traditionally have studied proliferation and it was a given that cells survive. The role of cell death for development, growth and survival of individuals was left outside of consideration. Only after Kerr, Wyllie and Currie [20] had discovered on basis of morphological appearance the existence of two different forms of cell death, researchers have become aware that death is the inevitable complement to cell division. To discriminate the natural cell death from accidental cell death they introduced the term apoptosis. This term is derived from the Greek: apo "apart" and ptosis "fallen" meaning the shedding of leaves from trees during the autumn.

There are many ways to die, but from cell biological point of view only two forms exist: physiological and pathological cell death (Figure 4-1).

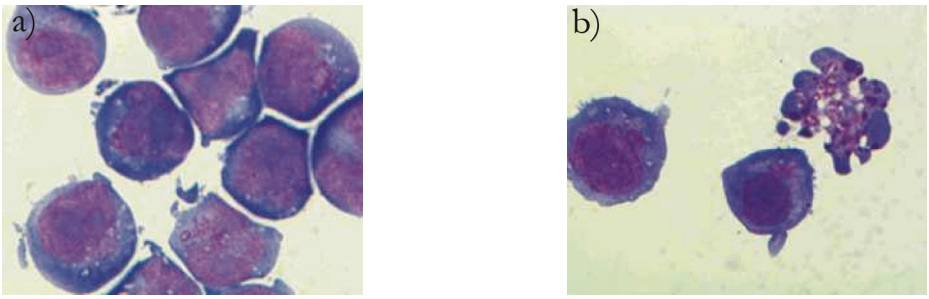

Figure 4-1: Apoptosis versus necrosis: a) Light microscopy of untreated control HL60 cells and b) cells treated with apoptotic inducer camptothecin and cultured 6 h in vitro.

Necrosis of cells occurs after a physical, chemical or osmotic injury, including hypoxia and complement attack [1, 20, 21]. During accidental cell death, the cell membrane looses its selective permeability and ion-pumping capacity. This leads immediately to swelling of the cell and its organelles and to leaking of the cellular contents into the extracellular space, eliciting an inflammatory reaction in the adjacent viable tissues.

Apoptosis is a physiological active bioenergy-saving cell elimination mechanism by which aged, unwanted or sublethal damaged cells are abolished and their contents are reutilized by macrophages or by phagocytosing adjacent cells. Physiological cell death occurs as "programmed cell death" (PCD) during the period of embryogenesis and goes on during post-embryonic life as "apoptosis", thus controlling cell numbers and organ size in a dynamic balance between cell proliferation and cell death [22-24]. Without continuous signalling by growth factors, hormones or cytokines, cells undergo apoptosis.

During apoptosis a specific pattern of cell abolition takes place. The earliest changes include the loss of cell junctions and specialized membrane structures such as microvilli. The integrity of the cell membrane and of the mitochondria remains initially intact, the cytoplasm condenses and the nucleus coalesces into large masses, which then break up into fragments. The endoplasmatic reticulum transforms into vesicles that fuse with the cytoplasmic membrane. These processes result in contraction of the cytoplasmic volume. The cell adopts a convoluted outline and subsequently the cell breaks up into small vesicles enclosing parts of the cellular contents and apparently intact organelles. These apoptotic bodies end up in the extracellular space, where they are phagocytosed by nearby cells and macrophages. The whole process takes only a few hours and the cell remnants do not elicit any inflammatory reaction (Figure 4-2).

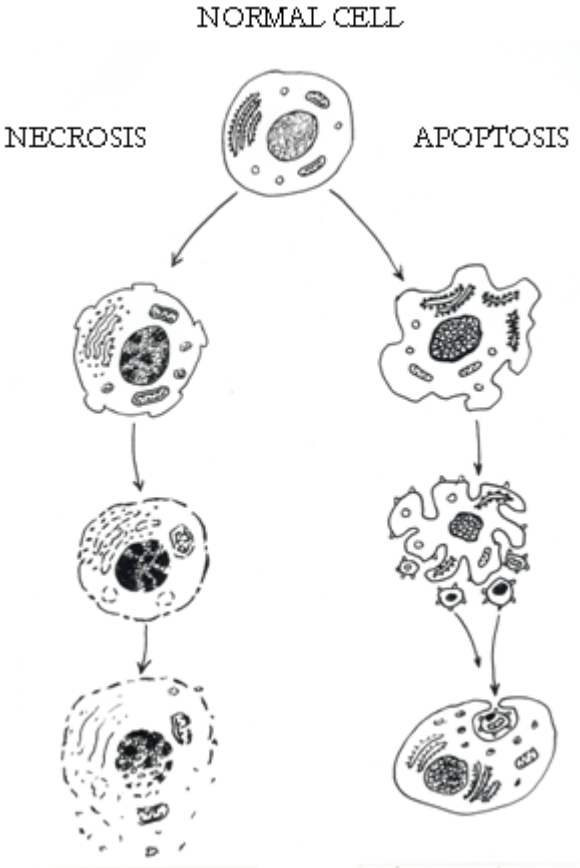

Figure 4-2: The most prominent differences between apoptosis and necrosis. From Vermes and Haanen [1], with permission of Academic Press.

In summary, apoptosis refers to a specific form of programmed cell death, which guarantees the welfare of the whole organism through the elimination of unwanted cells. The duration of apoptosis is short, involves single cells with morphological changes only after the point of no return, ending with phagocytosis without reaction in the neighbour cells. There are number of techniques to measure this cell death, but we still seeking after a simple, specific and sensitive technique which offers the possibility to measure apoptosis on single cell level, without staining, in real time, with high-throughput. The Lab-in-a-Chip concept by using chip technology offers such a tool.

In this chapter apoptotic cell death dynamics of HL60 cells studied using a microfluidic cell trap device is described. This work is published in Lab Chip, 5, (2005), pp.49-55.

4.3 Experimental

4.3.1 Instrumentation

An experimental system was designed and built which allows observation of the temporal evolution of fluorescent and light microscopy changes in HL60 cells following apoptosis and electroporation applications. The chip was mounted on to an X–Y–Z translation stage in an inverted microscope (Leica DM IRM, Leica Microsystems, Wetzlar, GmbH, Germany). The microscope system is equipped with a mercury lamp, 20x, 40x, 50x objectives, and the fluorescence filter set (BP 450-490, LP 515). In addition, a computer-controlled CCD camera (Colorview 8) is mounted in the microscope for imaging recording.

For the electroosmotic flow (EOF) control a computer-controlled high-voltage power supply (CU 4411, IBIS technologies BV, Hengelo, The Netherlands) with four independently controllable positive voltage outputs was used. Gold wires immersed in the reservoirs of a chip holder were used for making the electrical connection to the high voltage supply unit with the fluid in the chip.

4.3.2 Design and fabrication of the cell trap device

The microfluidic cell trapping device consists of two channels which join together in a crossway (Figure 4-3a). The cell trapping microstructures are located in the vicinity of this crossway acting as a filter, i.e. fluid can flow through the trap whereas the cells will block them at least partially. Feature sizes somewhat smaller than the cells that we want to trap, are required. For this purpose, narrow openings which consist in vertical sidewalls are designed across the channel (see Figure 4-4). Several different geometries of the mechanical trap were designed. The trapping microstructures differ from each other in the shape, size, number of trapping sites as well as the number of exits (narrow openings between traps). The diversity of designs should allow defining which trapping microstructure configuration is the

most suitable for analyzing apoptosis on chip. Figure 4-3b and 4-3c show the photographs of the two different trapping layouts used for the experiments in this work.

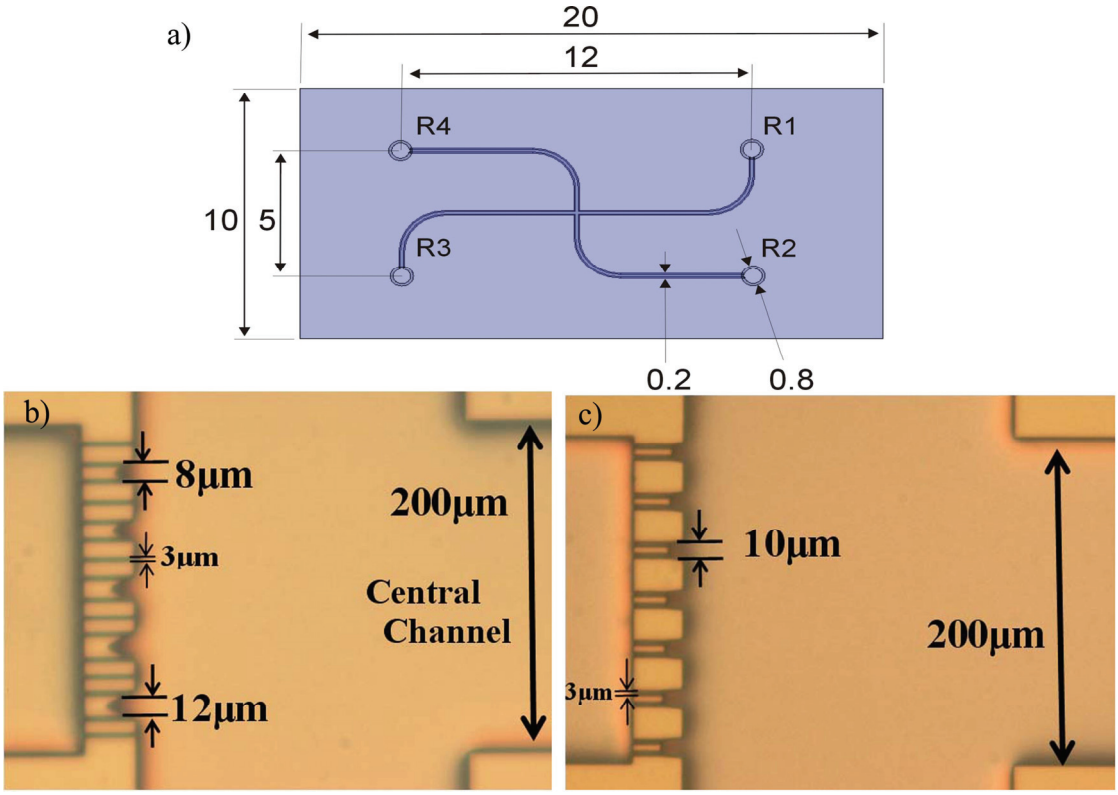

Figure 4-3: a) Drawing of the microfluidic chip with dimensions in mm. Photographs of the trapping sites, b) layout 1 and c) layout 2, in the microfluidic chip design.

The mechanical trap shown in Figure 4-3b (layout 1) contains traps that differ in size. The diameters of the trapping sites vary from 8 µm to 12 µm from top to bottom in this figure. In addition, narrow openings of 3 µm diameter are located between the trapping sites. This layout has been designed as a test structure to determine the most suitable size of the trap. The second layout shown in Figure 4-3c (layout 2) shows a mechanical trap with identical trap diameters (10 µm) and no exit channels are present between them. The 10 µm diameter of the traps was chosen because this is approximately the size of HL60 cells used for the experiments. Figure 4-4 shows a SEM picture of the trapping sites (close-up) designed in layout 1. For both layouts, the dimensions of the channels are 15 µm deep, 200 µm wide and 12 mm long, fabricated with the process that is described in the next paragraph.

The devices are made of a silicon/glass sandwich. The schematic of the fabrication process is shown in Figure 4-5. In the silicon substrate the microfluidic channels and trapping sites are etched by reactive ion etching using the Bosch process (a-d). Access holes from the back side of the silicon wafer are powderblasted (e). After this step the silicon wafer is thermally oxidized at 1100 °C (g). A glass wafer is anodically bonded to the silicon wafer (h), which allows the visualization of the channels and the trapping process as well as optical detection of the fluorescence signal.

4.3.3 HL60 cells

Human promyelocytic leukemic HL60 cells were obtained from the German Collection of Microorganisms (Braunschweig, Germany). HL60 cells were cultured in RPMI-1640 medium supplemented with 10% heat-inactivated and filter-sterilized Fetal Calf Serum, 100 IU/ml penicillin, 100 mg/ml streptomycin, 2 mM L-Glutamine and 250 μg/ml fungizone (RPMI + medium). RPMI-1640 medium was obtained from BioWhittaker (Verviers, Belgium). Supplements and antibiotics were all obtained from Life Technologies (Grand Island, NY, USA). Cell cultures were maintained in a 5% CO_2 humidified atmosphere at 37 °C.

4.3.4 Sample treatment

Different reagents were needed depending on the purpose of the experiment. Therefore, cell treatment differs for each experiment. To validate the estimations obtained with our simulations, HL60 cells suspended in RPMI+ medium (0.5×10^6 cells·ml^{-1}) were mixed with propidium iodide (PI) (Sigma, St. Louis, MO, USA) to obtain a final concentration of 4 μM, at room temperature and isolated from light one hour before the experiment took place. PI is a fluorescent nucleic acid dye that cannot penetrate a viable cell membrane and is thus used extensively as a tracer for surface membrane integrity in living cells.

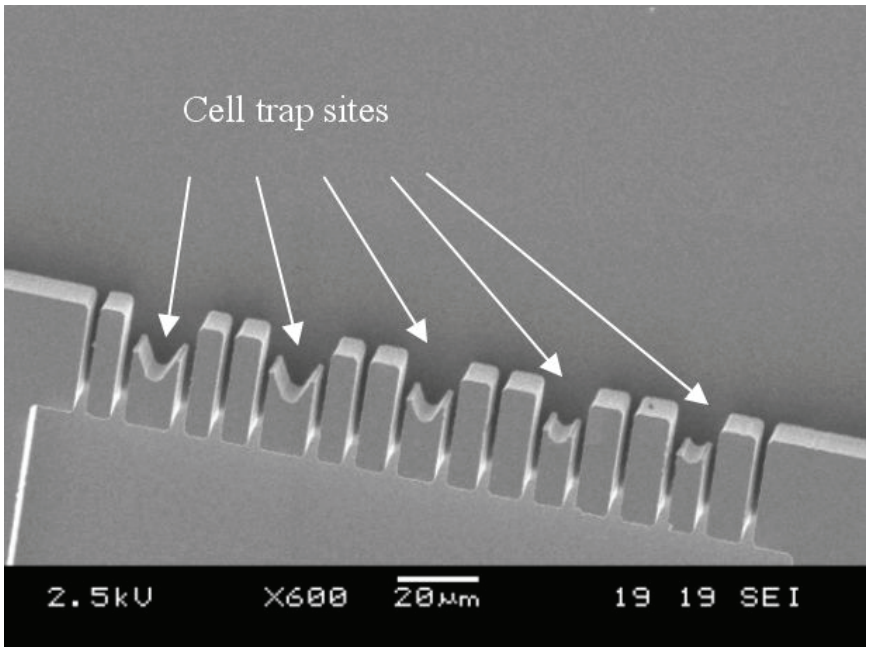

Figure 4-4: SEM picture of the trapping sites (close-up) for layout 1.

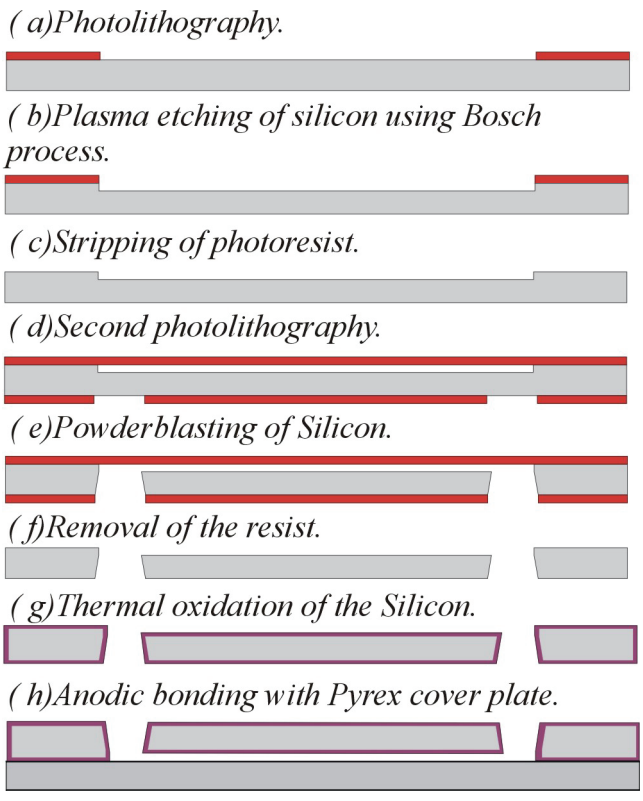

Figure 4-5: Schematic of the fabrication process.

If the cell membrane looses its integrity (late apoptosis and necrosis), PI rapidly enters the cell and readily binds to DNA in the nucleus, developing light to dark red fluorescence. The fluorescence intensity varies with the quantity of PI bound to the DNA providing quantitative information as PI saturates dead and dying cells.

To be able to discriminate between apoptosis and necrosis, the cell treatment was as follows; 125 μl of HL60 cells ($0.5x10^6$ cells·ml^{-1}) were treated with 15 μL of PI (1.5 μM final concentration) and 10 μL of the inhibitor FLICA (20 mM final concentration; FLICA is a mixture of 5 mM FAM-VAD-FMK and 15 mM z-VAD-FMK) obtained from Intergen Co. (purchase, NY, USA). FLICA blocks the activation of caspases and arrests further progress of the apoptotic cascade and prevents cellular disintegration.

In the last case, to study the effect of the apoptotic inducer TNF-α, 99.5 μl of HL60 cells (0.5×10^6 cells·ml^{-1}) were treated with 15 μL TNF-α/ 10.5 μL CHX (3nM /50 μM final concentrations) (Sigma, St. Louis, MO, USA), 15 μL of PI (1.5 μM) and 10 μL of the inhibitor FLICA (20 mM). Immediately after the cell sample preparation, 100 μl of this sample solution was introduced manually in the inlet reservoir of the central channel (see Figure 4-3a, inlet R1)

4.3.5 Procedures

Before starting experiments, the chip was conditioned by rinsing with 100 mM NaOH. In this way all the silanol groups of the wall become activated and we attain the same surface charge at each experiment. Afterwards, NaOH is first replaced by flowing DI water and then by RPMI+ medium that was used as the electrolyte for the electroosmotic flow (EOF) control. 100 μl of the cell sample treated was introduced manually in the inlet reservoir (R1) of the central channel (see Figure 4-3a). The same volume of RPMI+ medium was introduced in each of the rest reservoirs (R2, R3, and R4). A four point voltages scheme at all reservoirs is used to drive the cells towards the trap (see paragraph cell handling).

4.3.6 Cell handling on microfluidic cell-trap chip

The integrated trapping structure in a flow-through chip represents a way of handling single cells. Cells were here transported within the microfluidic channels by means of electroosmotic flow (EOF). EOF control experiments were carried out in both layouts in order to perform single cell handling and positioning.

The voltage scheme used for driving the cells from the central channel towards the trapping sites was set at the sample compartment (R1) to 100 V, at the reservoir behind the trap (R3) to 0 V and at the other two reservoirs to 50 V (see Figure 4-3a). These settings were maintained until the cells were getting close to the trapping sites. At this moment, the electrical resistance in the trapping site is increased due to the presence of the cells and in order to continue addressing the coming cells towards the trap the voltage in the reservoirs 2 and 4 was increased to a value of 80 V.

At first, by using the cell trap device with layout 1 (Figure 4-3b), we observed that cells get trapped also at the small side channels located between the traps. Therefore for the next series of experiments the mechanical trap with layout 2 (Figure 4-3c) was used, where all the traps have the same size.

4.4 Results and discussion

4.4.1 Simulation and determination of system parameters

Using equivalent electrical circuit design for the electrolyte-filled sections of the microfluidic network, an estimation of the potential drop across the trap feature can be made as shown in Figure 4-6. Conductivity of the medium (1.363 $S \cdot m^{-1}$), dimensions of the channels and traps/geometry and voltage scheme used during the EOF experiments were the input values for the program. It is assumed that cells sit perfectly at the traps and seal them nicely giving a high electrical resistance, Mega ohm sealing. At a driving voltage scheme indicated in the previous section (V_1=100 V, V_2=50 V, V_3=0 V and V_4= 50 V) and for the case where all the traps are free, the voltage drop across the trap (1 V) exceeds already the transmembrane potential and cell membrane permeabilization can occur [25, 26]. If the number of traps blocked increases the total voltage drop over the trap becomes higher.

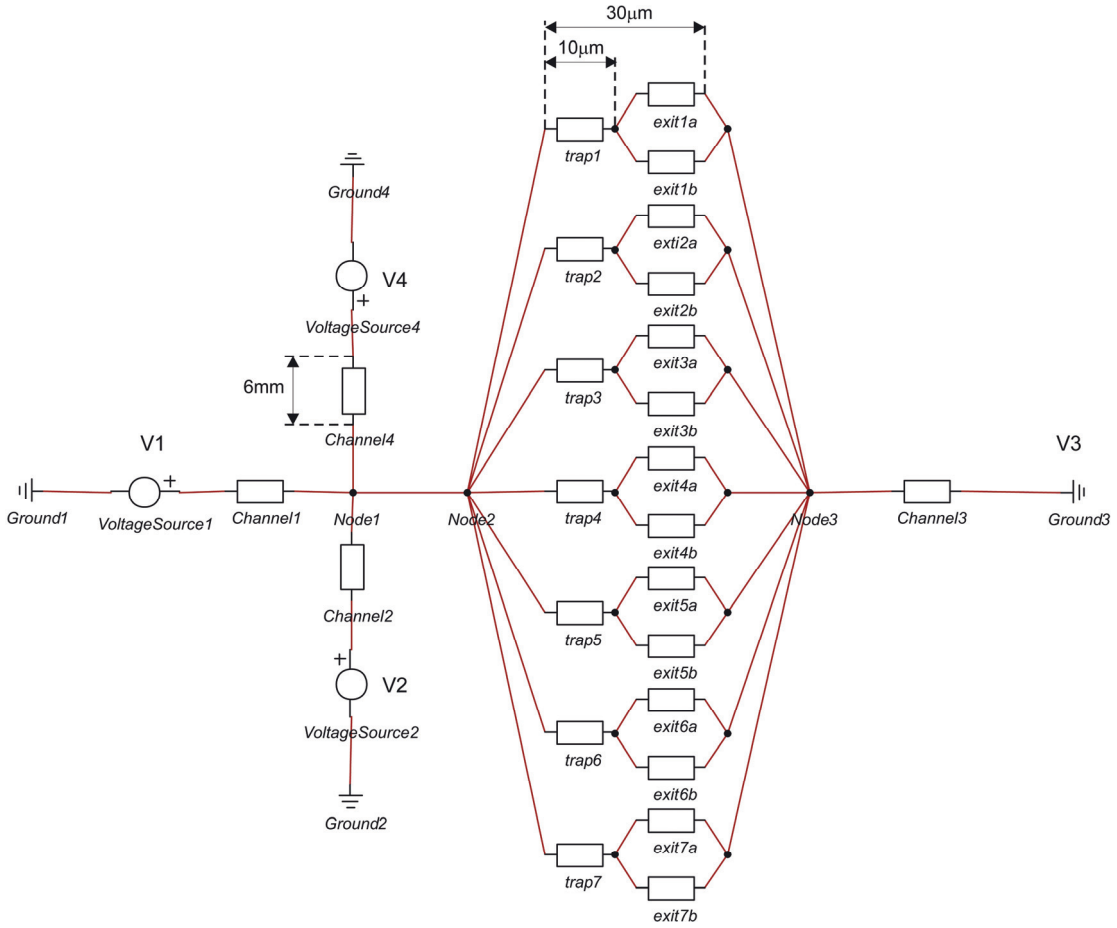

Figure 4-6: Equivalent electrical circuit of the cell trapping device (layout 2) using 20-Sim.

4.4.2 Apoptotic and necrotic cell death dynamics studies on chip. Morphological assessment of cell death by fluorescence microscopy.

1) Electric field mediated cell death

We performed the following assessment in order to check whether the potential drop over the trap will be powerful enough to create cell death (either via apoptosis or necrosis) due to cell membrane permeabilization. At the beginning of the experiment, the cell sample was viewed under the mercury lamp and no PI uptake was observed. However, at the time the cells were sitting in the trap, red fluorescence was shown, meaning that the cell membrane has lost its integrity by

the applied electric field. To determine if the loss in cell membrane integrity has been caused by the applied electric field or by mechanical lysis through the microchannels the following experiment was carried out. In this case, cells were driven towards the trapping sites by means of pressure driven flow (PDF). Once the cells were located in the traps no PI uptake was observed. At this point, by switching on the EOF voltage scheme mentioned above in the cell handling section, we observed the uptake of PI by the red fluorescence of the cells sitting in the traps (data not shown). Therefore, we can conclude that cell membrane disruption is caused by the applied electric field and no due to mechanical lysis.

In Figure 4-7 the result of the EOF driven cell trapping is shown. Figure 4-7a shows the fluorescence image of the first cells trapped when the voltage scheme is on; cells inside of the trap took up PI immediately after docking. Figure 4-7b shows the light microscopy image of the cells 10 seconds after the electroosmotic flow was stopped and Figure 4-7c is the fluorescence image of Figure 4-7b. Comparing Figures 4-7b and 4-7c, we can conclude that the cells inside of the trap show the red fluorescence but the cells in the vicinity of the trap do not, and they can be further investigated (as done in subsection 3). Observation of the cells located in other places apart from the trap, e.g. channels, did not show red fluorescence, therefore we can conclude that the presence of the EOF in the channels did not affect the cell viability as shown in Figures 4-7d and 4-7e. With this assessment we were able to show the electropermeabilization effect of the applied electric field used for the microfluidic control over the cells being located in the trap. Likewise, the experiment confirms the validity of our simulations. On the other hand, with the performed experiment it is not possible to discriminate whether the cells are dead (necrotic cell) or in the process of dying (late apoptotic cell), because in both cell states the cell membrane has lost its integrity, thus showing red fluorescence. In the next step an apoptotic indicator (FLICA) will be added to the cell sample in order to find out whether cells die through apoptosis or necrosis when an electric field is applied.

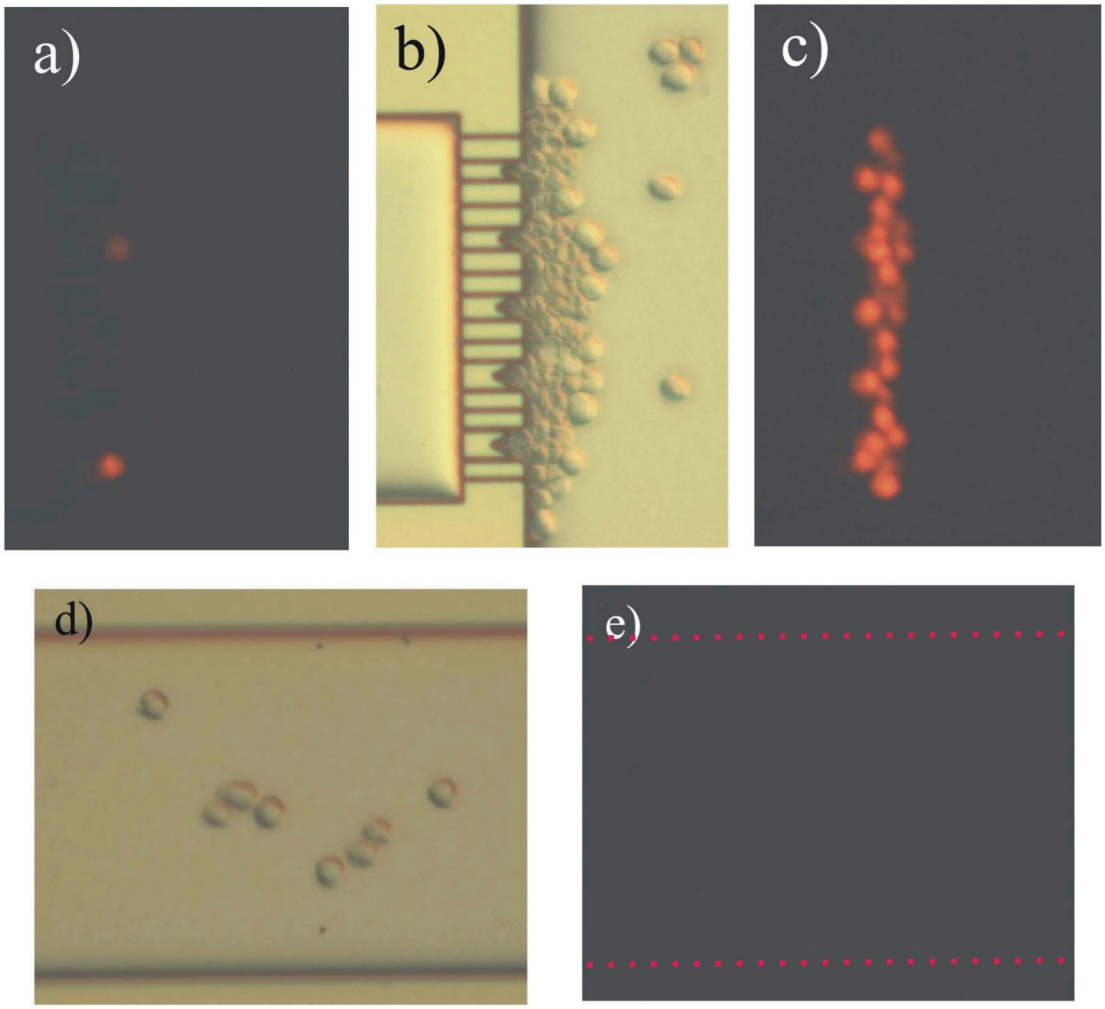

Figure 4-7: PI uptake in HL60 cells sitting at the trap due to the high electric field lines density. a) Fluorescence image at the time the HL60 cells arrive at the trap. b) Light microscopy image of the cells 10s after EOF control was stopped. c) Fluorescence image form image b). d) Light microscopy image of the central channel (R1). e) Fluorescence image from image d).

2) Discrimination between apoptotic and necrotic cells

In the previous experiment we confirmed that cell death was electric field mediated in HL60 cells sitting at the trap. In order to determine whether apoptotic or necrotic processes occurred an apoptosis indicator, FLICA, was used. When cells enter apoptosis, intracellular FLICA binds to activated caspases and blocks their action arresting further progress of the apoptotic cascade and preventing cellular disintegration.

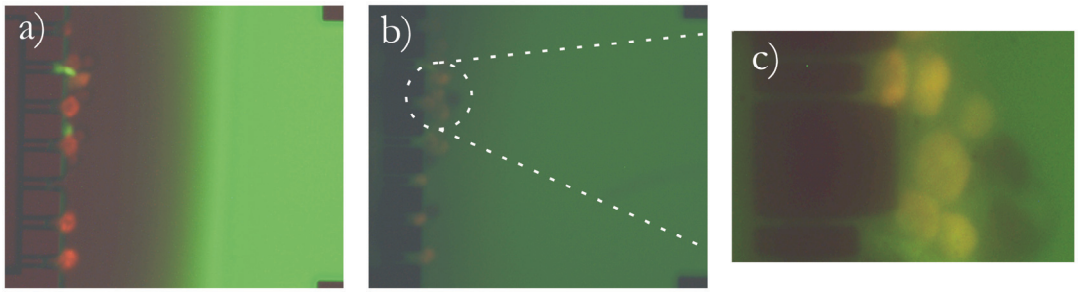

Figure 4-8: Cell discrimination by fluorescence. a) EOF control on; cells sitting at the trap get permeable and PI is uptaken. FLICA moves by means of its electrophoretic mobility. b) EOF control off; FLICA diffuses and enters in contact with the cells being located at the trap, c) zoom in from Figure 4-8b. Cells sitting in the traps show the green (FLICA+) and red (PI+) fluorescence. A second row of cells that have not received the influence of the electric field do not show any fluorescence label; no apoptosis has been induced, viable cells (FLICA-/PI-).

Figure 4-8a it is observed that during the EOF control cells moved towards the trap in the direction of the EOF, while FLICA, being a negative charged molecule moved by means of its electrophoretic mobility. The trapped cells showed red fluorescence, in agreement with the previous experiment. Once the EOF was stopped, FLICA diffused towards the trap where cells were located (see Figure 4-8b). At this point, the cells first showing red fluorescence now show red (PI) and green (FLICA) fluorescence (FLICA+/PI+, see Figure 4-8c). This bicolor fluorescence pattern is characteristic of cells being at the late apoptotic state. These results could suggest that apoptotic cell death was induced by the electric field applied. In the case that the electric field mediated cell membrane permeabilization is reversible, meaning that the cell membrane reseals after the EOF voltage is off, the presence of the green fluorescent label (FLICA+) will determine if the process of apoptosis is activated by the applied electric field, because FLICA only binds to activated caspases within the cell. At this point of the experiment, the reversible or irreversible electropermeabilization of the cell membrane remains uncertain and the green fluorescence label can be either by diffusion through a disrupted cell membrane or by caspase activation. However, impedance measurements could allow us to know if resealing of the cell membrane has occurred.

3) Apoptotic cell death dynamics on a chip.

To ensure that apoptotic cell death is induced, HL60 cells were incubated with a mixture of TNF-α and CHX. Apoptotic cell death dynamics was studied in real time on a chip (using layout 2) at single cell level. Time point zero is considered the moment that the cell sample (consisting of HL60 cells, FLICA, PI and TNF-α/CHX) was introduced in the chip reservoir R1.

As described in literature, inducing apoptosis and labeling cells with FLICA and PI makes it possible to identify four subpopulations with flow cytometry: (i) Viable or non- apoptotic cells show neither FLICA nor PI fluorescence. (ii) In the initial phase of apoptosis, the caspases become activated and FLICA binds to these activated caspases while the plasma membrane is still able to exclude PI. In the initial phase of apoptosis, HL60 cells are FLICA+/PI-, early apoptotic. (iii) Subsequently, HL60 cells loose their plasma membrane integrity and their ability to exclude PI. These late apoptotic cells are FLICA+/PI+. (iv) Finally, HL60 cells loose the ability to bind FLICA, because the caspases are either inhibited or degraded, and become FLICA-/PI+. This phase is called the 'necrotic stage' of apoptosis. In the continuous presence of FLICA, this latter phase (FLICA-/PI+) is normally not visible, due to the fact that FLICA arrests the apoptotic pathway in the late apoptotic phase.

Figure 4-9 shows the bivariate distributions of green and red fluorescence intensity from TNF-α/CHX-treated cells exposed to FLICA and PI in the microfluidic cell trap device. HL60 cells, in the continuous presence of FLICA, transit from the viable stage to the early apoptotic stage and then to the late apoptotic stage (see black dotted circles in Figure 4-9, lower and upper cell).

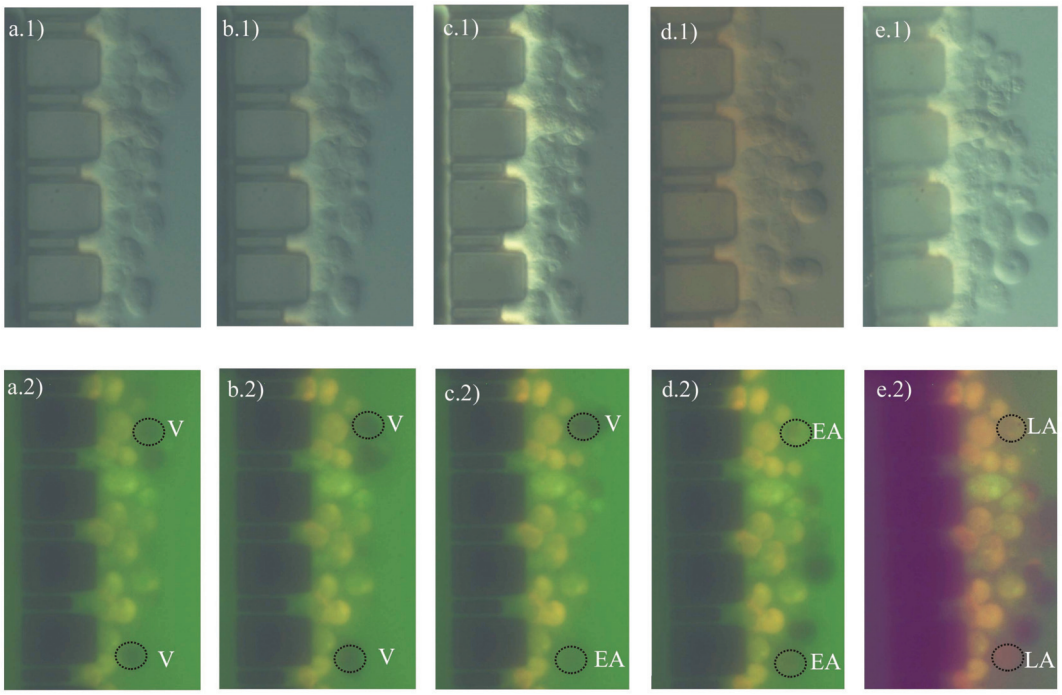

Figure 4-9: Optical images of cell death dynamics. Light (1) and fluorescence (2) microscopy images of HL60 cells sitting at the trap over time a) 1h, b) 2h, c) 4h, d) 6h, e) 24h. V: Viable cell; EA: early apoptotic; LA: late apoptotic.

At completion of the experiment, analysis of the fluorescence images from Figure 4-9 was performed. For each series of fluorescent images, areas of interest were defined manually for each cell (named upper and lower cell) upon their positions over time. Images areas of approximately of 92×93 pixels^2 containing one cell only, were estimated from the white light image. The average green and red scale intensity of each area of interest was then automatically calculated for each image. This was calculated, for the two cells of interest three times and an average value ± std dev. is given. Consequently, the temporal development of FLICA and PI fluorescence in individual cells across time could be graphed as mean fluorescence intensity (in arbitrary units) *versus* time, as shown in Figure 4-10. An increase in FLICA fluorescence (between 4 and 6 hours) determines that the apoptotic process has been activated.

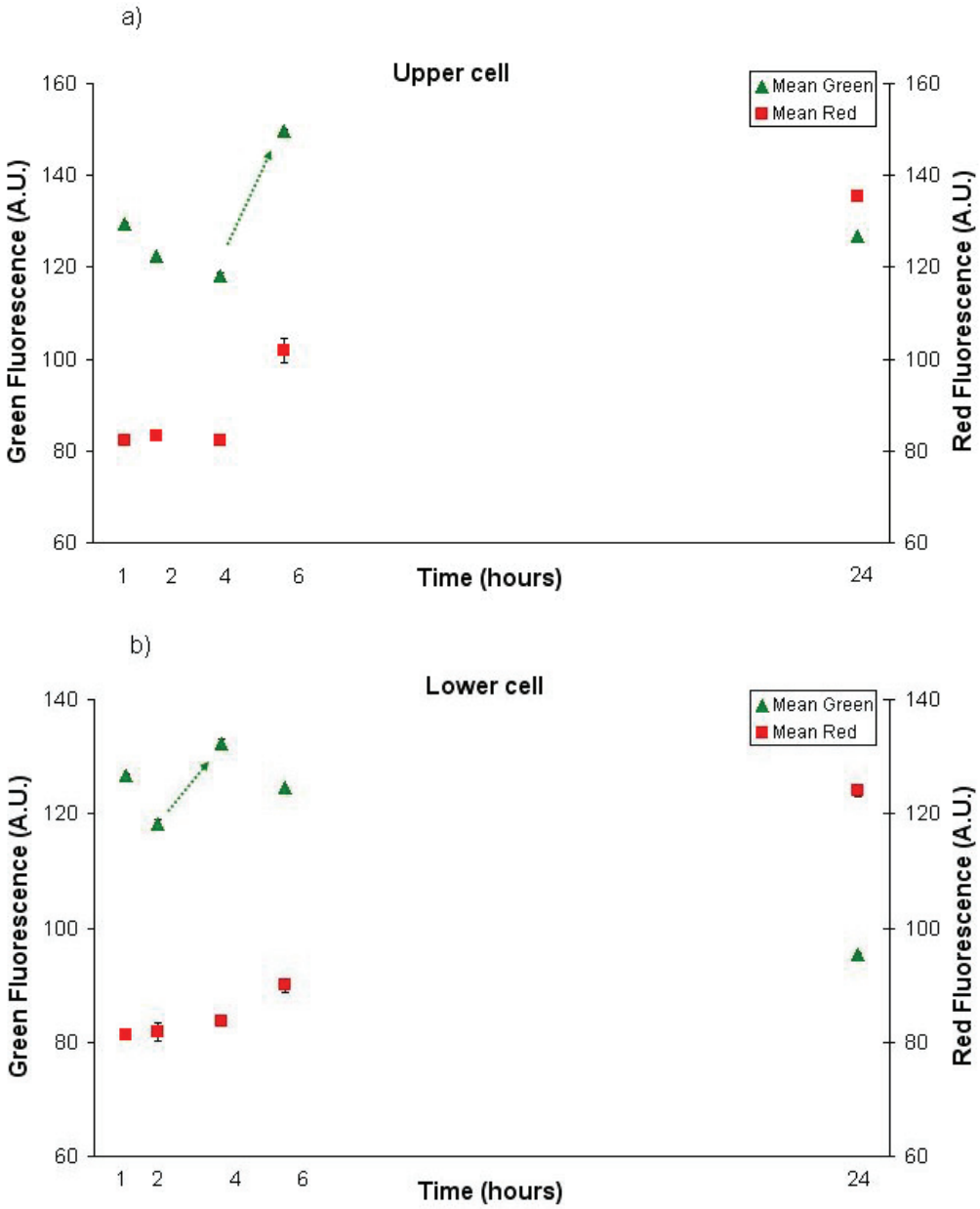

Figure 4-10: TNF/CHX induced apoptotic cell death dynamics. Green (FLICA) and red (PI) fluorescence intensity of upper a) and lower b) HL60 cell in time (trend is indicated by the arrow).

4.5 Conclusions

Here we present for the first time that it is possible to follow the steps in apoptotic cell death cascade in real time within our newly developed microfluidic cell trapping device. Localization of cells in the trap allows light and fluorescent imaging on several cells on a single cell basis simultaneously within the field of view. Therefore, the cellular changes appearing when inducing apoptosis can be visualized by both light microscopy and through the bivariate distributions of green (FLICA) and red (PI) fluorescence. HL60 cells incubated with TNF-α/CHX transit from viable to early apoptotic and eventually to late apoptotic in the continuous presence of FLICA, during the course of the cell death cascade.

It is known in literature that electric fields induce apoptosis in HL60 cells [27]. However, with the used biochemical assay we were not able to compare the effect of the two inducers (TNF-α/CHX and electric field) because uncertainty remains in electric mediated cell death.

In the near future impedance measurements will be performed to ensure that electric-field mediated apoptosis has occurred. This will make possible to compare the effects of different inducers on the apoptosis process. In addition, coupling a spectrometer to the microscope will allow quantitative measurements in fluorescent intensity from the different apoptotic stages of the cells in more detail.

Nowadays there are many assays present to detect cell death, however measuring apoptosis in a microfluidic cell trap device offers many advantages over the present conventional (flow cytometry) methods. Besides the benefits to measure apoptosis on a single cell level and in real time, it is now also possible to follow the intracellular changes within a cell. Conventional apoptotic methods use cell suspensions as a representation of the total cell culture (tissue), not knowing how the different cells react. However, in this device it is possible to investigate the reaction of one cell to a certain inducer and also investigate how cells react with each other in time. Further, fewer cells are needed, which is of special interest when primary cells (directly prepared from fresh tissue or fluids from an organism) are used [11]. Moreover, this device offers possibilities to investigate dose-response relations within the same cell and between cells in real time. Thus, adapting the present conventional techniques to chip technology will offer many benefits and will obtain new insight in the apoptotic cascade.

4.6 References

[1] I. Vermes and C. Haanen - *Apoptosis and Programmed Cell-Death in Health and Disease;* Advances in Clinical Chemistry, **31** (1994), pp 177-246.

[2] I. Vermes, C. Haanen and C. Reutelingsperger - *Flow cytometry of apoptotic cell death;* Journal of Immunological Methods, **243 (1-2)**, (2000), pp 167-190.

[3] F. Wolbers, P. Buijtenhuijs, C. Haanen and I. Vermes - *Apoptotic cell death kinetics in vitro depend on the cell types and the inducers used;* Apoptosis, **9 (3)**, (2004), pp 385-392.

[4] N. A. Thornberry and Y. Lazebnik - *Caspases: Enemies within;* Science, **281 (5381)**, (1998), pp 1312-1316.

[5] M. O. Hengartner - *The biochemistry of apoptosis;* Nature, **407 (6805)**, (2000), pp 770-776.

[6] H. Andersson and A. v. d. Berg, -*Lab on a chips for Cellomics;* Kluwer academic publishers (2004).

[7] H. Andersson and A. van den Berg - *Microfluidic devices for cellomics: a review;* Sensors and Actuators B, **92 (3)**, (2003), pp 315-325.

[8] H. Andersson and A. van den Berg - *Microtechnologies and nanotechnologies for single-cell analysis;* Current Opinion in Biotechnology, **15 (1)**, (2004), pp 44-49.

[9] H. Lu, S. Gaudet, M. A. Schmidt and K. F. Jensen - *A microfabricated device for subcellular organelle sorting;* Analytical Chemistry, **76 (19)**, (2004), pp 5705-5712.

[10] H. Lu, L. Y. Koo, W. C. M. Wang, D. A. Lauffenburger, L. G. Griffith and K. F. Jensen - *Microfluidic shear devices for quantitative analysis of cell adhesion;* Analytical Chemistry, **76 (18)**, (2004), pp 5257-5264.

[11] A. Tixier-Mita, S. Ostrovidov, M. Chiral, M. Frenea, B. Le Pioflue and H. Fujita -*Proceedings of MicroTotal Analysis System;* microTAS, (2004), pp 180-183.

[12] N. J. Dovichi and D. Pinkel - *Analytical biotechnology - Tools to characterize cells and their contents - Editorial overview;* Current Opinion in Biotechnology, **14 (1)**, (2003), pp 3-4.

[13] S. A. Sundberg - *High-throughput and ultra-high-throughput screening: solution- and cell-based approaches;* Current Opinion in Biotechnology, **11 (1)**, (2000), pp 47-53.

[14] S. D. H. Chan, G. Luedke, M. Valer, C. Buhlmann and T. Preckel - *Cytometric analysis of protein expression and apoptosis in human primary cells with a novel microfluidic chip-based system;* Cytometry Part A, **55A (2)**, (2003), pp 119-125.

[15] K. Kleparnik and M. Horky - *Detection of DNA fragmentation in a single apoptotic cardiomyocyte by electrophoresis on a microfluidic device;* Electrophoresis, **24 (21)**, (2003), pp 3778-3783.

[16] E. Tamaki, K. Sato, M. Tokeshi, K. Sato, M. Aihara and T. Kitamori - *Single-cell analysis by a scanning thermal lens microscope with a microchip: Direct monitoring of cytochrome c distribution during apoptosis process;* Analytical Chemistry, **74 (7)**, (2002), pp 1560-1564.

[17] S. Gawad, L. Schild and P. Renaud - *Micromachined impedance spectroscopy flow cytometer for cell analysis and particle sizing;* Lab on a Chip, **1 (1)**, (2001), pp 76-82.

[18] Y. Huang, N. S. Sekhon, J. Borninski, N. Chen and B. Rubinsky - *Instantaneous, quantitative single-cell viability assessment by electrical evaluation of cell membrane integrity with microfabricated devices;* Sensors and Actuators A, **105 (1)**, (2003), pp 31-39.

[19] P. Smolewski, J. Grabarek, B. W. Lee, G. L. Johnson and Z. Darzynkiewicz - *Kinetics of HL-60 cell entry to apoptosis during treatment with TNF-alpha or camptothecin assayed by the stathmo-apoptosis method;* Cytometry, **47 (3)**, (2002), pp 143-149.

[20] J. F. R. Kerr, A. H. Wyllie and A. R. Currie - *Apoptosis: A basic biological phenomenon with wide-ranging implications in tissue kinetics;* British Journal of Cancer, **26** (1972), pp 239-257.

[21] A. H. Wyllie, J. F. R. Kerr and A. R. Currie - *Cell death: The significance of apoptosis;* Int Rev Cytol, **68** (1980), pp 251-300.

[22] N. N. Daniel and S. J. Korsmeyer - *Cell death: Critical control points;* Cell, **116** (2004), pp 205-219.

[23] B. Fadeel - *Programmed cell clearance;* Cellular and Molecular Life Science, **60** (2003), pp 2575-2585.

[24] K. S. Ravichandran - *"Recruitment Signals" from apoptotic cells to a quiet meal;* Cell, **113** (2003), pp 817-820.

[25] J. L. Rae and R. A. Levis - *Single-cell electroporation;* Pflugers Archiv-European Journal of Physiology, **443 (4)**, (2002), pp 664-670.

[26] J. C. Weaver - *Electroporation: general phenomenon for manipulating cells and tissues* Journal of Cell Biochemistry, **51 (4)**, (1993), pp 426-435.

[27] J. Pinero, M. Lopez-Baena, T. Ortiz and F. Cortes - *Apoptotic and necrotic cell death are both induced by electroporation in HL60 human promyeloid leukaemia cells;* Apoptosis, **2 (3)**, (1997), pp 330-336.

5

Electroporation of cells in cell trap device

In this chapter single cell electroporation in different cell trapping devices is presented. A detailed electrical characterization for single cell electroporation is performed with two cell lines, viz. HL60 and C2C12. Successful gene transfection and protein expression in single cells is accomplished. Compared to bulk electroporation a much higher success rate is observed.

5.1 Introduction

In this chapter single cell electroporation and gene transfection in different cell trap devices is presented. In chapter 2 an overview of electroporation of cells in microfuidic devices is presented. Very few examples of gene transfection on a chip have been published [1-3]. Conventionally, gene transfection is performed in bulk, either by electroporation or others treatments like bombardment with micro-pellets coated with DNA, viral vectors [4-6] usually with very low yields. In section 5.2 simulations and experiments performed on the first generation of a cell trap device is discussed. This is followed by a section (5.3) in which a second generation is described, containing independently addressable cell traps. With both devices Single Cell Electroporation (SCE) is performed successfully. A detailed electrical characterization of single cell electroporation is performed with the second generation using two different cell lines, viz. HL60 cells (sections 5.3.3) and C2C12 cells (section 5.3.4). Finally, in section 5.3.5 the microfluidic cell trap device is used to efficiently transfer genes and express proteins in single cells.

5.2 Cell trap device: generation 1

5.2.1 Design and fabrication

The first microfluidic device developed for single cell electroporation studies is the so-called 'suction trapping device' which consists of two channels that are connected by microholes. These microholes act as trapping sites for living cells. The two channels (widths 50 μm and 20 μm, respectively), as well as the nine trapping sites (4 μm wide) are etched to a depth of 15 μm using (Deep) Reactive Ion Etching ((D)RIE). The fabrication process is identical to the process of the filter trapping devices as described in chapter 3 (section 3.3.4). There are two designs of trapping sites, a straight trap (type 1), and a trap with two side channels (type 2); both are shown in Figure 5-1. Gold wires immersed in the reservoirs of the chip were used to make electrical connections to a high-voltage supply unit.

5.2.2 Microfluidic control

The cell sample flows along the upper channel, while the lower channel is used to create a pressure gradient; this is accomplished by suction on the bottom access hole (4).

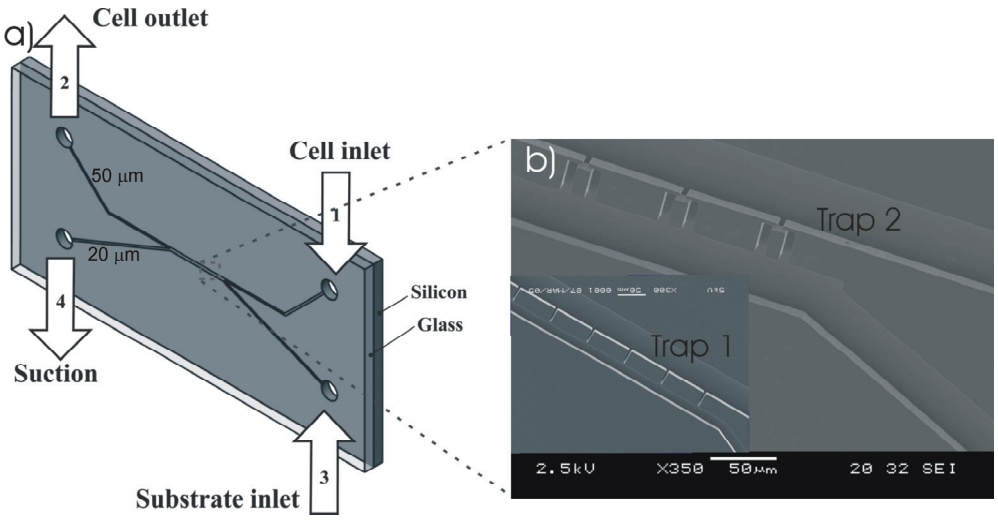

Figure 5-1: (a) Schematic drawing of microfluidic cell trap device and (b) SEM pictures of the two designs for the trapping structures.

The effect of this pressure gradient between the upper channel (containing the cell sample) and the lower channel is that the cells will be trapped (mechanically) at the trapping sites. The process sequence to trap cells at the sites in this chip is as follows. First, the chip is filled with the desired buffer using capillary forces. Then 100 μl of buffer solution is added to all the reservoirs. Subsequently 100 μl of cell sample is placed in inlet (1) (see Figure 5-1). Cells are then transported towards the trapping sites by means of pressure-driven flow, which is initiated by removing 50 μl of buffer solution from the top outlet reservoir (2). To trap single cells, a negative pressure is applied to the suction reservoir (4), either with a micropipette or via a pump. Once the cells are trapped, the pump is switched off and cells remain localized at the traps, ready to be used for electroporation studies. In Figure 5-2 this trapping principle is shown, as well as a picture of traps containing a cell.

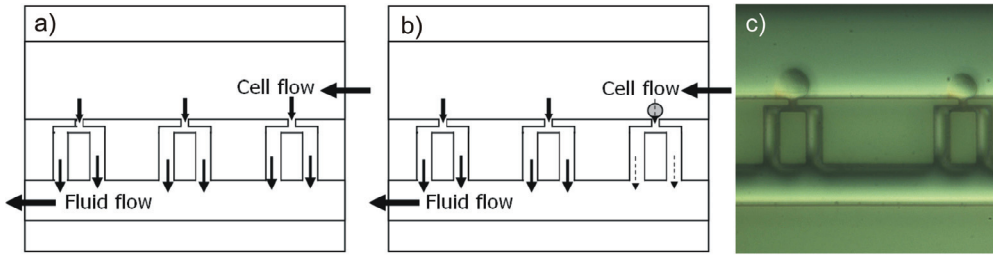

Figure 5-2: (a-b) Schematic drawing of the flow control for the cell trapping and (c) picture of two cells located at the trapping sites.

5.2.3 Electric field simulations

The electric field distribution for this suction trapping device is modeled using finite element software (Femlab 3.0, Comsol, Sweden). The DC conductive medium model was used for a steady state situation, which solves Gauss' differential equation. The boundary conditions are considered as being electrical insulated, with a voltage difference of 100 V. The channel has a conductivity of $0.1 \cdot S\ m^{-1}$.

The electric field distribution in this device clearly shows that the electric field is focused only at the outer trapping sites (Figure 5-3a), viz. the traps that are located close to the electrodes, gold wires immersed in the reservoirs, while nearly no electric field is present in the middle traps (Figure 5-3c).

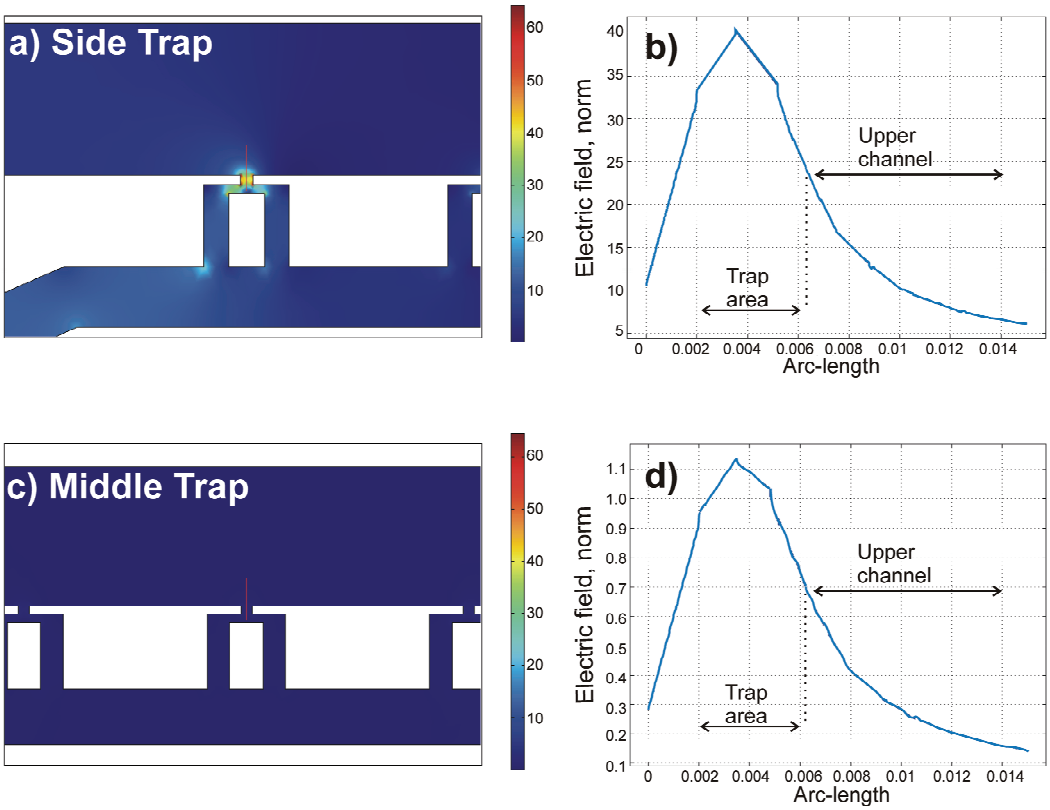

Figure 5-3: Electric field distribution in the cell trapping device (a-b) for the side traps and (c-d) for the middle traps.

5.2.4 Results and discussion

The results from the electric field simulations showed that only the side traps are effective for cell electroporation. To confirm these simulations cell experiments with human promyelocytic leukemic (HL60) cells are performed. HL 60 cells are cells in suspension, easy to handle and with an average size of 10 μm in diameter. In these experiments, gold wires immersed in all the reservoirs of the chip were used to make electrical connections to a high-voltage supply unit. Cells were loaded and trapped in the chip as described in section 5.2.2. Cell viability was checked immediately after cell trapping by adding Propidium Iodide (PI, 15 μM) to the microfluidic channels as a live/death stain, before the electroporation signal was delivered. PI is a cell impermeable membrane integrity indicator: it cannot permeate through the intact cellular membrane, but a damage

membrane cannot prevent PI to enter. PI will intercalate with the nuclear DNA causing red fluorescence.

After trapping, the cells did not show red fluorescence, indicating viable cells. Subsequently, PI was removed from the microfluidic channels by rinsing thoroughly with the electroporation buffer (10 mM HEPES, 140 mM NaCl, 2.68 mM KCl, 1.7 mM $MgCl_2$, 25 mM glucose, 2.5 mM $CaCl_2$, pH 7.4) supplemented with FITC-Annexin V (0.125% v/v). Annexin V is a phospholipid binding protein with high affinity for phosphatidylserine (PS) which is under viable cellular conditions located in the cytoplasmic side of the cell membrane (inner leaflet). Annexin V can not pass the cell membrane under normal conditions. Annexin V is coupled to FITC (fluorescein isothiocyanate) which enables the detection of the binding of the protein to PS. Next, a voltage difference was applied between the wires in the top reservoirs (1 and 2) and the wires in the bottom reservoirs (3 and 4). Results of this electroporation experiment are shown in Figure 5-4.

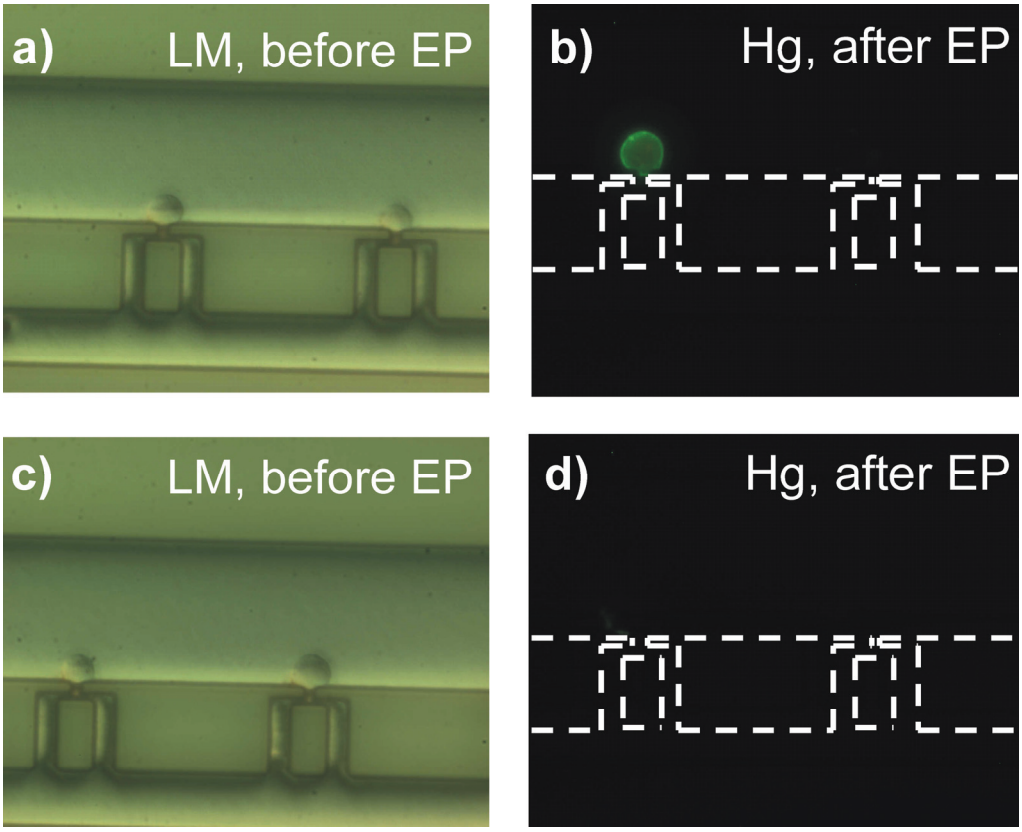

Figure 5-4: Light and Fluorescence images of cells before and after electroporation. (a-b) side traps. (c-d) middle traps.

As can be seen, indeed only the cell located at the side trap, the closest to the electrode, shows the green fluorescence, indicating Annexin V binding to PS and therefore cell permeabilization (Figure 5-4 a & b). The cells located in the middle traps (Figure 5-4 c & d) remain dark after electrical pulse is delivered, thus no cell membrane permeabilization took place. These experiments were also performed with PI as indicator and identical results were obtained (data not shown): in this chip only the side traps can be used for electroporation. A microfluidic cell trap device with significant better electroporation efficiency, a chip in which all nine traps can be used for single cell electroporation is discussed in section 5.3.

5.3 Cell trap device: generation 2

5.3.1 Design and fabrication

A chip (suction device) in which all trapping sites can be used for single cell electroporation can be achieved by implementing independent electrodes for all trapping sites. Thus, instead of using one electrode pair for all (nine) sites, in this redesigned chip each trap will have its own electrode pair for single cell electroporation of the trapped cell. In Figure 5-5 a picture of the second generation device for electroporation is shown: it contains strategically positioned electrodes for all traps. For the electroporation signal a voltage difference is applied between the top electrode and the bottom one (ground electrode, which is a common electrode for all the traps). Integration of the electrodes in the microfluidic device is done by sputtering a platinum thin-film on the Pyrex wafer (in recess areas, to avoid bonding problems). Besides this step, the fabrication is identical to the process in chapter 3. Channels and trap dimensions are identical to the values indicated in section 5.2.1.

The flow control and cell trapping in this chip is identical to the procedure described in section 5.2.2.

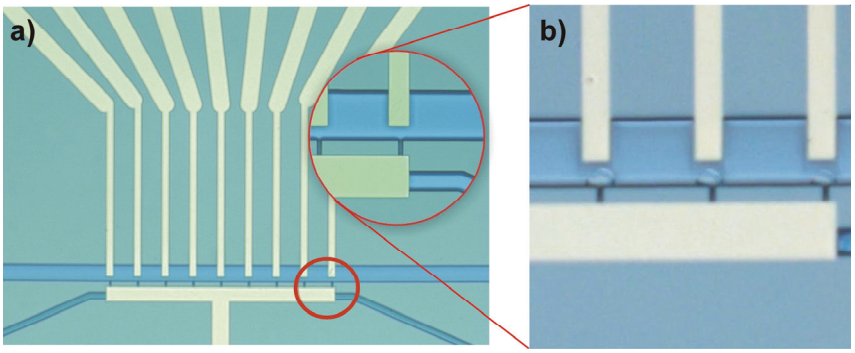

Figure 5-5: (a) Image of the microfluidic device with integrated electrodes and a zoom in of the trapping sites (4 μm width). (b) a close-up of trapping sites showing three cells being trapped and ready to be electroporated.

5.3.2 Electric field simulations

The electric field distribution is modeled for this device using finite element software (Femlab 3.0, Comsol, Sweden). The DC conductive medium model was used for a steady state situation, which solves Gauss' differential equation. The boundary conditions are considered as being electrical insulated, with the two electrodes being 1 V and grounded. The channel has a conductivity of 0.1 $S \cdot m^{-1}$. The electric field distribution in the second generation cell trapping device clearly shows that the electric field is focused at the site where the cell is trapped (Figure 5-6a). The electric field strength in the upper channel is negligible compared to the electric field strength at the trapping site, thus cells which are not trapped will not be influenced by the electric field. This is also found (see Figure 5-6b) when the electric field strength between the two electrodes is plotted along the line depicted in Figure 5-6a. Figure 5-6b also shows that a voltage difference of 1 V already gives an electric field strength of 0.57 $kV \cdot cm^{-1}$ over the trap. As the trapping device consists of nine parallel trapping sites, leakage currents between neighboring traps could occur. This has been verified in a multi-trapping site model: it is found that this issue is negligible since the resistance between the high voltage electrode of a trapping site and the grounded electrode of a neighbouring site is significantly higher than the resistance between the electrodes of the same trapping site. A more detailed study of the electric field distribution in this generation of cell trap device is given in chapter 6.

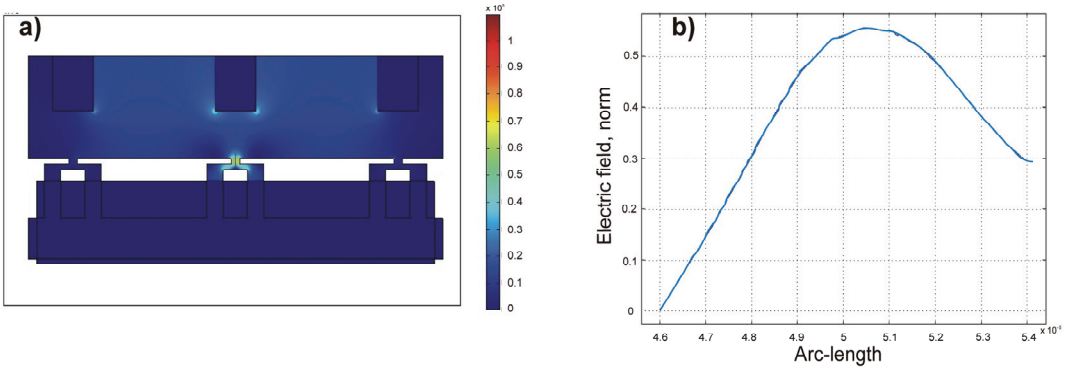

Figure 5-6: Electric field distribution in the cell trap device with integrated electrodes (generation 2).

5.3.3 Single cell electroporation of HL60 cells

The most important parameters for effective electroporation of a cell are the electrical field strength (E-field) and the time this field is applied (pulse length). However, a variety of other parameters influences the efficiency of electroporation as well, such as the shape of the electrical pulse, polarity, number of and interval between pulses, size of target cells, and thermal conditions during and after the pulse, as well as other cellular and environmental factors. The electroporation process can be followed by looking at the uptake of molecules (PI for example) by the treated cells. Besides the size of the initiated pores in the membrane by electroporation, the uptake of molecules depends also on their molecular size, charge, and other physico-chemical properties. It is beyond the scope of this chapter to discuss the state of knowledge about the importance of all these parameters, especially since conclusive studies are still lacking.

In this section we determine the voltage (or *E*-field) and pulse length needed for cell membrane permeabilization of individual HL60 cells that are trapped in the cell trap device. Cell membrane permeabilization of HL60 cells is studied by using PI as membrane integrity indicator. In a series of experiments pulses with different amplitudes and/or pulse lengths were applied to individual cells and the fluorescence intensity of the cell was detected one minute after each single pulse. At the start of each experiment, trapped cells were not red-fluorescent, indicating that

the cell membrane was intact. Figure 5-7 shows the relationship between the field strength and/or pulse length for PI uptake in HL60 cells.

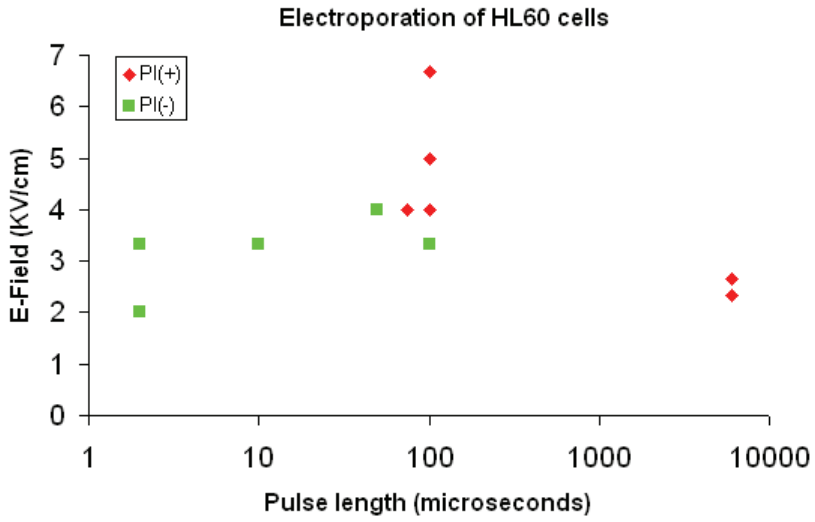

Figure 5-7: Relation between electric field strength and pulse length for PI uptake in electroporation of HL60 cells.

Field strengths above 4 kV·cm^{-1} and/or pulse lengths longer than 75 μs caused permeability of the cell membrane, thus successful electroporation. However, too high field strengths and/or pulse lengths will lead to an unstable situation where the cell can not reseal and will disintegrate (cell lysis) and die. If the field strength is too low (< 4 kV·cm^{-1}), the breakdown transmembrane potential is not achieved; similarly, if the pulse length is too short (below 75 μs), the membrane cannot be charged enough to reach the electroporation membrane potential. Overall, field strength and pulse length can be traded off to a certain extent to obtain electroporation. All experiments were performed twice, giving the same results in PI uptake. The experiments showed that single cell electroporation is achieved at each individual trap in this device, as predicted with simulations (5.3.2).

After the electrical parameters were determined, PI was removed from the microfluidic channels by flushing cell culture medium. 30 minutes after electroporation of the cells, FITC-Annexin V was added to the cell trap device. All the red fluorescent cells [PI (+)] showed FITC-Annexin V staining, as indicated by their green fluorescence (Figure 5-8). This means that either the electrical treatment

was too strong (cells are going to dye, apoptosis), that the cell membrane did not reseal completely or that phosphatidylserine (PS) is translocated from the inner to the outer leaflet of the plasma membrane during electroporation process (and thus exposing PS to the external cellular environment).

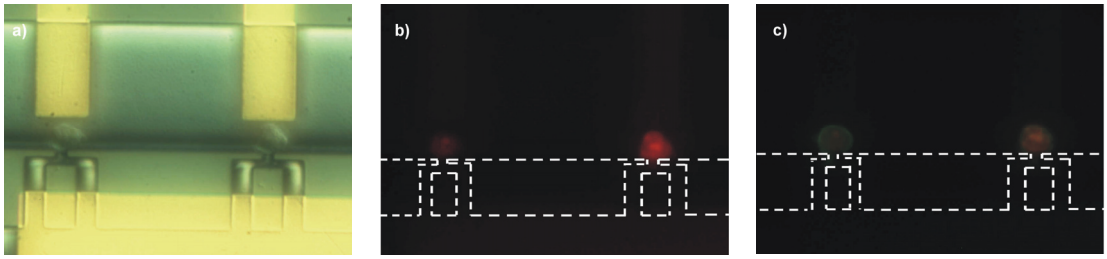

Figure 5-8: a) Light microscopy image of HL60 cells after EP, b) fluorescence image of picture a) showing PI (+) cells and c) fluorescence image of the same cells showing FITC-Annexin V staining.

The effect of the pulse length on the PI uptake by HL60 cells was further analysed. For these experiments the electric field was fixed at 4 $kV \cdot cm^{-1}$ and the pulse length had to be sufficiently long enough to allow PI to enter in the cell. PI was added to the microfluidic channels once the cells were trapped at the sites. Before the electrical pulses were applied, trapped cells were not red fluorescent [PI (-)], indicating that the cell membrane was intact. Fluorescence images were taken one minute after the electrical pulse was applied. The results are shown in Figure 5-9. As can be seen, an increase in pulse length from 50 μs to 100 μs gives rise to an increased fluorescence intensity of PI (more PI is uptaken by the cells).

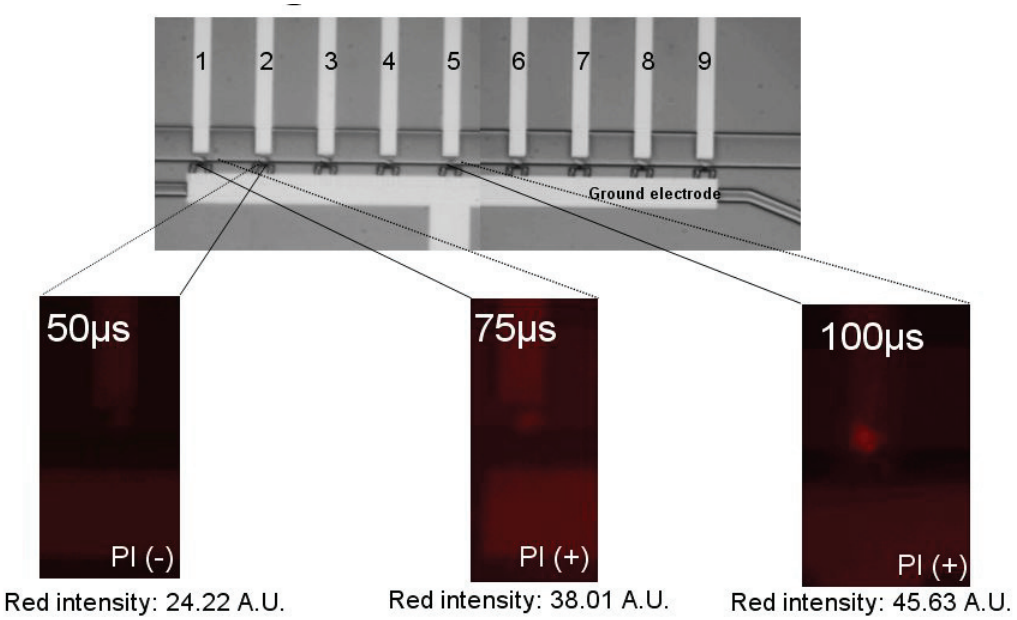

Figure 5-9: PI uptake in HL60 cells at different pulse lengths.

5.3.4 Single cell electroporation of C2C12 cells

The electroporation studies described for HL60 cells were also done for mouse myoblastic cells (C2C12). C2C12 cells are adherent cells, in contrast to HL60 cells which are cells in suspension. Moreover, C2C12 cells are bigger than HL60 cells (cell diameter 16-20 µm vs. ~10 µm, respectively). These cells are "stem cells like" since they can differentiate rapidly, forming contractile myotubes. C2C12 cells are used in this study as a model for stem cells and are investigated for gene transfection studies.

In general, it is known that the optimal electrical parameters differ for different molecules. For example, the delivery of low molecular weight drugs into mammalian cells typically requires fields of 1 $kV \cdot cm^{-1}$ and pulse lengths of 100 µs are effective, whereas for the delivery of genes lower fields ($>50 \cdot V \cdot cm^{-1}$) and longer pulses (20 ms) yield better results. The applied electrical parameters also depend on the application. If the goal is intracellular delivery of a chemotherapeutic agent to kill tumor cells, exceeding the upper limit of electroporation which leads to lysis of the cells is acceptable, whereas for the delivery of genes it is desirable to select the experimental parameters within the region of effective electroporation and high cell survival [7].

The most important question within C2C12 study is whether it is possible to perform successful gene transfection in stem cells by means of single cell electroporation. For this purpose, the electrical parameters need to be investigated. This section describes how the voltage and pulse length were determined for gene transfection into C2C12 cells.

First the minimum voltage for successful PI uptake was determined for a pulse length of 6 ms. Electrical pulses of 6 ms with increasing amplitude from 1 to 3 V (steps of 0.5 V) and an interval pulse of 1 min were applied to the cells (Figure 5-10).

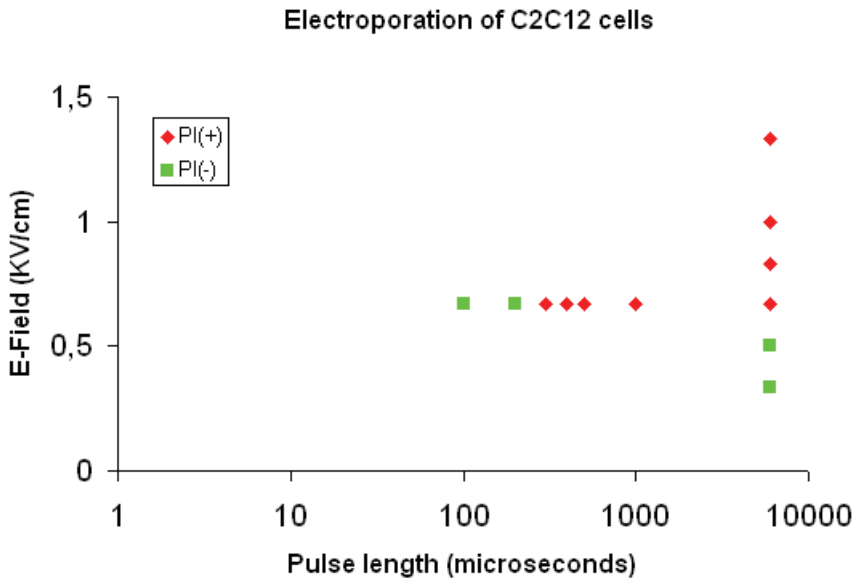

Figure 5-10: Relation between electric field strength and pulse length for PI uptake in electroporation of C2C12 cells.

Subsequently, then for the lowest voltage for electroporation (2 V), the effect of the pulse length on PI uptake was studied. As can be seen in Figure 5-11, an increase of the pulse length (from 100 µs to 6 ms) results in increased fluorescence intensity of PI, thus more PI is uptaken by the cell.

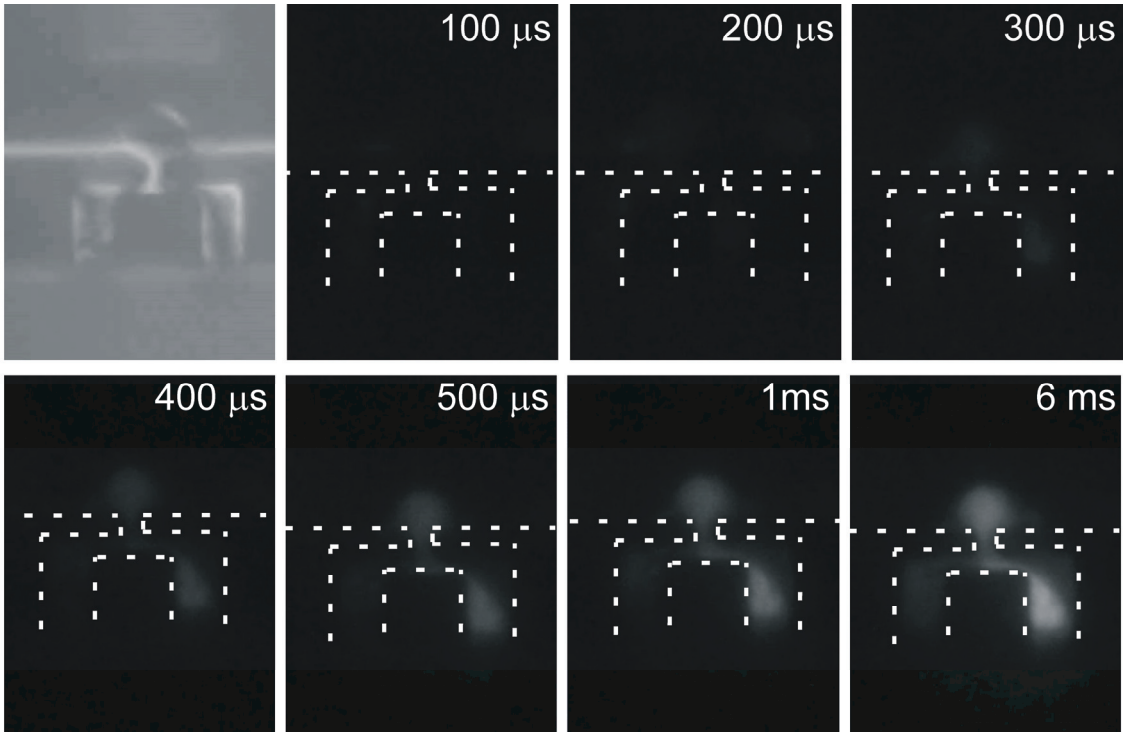

(a)

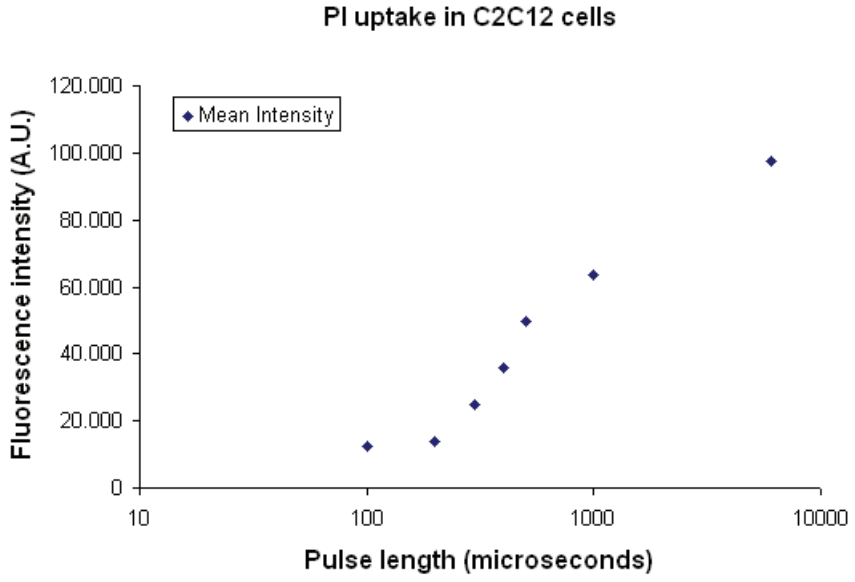

(b)

Figure 5-11: a) Snapshots of PI uptake for an E-field of 0.67 kV·cm^{-1} for different pulse lengths - b) PI-fluorescence intensity (A.U.) corresponding to the snapshots.

To get an indication of the lifetime of the pores in the cell membrane of C2C12 cells after electroporation, the following study was performed. Cells suspended in the electroporation buffer (10 mM HEPES, 140 mM NaCl, 2.68 mM KCl, 1.7 mM $MgCl_2$, 25 mM glucose, pH 7.4) were loaded and trapped in the microfluidic device (process described in section 5.2.2). Subsequently, identical electrical signals were applied to all the cells, viz. a pulse of 2 V and 6 ms. This signal was applied to the different cells with an interval time of 15 min (i.e. the cell in trap 2 was electroporated 15 min later than the cell in trap 1 etc.). Five minutes after electroporation of the last cell, PI was added to the microfluidic channels. In this way it was possible to determine pore resealing times (5, 15, 30, 45 or 60 min): when cells did not show the red fluorescence, i.e. no PI uptake, this indicates that the pores were resealed. In table 5-II the results are shown for three independent experiments.

Experiment I.D.	**Pore resealing time [min]**				
	5	15	30	45	60
1	PI(-)	**PI(+)**	PI(-)	PI(-)	PI(-)
2	PI(-)	PI(-)	PI(-)	PI(-)	PI(-)
3	PI(-)	**PI(+)**	PI(-)	**PI(+)**	PI(-)

Table 5-I: Pore resealing time of C2C12 cells based on PI uptake: PI(-) indicates pore resealing, PI(+) indicates cell membrane integrity disrupted.

As can be seen, for all experiments no PI uptake is observed 5 minutes after adding the PI to the cell traps. This means that the cells are resealed, and therefore it is reasonable to assume that for longer times the pores also reseal. However, this is not the case for all cells, presumably due to the fact that the cells in these traps were in a different cell state (for example, these cells were dying or dead before electroporation).

5.3.5 Gene transfection studies on C2C12 cells by electroporation

Transfer of DNA molecules into mammalian cells using electroporation is a powerful and a widely used method that can be directly applied to gene therapy [8-10]. We used the cell trap chip (generation 2) to immobilize, electroporate and transfect genes into individual C2C12 cells.

C2C12 cells resuspended in ice-cold electroporation buffer (10 mM HEPES, 140 mM NaCl, 2.68 mM KCl, 1.7 mM $MgCl_2$, 25 mM glucose, pH 7.4) were loaded and trapped in the microfluidic device as described in section 5.2.2. Once the cells are trapped, DNA encoding green fluorescent protein eGFP (100 ng/ml) is loaded into the cell trap device. DNA-cell contact is established within a pre-incubation period of 10 minutes before applying an electric field. In this way DNA adsorption in the cell membrane surface takes place. Subsequently, DNA transport across the cell membrane is initiated by one or several short electric pulses. A post-incubation time up to 10 min is given for the cell-DNA mixture (after the electric pulse). The actual permeation is a sequence of rather slow (milliseconds to minute range), but still unknown, "transfer steps" within the post-incubation period. The DNA transport is terminated by membrane resealing. Next, cell culture medium with 10 % serum is added to the microfluidic channels. Afterwards, the chip is placed in a small Petri dish with cell culture medium. This Petri dish is then placed in the incubator (37 °C and 5 % CO_2). If DNA is inside the cell, intracellular events lead to actual gene expression. Gene transfection was quantified by GFP expression 24 h after cell electroporation. Optical inspection of the cells was done 24 h and 48 h after electroporation. Figure 5-12 shows fluorescence images of successfully transfected C2C12 cells. The images were taken with a confocal microscope and a wide field microscope.

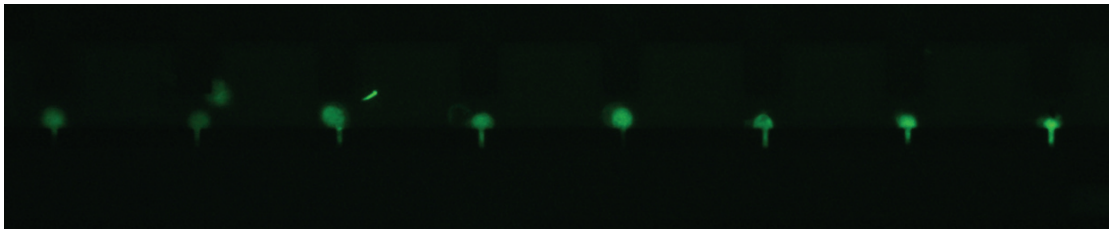

Figure 5-12: Fluorescence image of C2C12 cells in traps showing the expression of the green fluorescent protein 24 h after electroporation. To all cells a single pulse of 2 V-6 ms was applied.

It is observed that C2C12 cells have high transfection efficiency: 48 h after electroporation the cells showed a higher expression of GFP (higher fluorescence intensity) than after 24 h (Figures 5-12 & 5-13a). The cells also showed healthy morphology observed under light microscopy images. This healthy morphology was maintained at least 120 h post-transfection. Figure 5-13b shows a picture of two cells 120 h after of electroporation; just before imaging the cells were nucleus-stained with the life stain Hoechst. Transfection of DNA encoding yellow fluorescent protein (YFP) was also achieved (data not shown).

With these experiments we showed the use of microfluidic devices to efficiently transfer genes and express proteins in single cells.

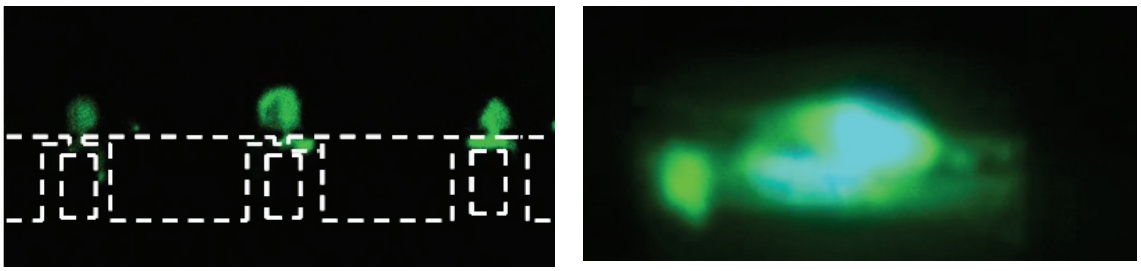

(a) (b)

Figure 5-13: a) Fluorescence images of the green fluorescence protein in three C2C12 cells located at trapping sites (indicated by the dashed lines). Images were taken 48 h after electric field application; applied signals were (from the left to right cell): 6 pulses of 2 V-6 ms, 1 pulse of 2 V-4 ms and 3 pulses of 2 V-4 ms. b) Fluorescence image of 2 cells showing the expression of GFP and the fluorescence (blue) of the nucleus stain (stain: Hoechst) - the image was taken 5 days after electroporation.

5.4 Conclusions

In this chapter the design and performance of cell trap devices for single cell electroporation and transfection are presented. In the first generation wires immersed in the reservoirs are used as electrodes. Electric-field simulations and experiments showed that only the side traps (the closest to the electrodes) are effective for single cell electroporation. Therefore, a microfluidic cell trap device with significant better electroporation efficiency is needed. For this reason a second generation of the cell trap device is designed: a chip in which all traps can be used for single cell electroporation. This is accomplished by integration of strategically positioned platinum electrodes, such that each trap can be electrically addressed individually. The results on the electric field distribution in this second generation cell trapping device clearly show that the electric field is focused at the site where the cell is trapped.

With the latter chip, electropermeabilization experiments were performed on two cell lines using the membrane-impermeable DNA stain PI and a plasmid encoding GFP as reporter molecules. Electrically driven molecular uptake, gene expression and cell viability after electropermeabilization were examined by fluorescence microscopy. The electrical parameters, voltage (or *E*-field) and pulse length needed for cell membrane permeabilization of individual cells were determined for HL60 and C2C12 cells. For identical pulse length (6 ms), it was found that the minimum electric field needed for electroporation of HL60 cells is 2.7 $kV \cdot cm^{-1}$ whereas 0.67 $kV \cdot cm^{-1}$ is sufficient for C2C12 cells. The difference in the electric field needed for successful electroporation between HL60 cells and C2C12 cells is a factor 4. This is due to the fact that C2C12 are bigger cells than HL60 cells and thus C2C12 block the trap sites better. In addition, it is known that lower voltages are needed to electroporate larger cells.

Besides electroporation, the resealing times of cells were studied. However, no conclusive data concerning resealing times could be obtained with the cell trap devices. This is due to complex nature of the cells: in order to get concise data, a significantly larger amount of experiments have to be done (stochastic process).

It is also demonstrated that the cell trap device can be used for gene transfection studies of individual cells. Gene transfection by electroporation of DNA encoding a green fluorescent protein and the subsequent protein expression

in C2C12 cells was achieved. For the first time it is shown that microfluidic cell trap devices can be use to efficiently transfer genes into single cells.

5.5 References

[1] Y. C. Lin and M. Y. Huang - *Electroporation microchips for in vitro gene transfection;* Journal of Micromechanics and Microengineering, **11 (5)**, (2001), pp 542-547.

[2] Y. C. Lin, C. M. Jen, M. Y. Huang, C. Y. Wu and X. Z. Lin - *Electroporation microchips for continuous gene transfection;* Sensors and Actuators B-Chemical, **79 (2-3)**, (2001), pp 137-143.

[3] Y. C. Lin, M. Li, C. S. Fan and L. W. Wu - *A microchip for electroporation of primary endothelial cells;* Sensors and Actuators A, **108 (1-3)**, (2003), pp 12-19.

[4] G. L. Andreason - *Electroporation as a technique for the transfer of macromolecules into mammalian cell lines.;* Journal of Tissue Culture Methods, **15** (1993), pp 56-62.

[5] I. Hapala - *Breaking the barrier: Methods for reversible permeabilization of cellular membranes;* Critical Reviews in Biotechnology, **17 (2)**, (1997), pp 105-122.

[6] A. G. Sabelnikov - *Nucleic-Acid Transfer through Cell-Membranes - Towards the Underlying Mechanisms;* Progress in Biophysics & Molecular Biology, **62 (2)**, (1994), pp 119-152.

[7] S. B. Dev, D. P. Rabussay, G. Widera and G. A. Hofmann - *Medical applications of electroporation;* IEEE Transactions on Plasma Science, **28 (1)**, (2000), pp 206-223.

[8] D. C. Chang, B. M. Chassy and J. A. Saunders -*Guide to electroporation and electrofusion;* San Diego: Academic Press (1992).

[9] E. Neumann, A. E. Sowers and C. A. Jordan, -*Electroporation and Electrofusion in Cell Biology;* Plenum Press, New York (1989).

[10] G. L. Prasanna and T. Panda - *Electroporation: Basic principles, practical considerations and applications in molecular biology;* Bioprocess Engineering, **16 (5)**, (1997), pp 261-264.

6

Electrical detection of electroporation

In this chapter two models are elaborated to characterize and simulate single cell electroporation in a microfluidic cell trap device. A Finite Element Model is used to investigate the potential distribution in the cell trap chip as well as the voltage drop over a trapped cell. An equivalent electrical circuit model of the chip with a trapped cell is developed to verify whether it is possible to measure electroporation electrically. Experiments were performed to identify the electrical signals that are needed for reversible electroporation, and to investigate whether electrical and optical detection of electroporation (i.e. staining) can be correlated.

6.1 Introduction

Biological cells contain highly conductive aqueous electrolytes separated by thin, low-conductivity membranes populated with electrically active macromolecules [1, 2]. As a result, multicellular systems are extremely heterogeneous with respect to their passive electrical properties (local resistance and capacitance). Electric field effects in biological systems have long-standing scientific interest [3, 4]. Electroporation is a phenomenon in which the cell membrane is exposed to high intensity electric field pulses, which results in temporarily destabilized specific regions of the cell, pore formation [5, 6]. During the destabilization period, the cell membrane is highly permeable to exogenous molecules present in the surrounding media [7]. When cells get electroporated, the cell membrane resistance suddenly decreases, causing a sudden increase in the current. Therefore, membrane permeation can be assessed electrically by measuring characteristic 'jumps' in current that correspond to drops in cell membrane resistance [8, 9].

In this chapter, two models are elaborated to characterize and simulate single cell electroporation (section 6.2). A Finite Element Model (FEM) is used to characterize the electrical behaviour of SCE (section 6.2.1) and the results of this model are described. With the FEM model the potential distribution in the cell trap chip is modeled as well as the voltage drop over the cell (section 6.4.1). Moreover, the electrical circuit model (of a trapped cell) is developed (section 6.2.3) and simulations are performed to verify whether it is possible to measure the increase in current when cell electroporation takes place (section 6.4.2). Finally, electroporation experiments were done to identify the signal configuration needed for reversible electroporation of cells (section 6.5). During these experiments it is investigated whether the current 'jump' occurs at the same moment as optical detection of electroporation (i.e. staining). Lastly, the conclusions and recommendations are given in section 6.6.

6.2 Electroporation model

To predict the occurrence of 'jumps' in the electrical currents, indicators for SCE in the chip, and to explain the response behaviour, a finite element model and

an electrical circuit model were made. In both models the permittivity (ε) and the conductivity (σ) of the materials (cell, buffer, chip) as well as the geometry and dimensions of the various elements of the chip are used (flow channels, traps, etc.) to calculate the voltages and the currents in the system.

In the finite element model the geometry of the chip is created, and the values of the conductivity are assigned to the various elements. In the electrical circuit model the geometry, the permittivity and the conductivity of the various parts of the chip are used to calculate the corresponding resistances and capacitances. The conductivities and the permittivities of the materials used are given in Appendix A, table 6-V.

First the FEM model of one trap will be discussed, followed by the electrical circuit model of one trap. Because of the symmetry of the cell trap device (Figure 5-1, chapter 5) it is sufficient to model only one trap (all traps behave identical).

6.2.1 Finite Element Model

The potential and the electric field distribution in the trapping device are modeled with finite element software (FEMlab 3.0, Comsol, Sweden). A 2D finite element model was made by drawing the structure of the chip. Subsequently, boundary conditions and different conductivities were assigned to the different parts (subdomains) of the chip. The DC conductive medium model was used for a steady state situation, which solves Gauss' differential equation. No time-dependent simulations were performed with FEMlab. The simulations were done for a DC signal of 10 V on the electrodes, and the simulations were purely resistive.

6.2.2 Electrical Circuit Model

The electrical circuit consists of the following elements (Figure 6-1); the resistance of the electrolyte solution in the channel, the resistance of the electrolyte solution in the trap, the double layer impedances of the electrode-liquid interfaces, the stray capacitances between the different electrodes, the impedances of the cell membrane and the resistance of the interior liquid of the cell. In Figure 6-1 the equivalent electrical model of a cell in a trap site is presented (the elements of the

model will be discussed separately in the following sections) and step by step the model of Figure 6-1 will be built up.

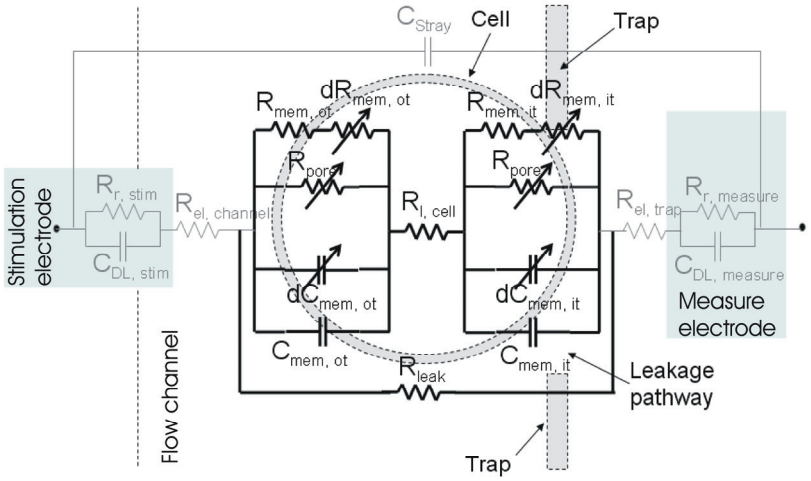

Figure 6-1: Equivalent electrical model of a cell in a trap.

The following equations are used to calculate the resistances and capacitances present in the model:

$$R = \rho \frac{l}{A} \qquad \text{eq.(1)}$$

where R is the resistance, ρ the resistivity, l the length, and A the surface of the material.

$$C = \frac{\varepsilon_0 \varepsilon_r A}{d} \qquad \text{eq.(2)}$$

where C is the capacitance, ε_0 the permittivity of vacuum, ε_r the relative permittivity of the dielectric material, A the surface of the conducting materials and d the thickness of the dielectric material.

Resistance of electrolyte solution

The resistance of the electrolyte solution in the chip is calculated with eq.(1). This resistance is modeled as the resistance of a block of the electrolyte solution in the top channel (R_{ch}) in series with the resistance of the electrolyte solution in the trapping structure (R_t). For R_{ch} a block is taken of length x and width y as is illustrated in Figure 6-3. The calculation of R_t for a cell trap device type 2 is shown in Figure 6-2. For the value of R_t for a trap type 1 the calculation is simpler since

this trap is a long thin straight channel and R_t is calculated simply with eq.(1). More details of the trap designs can be found in chapters 3 & 5.

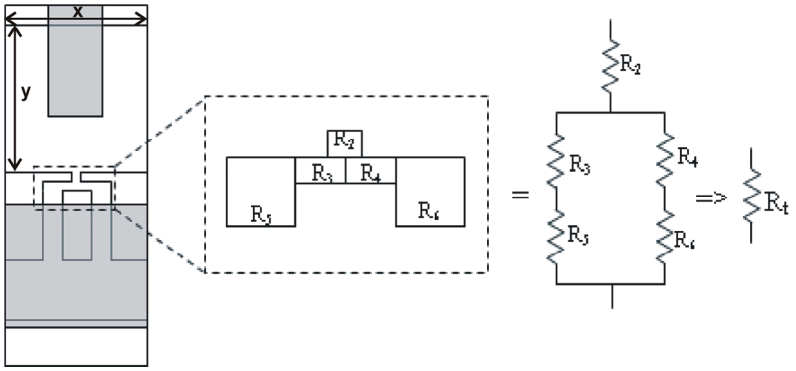

Figure 6-2: Method of calculating the resistance of the electrolyte solution in the trap.

Double layer impedance at the metal/liquid interfaces

At the surface of an electrode, chemical and physical interactions between the metal and the electrolyte solution ions at the metal/liquid interface cause a charge distribution that determines the impedance of the metal/liquid interface. One of the simplest and most common models for the double layer impedance is Randles cell model (Figure 6-3). The model consists of the double layer capacitance C_{DL}, and a reaction resistance R_r [10].

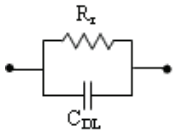

Figure 6-3: Electrical circuit model of the Randles cell.

with the elements described so far, a (very) simplified version of the model is shown in Figure 6-4:

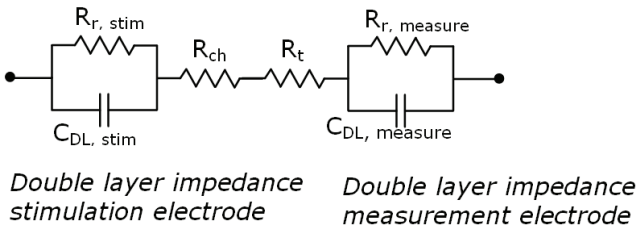

Figure 6-4: The electrical circuit model including the double layer impedances of the stimulation electrode and the measurement electrode.

Stray capacitance

Besides the double layer capacitance, there are two other capacitances present in the system, namely the two parallel capacitances between the electrodes themselves, which can be combined to form the stray capacitance C_{stray}.

There are two different pathways the current can follow from the stimulation electrode to the measurement electrode (Figure 6-5): (i) through the liquid, or (ii) via the SiO_2 and the Si. In case (i), the electrodes behave like two plates with liquid in between with a resulting liquid capacitance C_L. In case (ii) the electrode and the silicon represent the two plates of the parallel plate capacitance, with silicon oxide being the dielectric material between the plates. This results in two stray capacitances C_{Si}, one for each electrode (see Figure 6-6 for the two pathways between a stimulation electrode and the ground electrode). The stray capacitance of the silicon oxide is calculated with eq.(2).

Figure 6-5 shows that there are two stray capacitances from the measurement electrode through the silicon, since the measurement electrode is in contact with the silicon above and below the bottom channel. Since these two capacitances are in parallel, in the model one capacitance is implemented with that surface area, resulting in one capacitance C_{stray}.

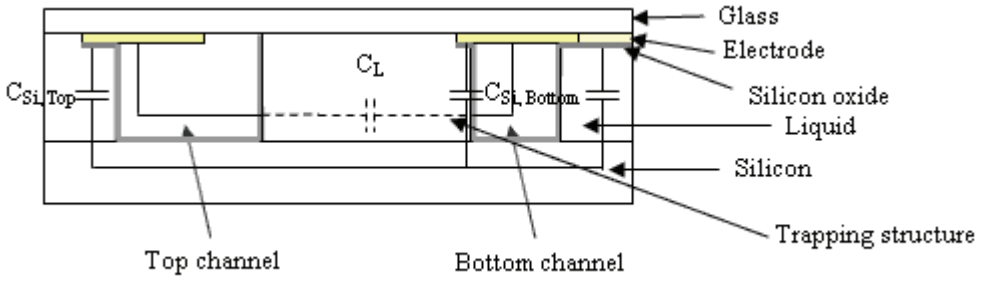

Figure 6-5: The two pathways of the stray capacitances (in a side view of the trap device).

The stray capacitance through the liquid is more difficult to calculate. The electrodes are not facing each other, but they are lying flat in the same plane (see Figure 6-6). Because of this the formula for the parallel plate capacitor (equation 2) is not applicable here.

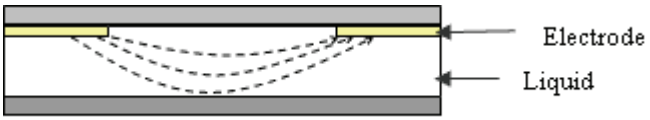

Figure 6-6: The current path between electrodes lying in the same plane.

An estimation of the capacitance between the electrodes through the liquid was made by means of the following formulas [11]:

$$C_L = (N-1)LC_l \qquad \text{eq. (3)}$$

with N the total number of electrode fingers, and L the finger length, and with

$$C_l = \frac{\varepsilon_0 \varepsilon_r}{2} \frac{K\left[(1-k^2)^{1/2}\right]}{K(k)} \qquad \text{eq. (4)}$$

where:

$$K(k) = \int_{t=0}^{1} \frac{dt}{\left[(1-t^2)(1-k^2t^2)\right]^{1/2}} \qquad \text{eq. (5)}$$

with k the modulus which can be approximated by:

$$k = \frac{s}{s+w} \qquad \text{eq. (6)}$$

where w is the electrode width and s the inter-electrode space.
Adding up this element the model becomes then as shown in Figure 6-7:

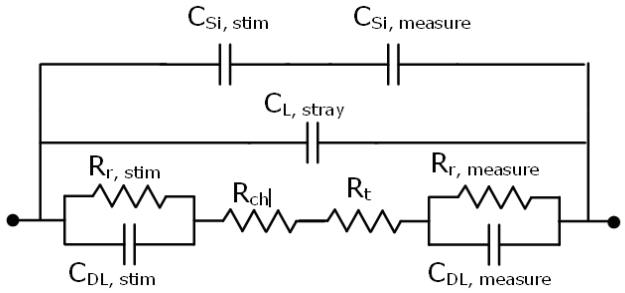

Figure 6-7: The electrical circuit model extended with the stray capacitances.

Capacitance between the stimulation electrodes

The model shown in Figure 6-7 is the equivalent circuit model of the stimulation electrode and the measurement electrode. However, between the stimulation electrode and its neighbouring electrodes, which are connected to the ground, identical impedances will be present (the resistance of the liquid between the electrodes R_{el}). The measurement electrode is grounded via a measurement

resistance (R_{meas}), while the neighbouring stimulation electrodes are directly connected to the ground. This measurement resistance R_{meas} is used to measure the current through the chip. Taking into account these issues, the model thus becomes (Figure 6-8):

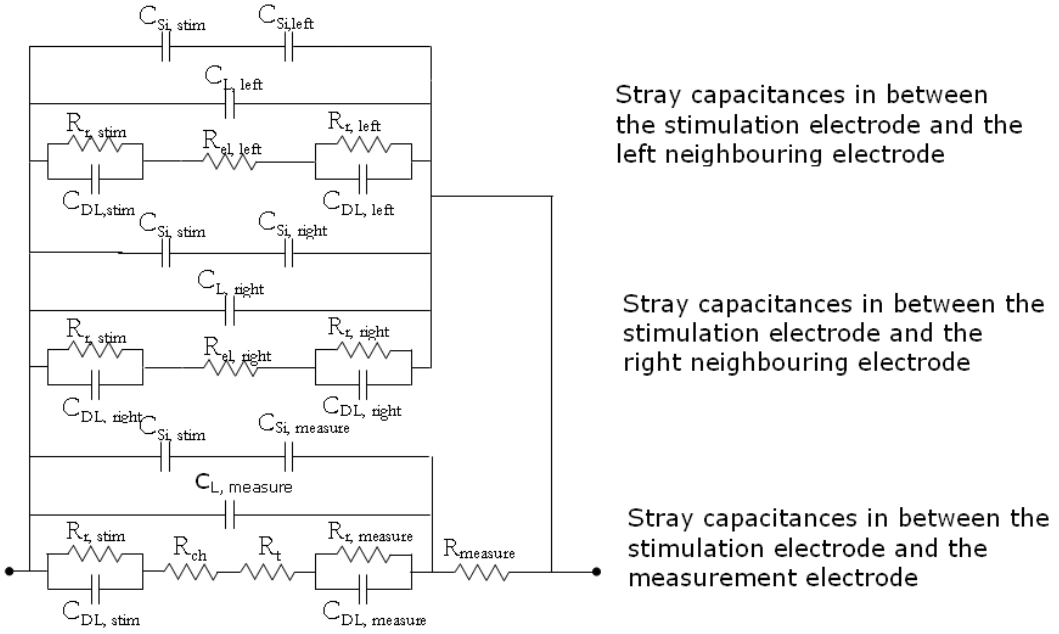

Figure 6-8: The electrical circuit model extended with the impedances in between the fingers.

The cell model

The last part to include in the model of Figure 6-8 is a cell model. One of the most simple models of a cell is a sphere of liquid (cytoplasm, the interior liquid of a cell) surrounded by a single shell (the membrane).

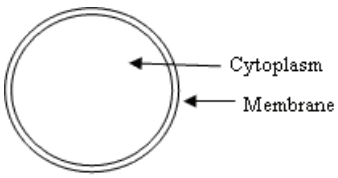

Figure 6-9: The simple cell model.

This cell model is converted to an electrical circuit model (Figure 6-10) that is implemented together with a leakage resistance (R_{leak}) in the circuit model of the chip (Figure 6-1).

The cell membrane itself is modeled as a parallel combination of a resistor (R_{mem}) and a capacitor (C_{mem}). The resistance and the capacitance of the cell membrane can be splitted into the resistance and capacitance of the membrane

inside the trap and the resistance and capacitance of the membrane outside of the trap. Overall the electrical circuit model of the cell (Figure 6-10) consists of the membrane capacitance and the membrane resistance of the part outside the trap ($C_{mem,\ ot}$ and $R_{mem,\ ot}$), the resistance of the cytosol ($R_{l,\ cell}$), the membrane capacitance and the membrane resistance of the part inside the trap ($C_{mem,\ it}$ and $R_{mem,\ it}$) and the resistance of a pore (R_{pore}). These resistances and capacitances are calculated with eqs. (1) and (2).

The resistance of the membrane increases with each pore opening, because the surface area of the membrane decreases. To model this, the difference in resistance between a membrane with one pore and an intact membrane ($dR_{mem,\ ot}$, $dR_{mem,\ it}$) is put in series with the membrane resistance. To model more pores, dR_{mem} for a single pore is multiplied with the number of pores.

The pore resistance of one pore is placed parallel to the resistance of the membrane. As more pores appear, they will be in parallel with both the membrane and the other pores. Therefore, the development of more pores is modeled by dividing the value of the pore resistance by the number of pores assuming an identical R_{pore} for all pores.

The capacitance of the membrane decreases with each pore opening because the surface area decreases. To model this, the difference in capacitance between an intact membrane and a membrane with one pore ($dC_{mem,\ ot}$, $dC_{mem,\ it}$, with negative values) is placed parallel to the membrane capacitance. To model more pores, that difference in capacitance is multiplied with the number of pores.

Finally, the leakage resistance is the resistance of the pathway where the current by-passes the cell, thus it is in parallel to R_{cell}. The leakage resistance represents the current pathway around the cell because a cell does not block the trap site completely (no giga-ohm sealing is achieved). The R_{leak} is modeled as a block of liquid above the cell, through which the current will flow. The model for the cell with the leakage resistance looks as follows (Figure 6-10):

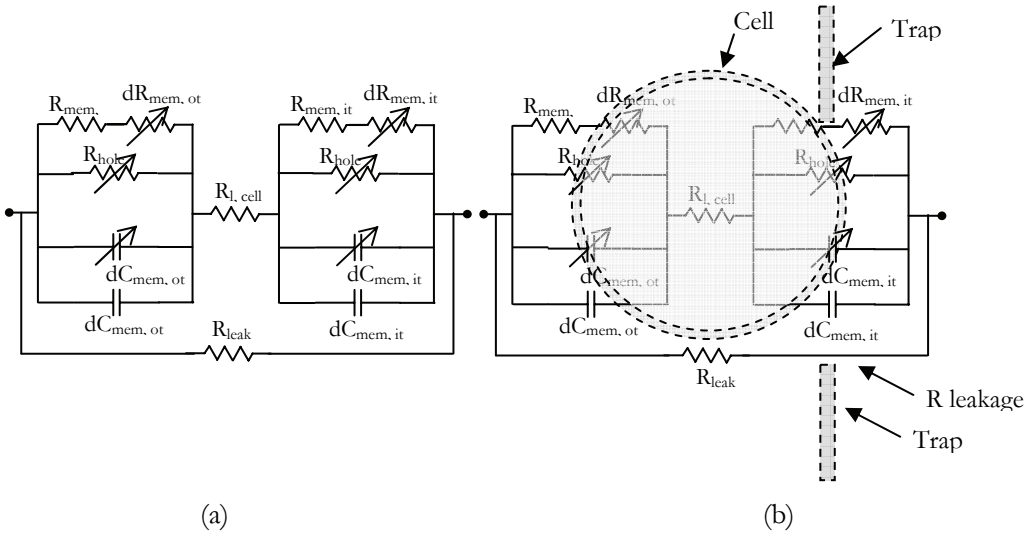

Figure 6-10: (a) The electrical circuit model of the cell. (b) The electrical circuit model of the cell model with the cell and the trap with the leakage pathway.

If this is implemented in the model of the trap, the whole electrical circuit model is finished and looks as presented at the beginning of this section in Figure 6-1.

6.3 Impedance spectroscopy

By measuring the impedance as a function of the frequency, information about the electrical properties of the chip can be obtained, for example, on the size of the double layer capacitance and the buffer resistance. During an impedance spectroscopy measurement, a small AC signal with an increasing frequency is applied to the electrodes, and the resulting current is measured. Subsequently, the impedance is calculated for each frequency. Ideally the impedance spectrum of two electrodes immersed in buffer solution looks like shown Figure 6-11.

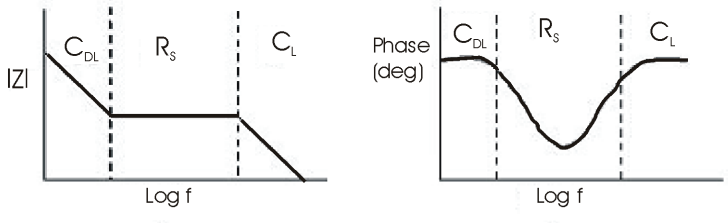

Figure 6-11: The result of an ideal impedance spectroscopy; the bode plot of the absolute impedance (right) and of the phase (left).

For both plots three different parts can be distinguished. In the plot of the impedance the two parts with the decay represent the double layer capacitance (C_{DL}) and the capacitance between the electrodes (C_L), respectively. The plateau represents the resistive part of the system. In the plot of the phase these three zones can also be distinguished: the dip in the phase represents the resistive part of the system, whereas the 'flat' parts represent the two capacitive parts.

6.4 Results

6.4.1 Results of FEM model

In this section, simulations of the electric potential distribution in the chip are discussed. The potential drop in the chip and over a cell was simulated for a DC signal of 10 V (applied to a stimulation electrode). For the simulations, different situations were taken into account:

a) The effect of the leak resistance R_{leak}: do cells completely block the electrical path via the buffer/electrolyte solution.

b) The influence of the electrical potential on cells trapped next to the stimulated trap.

c) The influence of non-grounded (floating) electrodes located close to the stimulated electrode/trap. (Neighbouring electrodes are the electrodes next to the stimulation electrode).

The values used for the different subdomains and boundaries are given in table 6-I. The DCM (conductive media DC model) module was used in all the simulations. In table 6-II model results are summarized for 8 different cases. Cases 1 and 2 are simulated without a leakage pathway and the outer electrodes are grounded. In case 3 to 5, simulations are done with a leakage pathway present while the outer electrodes are grounded, and last cases 6 to 8 are simulations with floating outer electrodes, with and without a leakage pathway present.

Parts of the model	Subdomain	Boundary
Buffer[a]	$\sigma = 1.572\ S{\cdot}m^{-1}$	Electrical insulation
Electrode G[b]	$\sigma = 8.99{*}10^{6}\ S{\cdot}\ m^{-1}$	Ground
Electrode L[b]	$\sigma = 8.99{*}10^{6}\ S{\cdot}\ m^{-1}$	Ground
Electrode R[b]	$\sigma = 8.99{*}10^{6}\ S{\cdot}\ m^{-1}$	Ground
Electrode M[b]	$\sigma = 8.99{*}10^{6}\ S{\cdot}\ m^{-1}$	Electrical potential V_0=10V
Cytosol[c]	$\sigma = 0.25\ S{\cdot}\ m^{-1}$	Continuity
Membrane[c]	$\sigma = 4{*}10^{-7}\ S{\cdot}\ m^{-1}$	Continuity

Table 6-I: Parameters used in the simulations. [a] value obtained from measurements, [b] values obtained from database FEMlab, [c] values from [12].

The resulting voltage drops over the stimulated cell ($V_{stimulated\ cell}$) and the neighbour cell ($V_{neighbour\ cell}$) are summarized for all the different situations in table 6-II.

Case	Outer electrodes	Outer trap	Middle trap	$V_{stimulated\ cell}$	$V_{neighbour\ cell}$
1	Grounded	Empty	Closing	9	-
2	Grounded	Closing	Closing	9	0.5
3	Grounded	Empty	Leakage	4	-
4	Grounded	Leakage	Leakage	3.9	0.15
5	Grounded	Closing	Leakage	4	0.49
6	Floating	Empty	Closing	9.7	-
7	Floating	Closing	Closing	9.8	8
8	Floating	Leakage	Leakage	4.3	3.5

Table 6-II: The resulting voltage drops over the cells: $V_{stimulated\ cell}$ is the potential over the stimulated cell, $V_{neighbour\ cell}$ is the potential over the neighbour cell.

Not surprisingly, it can be concluded that in the case of a leakage pathway around the trapped cell, the voltage drop over the stimulated cell is much smaller that in the situation where no leakage pathway is present (4 V *vs.* 9 V, case 3 *vs* 1 & 2). Thus, in case of a finite R_{leak} a higher stimulation voltage is needed to get the same voltage drop.

In cases of a leakage pathway the stimulated cell, $V_{stimulated\ cell}$ is significantly lower than in cases without such a pathway, independently of the status of the neighboring traps (cases 1 & 2 *vs* 3 & 5). In cases where neighbouring traps are (partially) blocked (cases 2, 4 & 5) across these cells only a small potential drop is found (0.15-0.5 V). Since this situation of a leakage pathway in all traps is the most realistic situation, it can be concluded that neighbouring trapped cells will not be influenced by the stimulation electrode. For this situation, case 4, the potential distribution in the chip is illustrated in Figure 6-12a and the potential distribution over the stimulated cell (middle cell) and over the neighbour cell (left cell) is shown in Figures 6-12a and b.

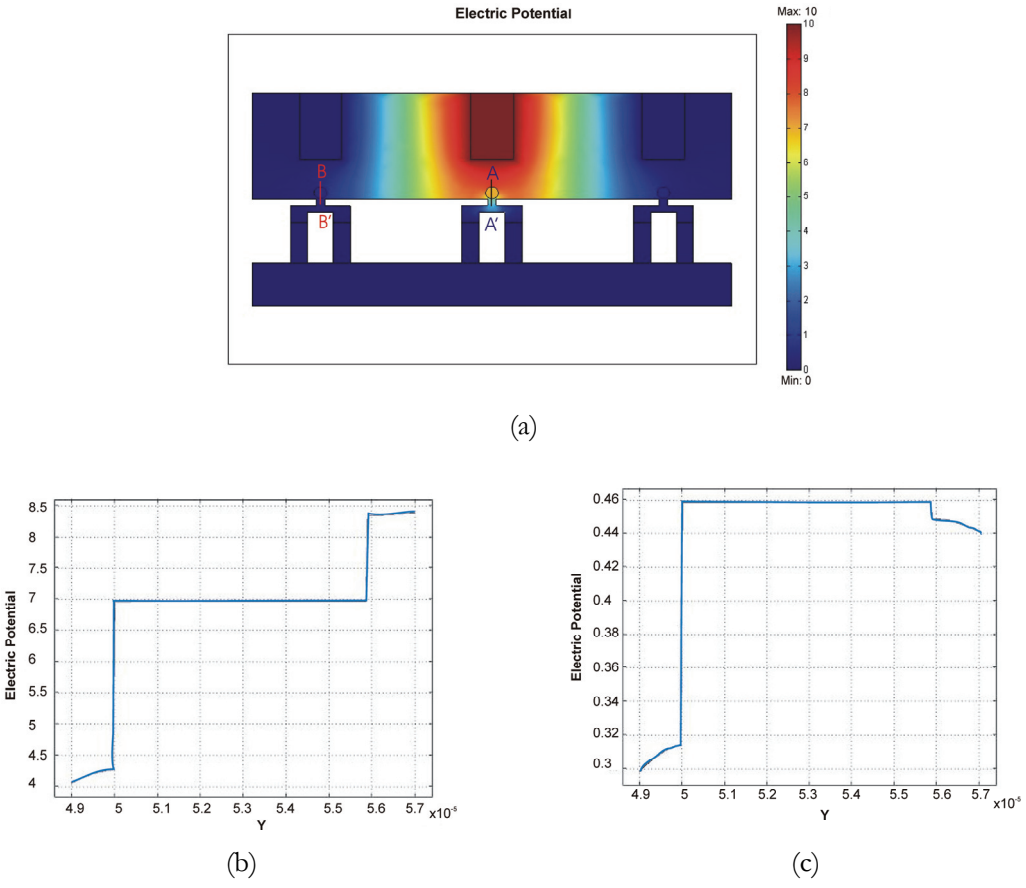

Figure 6-12: (a) Potential distribution in the chip in case 4. (b) potential drop over the cell in the middle trap (stimulated trap) across the line A-A' (black line depicted in (a)). (c) potential drop over the neighbour cell (left to the stimulated one) across line B-B' depicted in (a).

By looking at the influence of floating neighbouring electrodes (cases 6 to 8), it can be observed that floating electrodes have a significant influence on the

neighbouring cells. In cases of cell trapped at neighbouring traps (cases 8 & 9), the potential difference between stimulated and neighbouring cell is quite small (i.e. 0.8-1.8 V) and the potential over neighbouring cells is high. Therefore with this configuration, floating electrodes, it is likely that the stimulation signal will also affect the neighbouring cells probably leading to EP of neighbouring cells as well. To avoid this effect, during experiments it is important that neighbouring electrodes are grounded.

6.4.2 Results of electrical model

In this section, the theoretical electrical circuit model is elaborated and the values for the different components of the model are calculated. In Figure 6-13 the final model as shown in Figure 6-1, but now with the corresponding numerical values for all components. All the calculations are shown in Appendix A.

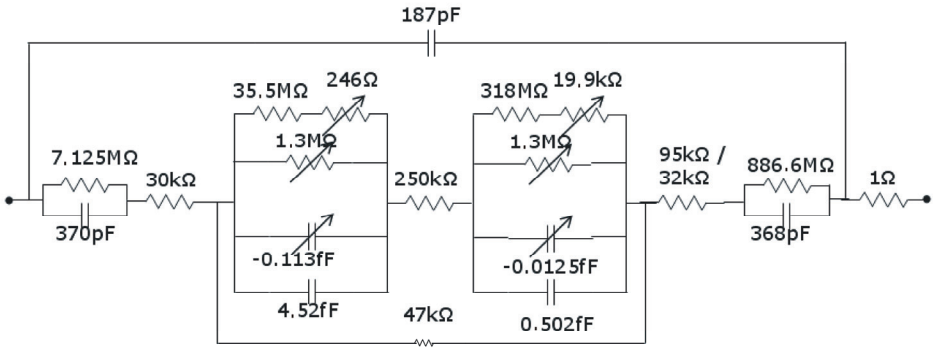

Figure 6-13: Electrical circuit model of the chip and a trapped cell with all the values of each element used for the simulations.

During SCE, the number of pores in the cell membrane increases, resulting in variations in C_{mem} and R_{mem}. The increase in membrane resistance and the decrease in membrane capacitance due to pore formation are implemented in the model by multiplying C_{mem} by the number of pores.

The model shown in Figure 6-13 was implemented in pSpice for both types of traps. The model for a chip with a trap type 2 is shown in Figure 6-14. In this model an extra resistor of 1 Ω is applied; it will be used to measure the current that 'flows' through the cell/trap model. Several simulations were done to verify whether it would be possible to see 'jumps' in current when a certain number of

pores are formed in the cell membrane (due to EP), and if these 'jumps' can be measured with the setup.

By changing the multiplication factor of the variable elements (R_{mem}, R_{pore}, C_{mem}), the opening of more than one pore is simulated. First, symmetrical pore formation will be simulated, meaning that the same amount of pores appear in both sides of the membrane (inside and outside of the trap). For the simulations two different stimulation signals are applied: (i) a pulse of 6 ms and 2 V, and (ii) a sine wave of 20 kHz and 0.2 V. The pulse signal is used to mimic the situation in which a pulse is used for both electroporating the cell and measuring the current. The sine wave is used to model the experiments in which the superposition of a pulse and a sine wave is used (where the pulse is used for electroporating the cell and the sine is used for measuring the current). The frequency of 20 kHz is chosen based on impedance spectroscopy (section 6.5.1).

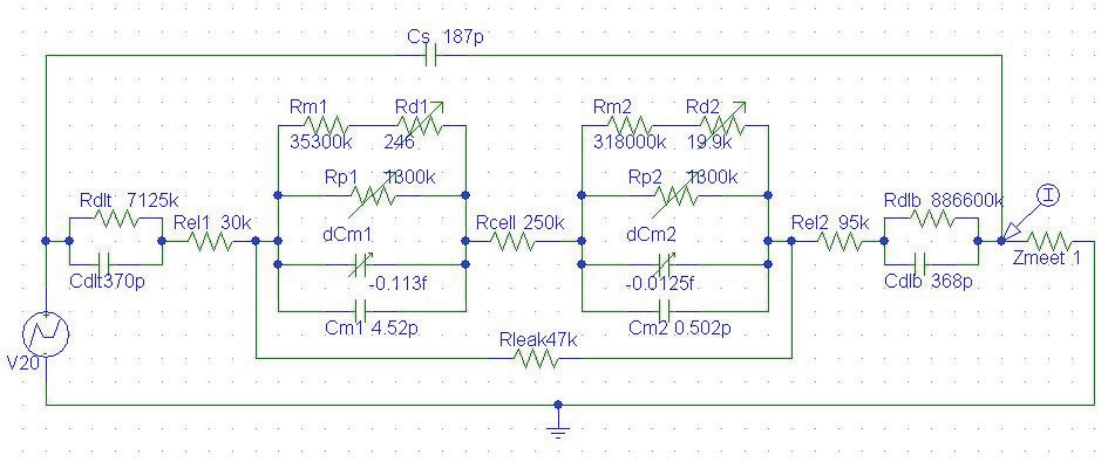

Figure 6-14: The pSpice model of a chip (trap type 2) when a pulse is applied with 2 pores present (inside and outside the trap).

The results of four simulations, i.e. signals (i) and (ii) for trap type 1 and 2, are shown in Figure 6-15. In this figure the current is plotted against the number of pores present in the membrane. The value of the current induced by the sine is measured at the plateau level of the resulting current. The values of the current resulting from the pulse are measured at 6 ms since there is no real plateau present during the pulse.

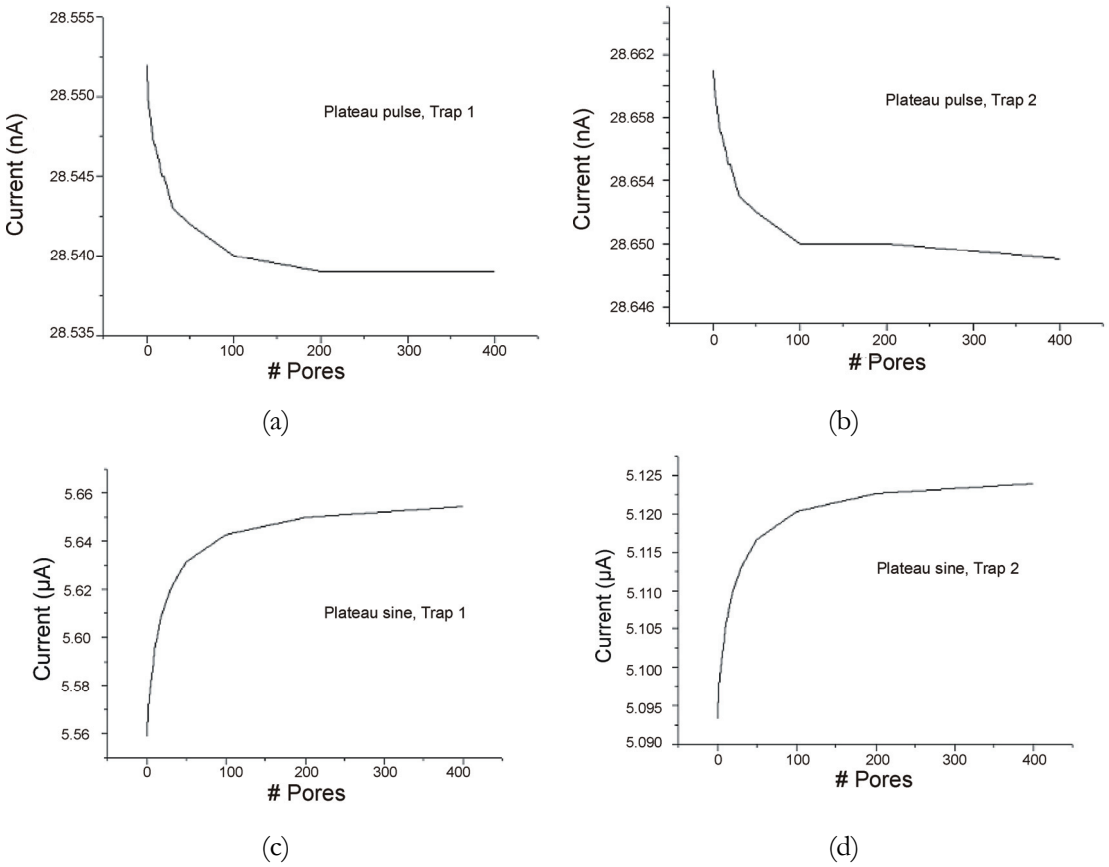

Figure 6-15: The current level of the pulse at 6 ms vs. the number of pores (a) for trap 1 and (b) for trap 2.The current level of the plateau of the sine vs. the number of pores (c) for trap 1 and (d) for trap 2.

The four figures above show that the values of the plateau of the sine increase with the opening of more pores, while the value of the pulse (at 6 ms) decreases. Also, the values of the plateau of the sine are higher in a chip with trap type 1 than in a chip with trap type 2. Moreover, the values of the pulse at 6 ms are higher in a chip with trap type 2 than in a chip with trap type 1. The increase in current due to the opening of more pores is also larger in a chip with trap type 1 than in a chip with trap type 2 when the sine is applied. On the other hand the decrease in current due to the opening of more pores is more or less the same for both types of traps when a pulse is applied. The currents found when a sine wave is applied are more than 100 times larger than the currents measured when a pulse is applied.

Since the currents found in the simulations are larger for a sine wave, the changes in the membrane resistance will (probably) be easier to measure with a sine

than with a pulse. Because the resistance of the trap type 1 is lower than the resistance of the trap type 2, the changes in current are larger in a chip with trap type 1. Why the current value of a pulse (at 6 ms) decreases when more pores are opened is not clear. Since the membrane resistance decreases, an increase in the current is expected. Probably for the pulse signal the decrease in membrane capacitance influences the signal more than the decrease in membrane resistance. This decrease in capacitance might explain the decrease in current. Another reason might be that the method of measuring the value of the pulse at 6 ms is not optimal: since there is no real 'plateau', it might be better to look at the RC time.

All the simulations above were done with symmetrical pore formation. However, changes in current were also modeled for asymmetrical pore formation. The results are given in table 6-III.

# Pores outside trap	# Pores inside trap	I sine trap 1 (μA)	I sine trap 2 (μA)	I pulse trap 1 (nA)	I pulse trap 2 (nA)
0	0	5,5589	5,0934	28,552	28,661
1	0	5,5591	5,0935	28,552	28,661
0	1	5,5704	5,0975	28,551	28,661
1	1	5,5701	5,0984	28,55	28,66
2	0	5,5591	5,0935	28,552	28,661
0	2	5,5714	5,0995	28,551	28,661
2	1	5,5718	5,0977	28,55	28,66
1	2	5,5748	5,0993	28,55	28,66
2	2	5,5778	5,0998	28,549	28,659

Table 6-III: The simulation results from the asymmetric pore formation.

The simulation results show that the changes in current for the plateau of the sine are larger when a pore appears on the part of the membrane inside the trap than when it does in the membrane part outside of the trap; e.g. for trap 1 dI_{in}= 0.0115 μA and dI_{out}= 0.0002 μA, and for trap 2 dI_{in}=0.0041 μA and dI_{out}= 0.0001 μA, respectively. Moreover, there is no difference between the values

of the plateau levels when one or two pores are formed at the part of the membrane outside the trap.
The difference in current between two pores in the part outside the trap and no (or one) pores in the part inside the trap is relatively large (0.0127 μA for trap 1 and 0.0041 μA for frap 2). This means that pores appearing on the inside of the trap will result in a change on the measured signal. Since the voltage drop over the membrane inside the trap is the highest, it is most likely that at this location the first pore will appear. With the pulse signal, however, it is very difficult to detect pore formation independent of the location of the pores.

In conclusion, from the simulations it appears that the current change when pore formation takes place can be detected. By using a sine wave it seems possible to measure pore formation at 20 kHz when more than 20 pores are formed.

A more detailed analysis of the current variations during pore formation using a sine wave is made. A frequency characterization of the currents flowing through the system is performed for different situations: no pore formation, 2 pores and 20 pores in trapped cell. In details, currents through the cell (I_{cell}), the leak resistance (I_{leak}), the stray capacitance (I_{stray}) and through the measurement resistance (I_{total}) are simulated and analyzed using frequency domain plots.

6.4.2.1 Model cell trap case A

The first situation considered is the one as given in Figure 6-14, with R_{leak} is 47 kΩ and platinum electrodes, which represents the used measurement setup. In Figure 6-16 the currents flowing through the system (model) are plotted versus the frequency when 20 pores are formed. It can be seen that the current flowing through the leak resistance (e.g. 1 μA at 20 kHz) is much higher over the complete frequency range than the current flowing through the cell (e.g. 100 nA at 20 kHz). In addition, for 20 kHz the total current flowing through the system is 1.2 order of magnitude larger than the current through the cell. Moreover, variations in the system, e.g. electrolysis, changes in ion concentrations, roughness of the electrodes, results in fluctuations of the measurement current. Assuming a change of 1% of the total current, this causes a variation of 50 nA on the measurement signal, which is in the same range as the extra current due to pore formation. Therefore, with the

actual configuration it will be very difficult to detect single cell electroporation (SCE), which is mainly due to low leak resistance.

In order to be able to measure electroporation, the system/measurement setup needs to be improved. Two cases are considered: reduction of the impedance of the electrodes and reduction of the leak pathway around the trapped cell (referred to as giga ohm sealing). These 2 cases are implemented and evaluated with the electrical circuit model. Currents through system are plotted versus the frequency.

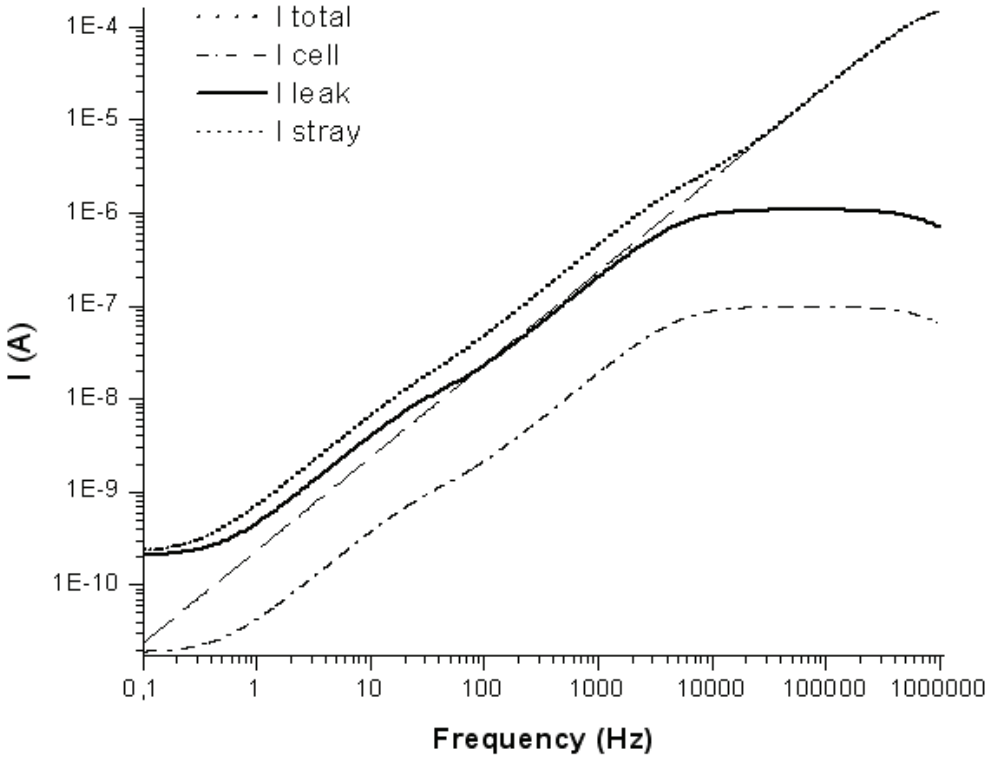

Figure 6-16: Currents through the system versus frequency of case A: R_{leak} is 47 kΩ and use of Pt electrodes.

6.4.2.2 Model cell trap case B

In case B the resistances of the electrodes are reduced to 10 kΩ, which can be obtained by replacing platinum by another material, for example Ag/AgCl-electrodes. In Figure 6-17 the currents flowing through the system (model) are

plotted versus the frequency when 20 pores are formed. It can be seen that the current flowing through the leak resistance (e.g. 1 μA at 20 kHz) is still higher over the complete frequency range than the current flowing through the cell (e.g. 100 nA at 20 kHz). Moreover, the current flowing through the stray capacitance is dominant at the initially selected measurement frequency of 20 kHz. Only for frequencies below 400 Hz, the current flowing through the cell is higher than through the stray capacitance. However, at these frequencies the current through the cell is still one order of magnitude smaller than the current through the leakage pathway. Therefore, changing the electrode material to a material with a lower impedance does not result in an 'easy' way of measuring the current through the cell due to electroporation. Nevertheless, this option improves the system in that sense that unwanted variations in current are reduced.

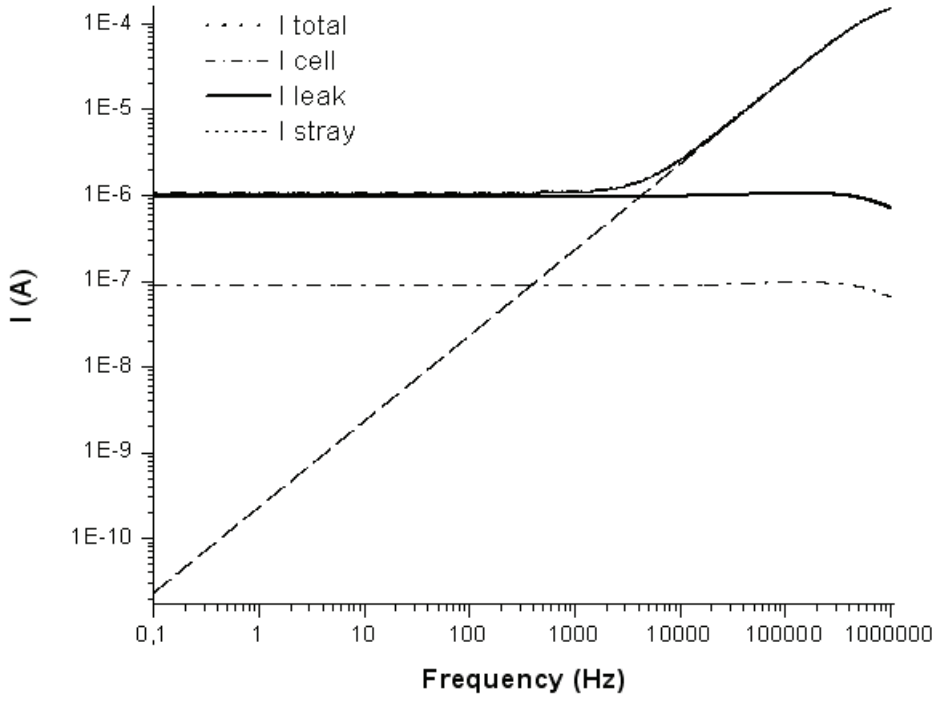

Figure 6-17: Currents through the system versus frequency for case B: R_{leak} is 47 kOhm and use of electrodes with a low impedance.

6.4.2.3 Model cell trap case C

For this case, the leak resistance is increased to 1 GΩ, meaning that the pathway where the current by-passes the cell is reduced. In Figure 6-18 the currents flowing through the system (model) are shown as function of the frequency for a situation of 20 pores. In this case, the current through the leak resistance (100 pA at 20 kHz) is considerably lower than the current flowing through the cell (800 nA at 20 kHz). At the initially selected measurement frequency of 20 kHz, the current through the stray capacitance is higher than the current through the cell. However, at frequencies below 200 Hz the current through the cell is higher than the current through the stray capacitance. Therefore, reducing the leakage pathway by proper sealing of the trap improves the system significantly, making it possible to detect pore formation for frequencies below 200 Hz. However, measuring at these low frequencies may pose problems, because for a statistically correct measurement a frequency beyond the pulse frequency (in this case 166 Hz) is recommended.

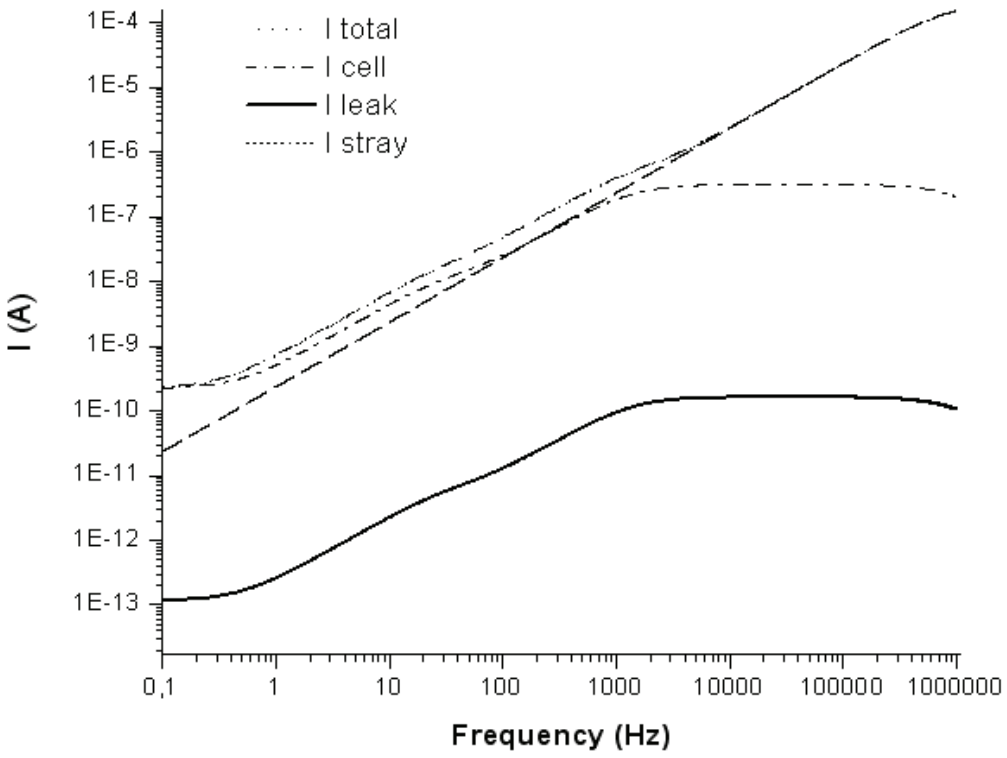

Figure 6-18: Currents through the system versus frequency for case C: R_{leak} is 1 GΩ and use of

Pt electrodes.

6.4.2.4 Model cell trap case D

For the last case, both options are implemented in the electrical circuit model, viz. reduction of both the electrode impedance and the leakage pathway. In Figure 6-19 the currents flowing through the system (model), when 20 pores are formed, are plotted versus the frequency. In this case, the current through the cell is significantly higher – more than 2 orders of magnitude – than the current through the leakage pathway. Moreover, at frequencies below 1 kHz the current through the cell is the dominant current: for these frequencies it is thus possible to detect single cell electroporation. At frequencies beyond this value, electroporation can be detected if the current through the stray capacitance is compensated [13].

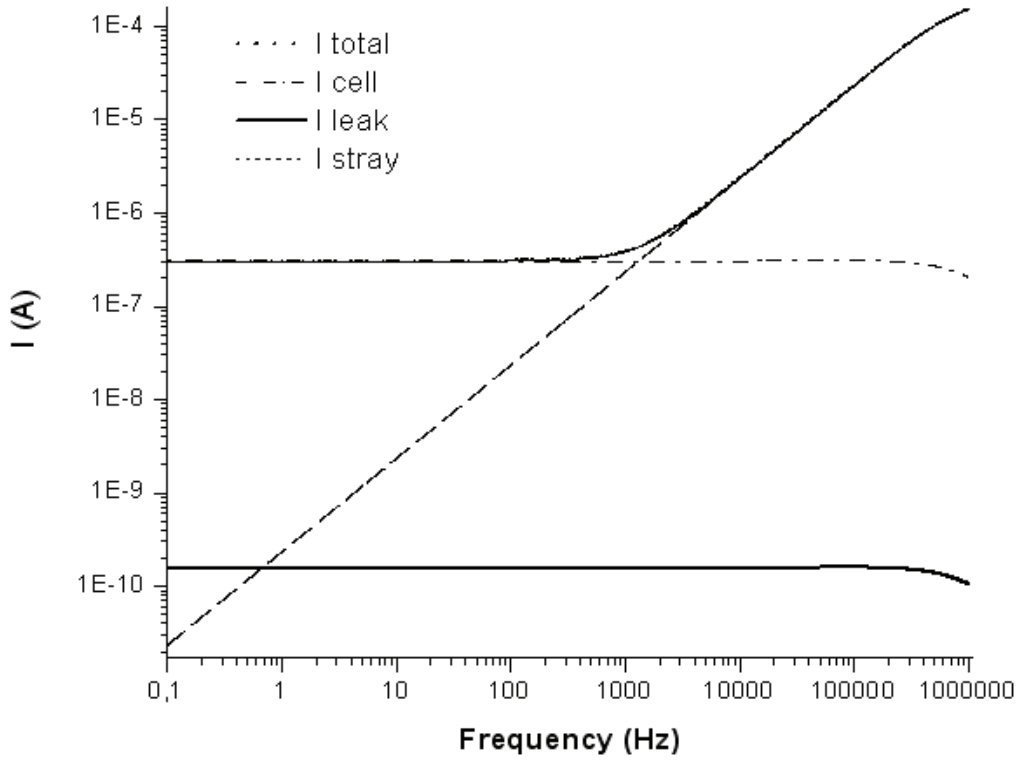

Figure 6-19: Currents through the system versus frequency for case D: R_{leak} is 1 GΩ and use of electrodes with a low impedance.

6.5 Experiments

6.5.1 Impedance spectroscopy

To measure the impedance of the chip as a function of the frequency, an impedance spectroscopy of the chip filled with the buffer solution was performed with a potentiostat. The impedance spectra for one of the electrodes are shown in Figure 6-16.

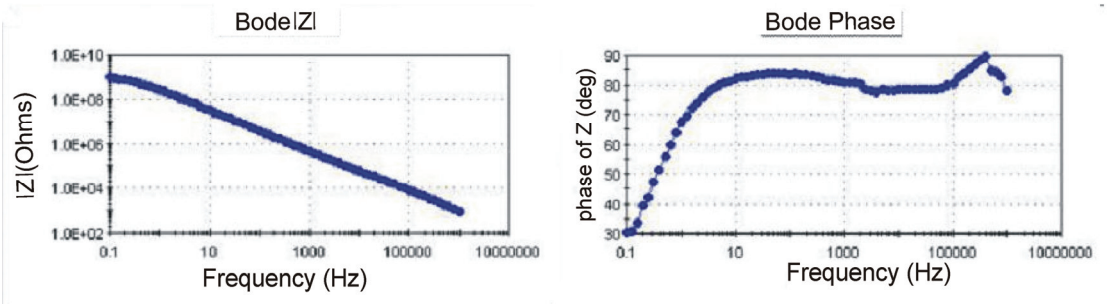

Figure 6-20: Bode plot of the impedance spectroscopy measurement of a chip filled with buffer solution.

The impedance spectra show that there is not real plateau present in the bode plot for the absolute impedance when compared to the ideal situation (see Figure 6-12). In the bode plot of the phase, a small dip can be distinguished at the frequency of 20 kHz. This means the system is mainly capacitive. Corresponding to this change in the phase, there also has to be a resistive part present, but this seems to be small (i.e. not observable Figure 6-16). The 'plateau' that is visible at very low frequencies is due to the measurement equipment, and not due to the chip.

The consequence of this capacitive behaviour is that it might be difficult to measure any changes in current when the resistance of the cell membrane suddenly decreases due to electroporation. This is further elaborated for C2C12 cells and discussed in section 6.5.2.

6.5.2 Electrical detection of C2C12 cells electroporation

6.5.2.1 Set-up

An experimental system was designed which allows optical inspection and electrical recording of cell electroporation. The chip is mounted on to an X-Y-Z translation stage in an inverted microscope (Leica DM IRM, Leica Microsystems, Wetzlar, GmbH, Germany). The microscope is equipped with a mercury lamp, 20x, 50x and 63x objectives, and a fluorescence filter set (BP 450-490, LP 515). A computer controlled CCD camera (Leica DFC300 FX) is mounted in the microscope for imaging recording. The electrodes, which serve to both apply the voltage and record the current, are connected to a function generator card (NI 5401, National Instruments) and a data acquisition card (NI PCI-6221, National Instruments) which are controlled via a Labview program. The DAQ-card records the current resulting from the electroporation signal which is amplified and convert to voltage via a current-to-voltage converter.

6.5.2.2 Electrical detection of EP of C2C12 cells

C2C12 cells were loaded and trapped in the chip. Optical inspection of cell electroporation was performed via the membrane-integrity DNA stain PI. A cell was stimulated with pulses of 6 ms with increasing amplitude from 1 V to 3 V with steps of 0.5 V. Electroporation was detected optically by PI uptake at 3 V. The resulting electrical signals of such an experiment are shown in Figure 6-17.

A jump in current at 3 V, the voltage where electroporation was detected optically, is however not observed. Figure 6-17 shows that the exponential decay is different for the pulses of 2.5 V and 3 V. Moreover, the increase in the 'plateau' level is not linear. The difference in the plateau levels between 2.5 V and 3 V is larger that the difference between 2 V and 2.5 V. The peak values do seem to scale linearly. Therefore, it is concluded that it is not possible to electrically detect electroporation from jumps in current signals. Why the increase in current is not visible is not fully understood, but it might be that the change jump in current due to the electroporation is too small to measure with respect to the exponential decay.

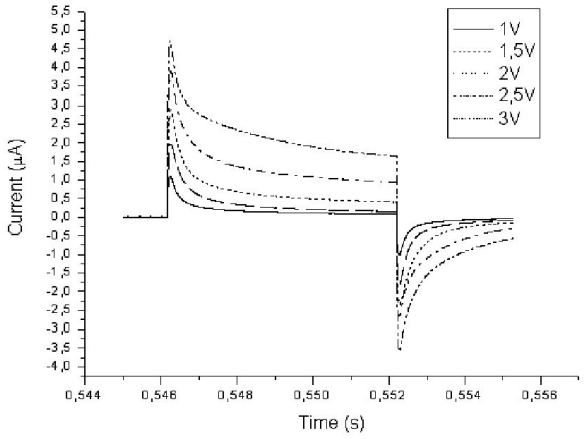

Figure 6-21: Currents measured during an electroporation experiment where a cell was stimulated with pulses of 6 ms, with increasing amplitude. EP is detected optically at 3 V.

A comparison between the signals from the experiment and the model results shows that the measured signals are not identical to the simulated signals. Even though for both signals an exponential decay is observed, the values for the plateau and the peak differ between the simulations and the experimental result. The plateau level of the simulations is lower than the plateau of the experimental result, whereas the peaks are higher in the simulations.

Therefore, it seems that the model does not fully simulate the situation during experiments since the model is quite simple, it consists only of perfect capacitors and resistors, it is too theoretical.

As mentioned before, the exponential decays of the signals from experiments seem to vary from each other. This difference in exponential decay could be an indication for electroporation. Therefore an analysis of the exponential decays shown in Figure 6-17 was done by fitting to a RC-network:

$$y = y_0 + A * e^{-t/\tau} \qquad \text{eq. (7)}$$

Where τ is the RC-time (the time required for the capacitor to be charged to 63.2% of the full charge) which is the product of the resistance and capacitance τ = R*C of a network with a resistor with a value R (in Ω) and a capacitor with a value C (in Farads).

The signals did not fit to equation 7, therefore another formula was tried. The best fitting was obtained with the eq.(8):

$$y = y_0 + A_1 * e^{-t/\tau_1} + A_2 * e^{-t/\tau_2} \qquad \text{eq. (8)}$$

This formula represents a circuit with two RC-networks with RC-times τ_1 and τ_2, (two dominant RC-networks).

In table 6-IV the parameters obtained from the fit are shown for the five pulses used for the experiments. The RC-times (τ_1 and τ_2) are plotted in Figure 6-18.

Parameters	**1V**	**1.5V**	**2V**	**2.5V**	**3V**
y_0	0.08084	0.14204	0.38565	0.89603	1.44367
A_1	0.27971	0.57032	0.8059	1.1654	1.6841
τ_1	0.000162	0.00167	0.0018	0.00196	0.0028
A_2	0.81104	1.13327	1.82104	1.92434	1.70399
τ_2	0.0002	0.00026	0.00024	0.00026	0.00017

Table 6-IV: Parameters of the fitting; pulses of 6 ms with different amplitudes in an open trap.

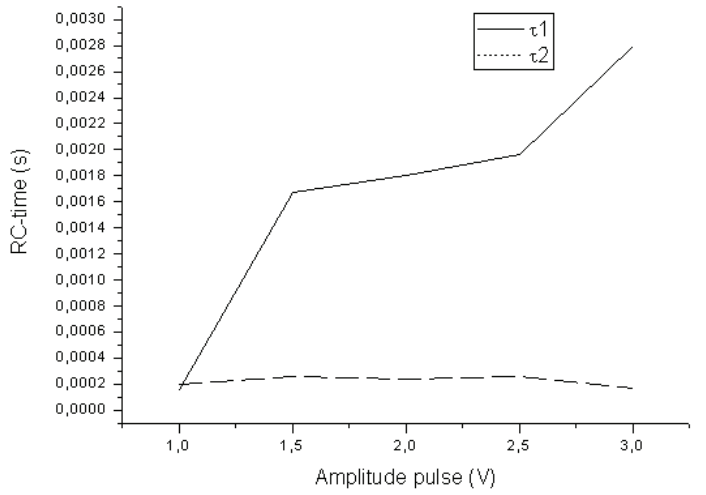

Figure 6-22: RC times (τ_1 and τ_2) for the different amplitudes of the pulse.

When comparing the two RC-times τ_1 and τ_2 there seems to be an increasing trend in the RC-time $\tau 1$ for increasing pulse amplitudes up to 3 V, especially for τ_1. It could be that τ_1 > 2.5 ms and τ_2~ 0.2 ms could be an indication for electroporation but it is uncertain. Instead it was investigated if a small AC signal could be used to detect electroporation electrically. A superposition of a pulse and a small AC signal is used, where the pulse is used for electroporating the cell and the

AC signal is used to measure the change in current when the cell gets electroporated.

A frequency of 20 kHz was chosen for the AC-sine wave, this frequency is based on the results of the impedance spectroscopy measurement (section 6.5.1). Since only information of the AC signal is of interest (the pulse will only be used for electroporating the cell), the recorded signal has to be filtered to remove the frequency components of the pulse. A third order elliptic band pass filter with cut-off frequencies of 19 kHz and 21 kHz was chosen to filter the AC signal.

By applying this signal, a superposition of a pulse of 2 V and 6 ms with a sine wave of 200 mV at 20 kHz, to an open trap it was found that the AC signal is larger after the pulse than before (Figure 6-19a). During the pulse the amplitude of the total signal is also higher than the amplitude before the pulse. The two extra peaks are most likely remaining pulse peaks after filtering caused by the frequency components of the pulse. The increase in amplitude after the pulse is probably caused by a decrease of the electrode impedance due to electrochemical cleaning of the electrodes. During electrochemical cleaning, hydrogen and oxygen ions that are absorbed in the platinum electrodes are released, resulting in a change in the double layer composition. Due to this change, the double layer capacitance increases which causes the increase in amplitude of the signal.

To prevent the influence of this electrochemical cleaning process on the current measurements, the electrodes need to be electrochemically cleaned before each experiment. This has to be done with relatively low amplitude of the pulse, to prevent Faradaic processes to take place. Several different approaches to electrochemically clean the electrodes were investigated. For all the approaches, a superposition of a sine wave of 20 kHz (0.2 V amplitude) and a pulse of 1 V was used. The length of the pulse as well as the number of pulses was varied. A pulse of 30 seconds gave the best results (i.e. nearly the same current levels before/after the pulse, Figure 6-19b) and therefore selected as a 'cleaning signal' of the electrodes prior to the experiments.

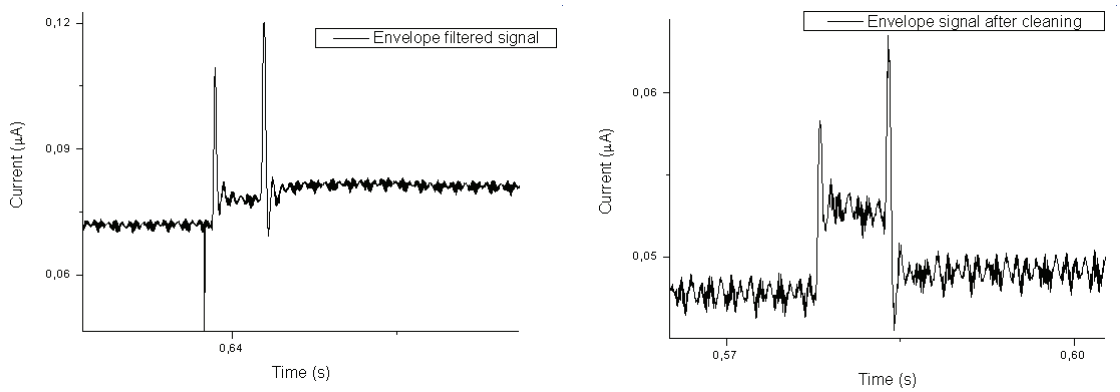

(a) (b)

Figure 6-23: (a) Envelope of the applied signal (superposition of a pulse of 2 V- 6 ms and a sine wave of 0.2 V and 20 kHz) to an open trap. (b) Envelope of the applied signal after the cleaning procedure.

After the cleaning procedure of the electrodes was established, it was tried to electrically detect electroporation by means of changes in the amplitude of the AC signal. Cells were stimulated with signals with a pulse of 6 ms with increasing amplitude (from 0.5 V to 2 V, in intervals of 0.5 V) and a sine of 20 kHz and 0.2 V, and the filtered response was recorded. Electroporation was detected optically via the fluorescent marker PI at 2V. The response of a pulse amplitude of 2 V showed that during this pulse there is a decay in the amplitude (Figure 6-20a) which was not present in the responses from the other amplitudes. Since the signal of 2 V gave PI uptake, this could be an indication for electroporation.

In a following experiment the cells were stimulated with signals of a pulse of 6 ms with increasing amplitude (from 0.4 V in intervals of 0.2 V) and a sine of 20 kHz and 0.2 V and the filtered response was recorded. Electroporation was optically detected at 3.8 V. In this case the cell was smaller than for the previous experiment and therefore a higher voltage was needed to obtain electroporation. The signal at 3.8 V shows an exponential decay during the pulse and a higher amplitude after the pulse (Figure 6-20b).

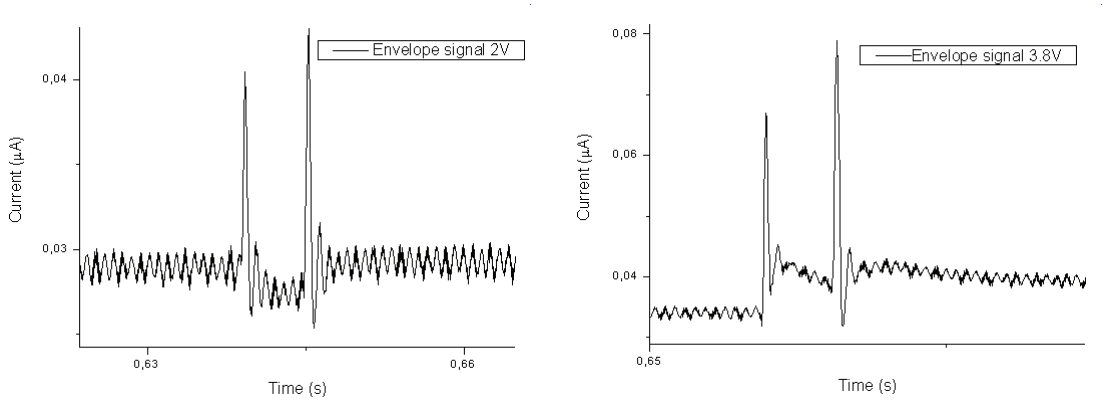

(a) (b)

Figure 6-24: (a) Envelope of the applied signal (pulse of 2 V-6 ms and a sine wave of 0.2 V at 20 kHz) when electroporation was detected optically. (b) Envelope of the applied signal (pulse of 3.8 V-6 ms and a sine wave of 0.2 V at 20 kHz) when electroporation was detected optically

Both signals in figure 6-20 are recorded for situations where electroporation was observed optically by PI uptake (cells showing red fluorescence). Figure 6-20b shows that the amplitude of the AC signal during the pulse was higher than the amplitude of the AC signal before and after the pulse (3.8 V). This is however not the case for Figure 6-20a, were the cell got electroporated at an amplitude of the pulse of 2 V. This might be due to the voltage dependent double layer capacitance. As a result the amplitude of the AC signal during pulse depends on the amplitude of the stimulation pulse. Thus, a higher stimulation pulse would increase the amplitude of the AC signal during pulse.

However, the results (current changes as indication for EP) are not conclusive to determine electroporation.

6.6 Conclusions and Outlook

In this chapter two models are elaborated to characterize and simulate single cell electroporation in a microfluidic cell trap device. A Finite Element Model is used to investigate the potential distribution in the cell trap chip as well as the voltage drop over a trapped cell. The FEMlab simulations show that when there is no leakage pathway, around 90% of the potential is across the cell and 10% (1 V of 10V) over the channel. When there is a leakage pathway, however, around 40% of the total potential is across the cell, while 15% is over the channel and 45% leaks around the trapped cell. The voltage over the stimulated cell is more than 50% smaller when there is a leakage pathway than when there is no leakage (4 V vs 9 V). This is a significant difference: it implies that, in order to obtain the same transmembrane potential, the stimulation voltage needs to be higher when there is a leakage path, which will always be the case during experiments. The voltage drop over the cells located in traps next to the stimulated cell is quite small compared to the voltage over the stimulated cell (0.15 V vs 3.9 V) if there is a leakage path around the trapped cell. Thus, adjacent cells are not influenced by the stimulated cell. Finally, the FEM simulations showed that stimulation electrodes that are not used should be grounded.

Since all the simulations with the FEMlab model are purely resistive, in future simulations it is necessary to add capacitive influences to the model in order to get insight in their influence. Furthermore, the cell model can be extended by implementing a two shelled model instead of a single shelled model, or by putting the nucleus of the cell into the model. Moreover, for the described simulations, the cytoplasm is modeled as a sphere of continuous liquid during the described simulations, but in practice the cytoplasm is filled with organelles (specialized organs within cells). These organs have different electrical parameters than the cytoplasm, and the results will therefore be different. Finally, implementation of transient elements in the FEM model, for example the change of the conductivity and permittivity of the cell membrane in time during electroporation, will result in a better model for studying/investigations on electroporation.

An equivalent electrical circuit model of the chip with a trapped cell is developed to verify whether it is possible to measure electroporation electrically. The electrical circuit model showed that electrical detection of electroporation should be possible with a sine wave at a frequency of 20 kHz.

Experiments performed with the cell membrane integrity marker (PI) showed that single cell electroporation was achieved: only the cell that was electrically addressed with the electroporation signal showed the red fluorescence, cells located at the neighbouring traps did not. However, these experiments revealed that electrical detection of electroporation is not completely clear and conclusive. This could be due to too large capacitive effects, but also electrochemical processes could play a role. Therefore, a more detailed analysis of the current variations during pore formation using a sine wave was made. A frequency characterization of the currents flowing through the system was performed. From these characterizations, several improvements for the measurement setup followed.

Solutions to get better electrical detection of electroporation are reduction of the leak resistance around the cell and of the electrodes' impedance. Better sealing of cells can be achieved by reducing the height of the traps: if the height of the traps is reduced, the cells will block better the traps, and the leakage resistance will increase. The model showed that an increase of the leakage resistance from the kiloOhm range to the gigaOhm range makes it possible to detect pore formation for frequencies below 200 Hz. However, complete blocking of the trap by the cell is unlikely and undesired in the current chips (e.g. because of cross talk to neighbouring cells). The use of low impedance electrode material (e.g. Ag/AgCl) is a better choice, since there is no polarisation at the electrode surface. According to the model, combination of these two improvements results in a setup that can be used to detect single cell electroporation electrically for frequencies below 1 kHz.

The used equivalent electrical circuit model of the chip with a trapped cell does, however, not take into account any imperfections which could be present in the chip, like the roughness of the electrodes or any electrode contamination. A better model can be obtained by implementing these imperfections, as well as transient components.

Other options to improve the method to detect SCE electrically could be the use of microfluidic cell trap devices entirely made of glass. Since glass is non-conductive, the stray capacitance will be smaller within such chips, and therefore have less influence on the current measurements (i.e. a broader frequency range). Another option to detect electroporation electrically could be the use of chips with individually isolated cell traps.

6.7 References

[1] W. Chen and R. C. Lee - *Altered ion channel conductance and ionic selectivity induced by large imposed membrane potential pulse;* Biophysical journal, **67** (1994), pp 603-612.

[2] J. C. Weaver and K. H. Schoenbach - *Biodielectris;* IEEE Transactions on Dielectrics and Electrical Insulation, **10** (2003), pp 715-716.

[3] J. C. Weaver - *Electroporation of cells and tissues;* IEEE Transactions on Plasma Science, **28 (1)**, (2000), pp 24-33.

[4] J. C. Weaver - *Electroporation of biological membranes from multicellular to nano scales;* IEEE Transactions on dielectrics and electrical insulation, **10 (5)**, (2003), pp 754-768.

[5] E. Neumann, A. E. Sowers and C. A. Jordan -*Electroporation and electrofusion in cell biology;* Plenum Press, New York (1989).

[6] J. C. Weaver and Y. A. Chizmadzhev - *Theory of electroporation: a review;* Bioelectrochemistry and bioenergetics, **41** (1996), pp 135-160.

[7] D. C. Chang, B. M. Chassy, J. A. Saunders and -*Guide to electroporation and electrofusion;* Academic Press, San Diego (1992).

[8] M. Khine, A. Lau, C. Ionescu-Zanetti, J. Seo and L. P. Lee - *A single cell electroporation chip;* Lab on a chip, **5** (2005), pp 38-43.

[9] Y. Huang, N. S. Sekhon, J. Borninski, N. Chen and B. Rubinsky - *Instantaneous, quantitative single-cell viability assessment by electric evaluation of cell membrane integrity with microfabricated devices;* Sensors and Actuators A, **105** (2003), pp 31-39.

[10] Gamry Instruments - *Electrochemical Impedance Spectroscopy Primer;* http://www.gamry.com/App_Notes/EIS_Primer/EIS_Primer.htm, (2005).

[11] W. Olthuis, W. Streekstra and P. Bergveld - *Theoretical and experimental determination of cell constants of planar-interdigitated electrolyte conductivity sensors;* Sensors and Actuators B, **24 (1-3)** (1995), pp 252-256.

[12] Y. T. C. Ko, J. P. Huang and K. W. Yu - *Dielectric behaviour of graded spherical cells with an intrinsic dispersion;* European physical journal E, **14 (1)** (2004), pp 97-104.

[13] J. W. Wood - *Stray-capacitance neutralisation for high-resistance microelectrodes - a simple analysis;* Medical & biological engineering and computing, **19** (1981), pp 230-236.

[14] A. J. A. Bard and L. R. Raulkner, - *Electrochemical Methods, Fundamentals and Applications;* J. Wiley & Sons, New York (1980).

Appendix A

First, the liquid resistances of the two trappings structures are calculated, together with the resistance of the liquid in between the stimulation electrode and the trap. Next, the double layer impedance at the metal/liquid interface is calculated as well as the stray capacitances. Last, the values for the different components of the cell model are calculated, together with the resistance of the leakage pathway. Most of the parameters used in the calculations are summarized in table 6-V.

Parameters		Numerical values
Cell diameter	d_c	10 μm
Cell membrane thickness	l_m	4 nm
Silicon oxide thickness	d_{sio}	300 nm
Vacuum permittivity	ε_0	8.85e-12 F/m
Buffer permittivity [3]	ε_l	80 * ε0 F/m
Buffer conductivity [0]	σ_l	1.572 S/m
Silicon oxide permittivity [2]	ε_{sio}	3.9 * ε0 F/m
Platinum conductivity [2]	σ_{pt}	8.99*106 S/m
Membrane permittivity [1]	ε_m	7.23 * ε0 F/m
Membrane conductivity [1]	σ_m	4.10-7 S/m
Cytoplasm permittivity [1]	ε_c	120 * ε0 F/m
Cytoplasm conductivity [1]	σ_c	0.25 S/m

Table 6-V: Parameters used for the model calculations. [0] = value obtained from measurements, [1] = values from [12], [2] = values obtained from database FEMlab, [3] = permittivity of water.

Resistance of the liquid in the chip

In this section the liquid resistance of the channel and the trapping structures is calculated using eq.(1). The resistance of a trap, type 1, taking into account that the trap is 4 μm wide, 15 μm deep and 30 μm long, is:

$$\rho_l = \frac{1}{\sigma_l} = \frac{1}{1{,}572}\Omega$$

$$R_{el,\ trap1} = \rho_l \frac{l_{t1}}{A_{t1}} \qquad \text{eq.(A1)}$$

$$R_{el,\ trap1} = \frac{1}{1{,}572} \times \frac{30 \cdot 10^{-6}}{4 \cdot 10^{-6} * 15 \cdot 10^{-6}} = 32k\Omega \qquad \text{eq.(A2)}$$

where l_{t1} is the length, and A_{t1} the cross-section of a trap type 1.

The resistance of a trap, type 2, is calculated below as follows;
The height of the structure is 15 μm.

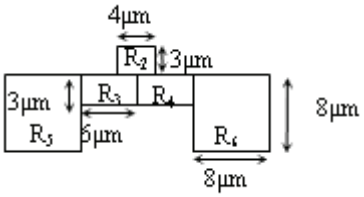

Figure 6-25: Modeling of the resistance of one trap (type 2).

with:

$$R_2 = \rho_l \times \frac{3 \cdot 10^{-6}}{15 \cdot 10^{-6} \times 4 \cdot 10^{-6}} = \rho_l \times 5 \cdot 10^4 \qquad \text{eq.(A3)}$$

$$R_3 = R_4 = \rho_l \times \frac{6 \cdot 10^{-6}}{15 \cdot 10^{-6} \times 3 \cdot 10^{-6}} = \rho_l \times 1{,}33 \cdot 10^5 \qquad \text{eq.(A4)}$$

$$R_5 = R_6 = \rho_l \times \frac{8 \cdot 10^{-6}}{15 \cdot 10^{-6} \times 8 \cdot 10^{-6}} = \rho_l \times 6{,}67 \cdot 10^4 \qquad \text{eq.(A5)}$$

and:

$$R_{trap} = R_2 + \frac{(R_3 + R_5)(R_4 + R_6)}{(R_3 + R_5) + (R_4 + R_6)} = R_2 + \frac{(R_3 + R_5)^2}{2(R_3 + R_5)} \qquad \text{eq.(A6)}$$

It follows that:

$$R_{trap} = 5 \cdot 10^4 \times \rho_l + \frac{\left(1{,}33 \cdot 10^5 \times \rho_l + 6{,}67 \cdot 10^4 \times \rho_l\right)^2}{2\left(1{,}33 \cdot 10^5 \times \rho_l + 6{,}67 \cdot 10^4 \times \rho_l\right)} = \left(5 \cdot 10^4 + \frac{4 \cdot 10^{10}}{4 \cdot 10^5}\right) \times \rho_l \cong 1{,}5 \cdot 10^5 \times \rho_l \qquad \text{eq.(A7)}$$

$$R_{trap} = \left(1{,}5 \cdot 10^5\right) \times \left(\frac{1}{1{,}572}\right) = 9{,}5 \cdot 10^4 \Omega = 95\Omega \qquad \text{eq.(A8)}$$

The resistance of the liquid between the stimulation electrode and the trap is located in series with the resistance of the trap. This resistance is estimated to be (eq.A9):

$$R_l = \rho_l \times \frac{l_{ch}}{A_{ch}} = \frac{1}{1{,}572} \times \frac{50 \cdot 10^{-6}}{15 \cdot 10^{-6} \times 70 \cdot 10^{-6}} = 30k\Omega \qquad \text{eq.(A9)}$$

where l_{ch} is the length of the channel and A_{ch} the cross-section of the channel. The resulting part of the model for the liquid resistances is shown in Figure 6-26.

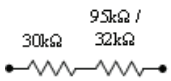

Figure 6-26: Electrical circuit model for the liquid resistances.

The double layer impedance at the metal/liquid interfaces

The differential capacity of the total double layer with charge σ_M is:

$$C_{DL} = \frac{d\sigma_M}{d\psi_M} \qquad \text{eq.(A10)}$$

The reciprocal value can easily be described as two capacitors in series: the Stern capacitance (C_{Stern}) and the diffusion capacitance (C_{diff}):

$$\frac{1}{C_{DL}} = \frac{d\left[(\psi_M - \psi_s) + \psi_s\right]}{d\sigma_M} = \frac{1}{C_{Stern}} + \frac{1}{C_{diff}} \qquad \text{eq.(A11)}$$

The values of these capacitances are by approximation:

$$C_{stern} = \frac{\varepsilon^*}{\delta} \qquad \text{eq.(A12)}$$

$$Cdiff = \varepsilon_l \times K \qquad \text{eq.(A13)}$$

with

$$\varepsilon_l = \varepsilon_{lr} \times \varepsilon_0 = 80 \times 8{,}84e^{-12} F/m \quad (\textit{The absolute permittivity of water}) \qquad \text{eq.(A14)}$$

with ε_{lr} the relative permittivity of water (80), and ε_0 the permittivity of vacuum (8.85e^{-12} F/m), ε^* the unknown dielectric constant of the Stern layer. Since δ is independent of the electrolyte solution concentration the Stern capacitance is constant (20 μF/cm^2) [14]. This capacitance needs to be multiplied by the surface of the electrodes to obtain the Stern capacitances. The diffusion layer capacitance is calculated using the equation A13. This equation gives the capacitance in farads per m^2. Therefore, this value has to be multiplied by the surface of the electrode to get the diffusion capacitance in farads. Since the surfaces of the stimulation and measurement electrode differ, the double layer capacitances will be different for both electrodes. The surface of one of the stimulation electrodes ($A_{e,stim}$) is 20 μm × 31 μm. For this electrode the double layer capacitance is:

$$C_{St,stim} = 0{,}2 \times 20 \cdot 10^{-6} \times 31 \cdot 10^{-6} F = 0{,}124 nF \qquad \text{eq.(A15)}$$

$$C_{di,stim} = \varepsilon_l \times \varepsilon_0 \times A_{e,stim} \times \kappa = \qquad \text{eq.(A16)}$$

$$80 \times 8{,}85 \cdot 10^{-12} \times 20 \cdot 10^{-6} \times 31 \cdot 10^{-6} \times 1/(50 \cdot 10^{-10}) = 87{,}8 pF$$

$$C_{DL,stim} = \frac{0{,}124 \cdot 10^{-9} \times 87{,}8 \cdot 10^{-12}}{0{,}124 \cdot 10^{-9} + 87{,}8 \cdot 10^{-12}} = 51{,}4 pF \qquad \text{eq.(A17)}$$

The surface of the measurement electrode ($A_{e,measure}$) is approximately (8+8) μm × 41 μm. The double layer capacitance is then calculated as follows:

$$C_{St,measure} = 0{,}2 \times 16 \cdot 10^{-6} \times 41 \cdot 10^{-6} = 0{,}131 nF \qquad \text{eq.(A18)}$$

$$C_{di,measure} = \varepsilon_l \times \varepsilon_0 \times A_{e,measure} \times \kappa = \qquad \text{eq.(A19)}$$

$$80 \times 8{,}85 \cdot 10^{-12} \times 16 \cdot 10^{-6} \times 41 \cdot 10^{-6} \times 1/(50 \cdot 10^{-10}) = 92{,}9 pF$$

$$C_{DL,measure} = \frac{0{,}131 \cdot 10^{-9} \times 92{,}9 \cdot 10^{-12}}{0{,}131 \cdot 10^{-9} + 92{,}9 \cdot 10^{-12}} = 54{,}4 pF \qquad \text{eq.(A20)}$$

Since the double layer resistance is very difficult to calculate its value was estimated from an impedance measurement of the chip. The electrical model described so far is given in Figure 6-27:

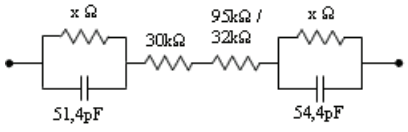

Figure 6-27: The electrical circuit model extended with the double layer impedances.

Stray capacitances

The stray capacitances through the silicon can be calculated with the formula for the parallel plate capacitor (eq.2). In order to do this the total surface of one of the stimulation electrodes and of the measurement electrode has to be known. These sizes are estimated using Figure 6-28.

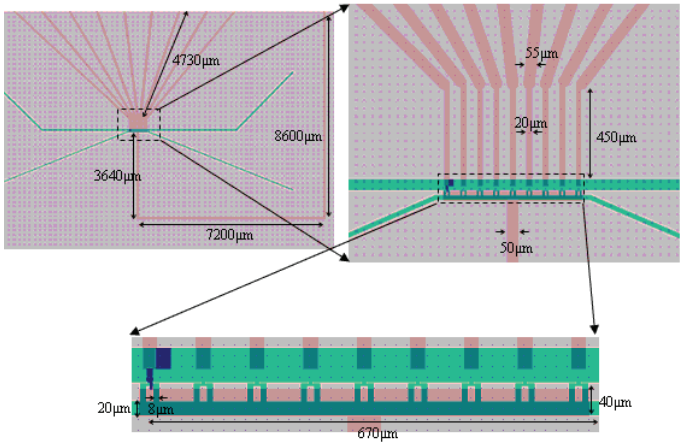

Figure 6-28: Estimation of the surfaces of the electrodes for calculating the stray capacitances through the silicon.

The stray capacitance through the silicon for the stimulation electrode is:

$$A_{T,stim} = \left(20\cdot10^{-6}\times450\cdot10^{-6}+55\cdot10^{-6}\times4730\cdot10^{-6}\right)m^2 = 0{,}27\cdot10^{-6}m^2 \qquad \text{eq.(A21)}$$

$$d_{sio} = 300\cdot10^{-9}m$$

$$C_{si,stim} = \frac{\varepsilon_{sio}\times\varepsilon_0\times A_{T,stim}}{d_{sio}} = \frac{3{,}9\times8{,}85\cdot10^{-12}\times0{,}27\cdot10^{-6}}{300\cdot10^{-9}} = 30{,}9pF \qquad \text{eq.(A22)}$$

where $A_{T,stim}$ is the total surface of one stimulation electrodes, and d_{sio} the thickness of the silicon oxide.

The stray capacitance through the silicon for the measurement electrode is:

$$A_{T,measure} = \left(3640\cdot10^{-6}+7200\cdot10^{-6}+8600\cdot10^{-6}\right)\times50\cdot10^{-6}+ \left(\left(670\cdot10^{-6}\times40\cdot10^{-6}\right)-\left(670\cdot10^{-6}\times20\cdot10^{-6}+18\times8\cdot10^{-6}\times19\cdot10^{-6}\right)\right) = 0{,}98\cdot10^{-6}m^2 \qquad \text{eq.(A23)}$$

$$d_{sio} = 300\cdot10^{-9}m$$

$$C_{si,measure} = \frac{\varepsilon_{sio}\times\varepsilon_0\times A_{T,measure}}{d_{sio}} = \frac{3{,}9\times8{,}85\cdot10^{-12}\times0{,}98\cdot10^{-6}}{300\cdot10^{-9}} = 0{,}113nF \qquad \text{eq.(A24)}$$

where $A_{T,measure}$ is the surface of the measurement electrode, and d_{sio} the thickness of the silicon oxide. With these two capacity values the total stray capacitance through the silicon can be calculated (eq.A25)

$$C_{stray,Si} = \frac{1}{\frac{1}{C_{stray,Si,meas}}+\frac{1}{C_{Stray,Si,stim}}} = \frac{1}{\frac{1}{30{,}9\cdot10^{-12}}+\frac{1}{0{,}113\cdot10^{-9}}}F = 24{,}3pF \qquad \text{eq.(A25)}$$

The calculation of the liquid stray capacitance $C_{stray,l}$ was done in Maple and the value is approximately 9.64 *f*F.

with the two values for the stray capacitance through the liquid and through the silicon, the total stray capacitance can be calculated ($C_{stray,Si}$ and $C_{stray,l}$ are in parallel). The total stray capacitance through the silicon is:

$$C_{stray} = C_{stray,Si} + C_l = 24{,}3 \cdot 10^{-12} + 9{,}64 \cdot 10^{-15} = 24{,}3 \cdot 10^{-9}\, F = 24{,}3\, pF \qquad \text{eq.(A26)}$$

Simulations were done with an electrical circuit model in pSpice to see if the stray capacitances between the stimulation electrodes have an important influence on the measured current. It was found that is not the case and therefore these capacitances are not included in our model. Adding the stray capacitance, the electrical circuit model becomes:

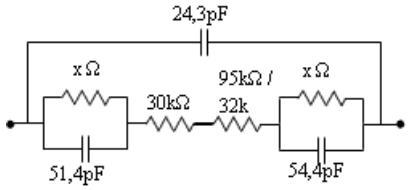

Figure 6-29: The electrical circuit model extended with the double layer impedances.

Cell model

First the resistances and capacitances of the cell membrane will be calculated, as well as the changes of these resistances and capacitances due to pore formation. Next, the resistance of a pore and the resistance of the cytoplasm and last the leak resistance are calculated.

a) Resistances and capacitances of the cell membrane

The cell membrane resistance, R_{mem}, are calculated using eq.(1), where

$$\rho_m = \frac{1}{\sigma_m} = \frac{1}{4 \cdot 10^{-7}} \Omega, \quad \textit{the resistivity of the membrane}$$

and

$$l_m = 4nm, \quad \textit{the thickness of the membrane}$$

For the part of the membrane outside of the trap (~90% of the membrane):

$$A_{mem,ot} = 0{,}9 * 4 * \pi * r^2 = 0{,}9 * 4 * \pi * (5 \cdot 10^{-6})^2 = 2{,}83 \cdot 10^{-10}\, m^2$$

$$R_{mem,ot} = \rho_m \frac{l_m}{A_{m,ot}} = (\frac{1}{4 \cdot 10^{-7}}) * (\frac{4 \cdot 10^{-9}}{0{,}283 \cdot 10^{-9}}) = 3{,}53678 \cdot 10^7\, \Omega \qquad \text{eq.(A27)}$$

where $A_{mem,ot}$ is the surface area of the membrane outside the trap and $R_{mem,ot}$ the resistance of the membrane outside the trap.

Similarly, the resistance of the part of the membrane inside the trap (~10% of the membrane) is:

$$A_{m,it} = 0{,}1 * 4 * \pi * r^2 = 0{,}1 * 4 * \pi * (5 \cdot 10^{-6})^2 = 3{,}1416 \cdot 10^{-11}\, m^2$$

$$R_{mem,it} = \rho_m \frac{l_m}{A_{m,it}} = (\frac{1}{4 \cdot 10^{-7}}) * (\frac{4 \cdot 10^{-9}}{0{,}0314 \cdot 10^{-9}}) = 3{,}1831 \cdot 10^8\, \Omega \qquad \text{eq.(A28)}$$

where $A_{m,it}$ is the surface area of the membrane inside the trap and $R_{mem,it}$ the resistance of the membrane inside the trap.

The cell membrane capacitance, C_{mem}, is calculated using the formula for the parallel plate capacitance (eq. 2).

For the part of the membrane outside the trap (90% of the membrane):

$$C_{mem,ot} = \frac{\varepsilon_m \times \varepsilon_0 \times A_{m,ot}}{l_m} = \frac{7{,}23 \times 8{,}85 \cdot 10^{-12} \times 2{,}82743 \cdot 10^{-10}}{4 \cdot 10^{-9}} = 4{,}5229 \cdot 10^{-12} \cong 4{,}52\,pF \qquad \text{eq.(A29)}$$

where $A_{m,ot}$ is the surface area of the membrane outside the trap, ε_m the permittivity of the membrane, l_m is the thickness of the membrane and $C_{mem,ot}$ the capacitance of the membrane outside the trap.

For the part of the membrane inside the trap (10% of the membrane):

$$C_{mem,it} = \frac{\varepsilon_m \times \varepsilon_0 \times A_{m,it}}{l_m} = \frac{7{,}23 \times 8{,}85 \cdot 10^{-12} \times 3{,}1416 \cdot 10^{-11}}{4 \cdot 10^{-9}} = 0{,}502\,fF \qquad \text{eq.(A30)}$$

where $A_{m,it}$ is the surface area of the membrane inside the trap, ε_m the permittivity of the membrane, l_m is the thickness of the membrane and $C_{mem,it}$ the capacitance of the membrane inside the trap.

The difference in resistance between a porated membrane (with one pore) and an intact membrane (without pores), $dR_{mem,ot}$ and $dR_{mem,in}$ is positioned in series with the membrane resistance. In this way, this simulates the increase in membrane resistance when a pore opens and is calculated as follows:

For the part of the membrane outside the trap (90% of the membrane):

$$\begin{aligned} A_{mp,ot} &= \left(0{,}9 \times 4 \times \pi \times r_c{}^2\right) - \left(\pi \times r_p{}^2\right) = \left(0{,}9 \times 4 \times \pi \times \left(5 \cdot 10^{-6}\right)^2\right) - \left(\pi \times \left(25 \cdot 10^{-9}\right)^2\right) \\ &= 2{,}82741 \cdot 10^{-10}\, m^2 \cong 283\,\mu m^2 \\ R_{memp,ot} &= \rho_m \frac{l_m}{A_{mp,ot}} = \left(\frac{1}{4 \cdot 10^{-7}}\right) \times \left(\frac{4 \cdot 10^{-9}}{2{,}82741 \cdot 10^{-10}}\right) = 3{,}53680 \cdot 10^{7}\,\Omega \cong 35{,}3M\Omega \qquad \text{eq.(A31)} \\ dR_{mem,ot} &= R_{memp,ot} - R_{mem,ot} = 3{,}53680 \cdot 10^{7} - 3{,}53678 \cdot 10^{7} = 246\Omega \end{aligned}$$

where $A_{mp,ot}$ is the surface area of the membrane outside the trap when one pore is formed, ρ_m the resistivity of the membrane, l_m the thickness of the membrane, $R_{memp,ot}$ the resistance of the intact membrane outside the trap, $R_{memp,ot}$ the resistance of the membrane outside the trap when one pore is formed and $dR_{mem,ot}$ the difference in resistance between a porated membrane and an intact membrane outside the trap.

For the part of the membrane inside the trap (10% of the membrane):

$$\begin{aligned} A_{mp,it} &= \left(0{,}1 \times 4 \times \pi \times r_c{}^2\right) - \left(\pi \times r_p{}^2\right) = \left(0{,}1 \times 4 \times \pi \times \left(5 \cdot 10^{-6}\right)^2\right) - \left(\pi \times \left(25 \cdot 10^{-9}\right)^2\right) \\ &= 3{,}1414 \cdot 10^{-11}\, m^2 \cong 31{,}4\,\mu m^2 \\ R_{memp,it} &= \rho_m \frac{l_m}{A_{mp,it}} = \left(\frac{1}{4 \cdot 10^{-7}}\right) \times \left(\frac{4 \cdot 10^{-9}}{3{,}1414 \cdot 10^{-11}}\right) = 3{,}1833 \cdot 10^{8}\,\Omega \cong 318M\Omega \qquad \text{eq.(A32)} \\ dR_{mem,it} &= R_{memp,it} - R_{mem,it} = 3{,}1833 \cdot 10^{8} - 3{,}1831 \cdot 10^{8} = 19{,}9k\Omega \end{aligned}$$

where $A_{mp,it}$ is the surface area of the membrane inside the trap when one pore is formed, ρ_m the resistivity of the membrane, l_m the thickness of the membrane, $R_{mem,it}$ the resistance of the intact membrane inside the trap, $R_{memp,it}$ the resistance of the membrane inside the trap when one pore is formed and $dR_{mem,it}$ the difference in resistance between a porated membrane and an intact membrane inside the trap.

The difference in capacitance between a membrane with one pore and a intact membrane (without pores), $dC_{mem,ot}$ and $dC_{mem,in}$, is positioned in parallel with the membrane capacitance to simulate the decrease in membrane capacitance when a pore opens and is calculated as follows:

For the part of the membrane outside the trap (90 % of the membrane):

$$C_{memp,ot} = \frac{\varepsilon_m \times \varepsilon_0 \times A_{mp,ot}}{l_m} = \frac{7{,}23 \times 8{,}85 \cdot 10^{-12} \times 2{,}82741 \cdot 10^{-10}}{4 \cdot 10^{-9}} =$$
$$4{,}5228 \cdot 10^{-12} F \cong 4{,}52 pF$$
$$dC_{memp,ot} = C_{memp,ot} - C_{mem,ot} = 4{,}5228 \cdot 10^{-12} - 4{,}5229 \cdot 10^{-12} =$$
$$-1{,}13 \cdot 10^{-16} F = -0{,}113 fF \qquad \text{eq.(A33)}$$

where $A_{mp,ot}$ is the surface area of the membrane outside the trap when one pore is formed, ε_m the permittivity of the membrane, l_m the thickness of the membrane, $C_{mem,ot}$ the capacitance of the intact membrane outside the trap, $C_{memp,ot}$ the capacitance of the membrane outside the trap when one pore is formed and $dC_{mem,ot}$ the difference in capacitance between a porated membrane and an intact membrane outside the trap.

For the part of the membrane inside the trap (10 % of the membrane):

$$C_{memp,it} = \frac{\varepsilon_m \times \varepsilon_0 \times A_{mp,it}}{l_m} = \frac{7{,}23 \times 8{,}85 \cdot 10^{-12} \times 3{,}1414 \cdot 10^{-11}}{4 \cdot 10^{-9}} =$$
$$5{,}0252 \cdot 10^{-13} F \cong 0{,}502 fF$$
$$dC_{mem,it} = C_{memp,it} - C_{mem,it} = 5{,}0252 \cdot 10^{-13} - 5{,}0254 \cdot 10^{-13} = \qquad \text{eq.(A34)}$$
$$-1{,}25 \cdot 10^{-17} F = -0{,}0125 fF$$

Where $A_{mp,it}$ is the surface area of the membrane inside the trap when one pore is formed, ε_m the permittivity of the membrane, l_m the thickness of the membrane, $C_{mem,it}$ the capacitance of the intact membrane inside the trap, $C_{memp,it}$ the capacitance of the membrane inside the trap when one pore is formed and $dC_{mem,it}$ the difference in capacitance between a porated membrane and an intact membrane inside the trap.

The membrane capacitance decreases with the formation of a pore, because the surface area decreases and therefore $dC_{mem,out}$ and $dC_{mem,it}$ are negative.

b) Resistance of one pore

The resistance of one pore, R_p, is calculated with eq.(1). Taking an average pore diameter of 50 nm [7]:

$$R_p = \rho_l \frac{l_m}{A_p} = \left(\frac{1}{1{,}572}\right) \times \frac{4 \cdot 10^{-9}}{1{,}96 \cdot 10^{-15}} = 1{,}30 M\Omega$$
$$l_m = 4nm$$
$$\rho_l = \frac{1}{\sigma_l} = \frac{1}{1{,}572} \qquad \text{eq.(A35)}$$
$$A_p = \pi \times r^2 = \pi \times (25 \cdot 10^{-9})^2 = 1{,}96 \cdot 10^{-15} m^2 = 0.00196 \mu m^2$$

Where A_p is the surface of the pore and R_p is the resistance of one pore.

c) The resistance of the cytoplasm

The resistance of the cytoplasm was estimated by calculating the resistance of a cylinder of liquid with the diameter of 10 µm (the diameter of a cell) and a length of 5 µm. The conductivity is given in table 6-V.

$$R_{l,cell} = \rho_c \frac{l_c}{A_c} = (\frac{1}{0{,}25}) * (\frac{5 \cdot 10^{-6}}{0{,}0785 \cdot 10^{-9}}) = 250k\Omega$$
$$l_c = 5um$$
$$A_c = \pi * r^2 = \pi * (5 \cdot 10^{-6})^2 = 7{,}85 \cdot 10^{-11} m^2 = 7{,}85 \mu m^2 \qquad \text{eq.(A36)}$$

where ρ_c is the resistivity of the cytoplasm, l_c the length of the cylinder, A_c the surface of the cylinder and $R_{l,cell}$ the resistance of the cytoplasm.

d) The leak resistance

The leak resistance is the resistance of the pathway where the current bypasses the cell. This resistance is parallel to the impedance of the cell. The leak resistance can be modeled as a block of liquid, with a height of 5 µm (channel depth is 15 µm and a cell has a diameter of ~10 µm), a width of 4 µm (the width of the trap) and a length of 1.5 µm (half of the length of the trap), see Figure 6-30.

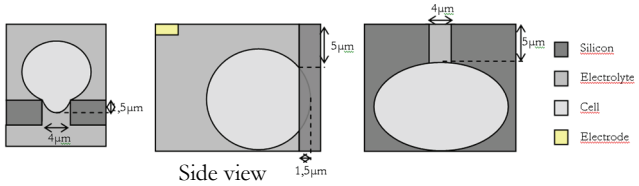

Figure 6-30: Method of calculating the leak resistance.

The leak resistance then becomes:

$$R_{leak} = \rho_l * \frac{l_L}{A_L} = \frac{1}{1.572} * \frac{1{,}5 \cdot 10^{-6}}{4 \cdot 10^{-6} * 5 \cdot 10^{-6}} \cong 47k\Omega \qquad \text{eq.(A37)}$$

where ρ_l is the resistivity of the buffer solution, l_L the length of the leakage path, A_L the surface of the leakage path and R_{leak} the leak resistance.

With all the elements described in a)-d); cell membrane, cytoplasm and R_{leak}, the electrical model of the cell becomes:

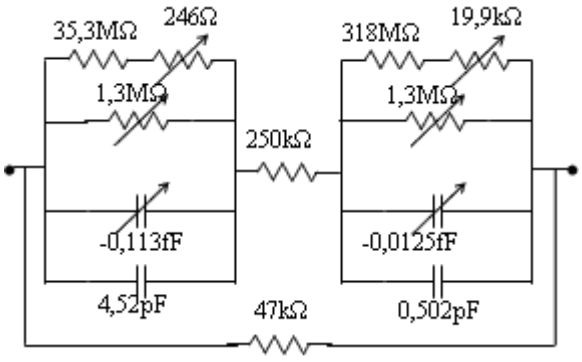

Figure 6-31: The cell model with calculated/estimated values for capacitances and resistances

Implementing the data from experiments

The resistance of the double layer is estimated from an impedance spectroscopy measurement done with a potentiostat. With the program ZsimpWin the equivalent circuit of the chip (trap 2) without a cell was

fitted to the experimental data. With the best fit the values for each element of the model were estimated (table 6-VI).

The results from this fitting show that the resistance of the liquid in the chip is in agreement with the calculated one (125 kΩ). However, the values for the other parameters (capacitances of the double layer and stray capacitance) differ from the calculated ones. In fact, the obtained values from ZsimpWin are larger than the calculated values, which can be explained by the roughness of the electrodes. This increases the surface area of the electrodes, and thus the capacitance. Therefore, it was decided to use the values from ZsimpWin.

Parameter	Value
C_{stray}	187 pF
$C_{DL,\ stim}$	370 pF
$R_{diff,\ stim}$	7.125 MΩ
$R_{el,channel+trap}$	125.5 kΩ
$C_{DL,\ measure}$	368 pF
$R_{diff,\ measure}$	886,6 MΩ

Table 6-VI: Values from the impedance spectroscopy.

The final model of a trapped cell (that is stimulated by one electrode):

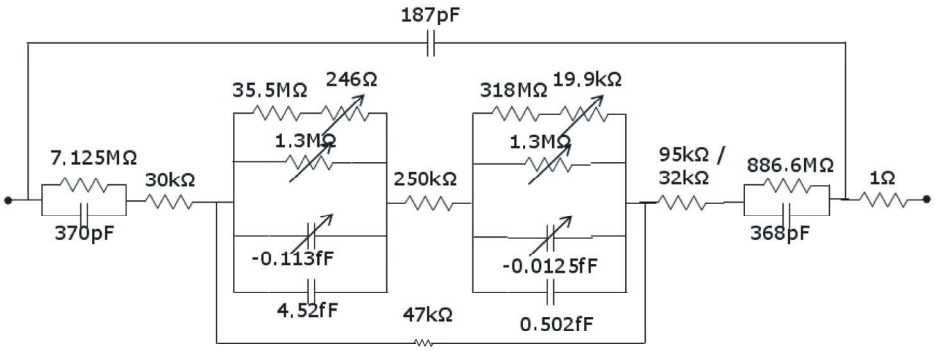

Figure 6-32: The final electrical circuit model.

Electroporation is a process where pores are created in the cell membrane. The above mentioned model takes only the formation of one pore into account, but it is easy to adopt the model to more pores. The increase in membrane resistance and the decrease in membrane capacitance will be multiplied with the number of pores, while the pore resistance will be divided by the number of pores.

7

Electroporation of yeast in a flow-through and single cell microdevice*

Microtechnology offers the opportunity to study biological processes at the cellular level. One of these processes is electroporation; the inactivation of microorganisms by high electric field pulses. In this study, electroporation of yeast was studied using two different microdevices; a single-cell electroporation device, which allows visual observation of the electroporation process of one cell in time, and a flow-through electroporation device, which gives quantitative kinetic data based on a population of cells. The electroporation process was studied using the membrane-impermeable fluorescent DNA stain PI. Visual observation and flow cytometry measurements revealed that the electroporation process is a progressive process, since the application of more pulses showed an increased PI uptake.

* This chapter is submitted to Biotechnology and Bioengineering: M.B. Fox, A. Valero, D.C. Esveld, A. van den Berg and R.M. Boom – *Electroporation of yeast in a flow-through and single cell microdevice*.

7.1 Introduction

Application of an electric field pulse to a biological cell leads to reversible membrane damage at low electric field strengths (lower than 1 kV·cm^{-1}) and inactivation of cells at high electric field strengths (generally higher than 1 kV·cm^{-1}), a phenomenon known as electroporation. When an external electric field (E) is applied to a cell, a potential difference will arise over the cellular membrane, the transmembrane potential. This transmembrane potential (VTM) is proportional to the cell radius (r) according to [1].

$$V_{TM} = 1.5\, r\, E \qquad \text{eq.(1)}$$

A transmembrane potential lower than ~1 V leads to reversible pore formation. This is extensively used for introduction of foreign molecules to cells, like DNA [2], whereby the aim is to keep the transfected cells viable. When the transmembrane potential is increased to values above 1 V, the pore formation becomes irreversible, and the extensive membrane damage will inactivate the cells. This is used for the novel pasteurization method named as pulsed electric fields (PEF) [3].

The use of microengineered systems offers major advantages for the study of electroporation process. Since the electrode distances are very small, relatively low voltages already give high electric field strengths. This facilitates the control of the electrical pulses. Secondly, since the size of the channels is in the same order of magnitude as the cells, it is possible to follow the electroporation process online, during the application of the electrical pulses. Microtechnological electroporation devices can roughly be divided into two categories [4]; microdevices that trap cells in an integrated microstructure located between two electrodes and microdevices that lead the suspended cells through a treatment-zone where the electrical pulses are delivered. The cell trapping devices are particularly suitable for the qualitative, online observation of the electroporation process since the trapped cells will not move during the treatment [5]. However, they are less suitable for quantitative measurements since the electric field is inhomogeneous and the measurements are laborious and time consuming, but do provide information about the difference between individual cells. In contrast, the flow-through devices are very suitable for quantitative measurements since samples with larger amounts of cells can be

collected after the electroporation process. However, qualitative measurements are hard to perform due to the continuous flow of cells during the application of the electrical pulses.

In this chapter, electroporation of S. cerevisae will be studied using two microdevices; a single cell trapping device and a flow-through PEF microreactor. Therefore it is possible to study the electroporation process both on single cell level and to accurately measure the average response of the ensemble of cells. The electric field distribution will be derived from a finite element model, which makes a coupling between the measurements in the single cell device and the PEF microreactor possible. The electroporation process itself will be followed by fluorescent staining. This work is submitted to Biotechnology and Bioengineering.

7.2 Material and methods

7.2.1 Microdevices: layouts and fabrication

7.2.1.1 Single cell trapping device

The cell trapping device consists of two parallel channels that are connected by microholes with dimensions smaller than cells (Figure 7-1). These microholes act as trapping sites for living cells by applying a pressure difference over the holes. The 50 μm wide top channels, the 20 μm wide bottom channel and the nine trapping sites with a width of 4 μm are etched by reactive ion etching (RIE) to a depth of 15 μm. The reservoirs are powderblasted from the backside of the silicon. On the whole substrate a silicon oxide layer is thermally grown to electrically insulate the conductive silicon. The channels are closed with a Pyrex wafer which allows the visualization of the channels as well as the trapping and the electroporation process. The platinum electrodes are sputtered into the recess Pyrex wafer, followed by anodically bonding of the two substrates.

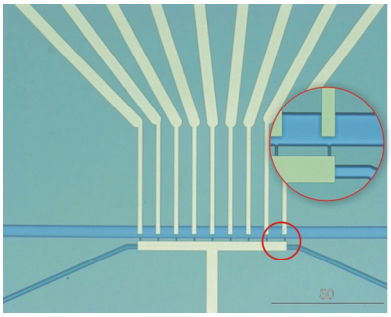

Figure 7-1: Image of the single cell trapping device with electrodes integrated and a zoom of the trapping sites (4 µm width).

7.2.1.2 PEF microreactor

The flow-through PEF microreactor was developed to study the PEF process in more detail [6] (Figure 7-2). It consists of a 50 µm deep channel with a 10 µm deep constriction. A 200 nm thick platinum electrode is placed at either side. This channel constriction acts as the treatment-zone for cell inactivation since it serves as an electrical resistance, concentrating the potential drop and thus creating a local high electric field strength. It was shown previously that this microreactor performs comparable to laboratory setups [6] and that it is suitable for bacterial inactivation [7].

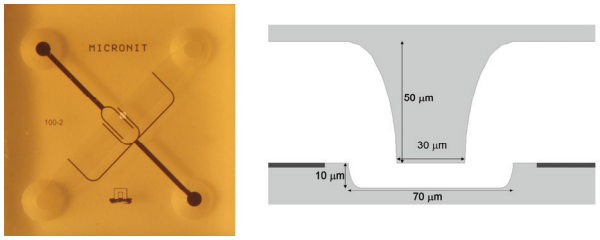

Figure 7-2: Image and schematic drawing of the PEF microreactor with dimensions.

7.2.2 Modeling the electric field distribution

The electric field distribution has been modeled both for the trapping device and the PEF microreactor, using finite element software (Femlab 3.0, Comsol, Sweden). The DC conductive medium model was used for a steady state situation, which solves Gauss' differential equation. The boundary conditions are considered

as being electrical insulated, with the two electrodes being 1 V and grounded. The fluid has a conductivity of 0.1 $S \cdot m^{-1}$.

7.2.3 Experiments

7.2.3.1 Single cell trapping device

For the experiments performed with the cell trapping device, the chip was mounted on to an X–Y–Z translation stage in an inverted microscope (Leica DM IRM, Leica Microsystems, Wetzlar, GmbH, Germany). The microscope system is equipped with a mercury lamp, 20x, 40x, 50x, 63x objectives, and the fluorescence filter set (BP 450– 490, LP 515). In addition, a computer-controlled CCD camera (Leica DFC300 FX) is mounted in the microscope for image recording. For the electroporation signal, a pulse generator (Avtech AVR-4-B-WUA) was directly connected to a specifically designed chip holder.

Experiments were started by filling the chip with buffer (5 mM HEPES, 6 mM NaCl solution with pH 7 and a conductivity of 0.1 $S \cdot m^{-1}$) by capillary forces. Then 100 µl of the buffer solution is added to all the reservoirs. To initiate the cell experiment the buffer solution in the top inlet reservoir is replaced by 100 µl of the cell sample consisting of 0.01% (w/v) *S. cerevisae* suspended in HEPES buffer mixed with the fluorescent probe PI (Invitrogen, The Netherlands) at a concentration of 30 µM. The cells were forced to flow along the upper channel. A pressure gradient over the trapping sites to the lower channel was created by suction on the bottom access holes. As a result, some of the yeast cells which flow in the upper channel are trapped at the trapping sites. Cells were electroporated using two different pulse widths (5 and 10 µs) and three different electric field strengths (6, 9 and 12 $kV \cdot cm^{-1}$). The degree of electroporation was optically monitored using the fluorescent staining as a result of the PI probe uptake.

7.2.3.2 PEF microreactor

For the inactivation experiments in the PEF microreactor, *S. cerevisae* was cultivated in the logarithmic growth phase from a 40 $g \cdot L^{-1}$ glucose, 5 $g \cdot L^{-1}$ bacterial peptone, 5 $g \cdot L^{-1}$ yeast extract solution and was washed twice. A syringe (Hamilton,

USA) was filled with a 0.1% (w/v) yeast solution and mounted to a syringe pump (Harvard Scientific, USA). The syringe was connected to a specifically designed chip holder via a 100 micrometer diameter glass capillary (Polymicro, USA). Experiments were done with a peroxide sterilized setup, and started with the most intense treatment, going towards milder treatments to reduce recontamination after the treatment chamber. Treated samples were collected and cell inactivation was studied using plating and PI staining.

An experiment was performed in which 8 pulses of 5 μs were applied at electric field strengths ranging from 0 to 26 $kV \cdot cm^{-1}$ to derive a working range for the inactivation experiments. Based on this experiment, inactivation experiments were done at electric field strengths of 3, 6, 9 and 12 $kV \cdot cm^{-1}$ with pulse widths of 5 and 10 μs, where the number of pulses was varied from 0 to 40 pulses on average. For the study of reversible electroporation, an experiment was done with pulses of 5 μs and 6 $kV \cdot cm^{-1}$ where PI was added in advance to the cell solution before the measurement and compared to an experiment where PI was added after treatment.

7.2.4 Probes and flow cytometry

The nuclear stain propidium iodide (PI) (Invitrogen, The Netherlands) was used as a cell impermeable membrane integrity indicator. PI will intercalate with the nuclear DNA, causing red fluorescence. However, it can only permeate through a cellular membrane if it is damaged. PI stained cells were incubated for 10 minutes after which flow cytometry (FCM) analysis was conducted. The FCM analyses were performed on a FACS Calibur flow cytometer (Becton Dickinson, USA), equipped with a 15 mW, 488 nm air-cooled argon ion laser. PI fluorescence was measured using a long-pass filter of 670 nm (FL3). Forward scatter was collected with a diode detector, side scatter and fluorescence were collected with photomultiplier tubes. Forward scatter and side scatter were collected using a linear amplification, PI fluorescence was measured using logarithmic amplification. Data were analyzed using CellQuest (Becton Dickinson, USA).

7.3 Results and discussion

7.3.1 Electric field distribution in cell trapping device and PEF microreactor

The electric field distribution in the microdevices has been modeled using finite element modeling software for a 2D situation (Figure 7-3). The distribution in the cell trapping device clearly shows that the electric field is focused at the site where the cell is trapped. The electric field strength in the upper channel is negligible compared to the electric field strength at the trapping site, so cells which are not trapped will not be affected. Analysis of the electric field strength distribution shows that a voltage difference of 1 V gives an electric field strength of 0.57 kV cm^{-1}. Since applied voltages are measured in following experiments, this factor has been used to calculate the electric field strength. As the trapping device consists of nine parallel trapping sites with one common grounded electrode (bottom electrode in Figure 7-1), leakage of current from one trapping site to the other could occur. This could cause a high electric field strength at the neighbouring site. This has been studied in a multi-trapping site model. However, the effect proves to be negligible since the resistance between the high voltage electrode of a trapping site and the grounded electrode via a neighbouring site is much higher than the resistance between the electrodes of the same trapping site. Therefore, the current leakage and thus the electric field strength will be very small. Secondly, neighbouring electrodes are grounded to reduce the leakage current even more.

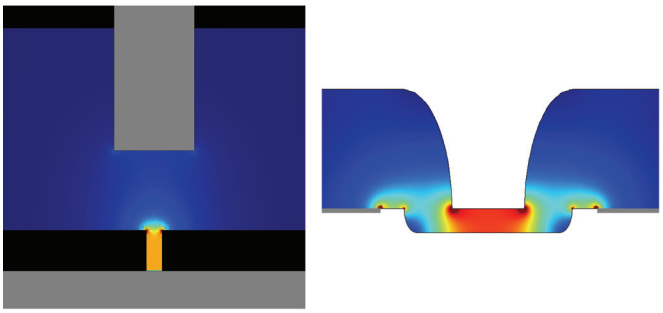

Figure 7-3: Electric field strength distribution in the cell trapping device (right) and the PEF microreactor (left).

The electric field strength distribution has also been determined for the PEF microreactor [6] (Figure 7-3), which shows that the electric field is focused at the treatment zone. A voltage difference of 1 V here gives an electric field strength of 0.14 $kV \cdot cm^{-1}$. This value is lower than the trapping device since the electrode distances are larger, but it is still much higher than comparable laboratory scale PEF equipment.

7.3.2 Flow cytometry and probing

Flow cytometric measurements of yeast inactivation were carried out using PI as a membrane integrity marker on samples obtained from the PEF microreactor. The FCM measurements (Figure 7-4) show that the application of increasing higher electric field strength pulses results in a higher average PI intensity. A similar pattern has been observed for the application of an increasing number of pulses. This indicates that the membrane is damaged more at higher treatment intensities (higher electric field strengths or more pulses), allowing more PI to enter the cell. When intact cells are compared to heat inactivated cells, two distinct populations can be distinguished (data not shown). Electroporated cells do not show these two distinct populations, but a more gradual increase of the PI fluorescence. This gradual increase of damage has been observed by others as well [8] and seems to be typical for electric field treated cells.

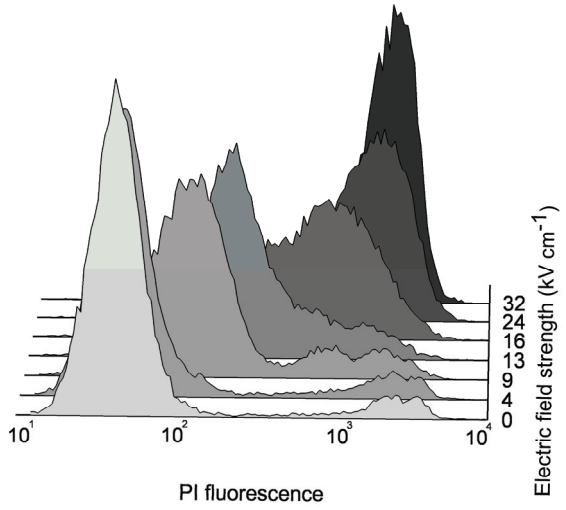

Figure 7-4: Fluorescence histogram of PI as measured with flow cytometry at increasing electric field strengths.

The electroporation of yeast in the single cell trapping device has also been studied using PI as a membrane integrity probe. In these measurements pulses were applied with a frequency of one pulse per minute and the fluorescence intensity was checked one minute after each pulse. These measurements showed a similar trend of gradual increase in the fluorescence intensity (Figure 7-5).

Figure 7-5: Light image of trapped yeast cell. PI response after 6 pulses and after 7 pulses of 10 μs and electric field strength of 9 $kV \cdot cm^{-1}$.

At the start of an experiment, trapped cells were not fluorescent, indicating that the cellular membrane was intact. After application of a certain amount of pulses, a relatively low fluorescent signal appeared, indicating that the membrane was damaged and PI could stain the cell. When a cell was inactivated by a pulse, it took approximately 30 seconds before it became red. However, the application of one additional pulse gave a large increase in PI fluorescence with a very bright coloured nucleus, which indicates that the membrane was damaged more severely. This is in accordance with the flow cytometry measurements of the PEF microreactor samples where this effect was observed as a gradual fluorescent increase. Cells did not shrink significantly when being inactivated which indicates that the membrane was electroporated, but the three dimensional structure was still intact. Moreover, when pulses were applied to one trapping site, cells at a neighbouring trapping site did not show red fluorescence and thus no PI uptake, which indicates that the electric field strength at that neighbouring site was negligible, as has been predicted by the electric field model.

7.3.3 Yeast inactivation as function of pulse width and number of pulses

Inactivation of yeast was carried out both in the cell trapping device and the PEF microreactor, with varying the electric field strength, pulse width and number of pulses. The effective range of the electric field strength was determined experimentally in the PEF microreactor at a constant average number of 8 pulses of 5 μs pulse width (Figure 7-6). The measurement shows that yeast is strongly inactivated in the range of 3 to 12 kV·cm^{-1}, where the process can be studied using PI as an indicator. Higher inactivation rates can be measured by counting the viability with plating, but these inactivation ranges are not measurable in the trapping device as only a single cell can be studied each time with PI fluorescence. Therefore, following experiments both in the PEF microreactor and the trapping device were conducted in the range of 3 to 12 kV·cm^{-1}.

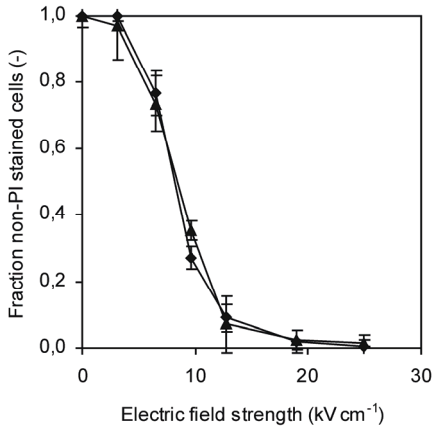

Figure 7-6: Effect of the electric field strength on the fraction of living cells after application of on average 8 pulses with a pulse width of 5 μs in the PEF microreactor, measured with flow cytometry (▲) and plate counting (♦).

For yeast inactivation experiments in the cell trapping device, pulses were delivered at a one minute interval to trapped cells. A cell was designated as inactivated when it showed red fluorescence due to PI uptake (Figure 7-5). The duplo measurements in the cell trapping device showed fairly large differences (Figure 7-7). This, most probably, has to do with the inhomogeniety of the electric field. The electrode behavior and electric field distribution could slightly be affected

by the presence of several cells being trapped at a trapping site or by the cleaning step with ethanol between measurements. The increase in the pulse width had a large impact on the required number of pulses to achieve yeast inactivation. For example at 6 kV·cm^{-1}, the number of pulses decreased from an average 17.5 to 6.5 pulses when the pulse width is doubled from 5 to 10 μs. In literature it is often reported that the required time constant to describe cell inactivation is the total treatment time, which is equal to the pulse width times the number of pulses ($t = \tau \cdot n$). It is therefore noteworthy that in these experiments a doubling of the pulse width gives somewhat more than a twofold reduction in the required number of pulses; i.e. the total treatment time at each electric field strength for 5 μs pulses seems to be higher than in case of 10 μs.

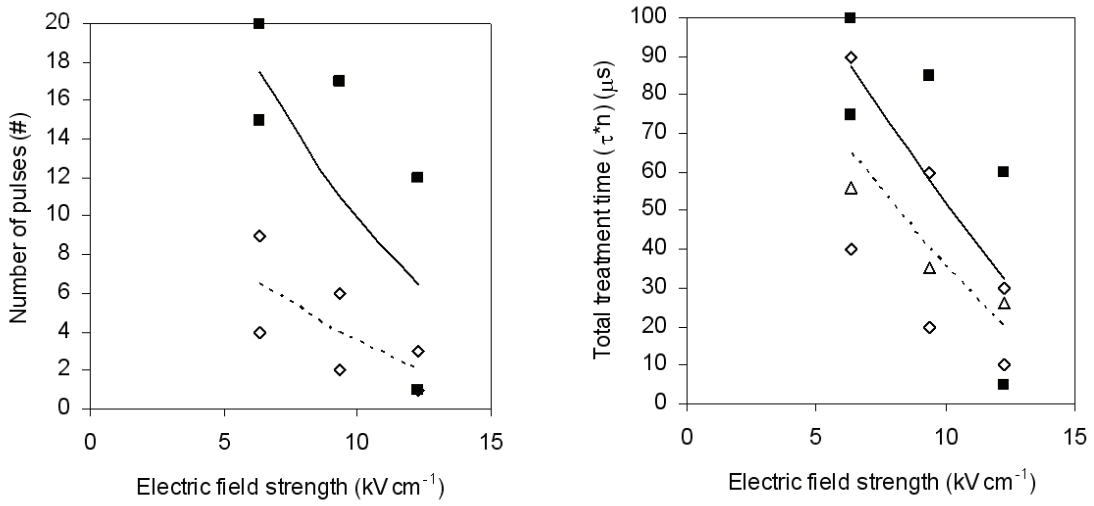

(a) (b)

Figure 7-7: Number of pulses and total treatment time (τ·n) required to inactivate *S. cerevisae* in the cell trapping device using 5 μs (■, solid line to guide eye) and 10 μs pulses (◊, dashed line to guide the eye). The PEF microreactor measurements, based on eq. 2 and 3 are depicted in figure (b) (Δ).

The effect of the number of pulses in cell inactivation was also studied in the PEF microreactor with increasing number of pulses at similar electric field strengths to the ones used in the cell trapping device. The inactivation was determined both by flow cytometry (Figure 7-8) and measuring by plating (Figure 7-9). The flow cytometry measurements also show that increasing the pulse width gives stronger inactivation (Figure 7-8). However when the inactivation is plotted, as the fraction of non-PI stained cells versus the total treatment time for the

different electric field strengths, it is clear that the total treatment time is in this case a good parameter for the description of cell inactivation since the 5 μs pulse width measurements are in good agreement with the 10 μs pulse width measurements.

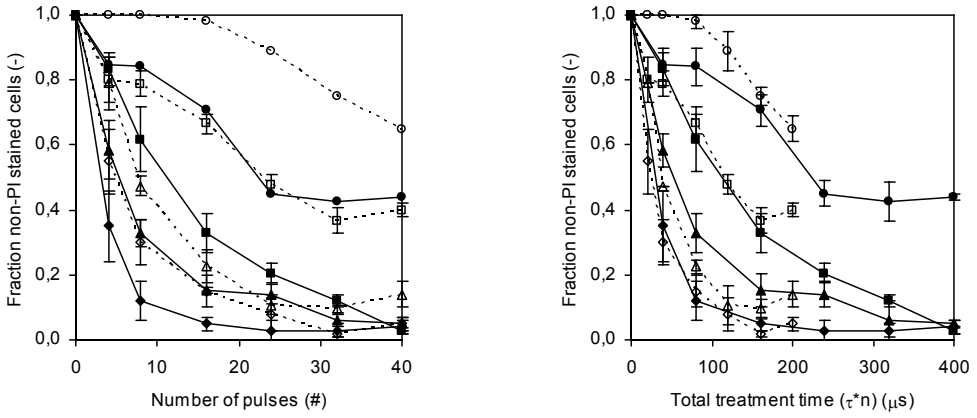

(a) (b)

Figure 7-8: Inactivation of yeast versus (a) the number of pulses and (b) the total treatment time (τ·n) at four different electric field strengths (3(●), 6(■), 9(▲) and 12 (♦) kV·cm^{-1}) and two different pulse widths (5 μs (open symbols, dashed line) and 10 μs (closed symbols, solid line)) as measured with flow cytometry.

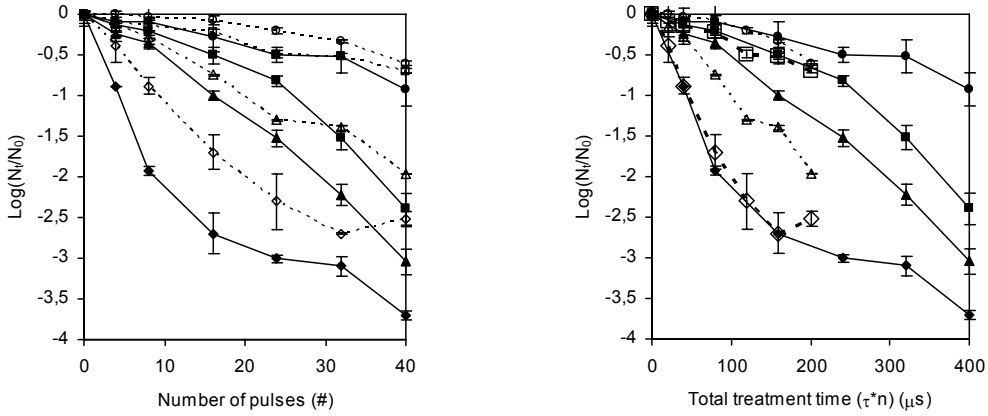

(a) (b)

Figure 7-9: Inactivation of yeast versus (a) the number of applied pulses and (b) the total treatment time (τ·n) at 4 different electric field strengths (3(●), 6 (■), 9 (▲) and 12 (♦) kV·cm^{-1}) and 2 different pulse widths (5 μs (open symbols, dashed line) and 10 μs (closed symbols, solid line) as measured with plating.

To compare the cell trapping device and the PEF microreactor, it is (arbitrarily) assumed that the threshold measured in the study of the cell trapping

device corresponds to a 50% fraction of living cells. Based on this assumption and the model data generated in the next paragraph, a comparison has been made (Figure 7-7b) between the two devices. This shows that the PEF microreactor equals the measurements with the 10 μs pulses in the cell trapping device. A disagreement is observed in the fact that the 5 μs pulses and 10 μs pulses behave similar in the PEF microreactor but not in the cell trapping device. However, the experimental setup of both experiments varied, since the pulses in the PEF microreactor were applied in a very short time frame (in the order of milliseconds), while the pulses in the cell trapping device were applied at one minute interval. In the cell trapping device, cells might therefore be able to partly recover after each single pulse, similar to reversible cell electroporation, while in the PEF microreactor the rapid pulses sequence lead to more irreversible electroporation. This would imply that for the experiments in the cell trap device, the application of one single pulse of 10 μs is more effective in cell inactivation than two 5 μs pulses, since it includes an extra recovery time for the pores.

To check whether reversible electroporation could take place in the PEF microreactor, an experiment was performed where PI was added at forehand to the cell suspension. It that way cells would be stained immediately when electroporated, irrespective whether the pore formation would be partly reversible or not. This experiment was then compared to a control experiment where PI was added after PEF treatment to measure only irreversible electroporation. A comparison of the two experiments at 5 μs, 6 kV cm-1 (Figure 7-10) shows that there is a fraction of cells which is PI positive when PI is present during treatment, but PI negative when added afterwards. A similar pattern has been observed for a 10 μs, 3 kV cm^{-1} experiment (data not shown). This is a strong indication that, despite the high field strengths applied, the electroporation is still partly reversible (20-40%) within a time scale of 10 minutes. The cells however do not stain PI positively after 10 minutes, indicating that they are still alive.

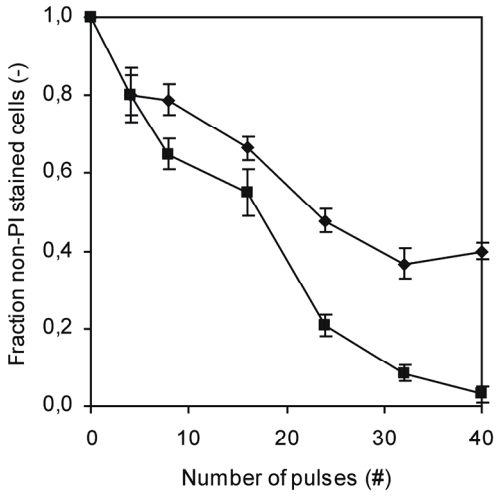

Figure 7-10: Inactivation of yeast measured with flow cytometry using 5 μs, 6 kV·cm^{-1} pulses. PI is present in the medium during the PEF treatment (■) and PI is added after the PEF treatment (♦).

7.3.4 Modeling of yeast inactivation

Yeast inactivation was also measured using plate counting as a viability measurement (Figure 6-10). Plate counting is a more suitable measurement method for fractions lower than 10% of living cells, since the measurements are done in a logarithmic fashion, opposed to the linear PI measurements. The plate counting measurements show that the effect of the treatment time ($t=\tau \cdot n$) at a constant electric field strength can be described by a first order kinetics model

$$\frac{dS}{dt} = -kS \Rightarrow k = \frac{-\ln(S)}{t} \qquad \text{eq.(2)}$$

The effect of the electric field strength (E) on the fraction of living cells is often described by the empirical model proposed by Huelsheger [9] using a rate constant (A) and a critical electric field strength (E_{crit})

$$k = A \cdot (E - E_{crit}) \qquad \text{eq.(3)}$$

The viability measurements were fitted to these equations, showing that the inactivation can be described with a critical electric field strength of 1.2 kV cm^{-1} and a rate constant of $2.4 \cdot 10^{-3}$ μs^{-1}·cm·kV^{-1}. These values are in the same order of magnitude as values measured by other researchers [10, 11]. The average diameter

of the cultured yeast was 7.3 μm, as has been measured with a coulter counter. The critical electric field strength can be translated to a transmembrane potential (Eq. 1), giving a critical transmembrane potential of 0.7 V. This value is within the range of 0.5 to 1 V that is reported as being the range where electroporation of cells starts.

For the cell trapping device, similar inactivation constants can be derived. However, a time and an electric field strength have been measured, but no fraction of living cells has been determined. If it is once again assumed that the fraction of living cells is 50% at the number of pulses that has been applied in the single cell electroporation device, a critical electric field strength of 4 kV cm^{-1} is calculated with a rate constant of $3 \cdot 10^{-3}$ $\mu s^{-1} \cdot cm \cdot kV^{-1}$. The critical transmembrane potential, based on this electric field strength, is 2.2 V. These values are in the same order of magnitude as in the PEF microreactor, which shows that the devices are well comparable. The small deviations with the PEF microreactor can be attributed to the fact that the fraction living cells has been assumed and the number of measurements is only 12, therefore giving larger standard deviations.

7.4 Conclusion

The inactivation of yeast by electric fields can be very well studied by combined measurements of a single cell trapping device and a PEF microreactor. The electroporation process was shown to be a progressive process, since staining with PI revealed that the fluorescent intensity increased gradually with increasing treatment (higher electric fields, longer pulse width or more number of pulses), observed both optically and with flow cytometry.

Applying pulses within a short period (e.g. milliseconds) is advantageous. Direct evidence was found that membrane recovery is reduced and that the effective irreversible pore formation favours cell inactivation. The electroporation process itself could be described by a combination of two models; a first order kinetics model for the description of the effect of the duration of the pulses of pulses and a Huelsheger-like model for the description of the electric field strength effect. This gave a critical transmembrane potential of 0.7 V for the PEF microreactor and 2.2 V for the trapping device, which is comparable to literature

values. The two devices were very well comparable in their electroporation behaviour.

7.5 References

[1] S. Y. Ho and G. S. Mittal - *Electroporation of cell membranes: a review;* Critical reviews in biotechnology, **16 (4)**, (1996), pp 349-362.

[2] G. L. Prasanna and T. Panda - *Electroporation: basic principles, practical considerations and applications in molecular biology;* Bioprocess engineering, **16** (1997), pp 261-264.

[3] D. Knorr, A. Angersbach, M. N. Eshtiaghi, V. Heinz and D. Lee - *Processing concepts based on high intensity electric field pulses;* Trends in food science & technology, **12 (3&4)**, (2001), pp 129-135.

[4] M. B. Fox, D. C. Esveld, A. Valero, R. Luttge, H. C. Mastwijk, P. V. Bartels, A. van den Berg and R. M. Boom - *Electroporation of cells in microfluidic devices: a review;* Analytical and Bioanalytical Chemistry, (2006), pp 474-485.

[5] A. Valero, F. Merino, F. Wolbers, R. Luttge, I. Vermes, H. Andersson and A. van den Berg - *Apoptotic cell death dynamics of HL60 cells studied using a microfluidic cell trap device;* Lab on a chip, **5 (1)**, (2005), pp 49-55.

[6] M. B. Fox, E. Esveld, R. Luttge and R. Boom - *A new pulsed electric field microreactor: comparison between the laboratory and microscale;* Lab on a chip, **5 (9)**, (2005), pp 943-948.

[7] M. B. Fox, D. C. Esveld, H. C. Mastwijk and R. M. Boom - *Inactivation of L. plantarum in a PEF microreactor The effect of pulse width and temperature on the inactivation;* submitted for publication in: Innovative Food Science & Emerging Technologies.

[8] P. C. Wouters, I. Alvarez and J. Raso - *Critical factors determining inactivation kinetics by pulsed electric field food processing;* Trends in food science & technology, **12 (3)**, (2001), pp 112-121.

[9] H. Huelsheger, J. Potel and E. G. Niemann - *Killing of bacteria with electric pulses of high field strength;* Radiation and environmental biophysics, **20** (1981), pp 53-65.

[10] Q. H. Zhang, A. Monsalve-González, B. Qin, G. V. Barbosa-Cánovas and B. G. Swanson - *Inactivation of Saccharomyces cervisiae in apple juice by square-wave and exponential-decay pulsed electric fields;* Journal of food process engineering, **17** (1994), pp 469.

[11] B. L. Qin, F. J. Chang, G. V. Barbosa-Cánovas and B. G. Swanson - *Nonthermal inactivation of S. cerevisiae in apple juice using pulsed electric fields;* Lebensmittel-Wissenschaft und -Technologie, **28 (6)**, (1995), pp 564-568.

8

Gene transfer and characterization of protein dynamics in stem cells using SCE in a chip*

Transfer of DNA molecules into mammalian cells using electric field pulses, electroporation, is a powerful and widely used method that can be directly applied to gene therapy. We have developed a flow-through chip that can immobilize, electroporate and transfect individual cells while being imaged using an inverted fluorescent microscope. With these chips we demonstrate transfection by electroporation of a green fluorescent-erk1 fusion protein and subsequent ERK1 protein tracking in mouse myoblastic cells (C2C12) and in human mesenchymal stem cells (hMSCs). Our silicon-glass chip enables, to our best knowledge for the first time, the immobilization, electroporation and real time monitoring of protein dynamics in single cells.

* This chapter will be submitted to Nature Biotechnology: A. Valero, J.N. Post, J.W. van Nieuwkasteele, H. Andersson, W. Kruijer and A. van den Berg.

8.1 Introduction

Stem cells differ from other cell types in the human body because of their capability to self-renew and their ability to give rise to multiple cell types. Adult stem cells, or somatic stem cells, are present in many adult tissues, like brain, bone marrow, skeletal muscle, skin, liver and others [1]. There are, however, often only small quantities of stem cells found in these different tissues, making it hard to isolate and purify these cells. Purification is yet needed for gene therapy and gene transfection.

In this work we utilized one of the more easily obtained stem cells, mesenchymal stem cells (MSCs) [2]. Mesenchymal stem cells have the capability for renewal and differentiation into a wide variety of cell types, like osteocytes, chondrocytes, adipocytes and stromal cells. These features of MSCs attract a lot of attention from researchers in the field of cell-based therapies of several human diseases. Human MSCs (hMSCs) can be isolated from bone marrow [1, 3] and can be expanded in culture for a limited amount of cell doublings [4]. Prolonged growth of MSC cells in culture can be achieved by genetic manipulation of the cells [4]. Also gene therapy based clinical applications require the introduction of genetic material [5]. The application of new approaches to the problems encountered in stem cell biology may provide information about human stem cell development that is not available using traditional cell culture methods [6]. Microfluidic devices offer the capability to study and analyze cells, both on single- and multi-cellular level with high-resolution and control over the cellular microenviroment in a way that is difficult to achieve using traditional methods [7-9].

Transfection of cells with foreign DNA is often accomplished by reversible electroporation [10]. However, the treatment protocols are often suboptimal [11] and based upon the application of high voltages and electric fields (i.e. thousands of volts per cm), which results in excess amounts of inactivated cells (low efficiency). Gene transfection by electroporation can, however, also be performed in microfluidic devices [12], benefiting from the small scale of these devices. This implies that relatively low voltages are sufficient due to close electrode spacing. Moreover, for microdevices only small amount of cells and transfection material are needed and the transfection efficiency is increased significantly. Furthermore,

optical inspection and real time monitoring of the electroporation and protein tracking is possible. In this report we show a successful method for introducing DNA into single cells using a microfluidic device for single cell electroporation, as well as the viability and prolonged responsiveness of the cells to extracellular stimuli.

Extracellular signal-regulated kinase, ERK1, is a protein that is important for transducing signals from the cells' environment to the cell nucleus [13]. Its action is important for a variety of cellular functions from proliferation and development to inflammatory responses and programmed cell death [14]. Binding of growth factors to receptors on the cell membrane results in ERK1 activation and subsequent nuclear translocation, where it can induce gene expression [15]. To examine whether the cells in the chip are still able to respond to their environment (ERK signalling pathway) after electroporation, we have utilized a green fluorescent protein (GFP) - erk1 fusion construct. This enables us to follow the movement of ERK1 from cytoplasm to the nucleus following receptor-mediated kinase activation.

This work highlights the relevant and potential use of a microfluidic device for single cell studies. We report the feasibility of this approach for trapping, electroporating and transfecting individual stem cells with high transfection efficiency as well as the possibility of online/real time spatiotemporal characterization of nuclear translocation of the ERK1 protein upon stimulation with growth factors.

8.2 Results

8.2.1 Electroporation of mouse myoblastic cells (C2C12)

For efficient electroporation the optimal electrical parameters differ for different molecules. For example, the delivery of low molecular weight drugs into mammalian cells typically requires fields of 1 $kV \cdot cm^{-1}$ and pulse lengths of 100 μs are effective, whereas for the delivery of genes lower fields (>50 $V \cdot cm^{-1}$) and longer pulses (20 ms) yield better results [16]. The applied electrical parameters also depend on the application. If the goal is intracellular delivery of a chemotherapeutic

agent to kill tumour cells, exceeding the upper limit of electroporation which leads to lysis of the cells is acceptable, whereas for the delivery of genes it is desirable to select the experimental parameters within the region of effective electroporation and high cell survival [16].

Mouse myoblastic cells (C2C12) are "stem cells like" since they can differentiate rapidly, forming contractile myotubes. C2C12 cells are used in this study as a model for stem cells and are investigated for gene transfection studies.

To test whether we can apply the microfluidic device for the electroporation of DNA into individual C2C12 cells, the electrical parameters were investigated. C2C12 cells were loaded and trapped into the microfluidic device as described in the Methods section under *Cell trapping*. Once C2C12 cells were trapped at the nine cell trapping sites, propidium iodide (PI) was added to the microfluidic channels and cell viability was checked before applying the electrical pulses. After trapping, the cells were not fluorescent, indicating that the cellular membrane was intact. Subsequently the minimum voltage for successful PI uptake was determined for a pulse length of 6 ms. The degree of electroporation was monitored optically using the fluorescent staining as a result of the PI probe uptake. Electrical pulses of 6ms with increasing amplitude from 1 to 3 V (steps of 0.5 V) and an interval pulse of 1 minute were applied to the cells. Electroporation was achieved for voltages of 2 V and higher. Next, the effect of the pulse length on PI uptake was studied for the lowest voltage for electroporation of C2C12 cells (2 V). An increase of the pulse length (from 100 μs to 6 ms) resulted in increased fluorescence intensity of PI, indicating that the cell has taken up more PI. The fluorescence intensity was checked one minute after each pulse was applied, to allow PI entering the cells.

8.2.2 eGFP transfection in C2C12 cells

C2C12 cells were loaded and trapped into the microfluidic device as described in the Methods section under *Cell trapping*. Once the cells were trapped, DNA encoding green fluorescent protein eGFP (100 $ng \cdot ml^{-1}$) was loaded into the cell trap device and a pre-incubation time (for DNA-cell contact) of 10 minutes was complied with before applying the electrical pulses. DNA transport across the cell membrane was initiated by one or several short electric pulses. Different electrical

parameters were used based on the PI uptake experiments. One or several (3 or 6) electrical pulses of 0.57 $kV \cdot cm^{-1}$ and two different pulse widths (4 and 6 ms) were applied to individual cells. All these configurations led to successful gene transfection (Figures 8-1 and 8-2a). Next, cell culture medium with 10% serum was added to the microfluidic channels for recovery of the cell by membrane resealing and terminates DNA transport. The chip was placed in a small Petri dish with cell culture medium and then placed in the incubator (37 °C and 5% CO_2). If the cell has taken up the DNA, intracellular events lead to actual gene expression. Gene transfection was quantified by measuring/imaging GFP expression 24 h after cell electroporation. Optical inspection of the cells was done 24 h and 48 h after electroporation. Figure 8-1 shows fluorescence images of successfully transfected C2C12 cells. The images were taken with a confocal microscope and a wide field microscope.

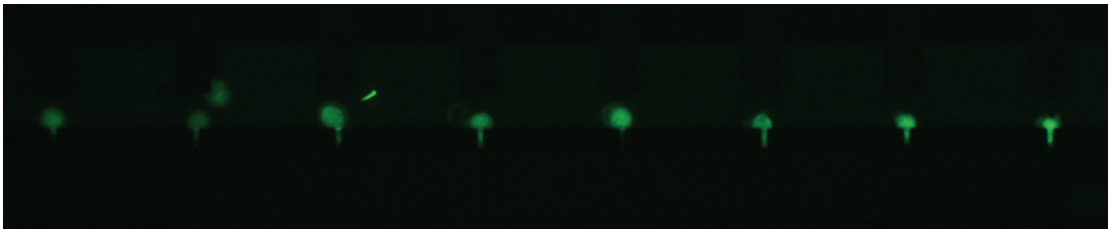

Figure 8-1: eGFP expression in C2C12 cells in the microfluidic cell trap device. Fluorescence image of C2C12 cells in traps shows the expression of the green fluorescent protein 24 h after electroporation. To all cells a single pulse of 2 V-6 ms was applied.

A high transfection efficiency (average TE of 75%) was achieved for C2C12 cells as observed by GFP expression in the majority of the cells that were electroporated. Results are summarized in Table 8-I. Furthermore, a higher fluorescence intensity of the eGFP was observed after 48 hours (Figure 8-2a) as compared to the intensity after 24 hours (Figure 8-1). The cells also showed healthy morphology observed under light microscopy images. Cells were attached to the surface of the chip and showed fibroblast morphology. This healthy morphology was maintained at least 120 h post-transfection. Figure 8-2b shows a picture of two cells 120 h after of electroporation; just before imaging the nuclei of the cells were stained with the life stain Hoechst. It was also observed that cells moved out from the trapping sites and adhered to the surfaces of the channel (see Figure 8-2b).

With these experiments we show the use of the microfluidic cell trap device to efficiently transfer genes by electroporation (and subsequent protein expression) in single cells.

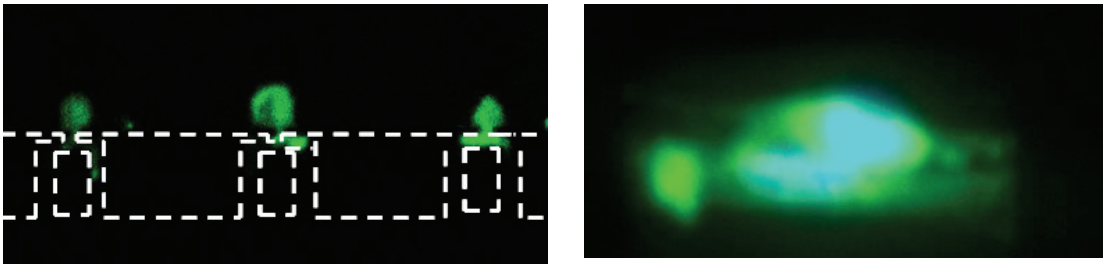

(a) (b)

Figure 8-2: (a) Fluorescence images of the green fluorescence protein in three C2C12 cells located at trapping sites (indicated by the dashed lines). Images were taken 48 h after electroporation. Applied signals were (from the left to right cell): 6 pulses of 2 V-6 ms, 1 pulse of 2 V-4 ms and 3 pulses of 2 V-4 ms. (b) Fluorescence image of 2 cells showing the expression of GFP and the fluorescence (blue) of the nucleus stain (stain: Hoechst) - the image was taken 5 days after electroporation.

8.2.3 eGFP-erk transfection in mouse myoblastic cells (C2C12)

A DNA construct encoding green fluorescent protein fused to erk1, peGFP-erk1 was electroporated in C2C12 cells. Cells were loaded and trapped in the microfluidic cell trap device described in the Methods section under *Cell trapping*. Since one single pulse of 2 V and 6 ms showed successful gene transfection for C2C12 cells (shown in previous section), this signal was used during the experiments. Twenty-four hours after electroporation, eGFP-ERK1 expression was visible mainly in the cytoplasm of the cells. The majority of the cells showed eGFP-ERK1 expression 24 hours after electroporation, with an average TE of 64 % (table 8-I). The cells were starved by removing all growth factors from the medium, resulting in localization of GFP-ERK1 protein to the cytoplasm. However, serum starvation led to a low cell survival, since most of the cells appeared to be dying as observed by the detachment of the cells from the surface (Figure 8-3) 24 h after starvation. Fourty-eight hours after electroporation, the medium was replaced for medium with serum (10%) and 10 $ng \cdot ml^{-1}$ bFGF to stimulate ERK phosphorylation and nuclear translocation. Addition of these growth-factors significantly increased

the nuclear localization of ERK1 (Figure 8-4a). Immediately after the addition of the growth factors, track images were taken every 5 minutes (described in the Methods section). The maximum intensity of eGFP-ERK1 in the nucleus was reached 30 minutes after bFGF addition, which corresponds with nuclear translocation of ERK1 in response to activation of extracellular signalling in a wide variety of cell types [13]. Fluorescence intensity changes in either the cytoplasm or nucleus of the cells were determined using ImageJ software [17]. Image areas of exactly the same size for the cytoplasm and for the nucleus were estimated and the average intensity of each area of interest was automatically calculated for each track image. Bleaching of the green fluorescence over time was observed and the fluorescence intensity was corrected (as explained in Methods section, *Bleaching correction*). Consequently, the temporal changes in fluorescence intensity in the cytoplasm (Icyt) and in the nucleus (Inuc) as well as the ratio between them (Inuc/Icyt) as function of time could be graphed as mean fluorescence intensity (in arbitrary units) versus time, as shown in Figure 8-4b. It can be seen that the fluorescence intensity of the cytoplasm decreased within time, while the intensity of the nucleus as well as the ratio (Inuc/Icyt) increased. These changes in intensity are more clear/evident in the first five minutes after adding the growth factors and level off after 15-20 minutes is observed.

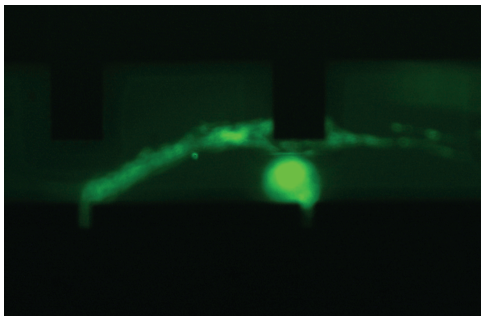

Figure 8-3: Serum starvation. After serum starvation (48 h after electroporation) some of the cells appeared to be dying as observed by the detachment of the cells from the surface.

The experiments clearly show that C2C12 cells trapped in the chip for 48 h are still able to respond to their environment (ERK signalling pathway) after electroporation. The movement of ERK from cytoplasm to the nucleus following receptor-mediated kinase activation could be followed optically.

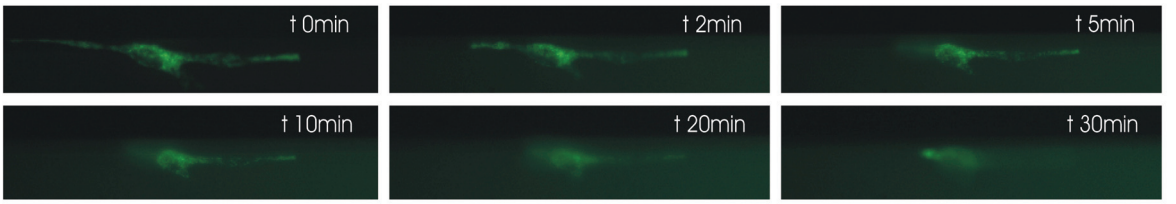

(a)

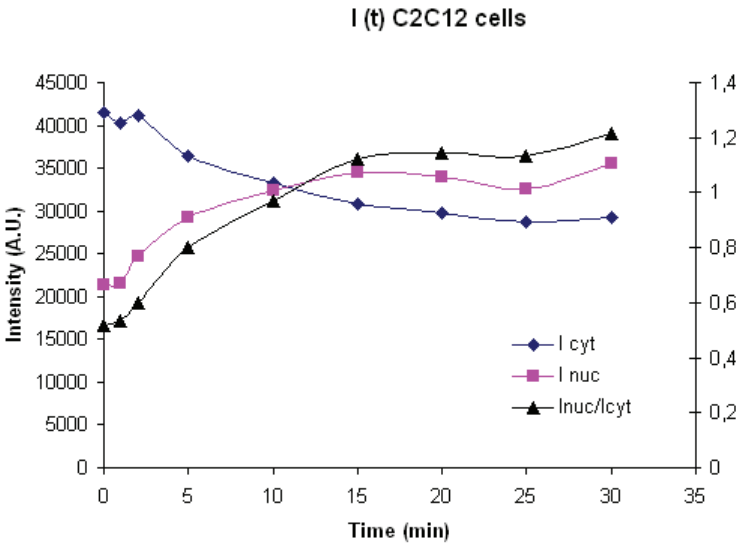

(b)

Figure 8-4: Nuclear translocation of eGFP-ERK after bFGF stimulation in C2C12 cells. eGFP-ERK1 is visible in cytoplasm while the nucleus remains dark (ERK1 is excluded from the nucleus, t = 0 min). After adding growth factors to the microfluidic chip, nuclear translocation of GFP-ERK1 is observed (t = 2 min to 30 min). In the graph time courses for GFP-ERK1 translocation following growth factor stimulation of C2C12 cells are plotted: fluorescence intensity of the cytoplasm (♦), the nucleus (■) and the ratio between eGFP intensity in nucleus and cytoplasmic (▲) was measured in time after adding growth factors. It can be observed that the maximum nuclear translocation was reached 30 min after addition of growth factors.

8.2.4 eGFP-erk transfection in human mesenchymal stem cells (hMSCs)

For human mesenchymal stem cells the same study, eGFP-erk1 transfection by single cell electroporation in a microfluidic cell trap device was performed, as well as the study of the ERK signalling pathway. The procedure used to investigate

this was identical to the one used for C2C12 cells and is described in the previous section (8.2.3).

Twenty-four hours after electroporation, eGFP-ERK1 expression was visible mainly in the cytoplasm of the cells (Figure 8-5). All electroporated cells showed eGFP-ERK1 expression after 24 hours of electroporation, average TE of 100% (Table 6-I).

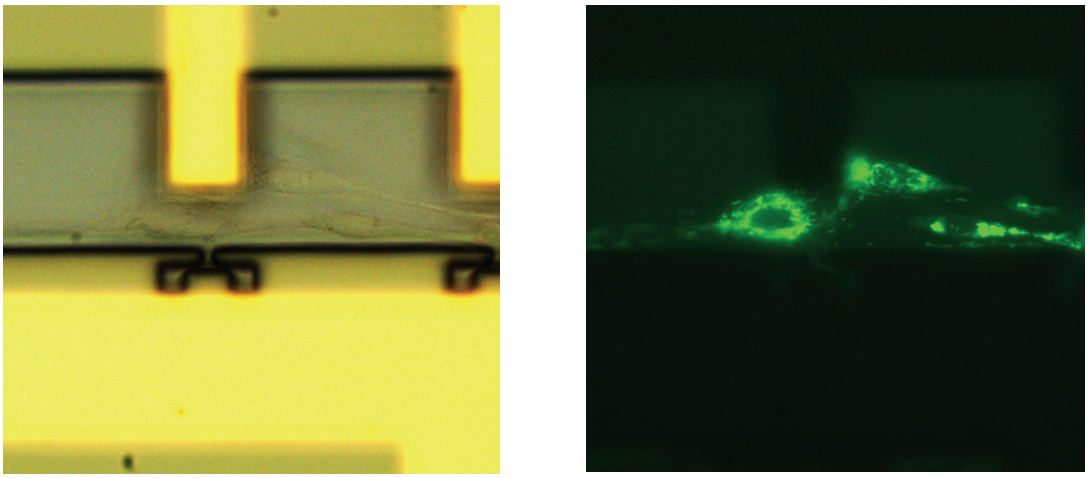

(a) (b)

Figure 8-5: eGFP-ERK expression in hMSCs 24 h after electroporation. (a) light microscopy image of hMSCs in the microfuidic cell trap device; (b) fluorescence image from image (a) shows eGFP-ERK expression 24 h after electroporation (and before serum starvation).

Cell type	**GFP experiments**			**GFP-ERK experiments**		
	# trapped cells	*# transfected cells (green cells)*	*TE* [%]	*# trapped cells*	*# transfected cells (green cells)*	*TE* [%]
C2C12	7	7	100	7	7	100
	8	3	38	5	3	60
	9	7	78	3	1	33
hMSC	6	5	80	4	4	100
	6	3	50	5	5	100

Table 8-I: Transfected C2C12 and hMSC cells for GFP and GFP-ERK experiments, performed in a microfluidic single cell trap device.

The cells were starved by removing all growth factors from the medium, resulting in localization of GFP-ERK1 protein to the cytoplasm. As observed for C2C12 cells, serum starvation also led to low cell survival in case of hMSCs (cell detachment from the surface). Fourty-eight hours after electroporation, the medium was changed for medium with serum (10%) and 10 $ng \cdot ml^{-1}$ bFGF to stimulate ERK phosphorylation and nuclear translocation. Immediately after the addition of the growth factors track images were taken every 5 minutes (described in the Methods section). The maximum intensity of eGFP-ERK1 in the nucleus was reached 30 minutes after bFGF addition, which corresponds with nuclear translocation of ERK1 in response to activation of extracellular signalling in a wide variety of cell types [13]. Fluorescence intensity changes in either the cytoplasm or nucleus of the cells were determined using ImageJ software [17]. Image areas of exactly the same size for the cytoplasm and for the nucleus were estimated and the average intensity of each area of interest was automatically calculated for each track image. Bleaching of the green fluorescence over time was observed and the fluorescence intensity was corrected (as explained in Methods section, Bleaching correction). Consequently, the temporal changes in fluorescence intensity in the cytoplasm (Icyt) and in the nucleus (Inuc) as well as the ratio between them (Inuc/Icyt) as function of time could be graphed as mean fluorescence intensity (in arbitrary units) versus time, as shown in Figure 8-6b. It can be seen that the fluorescence intensity of the cytoplasm decreased within time, especially during the first five minutes after the addition of the growth factors. On the other hand, the nuclear intensity slightly increased.

Although the addition of the growth factors (bFGF + serum) increases the nuclear localization of ERK1 (Figure 8-6) for hMSCs, this nuclear translocation is less pronounced than for C2C12 cells.

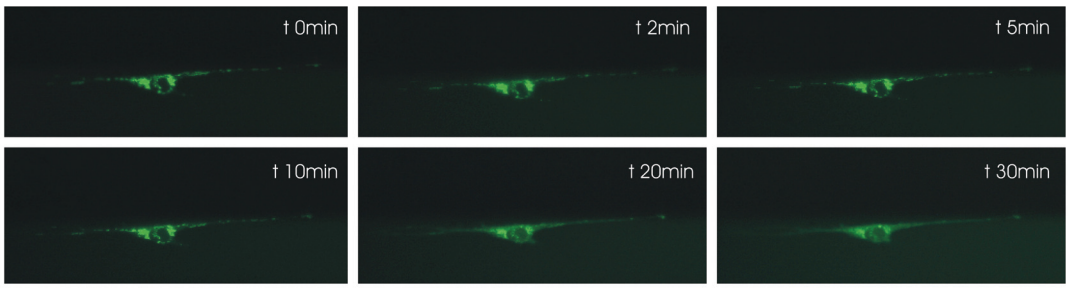

(a)

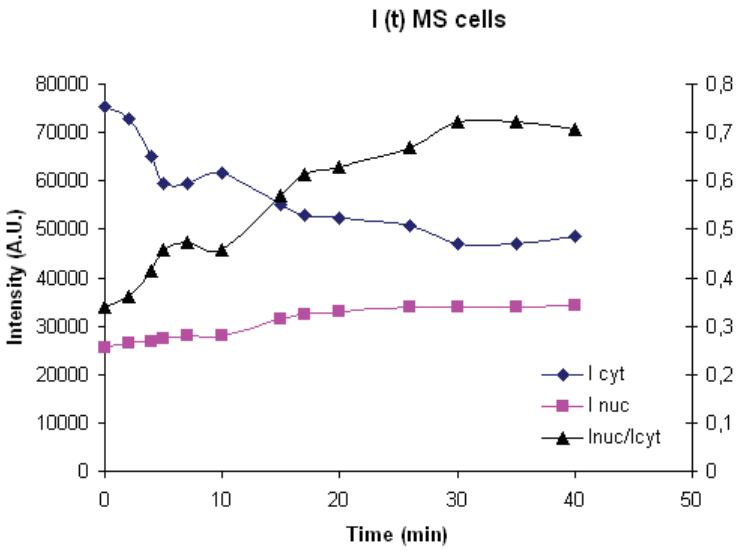

(b)

Figure 8-6: Nuclear translocation of eGFP-ERK1 in hMSC after bFGF stimulation. At t = 0 min, eGFP-ERK1 protein is visible in cytoplasm of the cell while the nucleus remains dark (ERK1 is excluded from the nucleus). After adding growth factors to the microfluidic chip, nuclear translocation of GFP-ERK1 is observed (t = 2 to 30 min). In the graph time courses for GFP-ERK1 translocation following growth factor stimulation of hMSCs are plotted in graph B: fluorescence intensity of the cytoplasm (♦), the nucleus (■) and the ratio between eGFP intensity in nucleus and cytoplasmic (▲) was measured in time after adding growth factors. It can be observed that the maximum nuclear translocation was reached 30 min after addition of growth factors. For hMSCs the nuclear translocation is less pronounced than in case of C2C12 cells (Figure 8-4).

8.2.5 Control experiments: no nuclear translocation of eGFP after bFGF stimulation in C2C12 and hMSCs cells

As a control, C2C12 cells and MSC were electroporated using eGFP-C1, resulting in GFP expression mainly in the cytoplasm of the cells 24 hours after electroporation. All growth factors were then removed and 24 hours after starvation 10 ng·ml^{-1} bFGF and 10% serum were added to the cells in the chip. After stimulation with growth factors, eGFP mainly localized to the cytoplasm and did not translocate to the nucleus (Figure 8-7). This shows that the nuclear localization of GFP-ERK1 is due to the presence and activation of ERK1 and that eGFP does not interfere with its activation.

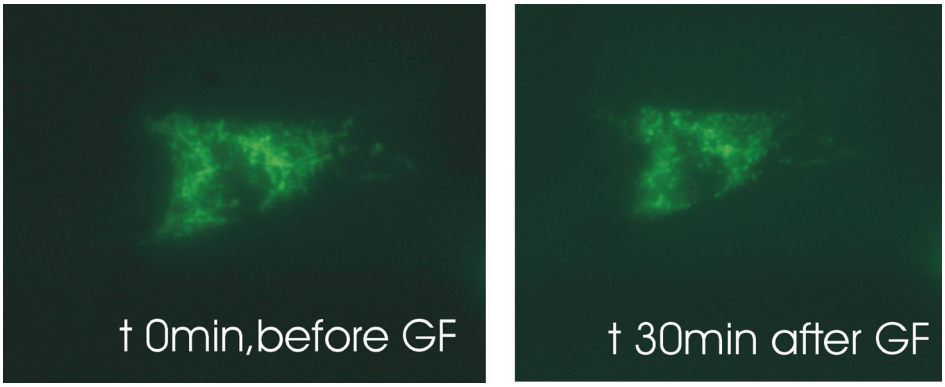

Figure 8-7: eGFP does not translocate to the nucleus after bFGF stimulation in hMSCs. Expression of GFP is visible in the cytoplasm 24 h after electroporation. After starvation cells were stimulated by adding growth factors (GF) and GFP remains in the cytoplasm as observed in the images taken before and after 30 min of GF addition.

8.3 Discussion

To our best knowledge, in this work for the first time the use of microfluidic cell trap devices is shown to efficiently transfer genes by single cell electroporation and protein expression in single cells (i.e. C2C12 and hMSC cells). In addition, the dynamics of the introduced protein can be followed in real-time for each individual cell. Numerous advantages are realised when gene transfection by electroporation in stem cells is performed in the microfluidic cell trap device. First of all, when compared to traditional bulk electroporation, the amount of cells as well as the

genetic material is significantly reduced. The risk of applying high voltages is avoided and the transfection efficiency as well as the cell survival is increased. In this work it is shown that a high transfection efficiency is achieved for both cell types: an average TE of 70% for C2C12 cells and 100% in case of hMSCs. When compared to other transfection methods, e.g. viral vector methods, the novelty of this non-invasive method is also emphasized since safety concerns are bypassed [18]. In addition, no special surface receptors are needed, making this promising technique more powerful in terms of non-cell specific transfection methods. This offers the possibility of using a mixed cell population in the chip, where no purification steps are needed since only the desired cells, the ones with the appropriate size/morphology, will be electroporated, or, in other words, will be genetically modified.

Different electroporation microdevices for gene transfection have been reported in literature [19, 20]. These devices are flow-type for continuous gene transfection, but all lack the ability to address an individual cell from a pre-defined cell batch by microfluidic or electronic means. In contrast, we developed a flow-through chip that can immobilize, electroporate and transfect genes in individual stem cells.

The long-term survival and responsiveness of the cells to external stimuli demonstrates the bio-compatibility of the device. C2C12 cells and hMSCs cells were able to respond to bFGF stimulation after electroporation and consequently ERK signalling pathway was followed real time in this device. This response was more pronounced for C2C12 cells than for hMSCs cells. However, a quite low cell survival was observed after serum starvation in both cell types.

We are currently applying this technique for transfection of genes into different types of adult stem cells. Because of the limited availability of adult stem cells, this method is a powerful tool for personalized gene therapy, tissue engineering and regenerative medicine.

8.4 Methods

8.4.1 Mouse Myoblastic cells (C2C12)

C2C12 (ATCC) cells are cultured in DMEM medium (Invitrogen) supplemented with 10% fetal bovine serum (Invitrogen), 100 IU·ml^{-1} penicillin, 100 mg·ml^{-1} streptomycin, 2 mM L-Glutamine, 250 mg·ml^{-1} fungizone and 1% pyruvate. No phenol red is present. Cells were harvested by incubation with trypsin (Invitrogen) and resuspended in medium with 10% fetal bovine serum to neutralize the effect of trypsin. To prevent cells for getting confluent, 10% of the cells are suspended in fresh medium twice a week. For experiments, the suspension is centrifuged after trypsination and resuspended in electroporation buffer (10 mM HEPES, 140 mM NaCl, 2.68 mM KCl, 1.7 mM $MgCl_2$, 25 mM glucose, pH 7.4). Note: cells are not used after 20 passages to be sure that the cells are not differentiated.

8.4.2 Mesenchymal stem cells (MSCs)

Mesenchymal stem cell growth medium consisted of 500 ml αMEM (Invitrogen), 10% fetal bovine serum (Cambrex), 1 ng·ml^{-1} bFGF (Invitrogen), 100 μg·100 units^{-1} ·ml^{-1} Penicillin/Streptomycin (Invitrogen) and 0.4 mmol·ml^{-1} ascorbic acid (Sigma). Cells were harvested by incubation with trypsin (Invitrogen) and were suspended in medium with 10% fetal bovine serum to neutralize the effect of trypsin. To prevent cells getting confluent, once a week 30% of the cells are suspended in fresh medium. For experiments, the suspension is centrifuged after trypsination and resuspended in electroporation buffer (10 mM HEPES, 140 mM NaCl, 2.68 mM KCl, 1.7 mM $MgCl_2$, 25 mM glucose, pH 7.4). Note: cells are not used after 10 passages to be sure that the cells are not differentiated.

8.4.3 Generation of an eGFP-erk1 fusion construct

ERK1 in pcDNA3 was a kind gift from Philippe Lenormand. Erk1 was amplified using PCR, adding an XhoI site to the 5' end of the sequence and a

BamHI site to the 3' end. This was ligated into PCR2.1 using the TOPO TA cloning kit (Invitrogen). Erk1 was isolated from PCR2.1 by digestion with XhoI and BamHI and ligated into the XhoI and BamHI site of eGFP-C1 (Clontech).

8.4.4 DNA purification

Purification of the plasmids was done with the use of the Endo Free® plasmid maxi kit (10), cat no. 12362 from QIAGEN®. The purification procedure of the handbook from the manufacturer was followed.

8.4.5 Probes

The nuclear stain propidium iodide (PI) (Invitrogen, The Netherlands) was used as a cell impermeable membrane integrity indicator. PI can not permeate through the intact cellular membrane, but a damaged membrane cannot prevent PI to enter. PI will intercalate with the nuclear DNA, resulting in red fluorescence.

8.4.6 Chip design and fabrication

The microfluidic cell trapping device consists of two channels that are connected by microholes. These microholes act as mechanical trapping sites for living cells. The two microfluidic channels are 50 μm and 20 μm wide, top and bottom respectively, and the nine trapping sites of 4 μm widths are etched by reactive ion etching (RIE) to a depth of 15 μm. The inlet/outlet reservoirs are powderblasted from the backside of the silicon. Subsequently, the silicon substrate was oxidized thermally to electrically insulate the silicon. The channel structure is capped with a Pyrex wafer which allows the visualisation of the channels as well as the trapping and the electroporation process. The strategically positioned platinum electrodes are sputtered into recessed areas in the Pyrex wafer, and then the two substrates are bonded anodically (Figure 8-8).

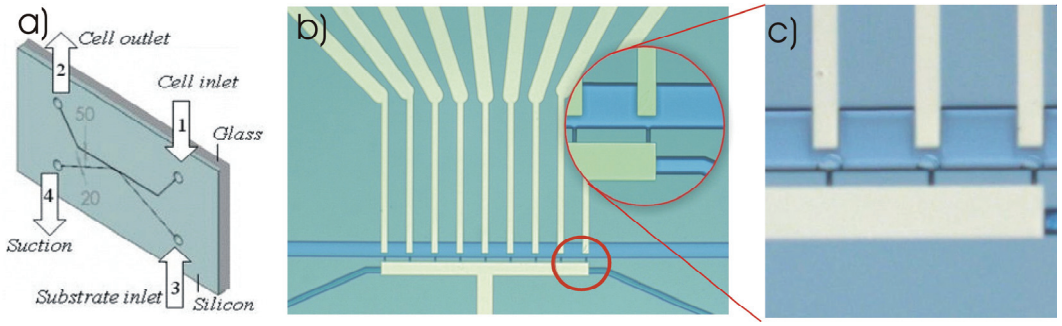

Figure 8-8: (a) Schematic drawing of the microfluidic chip (dimensions in µm); (b) image of the microfluidic chip with electrodes integrated and a zoom of the trapping sites (4 µm width); (c) close-up of a trapping feature showing three cells being trapped and ready to be electroporated.

8.4.7 Instrumentation

The chip was mounted on to an X–Y–Z translation stage in an inverted wide fluorescence microscope (Leica DM IRM, Leica Microsystems, Wetzlar, GmbH, Germany). The microscope system is equipped with a mercury lamp, 20x, 40x, 50x, 63x objectives, and the fluorescence filter set (BP 480/40, LP 515). In addition, a computer-controlled CCD camera (Leica DFC300 FX) is mounted in the microscope for image recording. For the electroporation signal, a custom-made Labview (National Instruments) application controls a function generator card (NI5041, National Instruments) and a data acquisition card (NI PCI-6221, National Instruments), which are connected to the electrodes via a specifically designed chip holder.

8.4.8 Cell handling and electrical parameters

8.4.8.1 Cell trapping

The integrated trapping structure in a flow-through chip represents a way of handling single cells. Experiments were started by filling the chip with buffer (10 mM HEPES, 140 mM NaCl, 2.68 mM KCl, 1.7 mM MgCl2, 25 mM glucose, pH 7.4) by capillary forces. Subsequently, 100 µl of the buffer solution was added to all the reservoirs (Figure 8-8a). To initiate the cell experiment the buffer solution

in the top inlet reservoir (1) was replaced by 100 µl of the cell sample. Cells were transported through the channel by means of pressure-driven flow. To trap single cells a negative pressure was applied to the suction reservoir (4) using a pump. Once the cells were trapped, the pump was switched off and cells were localized at the traps (Figure 8-8c).

8.4.8.2 Electroporation and gene transfection

Next, the transfection material (either DNA encoding eGFP or the DNA construct pegfp-erk1 at concentrations of 100 ng·ml) was loaded into the cell trap device. DNA-cell contact was established within a pre-incubation period of 10 minutes before applying an electric field. In this way DNA adsorption in the cell membrane surface took place. Subsequently, DNA transport across the cell membrane was initiated by applying a pulsed electric field (an electric pulse of 6 ms pulse width and a field strength of 0.57 $kV \cdot cm^{-1}$). A post-incubation time up to 10 minutes was given for the cell-DNA mixture. Cell culture medium with 10 % serum was added to the microfluidic channels and the chip was placed in a small Petri dish with cell culture medium and placed in the incubator (37 °C and 5% CO_2). If DNA is inside the cell, intracellular events lead to actual gene expression. Optical inspection of the cells was done 24 hours after electroporation and eGFP or eGFP-ERK1 expression was visible.

8.4.8.3 Serum starvation and bFGF stimulation

For egfp-erk1 transfection experiments, 24 h after electroporation medium was changed for medium containing αMEM, 10% FBS, 100 µg·100 $units^{-1} \cdot ml^{-1}$ Penicillin/Streptomycin and 0.4 $mmol \cdot ml^{-1}$ ascorbic acid. Fourty-eight hours after electroporation, the medium was replaced for medium with serum (10 %) and 10 ng·ml bFGF to stimulate erk phosphorylation and nuclear translocation. Track images were taken every 5 minutes with 488 nm excitation and a LP 515 emission filter. Fluorescence intensity changes in either the cytoplasm or nucleus of the cells was determined using ImageJ software [17]. Bleaching of the green fluorescence over time was observed and the fluorescence intensity was corrected (as explained in the next section).

8.4.9 Correcting for bleaching

It is assumed that the total intensity in the cell is constant. In order to determine the corrected intensity, the mean intensity is calculated inside a mask of the whole cell. Subsequently, each pixel in each frame was multiplied by the factor (I_0/I_t), where I_0 is the original intensity and I_t is the current frame intensity. For time zero (t = 0 min) the correction factor is 1, but as the image bleaches, the correction factor gets larger. This correction factor was applied to the track images for the nuclear translocation of eGFP-ERK as well as to the graphs of the fluorescence intensity versus time.

8.4.10 Electric field distribution

The electric field distribution in the cell trapping device has been modeled using finite element modeling software (Femlab 3.0, Comsol, Sweden) for a 2D situation (Figure 8-9). The DC conductive medium model was used for a static state situation, which solves Gauss' differential equation. The *E*-field distribution in the cell trapping device (Figure 8-9a) clearly shows that the electric field is focused at the site where the cell is trapped. The electric field strength in the upper channel is negligible compared to the electric field strength at the trapping site, so cells which are not trapped will not be affected. This is also found when the electric field strength between the two electrodes (Figure 8-9b) is plotted along the line depicted in Figure 8-9a. Analysis of the electric field strength distribution shows that a voltage difference of 1 V gives already electric field strength of 0.57 $kV \cdot cm^{-1}$ in the trap.

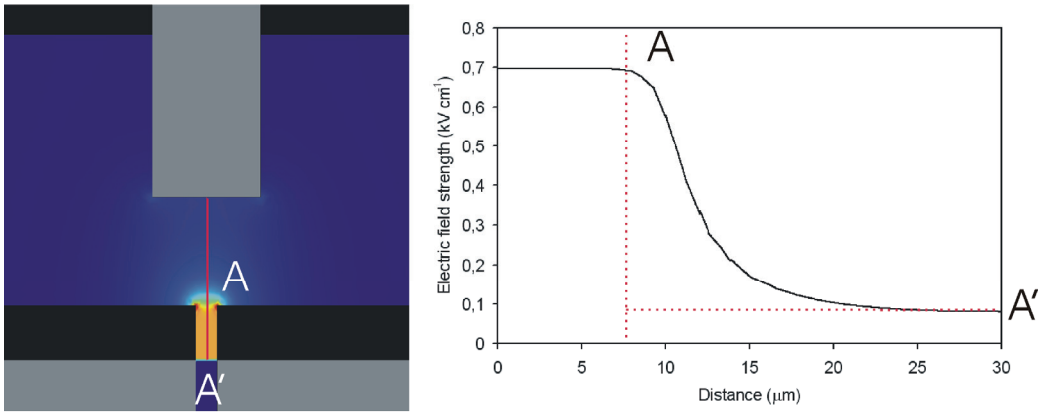

Figure 8-9: *E*-field distribution in the cell trap device. The electric field in the upper channel is negligible compared to the electric field at the trapping site. This is also shown when plotting the electric field strength between the two electrodes along the line A-A'. This shows that a voltage difference of 1 V already gives an electric field of 0.57 kV·cm^{-1}.

8.5 References

[1] M. Buehr and A. Smith - *Genesis of embryonic stem cells;* Philosophical Transactions of the Royal Society of London Series B-Biological Sciences, **358 (1436)**, (2003), pp 1397-1402.

[2] K. C. Kemp, J. Hows and C. Donaldson - *Bone marrow-derived mesenchymal stem cells;* Leukemia & Lymphoma, **46 (11)**, (2005), pp 1531-1544.

[3] J. J. Minguell, A. Erices and P. Conget - *Mesenchymal stem cells;* Experimental Biology and Medicine, **226 (6)**, (2001), pp 507-520.

[4] B. M. Abdallah, M. Azadali, F. Jacob, P. Hokland and M. Kassem - *Maintenance of differentiation potential of human bone marrow stroma cells immortalized by human telomerase reverse transcriptase gene;* Journal of Bone and Mineral Research, **18** (2003), pp S140-S140.

[5] R. Eiges, M. Schuldiner, M. Drukker, O. Yanuka, J. Itskovitz-Eldor and N. Benvenisty - *Establishment of human embryonic stem cell-transfected clones carrying a marker for undifferentiated cells;* Current Biology, **11 (7)**, (2001), pp 514-518.

[6] H. Andersson and A. van den Berg, -*Lab on a chips for Cellomics;* Kluwer academic publishers (2004).

[7] H. Andersson and A. van den Berg - *Microfluidic devices for cellomics: a review;* Sensors and Actuators B, **92 (3)**, (2003), pp 315-325.

[8] H. Andersson and A. van den Berg - *Microtechnologies and nanotechnologies for single-cell analysis;* Current Opinion in Biotechnology, **15 (1)**, (2004), pp 44-49.

[9] D. N. Breslauer, P. J. Lee and L. P. Lee - *Microfluidics-based systems biology;* Molecular Biosystems, **2 (2)**, (2006), pp 97-112.

[10] E. Neumann, A. E. Sowers and C. A. Jordan, -*Electroporation and Electrofusion in Cell Biology;* Plenum Press, New York (1989).

[11] D. C. Chang, B. M. Chassy and J. A. Saunders -*Guide to electroporation and electrofusion;* San Diego: Academic Press (1992).

[12] M. B. Fox, D. C. Esveld, A. Valero, R. Luttge, H. C. Mastwijk, P. V. Bartels, A. van den Berg and R. M. Boom - *Electroporation of cells in microfluidic devices: a review;* Analytical and Bioanalytical Chemistry, **385 (3)**, (2006), pp 474-485.

[13] M. J. Robinson and M. H. Cobb - *Mitogen-activated protein kinase pathways;* Current Opinion in Cell Biology, **9 (2)**, (1997), pp 180-186.

[14] A. V. Khokhlatchev, B. Canagarajah, J. Wilsbacher, M. Robinson, M. Atkinson, E. Goldsmith and M. H. Cobb - *Phosphorylation of the MAP kinase ERK2 promotes its homodimerization and nuclear translocation;* Cell, **93 (4)**, (1998), pp 605-615.

[15] A. Brunet, D. Roux, P. Lenormand, S. Dowd, S. Keyse and J. Pouyssegur - *Nuclear translocation of p42/p44 mitogen-activated protein kinase is required for growth factor-induced gene expression and cell cycle entry;* Journal of EMBO, **18 (3)**, (1999), pp 664-674.

[16] S. B. Dev, D. P. Rabussay, G. Widera and G. A. Hofmann - *Medical applications of electroporation;* IEEE Transactions on Plasma Science, **28 (1)**, (2000), pp 206-223.

[17] *http://rsb.info.nih.gov/ij/*

[18] J. Reiser, X. Y. Zhang, C. S. Hemenway, D. Mondal, L. Pradhan and V. F. La Russa - *Potential of mesenchymal stem cells in gene therapy approaches for inherited and acquired diseases;* Expert Opinion on Biological Therapy, **5 (12)**, (2005), pp 1571-1584.

[19] Y. C. Lin, C. M. Jen, M. Y. Huang, C. Y. Wu and X. Z. Lin - *Electroporation microchips for continuous gene transfection;* Sensors and Actuators B, **79** (2001), pp 137-143.

[20] Y. C. Lin, M. Li, C. S. Fan and L. W. Wu - *A microchip for electroporation of primary endothelian cells;* Sensors and actuators A, **108** (2003), pp 12-19.

9

Summary and Outlook

In this chapter the conclusions of the work described in the previous chapters of this thesis are summarized and compared with the project aims. Furthermore, several aspects are mentioned that can be useful for improvement of the microfluidic cell trap devices.

9.1 Summary

In this thesis the results of the development of microfluidic cell trap devices for single cell electroporation are described, which are to be used for gene transfection. The performance of two types of Lab-on-a-Chip trapping devices was tested using beads and cells, whereas the functionality for single cell electroporation of these chips was verified by means of gene transfection studies.

In order to be able to design microfluidic cell trapping devices for single cell electroporation (SCE), the fundamentals of the electrical permeabilization of cell membranes were discussed, as well as the advantages of using microdevices (chips) for SCE. The current status on micro-electroporation devices for analysis, transfection or pasteurization of biological cells is reviewed: most of the reported devices and concepts focus on the electroporation process itself, and do, however, not incorporate integrated separation and detection processes (analysis methods). The field of single-cell content analysis, where the cell content is released by electroporation, is promising, in particular when it is done in chips since it is difficult to accomplish this in a well-controlled way in larger structures. Clearly, microfluidic devices as a platform for electroporation fulfill the necessities to perform single cell electroporation and analysis, and are therefore important 'tools' to get more insight in the fundamentals of the electroporation process.

Trapping of cells by means of integrated microstructures, i.e. "mechanical filters", was identified as the best method to trap single cells in chips due to the simplicity of this method. The design and fabrication of silicon-glass chips containing two different micromachined trapping filters are shown. For both devices cells were trapped at the sites using two different methods (pinched injection and sheath flow), and the trapping performance of both methods was tested with beads (cell suspension model) and HL60 cells.

The analysis of apoptosis in HL60 cells was studied in these microfluidic cell trap devices. The silicon-glass chip enabled the immobilization of HL60 cells and real time monitoring of the apoptotic process. Induction of apoptosis of the cells was addressed in two ways: electric field mediated (i.e. electroporation) or

chemically. Fluorescent dyes (FLICA and PI) were used to discriminate between viable, apoptotic and necrotic cells. This work presented the first results to analyse programmed cell death dynamics using a chip and a first step towards an integrated chip for high-throughput drug screening on a single cellular level.

Single cell electroporation was carried out in chips containing mechanical trapping sites and integrated electrodes. The electrodes were positioned in such a way that each trapped cell could be addressed individually. Electropermeabilization experiments were performed on two cell lines, viz. HL60 and C2C12 cells, using a membrane-impermeable stain (PI) and a plasmid encoding green fluorescent protein (GFP). The experiments performed with the cell membrane integrity marker (PI) showed that single cell electroporation was achieved. Moreover, only the cell that was electrically addressed with the electroporation signal showed red fluorescence (PI uptake), cells located at neighbouring traps did not. For both cell lines, the electrical parameters, voltage (or *E*-field) and pulse length needed for cell membrane permeabilization of individual cells were studied in detail in these chips. Furthermore, for the first it was shown that microfluidic cell trap devices can be used for successful and efficient gene transfection.

Electrical detection is another method to detect single cell electroporation. In this method the current flowing through the cell membrane is measured. Since electroporation of a cell results in a resistance change of the membrane, membrane permeation can be detected by characteristic 'jumps' in current that correspond to drops in cell resistance. An electrical model was developed to verify whether it is possible to detect these characteristic current variations in the chips used in this thesis. The model showed that it is not trivial to electrically detect single cell electroporation with the current measurement set-up. Solutions to optimize the electrical detection of electroporation are presented, e.g. reduction of the leak resistance around the cell and of the electrodes' impedance.

Pulse electric field (PEF) electroporation can be used for the inactivation of microorganisms (e.g. pasteurization of foods). Two different microdevices were used to study PEF electroporation of yeast cells: a single cell trapping device and a flow-through electroporation device. The electroporation process was followed

using fluorescent DNA stain PI. It was found that electroporation of yeast cells is a progressive process.

Finally, the microfluidic single cell trapping devices were used successfully for studying gene transfection into stem cells by electroporation. After electroporation, green fluorescent-erk1 fusion protein was expressed in mouse myoblastic cells (C2C12) and in human mesenchymal stem cells (hMSCs) and subsequently the dynamics of the introduced protein were followed in real time. The long-term survival and responsiveness of the cells to external stimuli demonstrated the biocompatibility of the microdevice. This study clearly showed that single cell electroporation in microfluidic trapping devices is a powerful tool for personalized gene therapy, tissue engineering and regenerative medicine. Due to the limited availability of adult stem cells, the use of microdevices for SCE makes these chips extremely important and attractive for stem cell research.

9.2 Outlook

Based on the results shown in this thesis, it can be concluded that microfluidic devices are extremely useful tools for performing and studying single cell electroporation. By using chips, significant new insight and knowledge can be obtained in the fundamentals of the electroporation.

Microfluidic devices for single cell electroporation can be improved/adapted in a variety of ways, to make these chips applicable for even more purposes. Below several issues are discussed.

Integration of separation and detection processes in the chips is expected to add further value to the concept of an integrated electroporation microfluidic chip in the near future. In fact, on-chip combination of electroporation with analytical techniques such as capillary electrophoresis (CE) separation and mass spectroscopy (MS) or electrochemical (EC) detection is believed to be promising for performing single-cell genomics and proteomics studies. Integration of these processes is in particular valuable for the field of single-cell content analysis where the cell content is released by electroporation. The development and integration of new electrode materials and chemically or biologically modified electrodes can be a method to

improve the sensitivity of detection. Moreover, by applying advanced pulse schemes to the cells trapped in microfluidic devices, chips can facilitate research into intracellular electroporation.

Other materials than glass and/or silicon can be selected as base-material for the chips, for example polymeric materials (PDMS, SU-8 etc.). Reasons to use these materials can be the costs and ease of fabrication, flexibility, disposability and/or biocompatibility.

Clearly, by implementing one (or more) of the above-mentioned issues, the applicability of chips for single cell electroporation can be enlarged. These new devices offer new possibilities to investigate dose-response relations within the same cell and between cells in real-time, which open up new possibilities for single-cell analysis and new approaches for applications in drug discovery, combinatorial chemistry, and bioanalysis.

Most challenging and promising application of single cell electroporation in a chip is transfection of genes into stem cells. Because of the limited availability of adult stem cells, this method is a powerful tool for personalized gene therapy, tissue engineering and regenerative medicine.

Samenvatting

In dit proefschrift zijn de resultaten beschreven van de omwikkeling van microfluidische chips die gebruikt kunnen worden voor het tijdelijk immobiliseren (vangen/klemmen) van cellen om deze vervolgens individueel te kunnen elektroporeren. Het uiteindelijke doel is om deze chips te gaan gebruiken voor gen transfectie. De 'performance' van twee van deze 'Labs-on-a-Chip' is getest met behulp van 'beads' en cellen, en de functionaliteit met betrekking tot individuele cel elektroporatie is geverifieerd middels gen transfectie studies.

Om een goed ontwerp te kunnen maken van chips die geschikt zijn voor individuele cel elektroporatie zijn de fundamentele aspecten van elektrische permeabilisatie van celmembranen in kaart gebracht. Daarnaast is uitgelegd waarom het gebruik van microfluidische chips voor individuele cel elektroporatie (vele) voordelen biedt.

De huidige status van chips voor micro-elektroporatie die zijn ontwikkeld voor analyse, transfectie of pasteurisatie van biologische cellen is geïnventariseerd: de meeste gepubliceerde concepten en chips zijn vooral gericht op het elektroporatie proces, en zijn niet voorzien van geïntegreerde scheidings- en detectie technieken (analyse methoden). Het onderzoeksgebied dat zich richt op de analyse van de inhoud/samenstelling van individuele cellen is veel belovend, in het bijzonder wanneer dit uitgevoerd wordt in chips, daar het moeilijk is om dergelijke analyses gecontroleerd uit te voeren in grotere structuren. Microfluidische chips als platforms voor elektroporatie voldoen aan de eisen die nodig voor zijn individuele cel elektroporatie en bijbehorende analyses, en zijn derhalve belangrijke en nuttige 'tools' die gebruikt kunnen worden om meer inzicht te krijgen in het elektroporatie proces.

Het tijdelijk immobiliseren van cellen middels geïntegreerde mechanische filters is geïdentificeerd als de beste methode om individuele cellen tijdelijk vast te zetten in chips, daar deze methode relatief eenvoudig is. Het ontwerp en de

fabricage zijn beschreven van silicium-glas chips waarin twee verschillende types mechanische filters geïmplementeerd zijn. Deze chips zijn gemaakt met behulp van micromechanische technieken. In deze chips kunnen cellen tijdelijk gevangen/geklemd worden met twee technieken: 'pinched injection' en 'sheath flow'. De effectiviteit van deze technieken is getest met een cel suspensie model ('beads') en HL60 cellen.

In deze chips is de apoptosis van HL60 cellen geanalyseerd: in de silicium-glas chips kunnen de HL60 tijdelijk geïmmobiliseerd worden en kan het apoptotische proces *real-time* gevolgd worden. Het begin van apoptosis van de cellen is op twee manieren geïnitieerd: met een elektrisch veld (elektroporatie) of chemisch. Fluorescente kleurstoffen (FLICA en PI) zijn gebruikt om onderscheid te kunnen zien tussen gezonde, apoptotische en necrotische cellen. Met deze experimenten is bewezen dat microfluidische chips gebruikt kunnen worden om de dynamica van geprogrammeerde cel afsterving te analyseren. Dit werk is een eerste stap in de ontwikkeling van geïntegreerde chips die toegepast kunnen worden voor 'high-throughput' geneesmiddel onderzoek op individueel cel niveau.

Individuele cel elektroporatie is uitgevoerd in chips met mechanische immobilisatie locaties die voorzien zijn van elektrodes. Deze elektrodes zijn zodanig gepositioneerd dat elke geïmmobiliseerde cel individueel kan worden voorzien van elektrische signalen. Elektropermeabilisatie experimenten zijn gedaan met HL60 en C2C12 cellen, waarbij een membraan-impermeabele kleurstof en een plasmide coderende GFP gebruikt zijn. Middels de cel integriteits kleurstof (PI) kon aangetoond worden dat individuele cel elektroporatie bereikt is. In meer detail, alleen de cellen die blootgesteld waren aan elektrische (elektroporatie) signalen waren rood fluorescent (PI opname), cellen in aangrenzende locaties niet. De chips zijn gebruikt om voor beide cel typen de elektrische parameters te onderzoeken (elektrisch veld en lengte van de puls(en)) die nodig zijn om celmembraan permeabilisatie van individuele cellen te bereiken. Verder is voor de eerste keer aangetoond dat microfluidische chips met locaties om cellen tijdelijk te immobiliseren gebruikt kunnen worden voor succesvolle en efficiënte gen transfectie.

Een andere methode om individuele cel elektroporatie vast te stellen is elektrische detectie. In deze methode wordt de stroom door het celmembraan gemeten. Daar elektroporatie van een cel een verandering in de geleidbaarheid van het membraan tot gevolg heeft, kan membraan permeabilisatie gedetecteerd worden middels karakteristieke "sprongen" in de gemeten stroom. Een elektrisch model is opgesteld om te verifiëren of het mogelijk deze karakteristieke variaties in de stroom te kunnen detecteren in de chips. Uit dit model kwam naar voren dat het verre van triviaal is om individuele cel elektroporatie elektrisch te detecteren met de huidige chips en meetopstelling. Er zijn een aantal manieren onderzocht om elektrische detectie van elektroporatie mogelijk te maken in de chips, onder andere het beperken van de "lekweerstand" rond de geïmmobiliseerde cel en het aanpassen van de impedantie van de elektrodes.

Elektroporatie met behulp van gepulseerde elektrische velden (PEF) kan gebruikt worden voor het inactiveren van micro-organismen (bijvoorbeeld pasteurisatie van voedingswaren). Twee verschillende microsystemen zijn gebruikt voor het onderzoeken van PEF elektroporatie van gistcellen: een chip voor met locaties voor individuele cel elektroporatie en een flow-through elektroporatie systeem. Het elektroporatie proces is bestudeerd met de fluorescente DNA kleurstof PI. Geconcludeerd is dat het elektroporatie proces van gistcellen progressief is.

Tenslotte zijn de microfluidische chips met locaties om individuele cellen tijdelijk te immobiliseren succesvol gebruikt voor het uitvoeren en bestuderen van gentransfectie in stamcellen (middels elektroporatie). Na elektroporatie was de groen fluorescente-erk1 fusie proteïne zichtbaar in myoblastische cellen van muizen (C2C12) en menselijke 'mesenchymal' stamcellen (hMSC), en dynamica van de geïntroduceerde proteïne kon *real-time* gevolgd worden. De cellen in de chip bleven gedurende een lange periode gezond en vertoonden reactie op externe stimuli: dit illustreert duidelijk de bio-compatibiliteit van de chips. Deze studie bewijst dat individuele cel elektroporatie in microfluidische chips een belangrijke 'tool' is voor persoonlijke gentherapie, weefsel onderzoek en regeneratieve medicijnen. Vanwege de beperkte beschikbaarheid van volwassen stamcellen, zijn microfluidische chips

met voor locaties voor het elektroporeren van individuele cellen zeer belangrijk/aantrekkelijk voor stamcel onderzoek.

Acknowledgements

During four years I got to know a lot of people and here I would like to express my sincere gratitude to all of them, who in one way or another have been present in my life.

First I would like to thank my promotor, Professor Albert van den Berg, who gave me the opportunity to join his group as a Ph.D. student. Albert, thank you for all the freedom, trust and support you offered during this last four years. I truly appreciate how enthusiastic you have always been with my project, always pushing to get nice movies and pictures (sometimes too impatient: emailing-phoning, please Ana send me those beautiful pics of the green cells…) and always happy when those pics were there. Thanks also for all those BIOS-social activities, good and funny barbecues at Nijverdal, nice Christmas cadeautjes, the summer and winter 'workweek'; I really enjoyed them.

I would also like to thank my co-promotor, Helene Andersson. Despite the distance between Stockholm and Enschede, you were always there to answer emails/phone calls very quickly.

I am also very grateful to my supervisor during the first part of my thesis journey, Regina Luttge. Dear Regina, thanks for coaching me during this time. You always showed a lot of enthusiasm to manage the project and you seemed to never run out of energy, always positive and willing to discuss all kind of issues. Thanks for your support and encouragement.

If there is someone to whom I have to thanks most that is 'my technician', Jan van Nieuwkasteele, without his work this project would never have been completed. Dear Jan, thanks for being such a good technician, you have always tried your best not only at the cleanroom work but also helping me to build-up the best (and most fancy) setup. Thanks for all the good meetings and always accomplish deadlines in time.

Paul, Paulje, Paul, 'the cell culture smiling guy'; - could I have cells now?- Yes, but...first coffee and a cigarette, ok?. Thanks a lot for keeping happy the cells and doing the entire cell culture lab work. Thanks also for rolling your thumbs every time an experiment took place ;).

This work would have not been possible without the help and collaboration of different people. Part of this project/thesis has been done in collaboration with the group of Prof. Remko Boom from Food Science department at the University of Wageningen. I would like to thank Martijn Fox, the PhD at WUR University. Thanks Martijn for sharing and discussing ideas, for going up and down Wageningen-Enschede with your pulser and yeasts, for all the experimental work we have performed together and for your kindness. I owe my appreciation to Prof. Wiebe Kruijer and Janine Post from the group of Cell Molecular Biology in the University of Twente who were always very enthusiastic and positive with my project and willing to cooperate. Thanks Janine for all the time you have invested, for your help and support and for your good comments and tips.

Nicolas Demierre and Iris van Uitert, my two 'afstudeerstudenten', have also contributed to this thesis work. I am very grateful to them, the good way they did approach the project and their willingness to help. I am greatly indebted to Wouter Sparreboom, not only for his contribution in chapter 6 of my thesis but also to offer me all his time and knowledge. Thanks Wouter, I have learned a lot from you about electrical engineering. Thanks to Wouter Olthuis for good discussions and guidance during the afstudeer of Iris, Ad for his help with the electronics of the system, Rob Duwel for his help in labview and EdwinO for his help in modeling and simulations.

Working at the BIOS group has been all a pleasure, a fantastic place. I enjoyed a lot working in such a multidisciplinary environment where experts from different fields are met. I also liked a lot the daily life at the BIOS, always looking for an excuse to get cake in the coffee corner, the nice atmosphere in the coffee and lunch breaks and all the fun and laughs we got participating in different activities like karting, running, skating, squash, etc…Thank you to all the Bios boys 'n girls: Erik K., Wim, Paul, Wouter, Jacob, Woitek, Jan N., Floor, Han, Regina, Steven, Johan, Arjan, Svetlana, Anil, Egbert, Hermine, Jan E., Piet, Wouter O., Iris,

Jurjen, Erik F., Roald, Séverine, Celio, Lingling, Joke, Georgette, Kevin, Daniel, Ad, Tom, Hien-Duy, Gabriel and Edwin.

A special thanks goes to my roommates at the UT; Egbert, Jurjen and Floor for een leuke en gezellige kamer. Always making jokes, teasing each other, having fun and listening to each other complains. Jurjen, (Jur-Jur), the 'keyboard killer', loud music player and call center for arranging motorbikes issues. Egbert, (Egbertina), always listening to me, willing to play music every time I said; Egbert could you please play your nice music?? and for being always patient and smiling all those times I was having a deadline for a conference, presentations… and my mood was not so good at those moments. Floor, who despite all the mess and disorder is present in our room she keeps a tidy and clean desk! Always willing to answer any bio/cell-related question. (I wish you all a nice evening!!!!! every afternoon at the time of leaving).

Hermine, our dear secretary. Thanks for your kindness and for all the administrative support whenever was needed for conferences, meetings, appointments.

And of course I will not forget to thank all the former BIOS members: Sebaastian, Doro (thanks for the running training), Patrick (gnoe), Moni (che palle), Dragana, Koen, Rob, Annie, EdwinO, Martijn, Theo, Henk, Niels, Petra, Souke and Bjorn.

I would also like to thank Roald for reading the entire concept thesis as well as for providing me with valuable suggestions. Thanks a lot for translating the summary into Dutch. Roald, Roaldos, Roaldinho, no words to describe how supportive you have been since you came to the BIOS. You always manage to motivate me when I got hard times. Besides the time and effort (biking back and forward Hengelo-Deventer) you have dedicated reading my concept, thank you very much for always being there as a friend. Gracias amigo.

Séverine, the 'french-cocotte', who offered to correct the concept thesis, thanks for your corrections. Thanks also for your help at the confocal microscope. And… I will keep sharing the pump with you, ok? ;).

Extra thanks to Egbert and Roald for being my "Paranimfen". I am very happy that you will be up there with me.

During these years I have leaved in different places and with different people. Here I want to thanks all my housemates: Gemma, Alexander, Isabel, Sesé, Gabriel, Lourdes, Martine and Kim, for sharing nice times: cooking, eating, watching a movie, partying… Thanks Gemmocha, for your warmth welcome in Enschede, the homesick-feeling was less painful having you as my housemate and friend.

Estos años no hubieran sido lo mismo sin mis amigos 'los alopecianos'; Sesé (Aserejé y Cardhu), OlivaM (estamos sequitos), Seve (inolvidable, te llevo en mi corazón), Gabriel (si voy voy y si no, no voy), Marta (nuestra cocinera), Luisito (vamos a dar una vuelta o que???), Sonia (que bonito es Utrecht), Miguel, Juan, Isabel, Elisa, Jordi (que pasa Anitaaaaaa??), Astrid, Verena, Adelio, Mako (Valero?), Mauricio y Paco (pakito). Han sido muchos los momentos que hemos compartido y mucho lo que hemos disfrutado juntos. Gracias chicos por haber estado ahí, por haber sido mi familia, una pena que me hayáis dejado sola en Enschede….

Following the tradition of my friend 'Che palle'; dinner at 'De Baaird' every Thursday evening, I got to know almost all the SMCT members and they immediately make me feel as one more of the group!. Fernando, Lourdes, Olga, Alesio, Soco, Emiel, Moni, Michel, Marina, Bass, Xin Yi, In Yi, Martine, Christian, Francesca and Yanina: thanks for the laughs we have shared!

The Girl's night team -Unforgettable luxury dinners; Lourdes, Xin Yi, Soco, Marina, Martine and Janet -do you looooove me???, thanks for all these nice dinners and all the funny evenings.

Thanks to Henry (Quique) and Niels, my beer mates, always in for some beertje drinken and never-ending conversations, to Henny (+ the HAAL family) and Mako, leuke lunchs op vrijdagmiddag. Gracias Laura por nuestras conversaciones y Wim por compartir unas grimbergens los jueves noche.

Thanks to the ICT guys, Arjan and Ralph, always there to solve any computer problem and of course to tease me!

Gracias a mis amigas Rosana, Susana y Marta por estar siempre ahí cada vez que he estado de vuelta por España y por acompañarme en la distancia a través de e-mails y del messenger, que habríamos hecho sin el Messenger!!!

Jeroen gracias por dedicarme una bonita sonrisa todos los días que hemos compartido. Cari, gracias por tu cariño y compresión, por cuidar de mí y por escucharme y apoyarme siempre que lo he necesitado.

Estos años fuera de casa han servido para crecer mi amor hacia mi familia. Quiero agradecer enormemente a mis abuelas, tíos y primos por su constante amor y cariño. A mis padres y hermanos, Loli y Alejandro, que son lo más preciado para mí. Gracias papas por apoyarme siempre en todas mis decisiones, por vuestro incondicional apoyo y amor, por vuestros cuidados y mimos y por todo lo que me habéis enseñado. Estoy muy orgullosa de tener una familia tan maravillosa.

Ana